# Extracellular vesicles as potential therapies for paediatric neurovisceral diseases

***Maha Muwaffak***

**Thesis submitted in fulfilment of the requirements for the degree of Doctor of Philosophy (PhD)**

**University College London**

**School of Pharmacy**

**29-39 Brunswick Square London,**

**WC1N 1AX**

**2020**

I, Maha Muwaffak confirm that the work presented in this thesis is my own. Where information has been derived from other sources, I confirm that this has been indicated in the thesis.

# Acknowledgments

This PhD journey coincided with some of the toughest periods of my life followed by a global pandemic, but the fact that I am here today has proven to me that with enough determination, courage, and the right support network we can make anything happen. Many thanks are thus due for all those who were part of my support network.

First, I would like to thank my supervisors without whom this PhD project would not have come to light. Many thanks to Professor Ahad Rahim for taking me on as a PhD student in his lab and his continuous guidance throughout this project. I would also like to extend my profound gratitude to Professor Gareth Williams for all the support and guidance throughout these four years.

Many thanks are due to everyone in the Rahim lab for facilitating and making my PhD journey better with all their support in and out of the lab. Special thanks go to Dr Micheal Hughes for all his help with viral production and animal studies; Dr Laura Poupon and Amy Geard for their help with animal studies and primary neuronal cultures; and Dr Giuila Massaro for not only her support in the lab, but also her invaluable advice and guidance. Finally, I would also like to thank Dr Rita Trindade from the Williams group who gave me a great introduction to exosomes research.

I would also like to extend my acknowledgments to the EPSRC – Engineering Physical Sciences Research Council - for funding this project, as well as everyone at the School of Pharmacy from past and present research members; colleagues from other departments such as Dr Ben Allsop, Dr Trevor Askwith, and Dr Dave Gathercole; as well as all the friends I made along the way here.

Special thanks all my friends and family who in one way or another supported me throughout this PhD journey, especially during all the emotionally and psychologically challenging times. Biggest gratitude and love goes to my partner Petar whose support, encouragement, and motivation always kept me going and helped me be where I am today.

# Abstract

There are a large number of lethal diseases that affect the brain and visceral organs of children. Many of these neurovisceral conditions are caused by mutations in single genes leading to a lack of a particular protein or enzyme. These are intractable conditions for which there is no effective treatment available, and hence there is an overwhelming need to develop new therapies. Extracellular vesicles (EVs) offer one possible solution to this. EVs are anuclear cell-derived bodies that can deliver a desired therapeutic cargo to both the visceral organs and brain. Here we describe how a gene delivery strategy can be used to develop cellular factories that produce EVs loaded with proteins and enzymes of interest as prospective treatments for neurovisceral diseases.

Various EV producer cell types were first evaluated for transduction efficiency with lentiviral vectors carrying marker genes for enhanced green fluorescent protein (eGFP) and luciferase enzyme. HEK293T cells had the highest transduction efficiency and were hence used to produce EVs loaded with eGFP and luciferase. These loaded-EVs were isolated using an optimised differential ultracentrifugation method, and characterised for size, concentration, morphology, eGFP and enzyme content. *In vitro* experiments demonstrated that loaded-EVs can deliver active luciferase enzyme to HEK293T cells and eGFP to primary neurons. Additionally, eGFP was shown to be co-localised with lysosomes in primary neurons.

Injections of loaded-EVs into neonate mice through different routes of administration revealed that EVs delivered eGFP to both the brain and visceral organs, although to different extents. Significant eGFP content in the brain was only achieved following intracerebroventricular (ICV) injections. EVs were shown to cross the blood brain barrier following systemic administration but to a lower extent in comparison to the ICV route. Similar injections in adult mice resulted in eGFP only being detected in visceral organs at the same time points. The possibility of targeting delivery to the brain was evaluated through the use of the neuronal cell line SH-SY5Y to produce loaded-EVs. However,

EVs derived from HEK293T cells delivered a higher eGFP cargo to both the brain and visceral organs than those derived from SH-SY5Y cells.

Subsequently, Gaucher disease, a lysosomal storage disease caused by mutations in the *GBA1* gene leading to a defective glucocerebrosidase (GCase) enzyme, was chosen as a paediatric neurovisceral disease model. HEK293T cells were used to generate EVs loaded with the GCase enzyme, which were characterised and tested *in vitro*. These experiments revealed that the EVs can upregulate lysosomal GCase enzyme activity in cells, indicating that they can be used to deliver lysosomal enzymes to the lysosomal compartment.

Finally, the stability of HEK293T-derived EVs was evaluated, and it was determined that they are stable for two weeks at –80 °C but degrade over this time at 20 °C. The feasibility of freeze-drying using the lyoprotectant trehalose to improve stability of these EVs at higher storage temperatures was investigated, and freeze-drying with 2 %w/v trehalose enabled storage at 4 °C for two weeks and at 20 °C for one week without significant deleterious effects on the biological cargo. Overall, the work detailed in this thesis suggests that loaded-EVs could comprise potent therapeutic interventions for neurological disorders.

## Impact statement

Currently, the therapies available to treat neurovisceral diseases such as Gaucher disease are very limited or non-existent. Although rare, the outlook for patients suffering such conditions is extremely bleak: for instance, children affected by type II Gaucher disease usually do not reach their 2nd birthday [1] meanwhile those suffering from Batten disease can expect to become blind, demented and bedridden before dying at an early age from degeneration in the brain [2]. Enzyme replacement therapy is a potential treatment, but the inability of enzymes to cross the blood brain barrier (BBB) is a major impairment to treating neurological manifestations. Extracellular vesicle (EV)-based therapies directly address this issue because they have been proven to be highly effective drug delivery systems with the ability to cross biological membranes including the BBB [3]. Further, EVs can provide protection to incorporated enzymes/proteins, helping the latter to avoid rapid degradation, and the fact that EVs are non-immunogenic enables repeated administration without eliciting an immune response. Importantly, EVs have been shown to co-localize with lysosomes upon entry to cells, which gives them great potential as therapeutics for lysosomal storage diseases (including but not limited to Gaucher disease). It is estimated that there is around 50 lysosomal storage diseases with estimated combined frequency at birth of 1:7500 [4] and although some treatment options are available, most are associated with low efficacy, high cost, and immunogenicity problems. The development of a platform for the production of EVs loaded with a desired lysosomal enzyme could make major contributions to the treatment of these diseases.

This project develops a platform for producing “cellular factories” for loaded-EVs through transduction with lentiviral vectors and permanent expression of genes coding for a protein/enzyme of interest. Once these “cellular factories” are established, loaded-EVs can be obtained through the repeated culturing and passaging of cells that secrete these loaded-EVs into the media. Detailed *in vivo* biodistribution studies shed light on the largely unstudied pharmacokinetics of EVs following different routes of administration. These studies also lay the foundation for the comparison of EV pharmacokinetics between adult and neonate mice, which to our knowledge has not been

evaluated previously. Investigations into the storage stability of EVs, and how this is influenced by freeze drying, are reported.

Overall the work in this thesis shows that lentiviral vectors can be used to transduce cells to produce EVs loaded with a protein or enzyme of interest, that these EVs can be trafficked to the brain and visceral organs *in vivo*, and that they can be formulated to remain stable on the one-month timescale under standard refrigeration. These finding show the loaded-EVs to have therapeutic promise, and to be amenable to clinical conditions. This work thus provides a platform for the production and use of EVs as potential therapeutic delivery vectors for neurovisceral (and other) diseases. Ultimately, this could lead to great benefits for individuals affected by these conditions, their families, and healthcare providers.

# Table of contents

**Acknowledgments** ... 3

**Abstract** ... 4

**Impact statement** ... 6

**Table of contents** ... 8

**Abbreviations** ... 16

**Chapter 1: Introduction** ... 18

**1.1 Preamble** ... 19

**1.2 Gaucher disease** ... 19

**1.2.1 Genetics and epidemiology** ... 20

**1.2.2 Pathogenic basis of the disease** ... 21

**1.2.3 Diagnosis** ... 22

**1.2.4 Current available therapies** ... 23

**1.3 Extracellular vesicles** ... 23

**1.4 Biogenesis of exosomes** ... 26

**1.4.1 Formation** ... 26

**1.4.2 Sorting of cargo** ... 27

1.4.2.1 Protein cargo ... 27

1.4.2.2 RNA cargo ... 29

**1.4.3 Release** ... 30

**1.5 Nomenclature** ... 31

**1.6 Therapeutic potential of EVs** ... 31

**1.6.1 EVs in the treatment of neurovisceral disorders** ... 34

**1.6.2 EVs as delivery vectors of lysosomal enzymes** ... 35

**1.7 Lentiviral vectors** ... 36

**1.7.1 Lentiviral components** ... 37

**1.8 Current limitations in using EVs for therapy** ... 38

**1.9 Aims and objectives** ... 39

**Chapter 2: Materials and methods** ... 40

**2.1 Materials ..... 41**
**2.1.1 Antibodies ..... 41**
**2.1.2 Primer sequences ..... 42**
**2.2 Cloning ..... 42**
**2.2.1 Bacterial transformation ..... 42**
**2.2.2 Amplification and purification of plasmid DNA ..... 42**
**2.2.3 Restriction enzyme digest ..... 45**
**2.2.4 Gel electrophoresis ..... 45**
**2.2.5 DNA extraction from agarose gel ..... 46**
**2.2.6 Ligation ..... 46**
**2.2.7 Sequencing ..... 46**
**2.3 Lentivirus production ..... 46**
**2.3.1 Cell culture ..... 47**
**2.3.2 Transfection of cells and virus harvest ..... 48**
**2.3.3 Titration ..... 48**
**2.4 Production of EVs ..... 49**
**2.4.1 Maintenance of cell lines ..... 49**
**2.4.2 Vesicle depletion of FBS ..... 50**
**2.4.3 Cell viability assay ..... 51**
**2.4.4 Production of naïve EVs ..... 51**
**2.4.5 Production of loaded-EVs ..... 52**
2.4.5.1 Transduction ..... 52
2.4.5.2 Assessing successful transduction by flow cytometry ..... 53
2.4.5.3 Assessing successful transduction through analysis of GCase enzymatic activity ..... 54
**2.4.6 Isolation of EVs ..... 56**
**2.4.7 Concentration and purification of EVs ..... 59**
**2.5 Characterisation of EVs ..... 59**
**2.5.1 Nanoparticle tracking analysis ..... 59**
**2.5.2 Transmission electron microscopy (TEM) ..... 60**
**2.5.3 Quantification of total EV and cellular protein content ..... 61**
**2.5.4 Protein analysis using traditional western blot ..... 61**

**2.5.5 Protein analysis using the simple western system (WES) 62**
**2.5.6 Total RNA isolation ..... 64**
**2.5.7 Reverse transcription and quantitative real-time PCR analysis of RNA sequences isolated from EVs and HEK293T cells ..... 65**
**2.5.8 Quantification of ATP content in EVs ..... 66**
**2.5.9 Analysis of luciferase content in loaded-EVs ..... 66**
**2.5.10 Quantification of eGFP content in loaded-EVs ..... 67**
**2.5.11 Analysis of GCase enzymatic activity in loaded-EVs ..... 67**
**2.5.12 Delivery of loaded-EVs *in vitro* ..... 67**
2.5.12.1 Delivery of luciferase enzyme to cells of visceral origin 67
2.5.12.2 Delivery of eGFP to primary neurons ..... 68
2.5.12.3 Delivery of GCase to cells of visceral origin ..... 69
**2.6 *In vivo* biodistriubtion studies ..... 70**
**2.6.1 Animals ..... 70**
**2.6.2 EV administration ..... 70**
2.6.2.1 ICV route (neonates) ..... 71
2.6.2.2 IV route (neonates) ..... 72
2.6.2.3 IN route (neonates) ..... 72
2.6.2.4 IP route (neonates and adults) ..... 72
2.6.2.5 IV route (adult) ..... 72
2.6.2.6 ICV route (adults) ..... 73
**2.6.3 Harvesting of tissues ..... 73**
**2.7 Histological analysis of tissues ..... 73**
**2.7.1 Coating of slides ..... 73**
**2.7.2 Cryosectioning of tissue samples ..... 74**
**2.7.3 Immunohistochemistry ..... 74**
**2.7.4 Microscope imaging ..... 75**
**2.8 Protein analysis ..... 75**
**2.8.1 Protein concentration measurement from tissues ..... 75**
**2.8.2 GFP ELISA on frozen tissue ..... 75**
**2.9 Formulation of EVs and stability testing ..... 76**

**2.9.1 Freeze drying ..... 76**
**2.9.2 Evaluation of lyophilised EVs ..... 77**
**2.10 Statistical analysis ..... 77**
**Chapter 3: Production, optimisation and validation of loaded-EVs ..... 78**
**3.1 Introduction ..... 79**
**3.1.1 Isolation of EVs ..... 79**
**3.1.2 Characterisation of EVs ..... 84**
**3.1.3 Loading of EVs ..... 86**
**3.2 Aims and objectives ..... 90**
**3.3 Results and discussion ..... 90**
**3.3.1 Lentiviral production and titration ..... 90**
**3.3.2 Gene delivery to HEK293T and THP-1 cells ..... 91**
3.3.2.1 Fluorescence microscopy ..... 92
3.3.2.2 Flow cytometry ..... 95
3.3.2.3 Cell sorting to enrich eGFP in loaded EVs ..... 97
**3.3.3 Production of EV-free media ..... 99**
3.3.3.1 Depletion of EVs from FBS ..... 99
3.3.3.2 Cell viability ..... 103
**3.3.4 Isolation of EVs ..... 104**
3.3.4.1 Isolation of EVs using protocol 5 ..... 107
3.3.4.2 Concentration and further purification of EVs ..... 109
**3.3.5 Characterisation of loaded-EVs ..... 110**
3.3.5.1 Size and concentration ..... 110
3.3.5.2 TEM ..... 111
3.3.5.3 Evaluation of EV protein content ..... 112
3.3.5.4 Total RNA isolation ..... 115
3.3.5.5 RT and q-PCR analysis ..... 117
3.3.5.6 Quantification of ATP content in loaded-EVs ..... 119
3.3.5.7 Analysis of luciferase content in loaded-EVs ..... 121
**3.4 Conclusions ..... 123**
**Chapter 4: In vitro and in vivo delivery of cargo by loaded-EVs ..... 124**

**4.1 Introduction ..... 125**
**4.1.1 Cellular internalisation of EVs ..... 125**
**4.1.2 *In vivo* biodistribution of EVs ..... 127**
**4.2 Aims and objectives ..... 128**
**4.3 Results and discussion ..... 129**
**4.3.1 Delivery of luciferase enzyme to cells of visceral origin 129**
**4.3.2 Delivery of eGFP to primary neurons ..... 131**
**4.3.3 *In vivo* biodistribution study ..... 135**
4.3.3.1 Neonatal ICV route ..... 137
4.3.3.2 Neonatal IV route ..... 138
4.3.3.3 Neonatal IP route ..... 139
4.3.3.4 Neonatal IN route ..... 142
4.3.3.5 Adult ICV route ..... 144
4.3.3.6 Adult IV route ..... 145
4.3.3.7 Adult IP route ..... 146
4.3.3.8 Immunocytochemistry ..... 147
**4.4 Conclusion ..... 148**
**Chapter 5: Use of neuronal SH-SY5Y cells to produce loaded-EVs for targeting to the CNS ..... 150**
**5.1 Introduction ..... 151**
**5.2 Aims and objectives ..... 152**
**5.3 Results and discussion ..... 152**
**5.3.1 Gene delivery to SH-SY5Y cells ..... 152**
5.3.1.1 Fluorescence microscopy ..... 152
5.3.1.2 Flow cytometry ..... 153
5.3.1.3 Cell sorting to enrich eGFP in loaded EVs ..... 155
**5.3.2 Characterisation of loaded-EVs ..... 155**
5.3.2.1 Size and concentration ..... 155
5.3.2.2 TEM ..... 157
5.3.2.3 Evaluation of EV protein content ..... 158
**5.3.3 *In vivo* biodistribution study ..... 160**
5.3.3.1 eGFP content in the brain ..... 161

5.3.3.2 eGFP content in the liver ..... 164
5.3.3.3 eGFP content in the heart ..... 165
**5.4 Conclusion ..... 167**
**Chapter 6: Production of therapeutic GCase-loaded EVs ..... 168**
**6.1 Introduction ..... 169**
**6.2 Aims and objectives ..... 171**
**6.3 Results and discussion ..... 171**
**6.3.1 Cloning ..... 171**
**6.3.2 Lentiviral production and titration ..... 174**
**6.3.3 *GBA1Ub* gene delivery to HEK293T cells ..... 175**
**6.3.4 Characterisation of GCase-loaded EVs ..... 175**
6.3.4.1 Size and concentration ..... 175
6.3.4.2 TEM ..... 177
6.3.4.3 Protein analysis using western blot ..... 178
6.3.4.4 Analysis of GCase activity in loaded-EVs ..... 179
6.3.4.5 Evaluation of uptake of GCase loaded-EVs by cells ..... 180
**6.4 Conclusion ..... 182**
**Chapter 7: Freeze-drying of EVs for long term storage ..... 183**
**7.1 Introduction ..... 184**
**7.1.1 Storage of EVs ..... 184**
**7.1.2 Lyophilisation ..... 185**
**7.2 Aims and objectives ..... 187**
**7.3 Results and discussion ..... 188**
**7.3.1 Evaluation of stability of naïve non-lyophilised EVs ..... 188**
7.3.1.1 Concentration and modal size ..... 188
7.3.1.2 Total protein concentration ..... 190
**7.3.2 Evaluation of stability of lyophilised naïve EVs ..... 192**
7.3.2.1 Concentration modal size of lyophilised EVs stored at 4°C ..... 192
7.3.2.2 Total protein concentration of lyophilised EVs stored at 4°C ..... 195

7.3.2.3 EV surface markers of lyophilised EVs stored at 4°C.... 196
7.3.2.4 Concentration and modal size of lyophilised EVs stored at 20°C ..... 197
7.3.2.5 Total protein concentration of lyophilised EVs stored at 20°C ..... 199
7.3.2.6 EV surface markers of lyophilised EVs stored at 20°C.. 200
**7.3.3 Evaluation of stability of loaded-EVs containing luciferase enzyme ..... 202**
7.3.3.1 Concentration and size of lyophilised loaded-EVs stored at 4°C ..... 202
7.3.3.2 Total protein concentration of lyophilised loaded-EVs stored at 4°C ..... 203
7.3.3.3 EV surface markers of lyophilised loaded-EVs stored at 4°C ..... 204
7.3.3.4 Luciferase enzyme activity in lyophilised loaded-EVs stored at 4 °C ..... 205
7.3.3.5 Concentration and modal size of lyophilised loaded-EVs stored at 20°C ..... 207
7.3.3.6 Total protein concentration of lyophilised loaded-EVs stored at 20°C ..... 207
7.3.3.7 EV surface markers of lyophilised loaded-EVs stored at 20°C ..... 208
7.3.3.8 Luciferase enzyme activity in lyophilised loaded-EVs stored at 20°C ..... 209
**7.4 Conclusions ..... 212**
**Chapter 8: Discussion ..... 213**
**8.1 Overview ..... 214**
**8.2 Lentiviral vectors for generation of cellular factories for loaded-EVs ..... 214**
**8.3 EVs can deliver cargo *in vitro* and *in vivo* ..... 215**
**8.4 Neuronal cell derived EVs do not necessarily lead to enhanced or targeted delivery to neuronal cells ..... 216**

**8.5 EVs can deliver active lysosomal GCase enzyme to the lysosomal compartment ..... 216**

**8.6 Lyophilisation allows for storage of EVs at higher temperatures ..... 217**

**8.7 Study limitations and future considerations ..... 217**

**8.8 Conclusion ..... 220**

**References ..... 222**

**Appendices ..... 244**

**I. Chapter 3 ..... 244**

**II. Chapter 7 ..... 246**

# Abbreviations

| | |
|---|---|
| ANOVA | Analysis of variance |
| BBB | Blood-brain barrier |
| bp | Base pair |
| BSA | Bovine serum albumin |
| CMV | Cytomegalovirus |
| cDNA | Complementary DNA |
| CNS | Central nervous system |
| DAB | 3,3'- diaminobenzidine |
| DAPI | 4′,6-diamidino-2-phenylindole |
| dH2O | Distilled water |
| DMEM | Dulbecco's modified eagle medium |
| DMSO | Dimethyl sulfoxide |
| DNA | Deoxyribonucleic acid |
| ERT | Enzyme replacement therapy |
| ELISA | Enzyme-linked immunosorbent assay |
| EVs | Extracellular vesicles |
| FBS | Foetal Bovine Serum |
| g | g-force |
| GCase | β-glucocerebrosidase |
| eGFP | Enhanced Green fluorescent protein |
| ICV | Intracerebroventricular |
| IP | Intraperitoneal |
| IN | Intranasal |
| IV | Intravenous |
| Kb | Kilobase |
| LAMP1 | Lysosome-associated membrane protein 1 |
| LTR | Long terminal repeat |
| Mg | Miligram |
| MHC I | Major histocompatibility complexes class I |
| MHC II | Major histocompatibility complexes class II |
| miRNA | Micro RNA |
| mL | Millilitre |

| | |
|---|---|
| mRNA | Messenger RNA |
| MSC | Mesenchymal stem cell |
| MVBs | Multivesicular bodies |
| Nm | Nanometre |
| ns | Non-significant |
| NTA | Nanoparticle tracking analysis |
| Particles/mL | Particles per mililitre |
| PBS | Phosphate buffered saline |
| PEI | Polyethylenimine |
| PFA | Paraformaldehyde |
| RIPA | Radioimmunoprecipitation assay buffer |
| Rpm | Rotations per minute |
| RNA | Ribonucleic acid |
| SD | Standard deviation |
| TAE | Tris-acetate-ethylenediaminetetraacetic acid |
| TBS | Tris-buffered saline |
| TEM | Transmission electron microsospy |
| UC | Ultracentrifugation |
| W/V | Weight per volume |
| Vp | Viral particle |
| VSV-G | Vesicular-stomatitis virus G-protein |
| WPRE | Woodchuck post-transcriptional regulatory element |

# Chapter 1: Introduction

## 1.1 Preamble

There exist a number of inherited paediatric neurodegenerative metabolic diseases which are caused by the body's failure to produce key enzymes, for instance Gaucher's disease [1] and infantile neuroaxonal dystrophy (INAD) [5], and Batten disease [6]. In this project we will be focusing on Gaucher disease, the most common lysosomal storage disorder, which is caused by mutations in the *GBA1* gene that encodes for the lysosomal enzyme β-glucocerebrosidase (GCase). This results in a defective enzyme and subsequent accumulation of non-degraded substrate material in macrophages within the visceral organs and, in some forms of the disease, the brain. The current standard treatment is enzyme replacement therapy, which is efficient in ameliorating the visceral but not the neurological manifestations, as systemically administered enzymes cannot cross the blood brain barrier (BBB) [2]. Here we propose a novel approach to circumvent this problem through the use of EVs, which have been shown to be useful delivery vectors with a natural ability to cross biological membranes.

This introductory chapter will give an overview of Gaucher disease, EVs, and their potential as delivery vectors for enzymes. Moreover, lentiviral gene delivery vectors will be introduced and their use to produce stable "cellular factories" for EVs loaded with therapeutic enzymes discussed.

## 1.2 Gaucher disease

Gaucher disease is a multisystem chronic disease with signs and symptoms varying widely among patients. It can be broadly classified into three subtypes depending on age of onset and the presence or absence and rate of progression of neurological manifestations.

Type 1, or non-neuronopathic, Gaucher disease is the most common form and is mainly characterized by enlargement of the spleen and liver, but also blood disorders (such as anaemia and thrombocytopenia), orthopaedic complications (e.g. bone pain, fractures, and arthritis) and pulmonary involvement (pulmonary hypertension and interstitial lung disease) [7]. The

onset and severity of symptoms vary widely between patients, with appearance occurring from early childhood to adulthood. Type 1 Gaucher disease is purely visceral, and the central nervous system is usually not affected [7].

Types 2 and 3 Gaucher disease both have neuropathic in addition to visceral manifestations, with Type 2 being acute and Type 3 chronic [8,9]. Type 2 has a very early onset, with symptoms starting in early infancy and death occurring by the age of two to four years due to a rapid neurological decline. Central nervous system involvement results in an array of symptoms ranging from a hyperextended neck, spontaneous apnoea, difficulties in swallowing, seizures and progressive epilepsy [10,11]. Some of the characteristic visceral manifestations are similar to those of Type 1, but also include significant hepatosplenomegaly and pulmonary involvement [12]. Manifestations of Type 3 Gaucher disease are similar those of Type 2 but are less severe. The onset of symptoms starts between infancy and adolescence (and rarely in adulthood) in Type 3 Gaucher, and the rate of progression of symptoms is typically slower than with Type 2 [13]. This work will focus on Type 2 Gaucher disease, since this does not have any treatment options available and loaded-EVs could provide a viable therapy by delivering soluble GCase enzyme across the BBB to treat the lethal neurodegeneration.

### 1.2.1 Genetics and epidemiology

Type 2 Gaucher disease is inherited in an autosomal recessive manner whereby mutations in the *GBA1* gene located on chromosome 1 at position 22 (OMIM ID: 606463)[14] lead to greatly reduced or abolished GCase activity [7]. Over 300 mutations are known to cause the disease, including missense mutations (which represent the vast majority of cases), nonsense mutations, small deletions and insertions, and splice junction mutations [7]. The condition is very rare, with Type 1 being the most commonly occurring and representing 90-95 % of cases [11]. The overall occurrence of Gaucher disease is approximately 1 in 50,000 to 100,000 people in the general population.

### 1.2.2 Pathogenic basis of the disease

Human lysosomal beta-glucocerebrosidase is a glycosylated enzyme with 497 amino acids and a 67 kDa molecular weight[1]. In humans this enzyme is synthesised in the endoplasmic reticulum (ER), glycosylated in the Golgi complex and transported to the lysosome in endosomes, where it is activated by the acidic environment [1]. Glycosylation of the enzyme is essential for its catalytic activity [15]. In the lysosome, GCase takes part in a two-step reaction where first its active site is glycosylated by its natural substrate glucosylceramide (also known as glucocerebroside), followed by hydrolysis of the substrate into β-glucose and ceramide [16]. GCase also hydrolyses a minor lipid glucosylsphingosine, a deacylated form of glucosylceramide, into sphingosine and water [16]. In the body glucosylceramide is derived mainly from the degradation of plasma membranes, in particular senescent blood cells [17]. The catalytic activity of the enzyme is enhanced by the activator saponin C, which solubilises the membranes to release glucosylceramide and make it available for the GCase enzyme [18]. In Gaucher disease, as a consequence of the mutations in the *GBA1* gene, the enzyme produced has reduced catalytic function and/or stability due to, for example, a less flexible enzyme structure that cannot bind the substrate efficiently or a conformational change in the hydrophobic core of the protein that alters folding and hence stability [19].

As a result of reduced GCase activity, in Gaucher disease there is a build-up of glucosylceramide in the lysosomes of all cells, but this is more prominent in cells with monocyte/macrophage lineage. This is because these cells are responsible for eliminating erythroid cells and leukocytes, which contain large amounts of glycosphingolipids, a source of the GCase substrate glucosylceramide [20]. Macrophages become engorged with glucosylceramide and are termed “Gaucher cells”. They mainly infiltrate the liver, spleen and bone marrow, but also other organs including the lungs, skin, heart, kidney and the nervous system [21]. Gaucher cells are a hallmark of the disease, and due to the accumulation of glucosylceramide when visualised under the microscope they have eccentric nuclei and cytoplasm that resembles ‘wrinkled tissue paper’ (Fig. 1.1) [22].

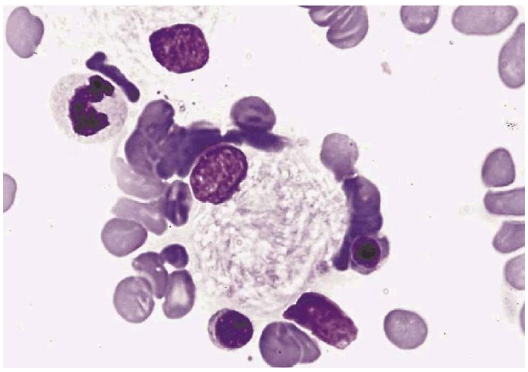

**Figure 1. 1:** Image of Gaucher cells. Reproduced from Aerts *et al*. [23] with permission from publisher Royal Society

Widespread accumulation of Gaucher cells underlies the multisystemic manifestations of the disease [7]. For example accumulation of Gaucher cells in the liver and spleen leads to hepatosplenomegaly [21], while build-up in the bone marrow (together with hypersplenism) results in cytopenia [24]. When they amass in the lung parenchyma and alveolar spaces, infiltrative lung disease and lipid pneumonia result [25,26]. The pathophysiological mechanisms underlying the neuronopathic manifestations of Type 2 and 3 Gaucher disease remain poorly understood, but it is suggested that neuronal loss, neuronal atrophy and necrosis occur due to direct toxic effects of accumulated glucosylceramide and glucosylsphingosine, which are produced endogenously in CNS neuronal cells [20].

### 1.2.3 Diagnosis

Unfortunately, as is often seen with progressive rare diseases, in many instances diagnosis of Gaucher disease is confirmed several years following the first clinical signs. The following signs often lead to suspicion of Gaucher disease: hepatosplenomegaly, thrombocytopenia with or without anaemia, characteristic bone lesions, or signs of CNS involvement (in Type 2 and 3) [27,28]. Currently, the gold standard to confirm diagnosis is by determining deficiency in GCase enzyme activity in total leukocytes or mononuclear cells, or cultured fibroblasts. Enzyme activity is determined fluorometrically using the substrate 4-methylumbelliferyl-β-D-glucopyranoside [1]. Positive tests for Gaucher disease are evident when enzyme activity is reduced to approximately 10–15% of that seen in healthy individuals [1,7].

### 1.2.4 Current available therapies

At the present the current available therapies for lysosomal storage diseases are limited. The standard of care for Gaucher disease is enzyme replacement therapy (ERT) administered alone or in combination with substrate reduction therapies (SRT). ERT aims to restore the levels of GCase in Gaucher cells. Commercially available ERTs include the recombinant enzymes Imiglucerase, Velaglucerase and Taliglucerase [29] . SRT relies on decreasing production of the GCase substrate (glucosylceramide). Examples of SRTs include Miglustat, which decreases synthesis of glucosylceramide by acting as a glucosylceramidase synthase inhibitor [30], and Eliglustat [31,32].

While ERT and SRT can be helpful in treating Type 1 Gaucher disease, none of the above therapies has an effect on the neuropathological manifestations of Type 2 and 3 Gaucher disease. ERT is effective in treating the visceral and haematological aspects of the disease but remains ineffective against neurological aspects, since the enzyme cannot cross the BBB [33,34]. Further, it is possible that after some time patients treated with ERT may develop neutralising antibodies against the enzyme, rendering it ineffective [29]. Miglustat has no major effects on either the haematological or neurological aspects, [30] and Eliglustat cannot cross the BBB and so has no efficacy against neurological manifestations [35].

Recently, there have been some studies evaluating strategies to increase enzyme delivery to the brain. Approaches include intra-cerebroventricular and intrathecal infusions, gene therapy, intranasal delivery, or using hyperosmotic solutions or ultrasound to shrink the brain's endothelial cells at the BBB and enable access to the brain [36]. Although some of these strategies have enjoyed measured success they are invasive and/or require further improvements. An alternative potential strategy is to use extracellular vesicles (EVs) delivery vectors for the lysosomal enzymes.

## 1.3 Extracellular vesicles

Nearly 40 years ago two reports from Harding *et al*. [37] and Pan *et al*. [38] described how multivesicular bodies in reticulocytes (immature red blood cells)

released vesicles of circa 50 nm into the extracellular space. It was initially thought that cells disposed of non-essential or excess cargo (such as proteins) by packaging this into EVs that are subsequently degraded by fusion with the lysosome or secreted from the cell into the extracellular space [39]. However, extensive research over the past decades on EV structure, origin, composition and role has proven otherwise, transforming EVs from garbage disposal tools to entities at the forefront of new therapeutics [40]. EVs are generally divided into three subtypes and these include exosomes, microvesicles (MVs) and apoptotic bodies (Fig. 1.2). These are mainly distinguished by their different origins and consequently by different protein profiles, as well as size, content, and function (Table 1.1) [41–43].

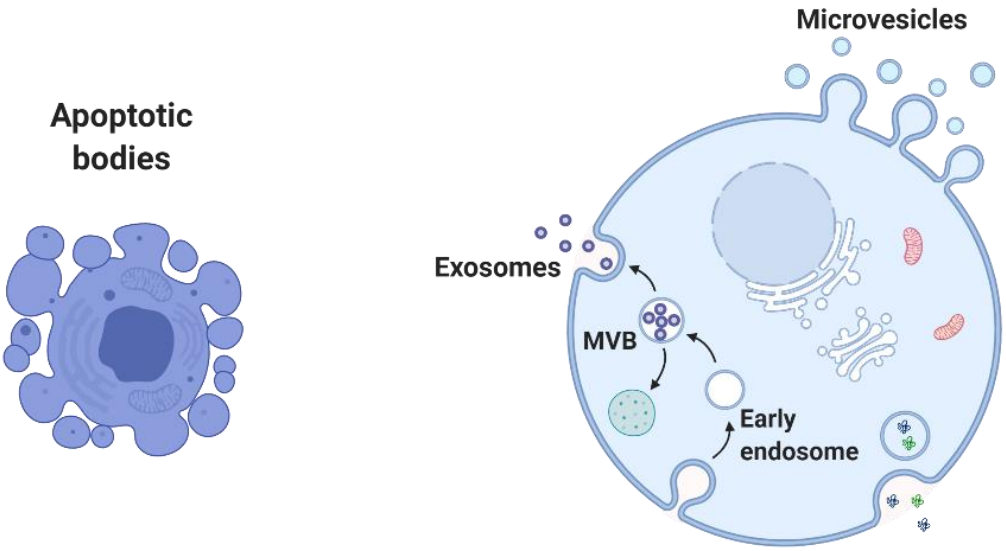


**Figure 1. 2:** Illustration of the different types of EVs (not drawn to scale). Created with BioRender.com

**Table 1. 1:** Characteristics of the different EV subtypes

| Vesicle origin | Characteristics | | | |
|---|---|---|---|---|
| | Origin | Size | Markers | Contents |
| **Exosomes** | Endosomal pathway: intraluminal budding of multivesicular bodies and consequent fusion with cell membrane | 40-150 nm | Tetraspanins (CD9,CD81,CD63), TSG101, Flotillin, ALIX | mRNA, miRNA and other non-coding RNAs, DNA, proteins, lipids |
| **Microvesicles** | Outward budding of plasma membrane | 100-1000 nm | Integrins, selectins, CD40 ligand | mRNA, miRNA and other non-coding RNAs; fragmented DNA; cellular organelles, proteins , lipids, |
| **Apoptotic bodies** | Outward blebbing of apoptotic cell membrane | 500-2000 nm | High concentrations of lipids such as phosphatidylserine | Nuclear fractions, cell organelles |

Exosomes are released by a large variety of cells in the body, such as cytotoxic T cells, neurons, platelets, or mast cells [44]. Exosomes can be isolated from almost all eukaryotic fluids [41], including blood, urine, saliva and media from cell cultures [45]. Some of the characteristic features of exosomes include enriched levels of tetraspanins (CD63, CD9, CD81), heat-shock proteins (HSP-27, HSP-60, HSP-70 and HSP-90), membrane transport and fusion proteins (Annexins I, II, RAB7), and the incorporation of lipids and nucleic acids such as DNA, mRNA and regulatory RNAs [44]. Moreover, exosomes derived from antigen presenting cells display major histocompatibility complex (MHC) I and/or II on their surface [46]. Mathivanan *et al*. have created an online database called ExoCarta (http://www.exocarta.org), where information from both published and unpublished studies involving exosomes is used to make a databank of their contents [47]. Currently, ExoCarta has collected information from 286 studies, and a total of 41860 protein entries, 4946 mRNA entries and 2838 miRNA entries have been made [47]. The precise composition of exosomes reflects their cells of origin, and contributes to their biological activity and potentially specific cell or tissue tropism [48].

Exosomes are the most characterised subtype and are currently evaluated as diagnostic and therapeutic entities in vast range of conditions [41,49–53]. The preference of using exosomes over the two other subtypes of EVs such as for example MVs stems from the difference in biogenesis and content. As exosomes are endosomal membrane derived vesicles this means that cargo incorporated into exosomes during their biogenesis, is that being actively processed by the parent cell [49]. It has been shown that this process of packaging and secretion of cargo in exosomes is finely tuned and has a role in intercellular communications in almost all physiological, and certain pathological, processes [54].The biological activity of exosomes is thought to be imparted by the cargo carried inside them, such as proteins, micro RNA (miRNA) and messenger RNA (mRNA) [55]. For example, in a study by Valadi *et al*. it was revealed that exosomes are involved in intercellular communication through the delivery of miRNA and mRNA, which when taken up by a target cell can be translated into functional proteins [56]. As such, exosomes can cause a multitude of responses in target cells [44]. In comparison, the biogenesis and sorting of cargo into MVs although less well defined results in fragments of cytosol fragments randomly enclosed by the budding of the plasma membrane and thus may not contain a similar repertoire of cargo as parent cell [49].

## 1.4 Biogenesis of exosomes

The precise mechanism by which exosomes are generated is not yet fully understood, but a number of studies have provided insight into their biogenesis [39,57–59]. Simplistically, the process can be split into three main parts: formation, sorting of cargo, and release (Fig. 1.3) [58].

### 1.4.1 Formation

This process is started with the formation of an early endosome which originates from inward budding of the plasma membrane (Fig. 1.3a) [58]. This is followed by inward budding of the endosomal membrane, leading to the formation of intraluminal vesicles (ILVs) [60]. The accumulation of ILVs in the endosomes results in their maturation into multivesicular bodies (MVBs) [39].

During this process of invagination, cargo such as proteins, lipids, etc. are sorted into the ILVs [58]. Finally, MVBs are transported to the plasma membrane and fuse with it, releasing the ILVs into the extracellular space. The released ILVs are termed exosomes [61] . It is established that there is fine tuning which determines the fate of these ILVs, but this process is complex [54] and the details are not yet understood.

## 1.4.2 Sorting of cargo

### *1.4.2.1 Protein cargo*

The endosomal sorting complex required for transport (ESCRT) machinery and associated accessory proteins (programmed cell death 6 interacting protein (ALIX), tumour susceptibility gene 101 protein (TSG101) and sorting vacuolar protein sorting 4 (Vps4)) are all thought to be involved in the sorting of proteins into exosomes [39] (Fig. 1.3b). The ESCRT is composed of four protein complexes: ESCRT-0, ESCRT-I, ESCRT-II, and ESCRT-III. The importance of the ESCRT has been confirmed by knockdown experiments, which resulted in a reduction of exosome release [62]. In addition the protein ubiquitin seems have a key role in the sorting process, through the provision of sorting signals [63].

The sorting processes is started by ESCRT-0, which recognises ubiquitinated proteins and then clusters them for delivery into MVBs [64]. ESCRT-0 binds to endosomal membranes through the interaction of Hrs (hepatocyte growth factor-regulated kinase substrate, a component of ESCRT-0) with phosphatidylinositol-3 phosphate (PI(3)P) in the endosomal membrane. Subsequently ESCRT-0 recruits ESCRT-I through interactions with TSG101 associated with ESCRT-I. Once ESCRT-I is activated it interacts with ESCR-II, and together this complex then promotes invagination of the membrane. ESCRT-II then associates with and activates the ESCRT-III complex. Here ALIX is enlisted to stabilise the ESCRT-III assembly. This complex then promotes vesicle budding, with ESCRT-III completing the scission of the membrane and resulting in the formation of ILVs [65]. Finally, the ESCRT-III complex separates from the MVB membrane through a process supported by

Vps4 and ATPase [65]. This mechanism of sorting protein cargo into exosomes is known as the ESCRT-dependent mechanism.

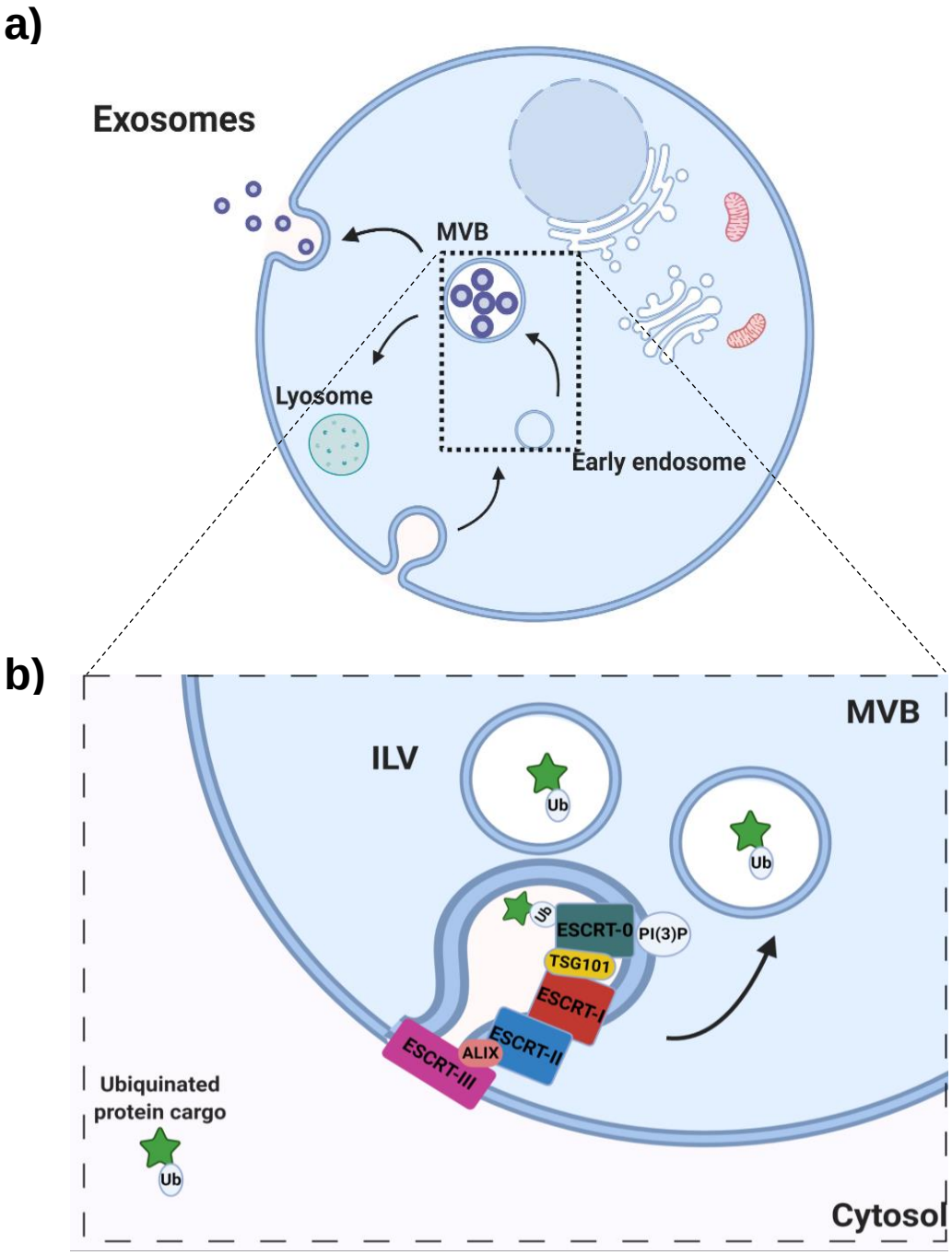


**Figure 1. 3:** Schematic of a) exosome biogenesis, and b) ESCRT dependent protein cargo sorting into ILVs in MVBs. These then fuse with the plasma membrane releasing exosomes into the extracellular space. Created using BioRender.com

Recently, it has been suggested that protein cargo may also be sorted into exosomes via ESCRT-independent mechanisms such as tetraspanin and lipid-dependent mechanisms. This was confirmed following a study by Stuffers

*et al*. [66], who showed that CD63-positive MVs were still produced by cells that were concomitantly depleted of all four subunits of the ESCRT complex. In addition, sorting of MHC II into exosomes derived from antigen presenting cells occurs without ubiquitination, suggesting that alternative mechanisms can be involved [67]. However, the details of these mechanisms are less well established.

Lipids such as ceramide and sphingosine-1-phosphate (S1P) have been shown to be enriched in exosomes [68,69] and may play key roles in the lipid-dependent sorting mechanism. Specific inhibition of the enzymes involved in the synthesis or modification of these lipids affects the cargo sorted into exosomes [68,69]. For example inhibition of neutral sphingomyelinase 2 (an enzyme that hydrolyses sphingomyelin to produce a ceramide) resulted in a decreased content of the tetraspanin CD63 in exosomes [68]. Inhibition of sphingosine kinase 1 (which phosphorylates sphingosine, resulting in the formation of S1P) led to a reduction in the sorting of CD63, CD81 and flotillin into exosomes [69]. The details of the mechanism that results in the altered cargo are yet to be elucidated.

It is thought that tetraspanins participate in cargo sorting by interacting with other transmembrane proteins, cytosolic proteins and lipids, and organising them into tetraspanin-enriched microdomains [70]. CD81 and CD9 have been specifically implicated here [71,72]. The enrichment of tetraspanins, ALIX and TSG101 in exosomes thus appears to be a direct consequence of their biogenesis.

Although all the above mechanisms for cargo sorting have been shown to exist, the signal that determines which is used remains to be elucidated. Furthermore, the mechanisms might work in a synergistic manner or separately, with different subpopulations of exosomes possibly relying on different mechanisms.

#### *1.4.2.2 RNA cargo*

The mechanisms by which RNAs are sorted into exosomes are generally not well understood [65]. Many studies have demonstrated that exosomes are

enriched in small RNAs such as miRNA, and that these perform a function once taken up by target cells [73–77]. Villarroya-Beltri *et al*.[78] were able to identify specific sequence motifs present in miRNAs loaded into exosomes (EXOmotifs), and found these to contribute to their sorting into exosomes (Fig. 1.4). The EXOmotifs bind to heterogeneous ribonucleoprotein A2B1 (hnRNPA2B1) which then facilitates their loading into exosomes. Directed mutagenesis of the EXOmotifs results in altered or reduced levels of miRNA cargo sorted into exosomes. In addition, hnRNPA2B1 found in exosomes is sumoylated (a post-translational modification involving the covalent binding of small ubiquitin-like modifier proteins), which is thought to be essential to its binding to miRNAs [78].

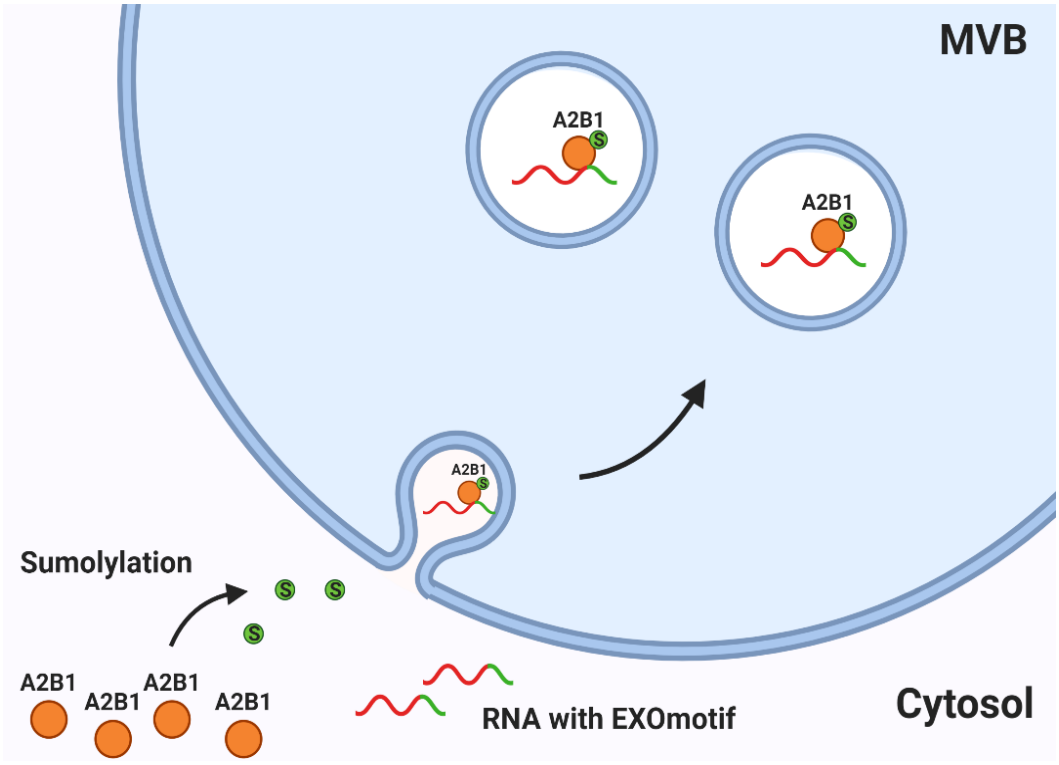


**Figure 1.4:** Schematic of the sorting process of RNA into exosomes. Created using BioRender.com (A2B1 is hnRNPA2B1)

### 1.4.3 Release

MVBs have two potential fates: they either undergo degradation by fusion with the lysosome, or fuse with the cell membrane and release the ILVs into the extracellular space as exosomes (exocytotic pathway) [58]. Transport of MVBs

to the plasma membrane occurs through their interactions with actin and the microtubule cytoskeleton [73,79,80]. Rab GTPases have also been implicated in release of exosomes, since knockdown of these components leads to reduced exosome secretion [81]. Rab GTPases are a family of small GTPases that regulate membrane trafficking, including vesicle formation, vesicle movement along actin and tubulin networks, and membrane fusion [81]. It is hypothesised that different stimuli lead to the fusion and release of exosomes from different cell lines [58]. For example, exosomes are released from platelets in response to thrombin receptor activation [82], from dendritic cells in response to activation by lipopolysaccharides [83], and from neuronal cells in response to plasma membrane depolarisation after an influx of $Ca^{2+}$ ions [84]. However, exosomes can also be released constitutively.

## 1.5 Nomenclature

As previously mentioned (**Section 1.3**) exosomes have a size range of 40-150 nm. However, throughout the literature extracellular vesicles with the same protein content and surface markers as exosomes have been reported with a range of sizes up to 250 nm, indicating that at present there is no precise size cut-off for the classification of vesicles as exosomes [85,86]. The currently available exosome isolation methods, as discussed later in this thesis, do not yet enable the isolation of pure particles within the exosomal size range. In addition, no specific markers for exosomes have been determined, which has led to some confusion in the literature. Therefore it is recommended to use the term “EVs” rather than exosomes when referring to isolated vesicles in the size range of 40-150 nm with markers enriched in exosomes (such as tetraspanins and TSG101), particular cargo and exosomal morphology [85]. Thus from this point onwards the term EVs will be used when referring to such isolated vesicles.

## 1.6 Therapeutic potential of EVs

Over the past decade research has demonstrated EVs to have therapeutic potential for a large range of diseases [52,87]. EVs from mesenchymal stem

cells (MSCs) have attracted particular attention in the regenerative medicine field [88–96]. The use of MSCs themselves has great potential for tissue regeneration, and they have been shown to have anti-inflammatory, immunomodulatory, angiogenic, antifibrotic, and anti-microbial properties, but there are some challenges that are yet to be solved [53,88]. These include the risk of iatrogenic tumour formation, cellular rejection, and infusion toxicity [92]. The therapeutic efficacy of MSCs is in large part mediated by the release of paracrine factors into the immediate extracellular environment; these then travel to nearby cells and take part in multiple processes such as angiogenesis, tissue regeneration and immune regulation [97,98]. This paracrine effect is a form of cell-to-cell communication mediated by EVs [99–103]. Compared to MSCs, EVs are smaller and have better access to target tissues, are easier to produce and store, and because there are no viable cells there is no risk of tumour formation and reduced immunogenicity [90]. MSC-derived EVs therefore represent a good option for cell-free therapy, and have the potential to replace the use of MSCs.

EVs are currently being evaluated in human clinical trials for a variety of conditions, mainly using materials derived from human MSCs (both with autologous and allogenic sources, Table 1.2) [104,105]. These are in the early stages of development (mainly phases I and II), with only a few that have reported results. For example, unmodified EVs derived from umbilical cord MSCs (allogenic) were given (1 dose intravenous followed by 1 dose via intra-renal artery injection a week later) to 20 chronic kidney disease patients in a phase I trial [87]. Administration of EVs was shown to be safe and effective in reducing the inflammatory immune reaction as well as improving the overall kidney function in comparison to placebo patient group [87]. Recently, EVs (ExoFlo™) from allogeneic bone marrow MSCs were evaluated in 24 patients with severe COVID-19 [106]. Here patients who were clinically deteriorating received a single intravenous (IV) dose of ExoFlo™ and the intervention evaluated for both safety and efficacy from days 1 to 14 post-treatment. ExoFlo™ was shown to be safe and effective in restoring oxygenation, downregulating cytokine storm, and reconstituting immunity. The therapeutic efficacy is to be further evaluated in a phase II trial (NCT04493242). EVs from

different sources such as human dendritic cells are also being evaluated in human clinical trials, with those from other cell sources still in pre-clinical studies [104].

**Table 1. 2**: Examples of EVs under investigation in clinical trials

| Indication & route of administration | Stage of development | EV source | Results |
|---|---|---|---|
| **Stage III & IV Chronic Kidney Disease, intra-arterial & IV injections** [87] | Phase II/III | Allogenic Umbilical cord MSCs | Safe and effective |
| **Acute Ischemic Stroke (NCT03384433), Intraparenchymal injection** | Phase I/II | Allogenic stromal MSCs (EVs enriched with miR-124) | Trial now recruiting |
| **Early Stage Novel Coronavirus Pneumonia (NCT04389385), Aerosol Inhalation** | Phase I | Allogenic COVID-19 T Cell | Active not yet recruiting |
| **Metastatic Pancreas Cancer (KrasG12D) (NCT03608631), IV injection** | Phase I | Stromal MSCs ( EVs loaded with KrasG12D siRNA) | Not yet recruiting |
| **Moderate-to-Severe Acute Respiratory Distress Syndrome in patients with Severe Covid-19 (NCT04493242), IV infusion** | Phase II | Bone marrow MSCs | Not yet recruiting |
| **Mild to Moderate Dementia due to Alzheimer's Disease (NCT04388982), Nasal drip** | Phase I/II | Allogenic Adipose MSCs | Recruiting |

EVs have inherent targeting capabilities and tropism for a particular cell or tissue, imparted by membrane proteins, ligands and surface receptors. Manipulation of these components can provide an added mechanism for the specific targeting of EVs to a certain tissue, cell type or microenvironment. This can potentially enable targeted delivery while avoiding off-target effects [48,107]. For example, Alvarez-Erviti and collegues generated EVs that can be targeted to neurons by transfecting dendritic cells ( derived from C57BL/6 mice) with a plasmid construct that contains lysosome-associated membrane glycoprotein 2b (Lamp2b) fused to a rabies virus glycoprotein (RVG) tag [108]. Following IV administration, these EVs were shown to preferentially localize in the brain, which was attributed to the recognition of the RVG tag by specific receptors on cells in the brain [108]. This approach exploits the fact that if a protein is overexpressed in an EV producer cell line, via for example plasmid transfection or viral transduction, that protein will subsequently be present in the EVs produced by the cells.

Another major advantage of EVs as delivery vectors is that they tend to be less immunogenic than their cells of origin due to the reduced presence or absence of MHC molecules on their surfaces [109]. They can hence be given repeatedly for the treatment of chronic diseases without eliciting an immune response and production of neutralising antibodies [109]. Zhu *et al*. [110] evaluated the immunogenicity of EVs derived from HEK293 cells following repeated IV administration for 3 weeks, and demonstrated negligible immunogenicity. EVs can potentially be used in place of similar synthetic drug delivery vehicles such as lipid nanoparticles, liposomes or polymeric micelles. Finally, EVs have good durability in culture, permitting large quantities of EVs to be harvested and collected from cell culture media and thus enabling ease of generation for use as delivery vesicles in therapeutics [111,112]. Therefore, EVs could potentially be highly effective delivery vectors for therapeutics or small molecules in treatments for various diseases.

### 1.6.1 EVs in the treatment of neurovisceral disorders

The use of EVs to treat neurovisceral diseases such as Gaucher disease is particularly promising because they have been shown to be able to deliver

cargo (e.g. enzymes, nucleic acid and lipids) to visceral organs such as the liver, spleen, lung, heart and kidney due to their intrinsic tissue-penetrating ability [113]. In addition, they have been shown to be able to cross the BBB and deliver cargo to the CNS, which is currently the major bottleneck to brain drug delivery [3]. EVs play key roles in CNS homeostasis, pathology and subsequent recovery [114], and are produced by various cells in the CNS (such as cortical and hippocampal neurons, glial cells, astrocytes and oligodendrocytes) [114].

Several reports demonstrated the potential of EVs in the treatment of neurological diseases such as Parkinson's disease, Alzheimer's disease, and multiple sclerosis [115–120]. For example, Reza-Zaldivar *et al*. [120] injected either MSCs or EVs derived from MSCs via the intracerebroventricular (ICV) route into an Alzheimer's mouse disease model and evaluated the effects of each treatment. It was demonstrated that MSC-derived EVs stimulated neurogenesis in the subventricular zone, which is typically affected in Alzheimer's disease, and alleviated cognitive impairment. In addition, these results were similar to those observed in the animals treated with MSCs. These findings were attributed to the secretory activity of MSCs, resulting in neurotrophic factors that can protect neurons from apoptosis, the production of anti-inflammatory cytokines, and miRNA that induces proliferation and differentiation of neural precursors and in turn could lead to the formation of new neurons or glial cells. Similar therapeutic effects were achieved through administration of MSC-derived EVs because EVs have been shown to be one of the most important components of the secretory activity of MSCs [121–123].

### 1.6.2 EVs as delivery vectors of lysosomal enzymes

We aim in this work to exploit the fact that the precise composition of biomolecules in EVs is dependent on the molecules being produced in the parent cells [44]. This will be used to develop a platform for the production of enzyme-rich EVs. The hypothesis is that cell lines known to produce a high level of EVs can be transduced with a clinically relevant lentiviral gene delivery vector to overexpress a reporter protein/enzyme or a therapeutic lysosomal enzyme. These cells should excrete the excess of this protein/enzyme inside EVs. GCase is intrinsic to all cells and thus, if the gene for GCase is

incorporated into the genome, when this gene is expressed it will naturally undergo the posttranslational modifications necessary its activity (glycosylation), before loading it into EVs [124].

The use of lentiviral gene delivery ensures that the gene of interest is integrated into the cell's genome and expressed in both the originally transduced cell and any resulting progeny [125]. This is advantageous over other approaches. Almost all published studies attempting to load EVs through genetic engineering a producer cell line have relied on transient transfection of the cells with a plasmid containing the gene of interest. Transient transfection with a plasmid means that the gene of interest is not integrated into the host genome, and hence the resulting progeny will not contain the gene of interest[125]. Hence, prior to production of each batch of EVs the cells have to be re-transfected, which is time consuming and can result in non-reproducible results and inhomogeneous samples. Using lentiviral vectors removes the need for such constant manipulation of cells prior to production of loaded-EVs.

Loaded-EVs, when incubated with cells, are taken up through the endocytic pathway in early endosomes; these then mature into late endosomes before fusing with the lysosome [109]. Do *et al*.[126] incubated loaded-EVs with a number of cell lines, and found that first the EVs become co-localised with early endosomal markers, followed by late endosomal markers and finally lysosomal markers. Furthermore, in addition to the demonstrated ability of EVs to incorporate and transport a large payload, the presence of the lipid bilayer ensures that this payload is protected from possible deleterious effects such as degradative enzymes or chemicals [44]. This suggests that our hypothesis that EVs loaded with lysosomal enzymes such as GCase can deliver active enzyme to the lysosome in cells is credible and possibly achievable.

## 1.7 Lentiviral vectors

Lentiviruses are members of the Retroviridae (retroviruses) family and are derived from the human immunodeficiency virus (HIV-1). They are frequently

used as gene delivery vectors as they have various advantages such as offering long term gene expression, since they integrate into the host genome [125,127], as well as :

I. being capable of infecting a wide variety of cells, including dividing and non-dividing cells [125];
II. not eliciting immunogenic reactions following transduction
III. carrying transgenes of up to 11kb [128];
IV. being relatively easy to manipulate and produce [127]

### 1.7.1 Lentiviral components

Currently used lentiviral vectors were developed through continuous improvements of early marker gene-carrying HIV vectors. Pathogenic components and their ability to self-replicate were removed to minimise the risk of generating replication competent lentiviruses (RCLs), without hampering their efficiency in entering cells and delivering the inserted therapeutic gene. To reduce the risk of generating RCLs a number of generations of lentiviral vectors were developed. Second generation vectors are most commonly used [125]. These are made from three separate plasmids. One of these is a packaging plasmid, which contains sequences coding for viral structural proteins and essential regulatory elements needed to make the viral shell. The second is a pseudotyping plasmid, encoding a viral glycoprotein such as the G protein of the vesicular stomatitis virus (VSV-G) envelope gene; this is required to provide the vector particles or virions with a receptor-binding protein. The third is a lentiviral expression plasmid containing the *psi* packaging sequence, with the transgene gene inserted between the lentiviral long terminal repeats (LTRs) [125].The *psi*-sequence acts as a signal to ensure the packaging of the transgene into virions [125]. This expression plasmid also typically contains a sequence for an internal promoter such as the cytomegalovirus (CMV) or mammalian ubiquitous spleen focus forming virus (SSFV), and these drive the transcription of the downstream transgene in transduced cells [125].

Splitting the genes required to make the virus into three plasmids, and the fact that both the packaging and envelope plasmids lack a packaging signal or LTRs, results in reduced risk of generating RCLs. This is because for RCLs to be produced, at least two recombination events would have to occur [127]. The use of VSV-G, rather than the HIV-1 envelope protein, provides further advantages such as higher viral particle stability that consequently allows for concentration to higher titres through ultracentrifugation [129]. Another major advantage of pseudotyping with VSV-G is that it confers the ability of lentiviral vectors to transduce a broad range of cells through the binding of VSV-G to ubiquitous cell membrane receptors [129]. These second generation lentiviral vectors will be used in this study to deliver genes of interest to target cells.

Given the efficacy of lentiviral vectors in transducing both proliferating and non-proliferating cells, resulting in stable expression of the transfer gene in both parent cells and progeny, they have become very popular tools for genetic engineering in both academic and industrial research [130]. In addition lentiviral vectors are currently being evaluated in *ex vivo* gene therapy for the treatment of various genetic diseases such β-thalassemia [131], X-linked adrenoleukodystrophy [132] and metachromatic leukodystrophy [133,134]. Here, lentiviral vectors are used to transduce haemopoietic stem cells such that they express the desired gene. After purification and characterisation, the transduced cells are then transplanted into the patient. This approach has shown some clinical benefits, but more importantly no adverse effects due to the lentivirus were reported.

## 1.8 Current limitations in using EVs for therapy

One problem impeding advancement in EV research is the lack of standardized methods for their isolation from different sources (such as serum or cell culture medium), purification and characterization. Current isolation methods have been reported to give variable yields and EV purity levels [45]. Standardization would not only allow meaningful comparison of results from different research studies, but is also crucial to allow us to obtain reproducible biological effects of EVs on target cells [45].

Furthermore, despite an upsurge in research into the therapeutic potential of EVs, there is still little work being carried out into possible formulation strategies. Most studies into EVs efficacy use the intravenous (IV) delivery route, which is often shows that EVs have a relatively short half-life following IV administration [135–137]. Additionally, IV therapy is complex, potentially dangerous, and is associated with high incidence of error as well as low patient compliance [138,139]. EVs are typically stored in phosphate buffered saline (PBS) at –80 °C, and during long term storage have been shown to be susceptible to aggregation and degradation following freezing and thawing cycles [140]. This hampers the potential use of EVs for translation [141]. Thus, to harness their full therapeutic potential, there is clearly a need for the development of stable EV formulations that can be delivered via an appropriate route of administration for the disease in question.

## 1.9 Aims and objectives

This project aims to develop a platform for the production of EVs loaded with enzymes from paediatric storage disorders, specifically Gaucher Disease type 2. The specific objectives to be met are:

- Use lentiviral vectors to deliver genes for marker enzymes and proteins to EV producer cells, and use these cells to produce loaded-EVs. Investigate and evaluate the characteristics of these EVs to ensure reproducible production.
- Assess the ability of the loaded-EVs to deliver cargo *in vitro* and *in vivo*, as well as evaluating *in vivo* biodistribution in adult and neonate mice.
- Produce EVs loaded with GCase enzyme and evaluate *in vitro* upregulation of this enzyme in cells.
- Determine the stability of naïve and loaded-EVs under different storage conditions. Ascertain whether freeze drying can enable stable storage of EVs at higher temperatures.

# Chapter 2: Materials and methods

# 2.1 Materials

## 2.1.1 Antibodies

The antibodies used in this study are detailed in Table 2.1.

**Table 2.1:** The antibodies used in this study

| Antibody | Host* | Dilutions | Dilutions used in simple western |
|---|---|---|---|
| ***Primary antibodies*** | | | |
| *Anti CD9 (ab223052, Abcam)* | Rabbit | 1:100 | 1:10 |
| *Anti TSG101 (ab30871, Abcam)* | Rabbit | 1:1000 | 1:50 |
| *Anti Calnexin (ab10286, Abcam)* | Rabbit | 1:1000 | 1:100 |
| *Anti-GBA (G4171)* | Rabbit | 1:2000 | 1:100 |
| *Anti-GFP (ab209)* | Rabbit | 1:10 000 | 1:100 |
| *Anti LAMP1 (ab24170, Abcam)* | Rabbit | 1:2000 | N/A |
| ***Secondary antibodies*** | | | |
| *Goat anti mouse HRP (ab6789, Abcam)* | Goat | 1:2000 | N/A |
| *Goat anti rabbit HRP (ab6721, Abcam)* | Goat | 1:3000 | N/A |
| ***Fluorescent secondary antibody*** | | | |
| *Alexa fluor 546 (ThermoFisher A-11010)* | Goat | 1:200 | N/A |

* Host information as obtained from the manufacturer.

### 2.1.2 Primer sequences

The names and sequences (5'-3') of the primers used in the study (all obtained from Sigma-Aldrich) are shown in Table 2.2.

**Table 2. 2:** Primer sequences

| **eGFP primers** | **Sequence** |
|---|---|
| Set 1 | F 5'-AAGCTGACCCTGAAGTTCATCTGC-3' |
| | R 5'-CTTGTAGTTGCCGTCGTCCTTGAA-3' |
| Set 2 | F 5'-TCTTCAAGTCCGCCATGCC-3' |
| | R 5'-TGTCGCCCTCGAACTTCAC-3', |
| ***GBA1* primers** | |
| F1 | TTCAAGTCCTTCCAGAGAGGAATG |
| F2 | AGCTGTGACTTCTCCATCCG |
| F3 | GGAGACAATCTCACCTGGCTACTC |

## 2.2 Cloning

### 2.2.1 Bacterial transformation

Plasmid DNA was amplified into chemically competent *E. coli* bacterial cells (One Shot® Stbl3™, ThermoFisher Scientific) following the manufacturer's protocol. The transformation mix was spread on to lysogeny broth (LB) agar (ThermoFisher) plates containing either ampicillin (100 µg/ml, Sigma-Aldrich) or kanamycin (50 µg/ml, Sigma-Aldrich) and incubated overnight at 37 °C to select for positive colonies. Positive colonies were used to inoculate 5 ml of lysogenic broth (Sigma-Aldrich) as starter cultures, with either ampicillin (100 µg/ml) or kanamycin (50 µg/ml). Cultures were incubated at 37 °C overnight under constant shaking at 225 rpm.

### 2.2.2 Amplification and purification of plasmid DNA

Plasmid DNA was purified using the QIAprep Spin Miniprep kit (QIAGEN) according to the manufacturer's instructions. The plasmid DNA was eluted into 50 µl of distilled water, and the concentration was determined by

spectrophotometry (NanoDrop 1000, Thermo Scientific). Absorbance of the sample was measured at 260 nm, and the ratio of absorbance at 260 nm and 280 nm (~1.8) was used to assess the purity of the DNA sample.

For large-scale plasmid DNA preparations, 500 µl of bacterial culture was incubated with 500 ml of lysogenic broth with either ampicillin (100 µg/ml) or kanamycin (50 µg/ml) at 37 °C overnight under constant shaking at 225 rpm. Plasmid DNA was purified using the Plasmid Maxi kit (QIAGEN) according to the manufacturer's instructions. The plasmid DNA was resuspended in 500 µl of distilled water ($dH_2O$) and the concentration was assessed (NanoDrop 1000, Thermo Scientific).

Sources and details of all the plasmids used in this study are listed in Table 2.3.

**Table 2.3:** Plasmids used in this study

| Plasmid Name | Relevant Characteristics | Source |
|---|---|---|
| *pSFFV.LUC.2A.eGFP* | Lentiviral construct with SSFV promoter driving Luciferase and *eGFP* reporter | Dr. Michael Hughes, Department of Pharmacology, UCL, UK |
| *p.CMV.eGFP.WPRE* | Lentiviral construct with CMV promoter driving *eGFP* reporter and WPRE element | This study |
| *pSSFV.IRES.eGFP* | Lentiviral construct with CMV promoter driving *eGFP* reporter | Dr. Michael Hughes, Department of Pharmacology, UCL, UK |
| *pGBA1Ub* | Plasmid sequence of GCase enzyme tagged with human Ubiquitin sequence | Invitrogen by Thermo Fisher Scientific |
| *pSFFV.GBA1Ubi.WPRE* | Lentiviral construct with SFFV promoter driving *GB1Ubi* | This Study |
| *pSFFV.GBA1.IRES.eGFP* | Lentiviral construct with SFFV promoter driving *GBA1 and eGFP*. | Dr. Michael Hughes., Department of Pharmacology, UCL, UK |
| *pGBA1.2A.eGFP* | Lentiviral construct with SFFV promoter driving *GBA1 and eGFP*. | Invitrogen by Thermo Fisher Scientific |
| *pMDG2* | Vesicular stomatitis virus envelope expression plasmid | Plasmid Factory |
| *pCMVdR.8.74* | Encapsulation plasmid lacking Vif-,Vpr-,Vpu, and Nef-accessory HIV-1 proteins | Plasmid Factory |

### 2.2.3 Restriction enzyme digest

To select the appropriate restriction digest sites, DNA sequences were analyzed with the SnapGene Viewer 5.0.4 software. 2 µg of DNA was digested with the selected restriction enzymes (New England Biolab) for a minimum of 1 hour at 37 °C unless stated otherwise, according to the manufacturer's instructions. The resulting DNA fragments were separated by size on an agarose gel via electrophoresis.

An example of a typical restriction enzyme digest reaction mix is:

| | |
|---|---|
| DNA | 2 µg |
| 10X Restriction Buffer | 2.5 µl |
| Enzyme (eg. BamHI,MluI) | 0.75 µl |
| Enzyme (eg. XhoI) | 0.75 µl |
| Make up with $dH_2O$ to final volume of | 25 µl |

### 2.2.4 Gel electrophoresis

50X Tris acetate-EDTA (TAE) buffer was prepared by combining 242 g Trizma (Sigma-Aldrich), 57.1 ml glacial acetic acid (Fisher Scientific), 100 ml of 0.5 M ethylenediaminetetraacetic acid (EDTA, Sigma-Aldrich), and adding $dH_2O$ to final volume of 1 l.

DNA fragments were separated on a 1-2 % agarose gel (Invitrogen) depending on fragment size. Gels were prepared using 1X TAE buffer and Safeview (Applied Biological Materials) at a dilution of 1:10,000 to aid with DNA visualisation. 27 µl of each sample was loaded onto wells using 1X Orange G-gel-loading buffer (Sigma-Aldrich). To determine the size of DNA fragments 1 Kb plus molecular weight marker (Invitrogen) was also loaded onto the gels, which were run at 110 V (PowerPac Basic, Biorad) for a minimum of 30 minutes, depending on the expected band size. The results were visualized using a UV transilluminator and images were captured with the attached CCD digital camera (InGenius, Syngene).

### 2.2.5 DNA extraction from agarose gel

The desired DNA fragments of the correct band sizes were excised from the agarose gel under limited exposure of UV light. These fragments were then extracted and purified using the QIAquick Gel Extraction kit (QIAGEN) following the manufacturer's instructions. The purified plasmid DNA was eluted in 30 µl of $dH_2O$.

### 2.2.6 Ligation

A rapid DNA ligation kit (ThermoFisher Scientific) was used to clone DNA fragments into a lentiviral plasmid, according to the manufacturer's instructions. Different molar ratios (1:1 or 1:3) of vector: insert DNA were tested to establish the optimal ratio for single insertion into the lentiviral backbone.

An example of a ligation reaction mix is detailed below:

| | |
|---|---|
| Linearised vector DNA | 100 ng |
| Insert | 1:1 or 1:3 (ratio of vector:insert) |
| 5X rapid ligation buffer | 4 µl |
| T4 DNA ligase, 5 u/µl | 1 µl (5 units) |
| $dH_2O$ to final volume of | 20 µl |

The reaction was incubated at room temperature for 5 -10 minutes.

### 2.2.7 Sequencing

Automated Sanger sequencing of the plasmids was outsourced to SourceBioscience (www.lifesciences.sourcebioscience.com, UK). The primers in Table 2.2 were used for sequencing during *GBA1* cloning. The resulting sequences were aligned to the original consensus and analyzed with the SnapGene V 5.0.4 software.

## 2.3 Lentivirus production

A second generation lentiviral vector packaging system was used to produce the vectors in this study. Standard lentiviral production typically relies on the

transient transfection of human embryonic kidney cells (HEK293T) with a packaging plasmid, an envelope glycoprotein-encoding plasmid, and a lentiviral transfer vector plasmid. Following transfection, lentiviral particles are produced and released into the culture supernatant of the HEK293T cells. The particles are then harvested and purified by ultracentrifugation (Fig. 2.1).

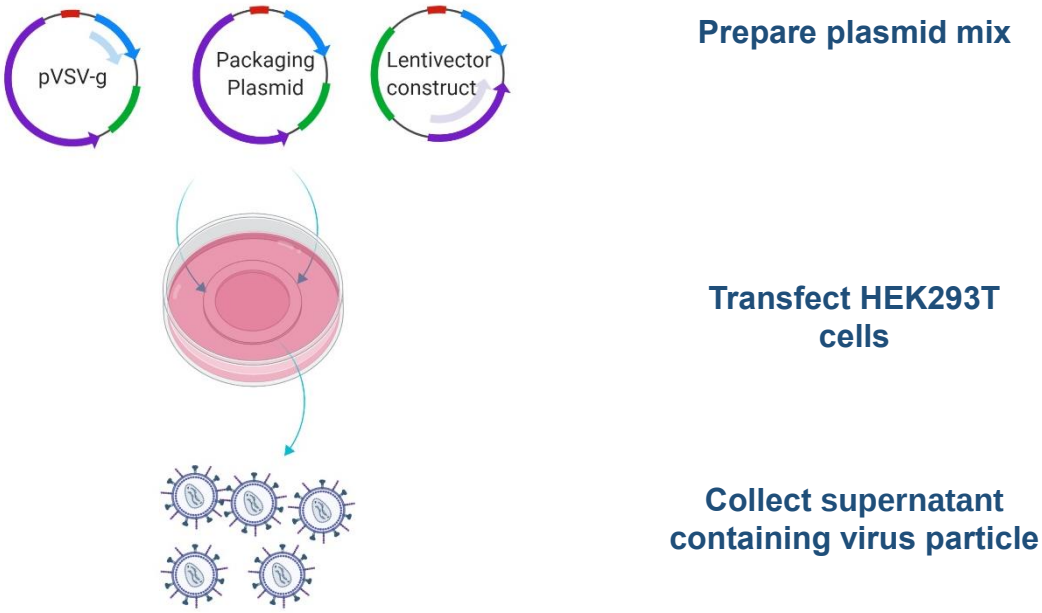


**Figure 2.1:** A simplified schematic showing the production of lentiviral vectors. Created using Biorender.com

## 2.3.1 Cell culture

HEK293T cells were used for virus production in this study. These cells were cultured in Dulbecco's Modified Eagle Medium (DMEM) GlutaMax™ (ThermoFisher Scientific). Where specified, 10 % v/v heat-inactivated foetal bovine serum (FBS; Sigma-Aldrich, inactivated at 56 °C for 30 minutes) and/or 1 % v/v of a pen/strep antibiotic solution (compromising penicillin at 5,000 units/ml, and streptomycin at 5,000 µg/ml, Gibco) were added to make complete media. Cells were maintained in a 5 % $CO_2$ atmosphere at 37 °C and passaged every 48-72 hours at 80-90 % confluency. Briefly, media was removed, cells rinsed with phosphate buffered saline (PBS, Gibco), followed by trypsinisation (trypsin-EDTA 0.05 %, Gibco) to detach cells. The culture

containing detached cells was spun at 200 g for 5 minutes and the resulting pellet was resuspended in fresh growth media.

The culture was regularly split at a 1:5 ratio into a new flask or dish. To avoid genetic drift, cells beyond passage 20 were discarded and freshly thawed passage three cells were allowed to recover until passage five, before being utilised.

### 2.3.2 Transfection of cells and virus harvest

Fifteen 100 mm dishes (Nunc) were seeded with 1 x $10^7$ HEK293T cells in complete DMEM GlutaMax™ before being left overnight to reach 70-80 % confluence. The cells were then triple transfected with 40 µg of the transfer vector plasmid, 10µg of the envelope plasmid PMD.G2, and 30 µg of the packaging construct plasmid p8.74 per dish. Firstly, 8 µl of a 10 mM stock of polyethylenimine (PEI; Sigma) was added to 40 ml of Opti-MEM® and filtered through a 0.22 µm membrane filter (BD Biosciences). The PEI was added to the plasmid mix and left at room temperature for 20 minutes to make the transfection master mix. The cells were then washed with PBS (concentration 1x, pH 7-7.3, without magnesium and calcium salts) followed by addition of 2.5 ml of transfection mix per dish. The cells were incubated at 37 °C under a 5 % $CO_2$ atmosphere for 24 hours, following which the transfection medium was removed and replaced with DMEM GlutaMax™ (Gibco). The supernatant was collected 48 hours post transfection, replenished with fresh DMEM GlutaMax™ (Gibco), and supernatant collected again 24 hours later. The supernatant was then centrifuged at 3000 g for 10 minutes at room temperature and filtered through a 0.22 µm filter to remove all cell debris. The virus was pelleted by centrifugation (16-18 hours) overnight at 3000 g and 4 °C. The resulting pellet was re-suspended in Opti-MEM® and stored at -80 °C

### 2.3.3 Titration

The lentiviral titre was obtained by the quantification of the viral envelope protein p24. The ZeptoMetrix p24 antigen enzyme linked immunosorbent assay (ThermoFisher Scientific) was used as per the manufacturer's protocol. Here the quantity of sample viral envelope protein p24 is determined by

comparison to a standard curve, created by standards of known p24 concentration.

## 2.4 Production of EVs

### 2.4.1 Maintenance of cell lines

The following cell lines were chosen for study, as they are known to produce high levels of EVs: HEK293T, human bone marrow derived stem cells (BMSCs), THP-1 cells and SH-SY5Y cells. The base medium for HEK293T was DMEM GlutaMax™ (ThermoFisher Scientific), for BMSCs MEM Alpha Medium (1x) (Gibco), and for SH-SY5Y cells a 1:1 v/v mixture of Minimum Essential Medium Eagle (MEM) and Ham's Nutrient Mixture F12 (Sigma-Aldrich). To complete the growth medium 10 % v/v heat-inactivated FBS and 1 % v/v of a pen/strep antibiotic solution (compromising penicillin at 5,000 unit/ml and streptomycin at 5,000 µg/ml, Gibco) were added to the respective medium. Additionally, 10 % Non-Essential Amino Acid solution (100X, Sigma-Aldrich) was added to complete the basal media for SH-SY5Y cells.

Cell lines were maintained in a 5 % $CO_2$ atmosphere at 37 °C in the appropriate culture medium. Passage of HEK293T and SH-SY5Y cell lines and BMSCs cells was attained by rinsing them with phosphate buffered saline (PBS, Gibco), followed by trypsinisation (trypsin-EDTA 0.05 %, Gibco) when they reached 70 % confluency. They were then split with a standard ratio of 1:10 every 48 hours for HEK293T cells, 7 days for BMSCs and 5 days for SH-SY5Y cells.

Non-adherent THP-1 cells were maintained at 1 x $10^6$ cells/ml in growth medium comprising RPMI 1640 (Gibco) supplemented with 10% v/v FBS and 1% v/v penicillin-streptomycin at 37°C in 5 % $CO_2$ atmospheric conditions. The cells were split every 3 to 4 days after washing twice with serum-free RPMI 1640. The cells were transferred into 50 mL centrifuge tubes and spun at 160 *g* for 5 minutes. The resulting supernatant was discarded, and cells were gently re-suspended in the remaining medium. 5 mL of RPMI was added and cells were centrifuged as before. The supernatant was again discarded and cell pellets were re-suspended in the appropriate volume of complete growth

medium to give a concentration of 1 x $10^6$ cells/ml. Cells were then seeded at the desired dilution into new culture flasks

When cell lines were being established, cryopreserved cells were quickly thawed at 37 °C. The thawed cells were diluted 10-fold with pre-warmed complete growth medium and centrifuged at 200 *g* for 5 minutes at 21°C. The cell pellet was re-suspended in complete medium and incubated at 37 °C and 5 % $CO_2$.

### 2.4.2 Vesicle depletion of FBS

FBS contains a significant quantity of EVs. Thus, to avoid contamination, culture media used in subsequent EV isolation must be depleted of these EVs. There are two options for depleting medium of FBS-derived EVs. One option is to grow the cells in the presence of all relevant nutrients and antibiotics but without FBS. If the cells need some proteins to survive then 1 % w/v bovine serum albumin (BSA) can be added instead of FBS. The second approach can be used for cells that do not survive in serum-free media: here the EVs are pre-depleted from either raw FBS or FBS-containing medium.

Two protocols have been reported in the literature to deplete FBS of EVs. Both were investigated to establish the optimal route for the cells used in this study. In the first protocol, raw FBS was spun at 100 000 g using a T-647.5 rotor on a Sorvall WX+ Ultra centrifuge (ThermoFisher Scientific). Centrifugation was performed for 18 hours at 4 °C to pellet FBS EVs. The light-coloured top layer of the resulting supernatant was then filter sterilised using a 0.22 µm syringe filter (Millipore). This was then used to make 10% v/v FBS-media. In the second protocol, 20 % v/v FBS media was prepared and then spun as detailed above. The light-coloured top layer of the supernatant was again filter sterilised and then diluted with media supplemented with all the nutrients and antibiotics but without FBS, to reach a final concentration of 10% v/v EV-depleted FBS. EV-depleted media was stored at 4°C and used within 2 weeks.

The efficiency of each protocol in depleting in EVs was analysed by measuring the particle concentration using nanoparticle tracking analysis, as will be

described in **Section 2.5.1**.The particle concentration was then compared to that of raw FBS and commercial EV-depleted FBS (System Biosciences).

### 2.4.3 Cell viability assay

To assess the cell viability in a) media with all the relevant supplements except FBS and b) in media with vesicle depleted FBS (prepared using the protocols in **Section 2.4.2** above), the CellTiter-Glo® luminescent cell viability assay (Promega) was used according to the manufacturer's instructions. As a control, the cell viability of cells grown in complete growth media with 10 % v/v unprocessed FBS was also determined. This assay relies on the generation of a luminescent signal proportional to the amount of ATP. Since the amount of ATP is proportional to the number of metabolically active cells present in culture the luminescent signal can be used as an indicator of cell viability. However, a limitation of this assay is that it does not distinguish between quiescent/senescent and actively dividing cells and thus it cannot be used as an indicator of cell proliferation.

Briefly, 10 000 cells were seeded into opaque-walled 96 well plates (NUNC) and incubated with the appropriate media (100 µl) at 37°C and 5% $CO_2$ for 48 hours. 100 µl of CellTiter-Glo® reagent was then added to each well and mixed for 2 minutes at room temperate on a plate shaker, to induce cell lysis. The plate was incubated at room temperature for 10 minutes to allow the stabilisation of the luminescent signal. Luminescence was then recorded using a SpectraMax M2 plate reader (Molecular Devices). A direct relationship exists between the luminescence measured using CellTiter-Glo® assay and the number of cells in culture.

### 2.4.4 Production of naïve EVs

To produce naïve EVs from the different cell lines, cells were cultured as detailed in Table 2.4. EV-depleted media was used throughout. Conditioned media from each of the cell lines (transduced and non-transduced) was collected and either processed to isolate EVs or aliquoted into 50 ml Falcon tubes and stored at -80°C.

**Table 2.4:** Numbers for cell culture of the different cell lines.

| Cells | HEK293T | THP1 | MSC | SH-SY5Y |
|---|---|---|---|---|
| **Number of cells seeded** | 5.5 x$10^6$ | 6 x$10^6$ | 1 x$10^6$ | 5.2x$10^6$ |
| **Cells at confluency** | 40x$10^6$ | 30x$10^6$ | 4x$10^6$ | 25x$10^6$ |
| **Flask** | T225 | T175 | T175 | T225 |
| **Growth media (ml)** | 65 | 37 | 37 | 65 |
| **Time to reach confluency (days)** | 3-4 | 3-4 | 7 | 4-5 |

## 2.4.5 Production of loaded-EVs

EVs loaded with luciferase and eGFP were produced from cells that were transduced with VSV.G.SFFV.LUC.2A.eGFP.WPRE lentiviral vector and sorted using fluorescence activated cell sorting (FACS) to ensure only cells with the highest gene expression are used for EV production. To generate EVs loaded with GCase enzyme the relevant cells were transduced with SFFV.GBA1Ub.WPRE lentiviral vector. These cells were cultured according to the details in Table 2.4.

When required, large scale production of loaded-EVs was achieved using a 10 layer EasyFill Cell Factory system (NUNC, ThermoFisher Scientific) instead of T225 tissue culture flasks. Briefly, 25x$10^7$ cells were used to seed the cell factory and 1.5 L of EV-depleted media was used, ensuring equal distribution in each layer of the cell factory. Cells were incubated at 37 °C and 5 % $CO_2$ for 4 days. The conditioned media was collected, aliquoted and stored at -80 °C for later EV isolation.

### *2.4.5.1 Transduction*

On day 1, 150 000 cells in 3 ml of the respective medium were added to each well in a 6-well plate. This number was chosen to accommodate a confluence of 70 % upon transduction. The cells were incubated at 37 ºC and 5 % $CO_2$ for 24 hours, to allow adhesion of cells to the plates.

On day 2, the cells were counted and the medium was replaced with fresh medium. The appropriate volume of lentiviral particles was added to three wells only, keeping the remaining three as controls. A range of multiplicities of infection (MOIs) was tested (MOI of 1, 10 and 100 for HEK293T and THP-1 cells, 25, 40 and 50 for SH-SY5Y cells) to determine the optimal number of lentiviral particles needed for efficient transduction. The MOI refers to the ratio of viral particles per cell. The MOI was calculated using Equation 2.1:

**(Equation 2.1)**

$$\frac{\text{Total number of cells x desired MOI}}{\text{Lentiviral titre (vp/ml)}} = \text{Total volume of lentiviral preparation to add to each well}$$

Following addition of the viral particles, the plates were gently swirled and incubated at 37 °C and 5 % $CO_2$. 72 hours post transduction, lentiviral mediated enhanced green fluorescent protein (eGFP) expression was assessed using a fluorescence microscope (ECOS FL, Life Technologies) equipped with a filter set for detection of enhanced eGFP (excitation maximum, 488 nm; emission maximum, 507 nm). Successfully transduced cells were propagated into larger flasks for subsequent analysis and EV production. Non-transduced cells were also propagated in parallel to serve as controls.

#### *2.4.5.2 Assessing successful transduction by flow cytometry*

For cells transduced with a lentiviral vector containing eGFP, successful transduction was evaluated using flow cytometry (MACS Quant flow cytometer). Successfully transduced cells will contain the eGFP gene and its expression will result in production of eGFP in these cells, which will fluoresce green. Flow cytometric analyses was also used to quantify the transduction efficiency of the different cell lines at the various MOIs. Briefly, adherent transduced cells were washed with PBS and trypsinised (as detailed in **Section 2.3.1**), then centrifuged to obtain a cell pellet. The latter was then re-suspended in 5 ml of the appropriate complete culture medium (but with only 2 % v/v FBS) that had been pre-filtered through a 0.22 µm membrane filter

(BD Biosciences). Just prior to analysis, all samples were filtered through a 70 µm cell sieve (Corning) into flow cytometry tubes, to ensure that only individual cells are present. Fluorescent cells were separated from non-fluorescent cells by setting a minimum fluorescence value (thresholding) on the histograms generated by the cytometer. By setting the threshold just to the right of the dimmest peak, cells to the left of the threshold were excluded from those counted as fluorescent within a given channel.

*Cell sorting*

Once transduction efficiency of the different cell lines and the appropriate MOI was established, cells were then sorted to select single cell colonies with the highest expression of eGFP and use these to establish cell lines for the production of loaded-EVs. To do this, transduced cells at the appropriate MOI were first analysed using flow cytometry (as detailed in **Section 2.4.5.2**) and a threshold was chosen to sort the cells that have the highest expression of eGFP into each well of a 96 well plate (NUNC) containing complete media with 20 % v/v FBS. HEK293T cells were sorted using the MACS Quant flow cytometer and SH-SY5Y cells using a BD FACSAria III.

Sorted cells were maintained at 37 °C and 5 % $CO_2$. Media was changed every 5 days initially and more frequently as cell numbers increased. When cells reached 80 % confluency they were passaged into a 24 well plate (NUNC), then a 6 well plate (NUNC), a T25 flask (Corning) and eventually a T75 flask (ThemoFisher Scientific), at which point the cells numbers were high enough to be used for production of EVs.

### *2.4.5.3 Assessing successful transduction through analysis of GCase enzymatic activity*

To establish successful transduction with SFFV.GBA1Ub.WPRE lentiviral vector, GCase enzyme activity of transduced cells was evaluated and compared to that of non-transduced cells. GCase enzyme activity was determined fluorometrically using 4-methylumbelliferyl-β-D-glucopyranoside (4-MUβGlu) as a substrate. First the following assay stock reagents were prepared.

0.2 M citrate buffer was prepared by mixing 46.5 ml of 0.15 M citric acid (Sigma-Aldrich) with 53.5 ml of 0.3 M $Na_3PO_4$ (Sigma-Aldrich). To make the Gaucher extraction buffer (GEB), first 10 % Triton X-100 (Sigma-Aldrich) was made by adding 5 ml of Triton X-100 to 45 ml of 0.2 M citrate buffer. Then 5 ml of 10 % Triton X-100 was added to a bottle containing 1 g of sodium taurodeoxycholate (Sigma-Aldrich) and the solution transferred to a measuring cylinder. 3 x 5 ml of 10 % Triton X-100 were added to the bottle and transferred to the cylinder each time, to ensure that all sodium taurodeoxycholate in the bottle has been dissolved and collected. The solution in the cylinder was made up to 100 ml with 0.2 M citrate buffer. The pH of the resultant GEB buffer was adjusted to 5.2, and the solution then aliquoted and stored at 4 °C.

Gaucher substrate buffer (4-MUβGlu**)** was prepared by adding 2.3 ml of dimethyl sulfoxide (DMSO) (Sigma-Aldrich) to 778 mg of 4-MU (Sigma-Aldrich). The solution was mixed and aliquots were stored at -20 °C. Gaucher standard solution 4-methylumbelliferone (4-MU) was prepared by dissolving 1.76 mg of 4-MU (Sigma-Aldrich) in 10 ml of methanol. 100 µl of this solution was then diluted in 19.9 ml of $dH_2O$, aliquoted and frozen at -20 °C. All stock solutions were stored protected from light, and placed in bags with desiccant sachets. On the day of the assay Gaucher working solution (GWS) was prepared fresh by diluting 14 µl of 4-MUβGlu in 2.9 ml of GEB.

GCase enzymes were extracted from transduced and non-transduced cells by first lysing them ice-cold GEB. Briefly, 250 µl of GEB was added to each well and the plate kept on ice for 5 minutes, swirling the plate every minute. The cells were then scraped and the lysate transferred to 1.5 ml microcentrifuge tubes. The resulting lysates were incubated on ice for 20 minutes, after which debris was pelleted by centrifugation at 14000 g and 4 °C for 20 minutes. The lysate was carefully extracted and total protein concentration was quantified using Pierce BCA Protein Assay Kit (ThermoFisher Scientific) according to the manufacturer's instructions**.**

To quantify the GCase enzyme activity, for each sample 4 wells of a 96 well plate (NUNC) were used. In the first and second well, 3 µl of sample and 30 µl of GWS were added. The plate was incubated at 37 °C for 2 hours, then 200

µl of Gaucher Stop Solution (GSS, 0.5 M EDTA pH 11.3-12) was added to these wells to stop the reaction. For each sample a standard and a standard blank were set up as follows: 40 µl of Gaucher standard solution (4-MU), 190 µl of GSS and 3 µl of sample were added to well 3 and 40 µl of $dH_2O$, 190 µl of GSS and 3 µl of sample to well 4. The fluorescence signal at a wavelength of 365 nm excitation and 450 nm emission was then recorded using a SpectraMax M2 (Molecular Devices) plate reader.

The enzymatic activity (nmol/hr/µg) was calculated using Equation 2.2.

**(Equation 2.2)**

$$\frac{\text{Fluorescence of sample}}{\text{Fluorescence of 1 nmol 4-MU}^{*}} \times \frac{60\ \text{mins}}{120\ \text{mins}} \times \frac{1000(\mu l)}{3(\mu l)} \times \frac{1(\mu g)}{\text{sample concentration } (\frac{\mu g}{\mu l})}$$

*(* Fluorescence of 1 nmol 4-MU = Fluorescence of standard- Fluorescence of standard blank)*

## 2.4.6 Isolation of EVs

In the initial stages of this study the following isolation protocol was employed to isolate EVs, before being developed further to improve the efficiency of isolating vesicles in the size range of EVs. Firstly, conditioned medium collected from the cell lines was centrifuged at 300 g for 10 minutes to remove cell debris, and then at 2000 g for 10 minutes, followed by filtration through a 0.22 µm membrane (BD Biosciences) to remove MVs. Next, EVs were pelleted by ultra-centrifugation at 100 000 g for 90 minutes at 4 °C, using rotor T-647.5 on a Sorvall WX+ Ultra centrifuge (ThermoFisher Scientific). The pellets were washed once in PBS (pH = 7.4, Life Technologies). For maximal EV retrieval, the EV enriched pellet was re-suspended repeatedly (21 times) in a small volume (100 µl) of an appropriate buffer, until the pellet was fully re-suspended. The buffer employed depends on the downstream experiments planned following the EV isolation. For example, lysis buffer is used for protein and RNA isolation, PBS for electron microscopy, nanoparticle tracking analysis and flow cytometry, and for functional studies culture medium may be preferred.

The most commonly used method to isolate EVs is the differential centrifugation method. However, as there is no standardised method each research group has optimised their own version to ensure the majority of particles obtained are within the size range of 30-150 nm, with a minimum amount of larger contaminating particles. Differences in culture procedures lead to production of EV suspensions with different viscosities, size ranges and other contaminants; therefore, it is essential to develop a method for each culture procedure. Different isolation methods were investigated by varying either the speed or time at different steps of the initial centrifugation method (Fig. 2.2).

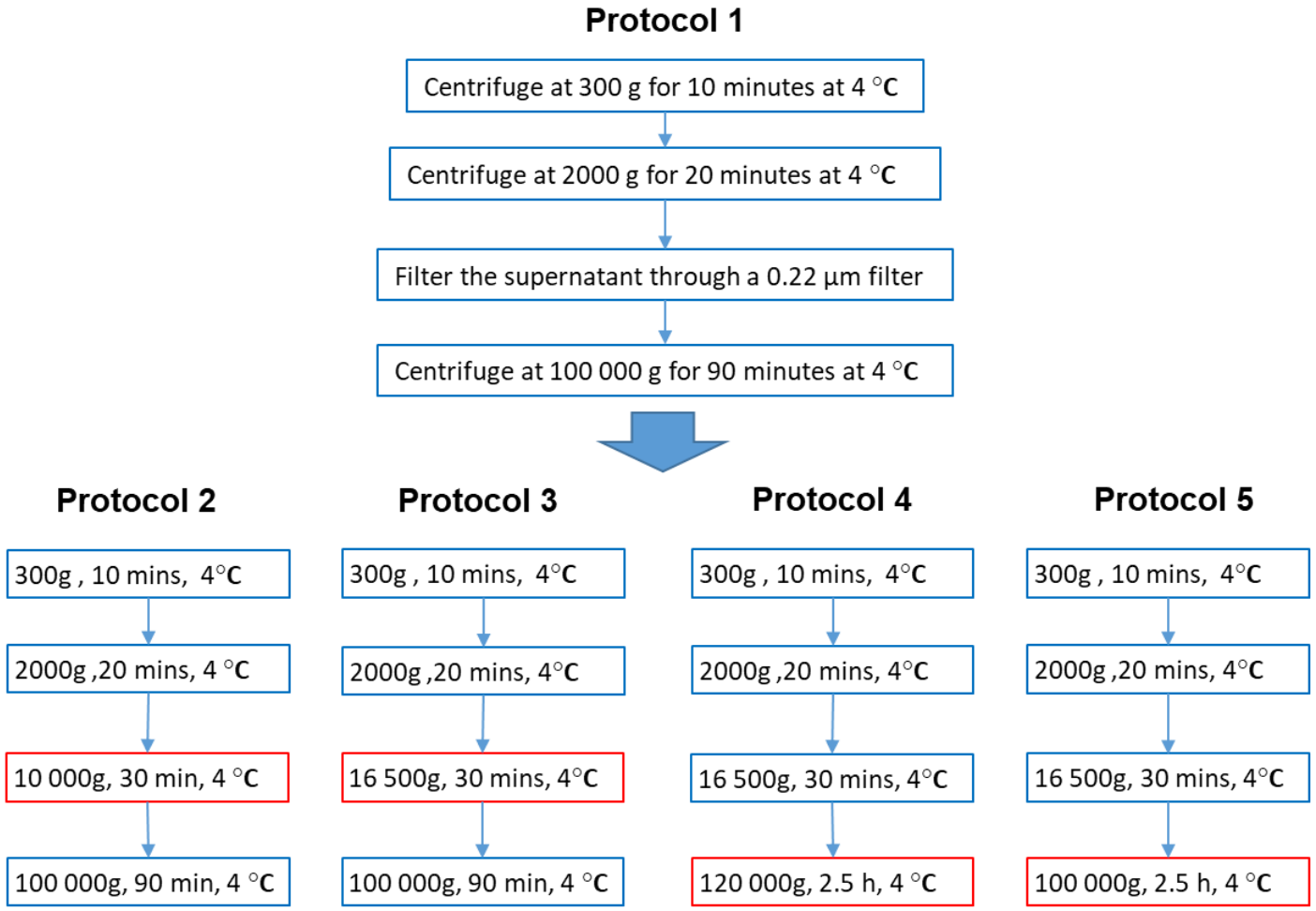


**Figure 2.2:** A schematic describing the isolation protocols explored. Stepwise alternations of the initial protocol (1) were executed to reach the final protocol (5).

### 2.4.7 Concentration and purification of EVs

To purify EVs further, a second ultracentrifugation step was assessed for its ability to produce a pure suspension of EV subpopulation. Six EV pellets isolated using protocol 5 in **Section 2.4.6** were pooled and diluted with PBS to 13.8 ml in a 14 x 95 mm Ultra-ClearTM Beckman Coulter tube. The tube was then placed in a SW40-Ti swing-out bucket, balanced to within 0.001 g and centrifuged at 100 000 g (Beckman Coulter Optima L-90K ultracentrifuge; acceleration fast, deceleration slow) at 4 °C for 2.5 hours. For maximal EV retrieval, the EV enriched pellet was re-suspended repeatedly (21 times) in 300 µl of an appropriate buffer, until the pellet was fully re-suspended.

## 2.5 Characterisation of EVs

### 2.5.1 Nanoparticle tracking analysis

EVs were analysed using nanoparticle tracking analysis with a NanoSight LM10 instrument (Malvern Panalytical) equipped with a sCOMs camera and a 532 nm green laser. The instrument was calibrated using colloidal silica microspheres (50 and 100 nm, Polysciences), rather than the usual polystyrene beads that are most commonly used for NTA standardisation. The reason for this is that although polystyrene beads are useful for verifying size measurements, they have a higher refractive index (approximately 1.59) than that reported for EVs (approximately 1.39) [142]. Silica microspheres, with a refractive index of 1.45, are a more appropriate standard for concentration measurements made by NTA as they thought to scatter a similar amount of light to EVs of similar size. Using the polystyrene beads for calibration of the NTA settings would lead to underestimation of EV numbers.

Briefly, ca. 1 ml of EV sample diluted in filtered PBS (220 nm cut-off PVDF membrane, BD Biosciences) was analysed at a concentration range between 3 x $10^8$ to 5 x $10^9$ particles/ml (30-80 particles per field of view), as recommended by the manufacturer. Following the establishment of the best capture (camera level 14-16) and analysis settings (detection threshold 4) for EV measurement by NTA, a 30-second video was first captured, then a fresh volume of sample was introduced into the chamber to make another recording.

This was repeated until 8 videos had been captured. The chamber was cleaned by wiping the chamber with distilled water followed by 10 % v/v aqueous ethanol between samples.

Prior to NTA analysis, the PBS used was checked for the presence of particles. If particles were present (more than 3 particles per frame of view), then PBS was ultracentrifuged for 3 hours at 100 000 g and 4 ºC (rotor T-647.5, Sorvall WX+ Ultracentrifuge, ThermoFisher Scientific) and filtered through a 0.22 µm membrane. This protocol was previously determined adequate to clear any particles.

One limitation of using the NTA to measure the concentration of EVs is that it does not distinguish between EV and non-EV particles and thus to improve the validity of the characterisation data, this results from this experiment need to be analysed in conjunction with that obtained from other EV characterisation methods such as TEM and western blot analysis of EV markers.

### 2.5.2 Transmission electron microscopy (TEM)

A drop (50 µl) of intact EVs resuspended in PBS was spotted onto Parafilm. Then, with forceps, a formvar carbon coated copper grid (400 mesh, TAAB) was gently positioned on top of each drop for 7 minutes. The grid was positioned with the coated side facing the drop containing EVs. Three drops, each 30 µl, of PBS were then placed on the Parafilm and the grid washed by sequentially positioning the grid on top of the droplets of PBS for 30 seconds, and using an absorbing paper in between. The absorbing paper was used gently by holding it closely to the side of the grid, without making contact with the coated area. The grids were then moved onto 20 µl drops of contrasting mixture, which was prepared by diluting 1 % uranyl acetate (UA) with 2 % phosphotungstic acid (PTA) in a ratio of 1:10. 5 minutes after incubation with this contrasting mixture, the grids were washed 3 times with PBS as described above. Excess liquid was removed using filter paper at 45°, and grids were left to dry before analysis. Different magnifications were used for TEM samples, with micrographs recorded using a JEOL-1010 TEM (100 kV, JEOL)

### 2.5.3 Quantification of total EV and cellular protein content

The total protein concentration of EVs was estimated using the Pierce BCA Protein Assay Kit (ThermoFisher Scientific) according to the manufacturer's instructions. Briefly, EVs were diluted either 1:2 or 1:3 in cold RIPA) lysis buffer (ThermoFisher Scientific) supplemented with 1X protease inhibitor cocktail (ThermoFisher Scientific) and left on ice for 10 minutes. BCA was then performed directly on the lysate.

Prior to cellular protein concentration analysis, cells were washed with an appropriate amount of PBS (Gibco). 250 µl of ice-cold RIPA lysis buffer (ThermoFisher Scientific) supplemented with 1X protease inhibitor cocktail (ThermoFisher Scientific) was added. The plate was kept on ice for 5 minutes, swirling the plate every minute. The cells were then scraped into 1.5 ml microcentrifuge tubes. The resulting lysates were incubated on ice for 30 minutes, after which debris was pelleted by centrifugation at 14 000 g and 4 °C for 20 minutes. Lysate was carefully extracted and total protein concentration determined using BCA, before being stored at -20 °C for further analysis.

### 2.5.4 Protein analysis using traditional western blot

The following buffers where prepared prior to the western blot: a) 1X Tris buffered saline (TBS): 6.04 g Trizma, 8.5 g NaCl, 3.2 ml 1M HCl (Sigma-Aldrich), $dH_2O$ to final volume of 1 l and b) 1X TBS-Tween**:** 1X TBS with 0.1 % v/vTween (Sigma-Aldrich).

Protein concentrations from cell samples were normalised to 3 µg/µl. 1X NuPAGE™ LDS sample buffer (ThermoFisher Scientific) and 1X reducing agent (ThermoFisher Scientific) were added to each sample. The samples were boiled at 70°C for 10 minutes to denature the proteins. 20-40 µg of protein sample and 5 µl of molecular weight marker (RPN800E, GE Healthcare) were then loaded into a NuPAGE Bis-Tris 4-12 % polyacrylamide gel (Novex, Life Technologies ThermoFisher Scientific) with 1X SDS Running buffer. The gel was run at 90 V for 1.5 hours (PowerEase, Life Technologies). A PDVF membrane (Millipore) was incubated in methanol for 1-2 minutes, and

the membrane and the gel then separately equilibrated in ice-cold transfer buffer for 5 minutes. A sandwich of filter paper/PVDF membrane/gel/filter paper wetted in transfer buffer was placed into the transfer apparatus (Trans-Blot SD, Bio-Rad). The transfer was performed at 400 mA for 1 hour. The membrane was washed in TBS-Tween buffer and blocked in 5 % w/v BSA in TBS-Tween at 4 °C for 1 hour, with agitation.

The membrane was then incubated with the primary antibody diluted in TBS-Tween with 3 %w/v BSA at 4 °C overnight, again with agitation. The membrane was then washed 3 times in TBS-Tween buffer while agitating (5 minutes per wash). The membrane was incubated with the secondary HRP-conjugated antibody (Abcam) diluted in TBS-Tween with 3 % w/v BSA at room temperature for 2 hours with agitation, and finally washed 3 times in TBS-Tween. The membrane was developed using SuperSignal West Pico kit (Thermo Fisher) according to the manufacturer's instructions. The imaging of the membrane was performed with UVP ChemStudio (Analytik Jena).

As there are no EV specific markers, proteins that are enriched in EVs, from all different cellular origins, are commonly used for detection. These are proteins such as tetraspanins (e.g. CD9, CD63 and CD81), cytoskeleton associated proteins (e.g. ezrin) and proteins involved in multivesicular biogenesis (e.g. TSG101 and ALIX). As other compartments of the cell also can produce vesicles, it is further recommended to determine the presence of proteins from these compartments such as the endoplasmic reticulum (e.g. Calnexin) and the Golgi apparatus (e.g. GM130). A lack of these proteins indicates no or little contamination of vesicles by other compartments in the sample studied. In this study, CD81, CD9 and TSG101 were used as EV markers and Calnexin for the absence of other contaminating vesicles.

### 2.5.5 Protein analysis using the simple western system (WES)

Analysis of EV proteins using the traditional western blot method failed to give reliable results, so analysis was instead carried out in the capillary gel electrophoresis format using a WES instrument from Protein Simple (Biotechne Ltd). In WES, the size separation and the immunoassay are

automatically performed in small capillaries, with results ready in 3 hours. First, the stacking and the separation matrices are successively loaded into the capillaries, before small volumes of samples (3 µl) are drawn up into the capillaries and separated according to size. Illumination by UV light immobilizes the separated proteins to the capillary wall. Appropriate primary and secondary antibodies are used to identify the proteins of interest using chemiluminescence. The chemiluminescent signal is detected and quantitated by the Compass software, and results are presented as an image showing a computer generated lane view. All experiments in the present thesis were performed under reducing conditions using the 12-230 kDa separation system (Protein Simple, Biotechne). Reagents were prepared by reconstitution of supplied materials according to the manufacturer's protocol, as described below.

Firstly, 400 mM dithiothreitol (DTT) solution was prepared by adding 40 µl of deionized water to the DTT tube provided. Fluorescent 5X Master Mix was then prepared by adding 20 µL of 400 mM DTT solution and 20 µL of 10X sample buffer to the Master Mix tube provided. A biotinylated ladder solution was also prepared through reconstitution of the pellet (provided in the kit) in 20 µL dionised water. Primary antibody solutions were then prepared by diluting the relevant antibody with Antibody Diluent II solution to achieve dilutions of 1:10 to 1:100 (Table 2.1). Samples were prepared by normalising their concentration with 0.1X sample buffer provided. The manufacturer recommends a working concentration of 0.2-1 µg/µl (with a lower limit of detection of 0.02 µg/µl).

4 µl of each sample was mixed with 1 µl of loading buffer (fluorescent 5x Master Mix, prepared as detailed above). The samples and biotinylated ladder were then denatured on a 95 °C heat block for 5 minutes, before being briefly vortexed, centrifuged and loaded onto the detection module assay plate. Anti-CD9, anti-TSG101, anti-GFP, anti-GBA and anti-Calnexin primary antibodies and corresponding rabbit-secondary antibodies were added, followed by the chemi-luminescent substrate. The fully loaded plate was centrifuged at 2000 RPM for 5 minutes before being inserted into the WES system, in conjunction

with a 13-capillary cartridge. Detection and quantification was conducted via a CCD camera and the Compass software, version 3.1.7.

### 2.5.6 Total RNA isolation

According to the manufacturer's protocol, the RNeasy® Mini Kit (QIAGEN) only isolates RNA molecules larger than 200 nucleotides. To also extract small RNA from EVs, a modified version of the RNeasy® Mini Kit was used. In brief, cells or EVs were separately disrupted and homogenized in 700 µl RLT buffer containing 1% β-mercaptoethanol, by passing the lysate at least 5 times through a blunt 20-gauge needle (0.9 mm diameter) fitted to an RNase-free syringe. 2.45 ml of ethanol was added to the samples prior to the use of the RNeasy® mini spin column. The samples were washed twice in 500 µl RPE buffer and eluted in 30 µl of RNase free water. Sample concentrations were then assayed by spectrophotometry (NanoDrop 1000, Thermo Scientific). Absorbance of the sample was measured at 260 nm, and the ratio of absorbance at 260 nm and 280 nm (~2) was used to assess the purity of the RNA sample. Samples were stored at –80 ºC for future analysis.

RNA was isolated from both sorted-transduced (MOI 100) and non-transduced HEK293T cells, and EVs derived from each cell source. To isolate RNA larger than 200 bp only (including eGFP RNA) from EVs and cells, the RNeasy® Mini Kit was used according to the manufacturer's protocol without any modifications.

One limitation of this experiment comes from the fact that EVs were not treated with RNase A prior to isolation of RNAs. RNase A would have served to degrade any RNA that is not incorporated in EVs and protected by the lipid bilayer [143]. Therefore, in this case we cannot distinguish if the RNA isolated is purely that incorporated in EVs or whether that attached to the surface of EVs.

### 2.5.7 Reverse transcription and quantitative real-time PCR analysis of RNA sequences isolated from EVs and HEK293T cells

Reverse transcription (RT) master mixes were prepared for each sample using the high capacity cDNA reverse transcription kit (Applied Biosystems), according to the manufacturer's instructions. Briefly, 10 µl of RT master mix was pipetted into individual tubes and 10 µl of RNA sample was added to each tube. The tubes were centrifuged briefly to eliminate any air bubbles. The samples were then placed into a thermocycler (Veriti 96-Well Thermal Cycler, Applied Biosystems) and incubated as follows: 25 °C for 10 minutes; 37 °C for 120 minutes; and 85 °C for 5 minutes. Reaction mixes were kept at 4 °C until use. qPCR master mixes were prepared for eGFP mRNA containing 5 µl of SsoAvanced universal SYBR green supermix (2x) (Bio Rad), 1 µl of forward primer, 1 µl of reverse primer and 1 µl of nuclease free water. After mixing, 8 µL of each master mix was placed into the wells of a 96-well plate. 2 µl of each RT reaction was added in triplicate to the master mix and the plate was sealed with an optical adhesive cover. Plates were spun down to remove air bubbles then placed into the StepOne Plus Real Time PCR system (Applied Biosystems) and run using the following thermocycler protocol: 95 °C for 10 minutes then 40 cycles of 95 °C for 15 s / 60 °C for 60 s. Once the run was complete, automatic cycle threshold (Ct) analysis was performed with the SDSv2.3 software.

One limitation of this experiment comes from the fact that the EV RNA expression data are not normalised to that of household genes as routinely done when determining and comparing expression levels between samples. This means that the data to be obtained from this experiment cannot be regarded as conclusive. Normalisation allows for accurate determination of analysed mRNA levels and improves the validity of the data. It was not conducted here because it remains difficult to determine appropriate normalisation controls for EV experiments. Moreover, the reference genes that are normally used to normalize expression levels between samples of cellular RNA are not appropriate normalization controls in this case [143].

### 2.5.8 Quantification of ATP content in EVs

The CellTiter-Glo® (Promega) kit was used to measure the amount of ATP in EVs. This is a method typically used to determine the number of viable cells based on quantitation of ATP. The assay procedure involves adding a single reagent (CellTiter-Glo® reagent) directly to cells and this homogeneous "add-mix-measure" format results in cell lysis and generation of a luminescent signal proportional to the amount of ATP present. The hypothesis is therefore that it would work in a similar way to detect the amount of ATP present in EVs. Briefly, three wells of a 96 well plate were seeded with 10 000 HEK293T cells in 100 µl of complete growth medium and three wells with 100 µl of EVs re-suspended in serum free media (DMEM GlutaMax™, ThermoFisher Scientific). 100 µl of CellTiter-Glo® reagent was added to each well and the contents mixed for two minutes on an orbital shaker to induce lysis. The plate was allowed to incubate at room temperature for 10 minutes to stabilize the luminescent signal. The luminescence of cells, EVs and the CellTiter-Glo® Reagent (to serve as a negative control) was then recorded using a plate reader (SpectraMax M2, Molecular Devices)

### 2.5.9 Analysis of luciferase content in loaded-EVs

The luciferase assay system (Promega) was used to investigate the presence of functional luciferase in loaded-EVs containing the enzyme, according to the manufacturer’s instructions. Briefly, EVs were lysed by adding 20 µl of lysis buffer (CCLR) to 10 µl of EVs re-suspended in PBS in a 1.5 ml microcentrifuge tube, mixed gently, and left at room temperature for 5 minutes to ensure complete lysis. 100 µl of the luciferase assay reagent was added to each sample, mixed gently by pipetting up and down 2-3 times, and the luminescence measured using a luminometer (GLOMAX 20/20, Promega). The luminescence of non-lysed EVs as well as the luminescence of naive EVs derived from non-transduced HEK293T cells (to serve as a negative control) were measured in triplicate.

## 2.5.10 Quantification of eGFP content in loaded-EVs

A GFP ELISA kit (ab171581, Abcam) was used to quantify the amount of eGFP in loaded-EVs, according to the manufacturer's instructions. EV suspensions were diluted in 1x Extraction Buffer PTR, vortexed for 15 seconds and left on ice for 10 minutes. 50 µl of samples and GFP standards were added to pre-coated wells in microplate strips provided in the kit. 50 µl of antibody cocktail was added to each well and the strips were incubated at room temperature on a plate shaker set to 400 rpm for 1 hour. Subsequently, the wells were washed three times with 1x wash buffer PT, 100 µl of 3,3',5,5'-tetramethylbenzidine (TMB) substrate added to each well, and the plate was incubated for 10 minutes at room temperature in the dark on a plate shaker set to 400 rpm. The reaction was stopped by addition of 100 µl of stop solution and shaking at room temperature for 1 minute on a plate shaker set to 400 rpm. The absorbance was recorded at 450 nm using a SpectraMax M2 (Molecular Devices) plate reader.

## 2.5.11 Analysis of GCase enzymatic activity in loaded-EVs

GCase activity in loaded EVs was determined fluorometrically using 4-methylumbelliferyl-β-D-glucopyranoside (4-MUβGlu*)* as a substrate, in the same manner as that for cells (**Section 2.4.5.3**) Briefly, loaded-EVs were resuspended in ice-cold GEB and kept on ice for 20 minutes, after which debris was pelleted by centrifugation at 14 000 g and 4 °C for 20 minutes. The lysate was carefully extracted and total protein concentration first quantified using BCA according to the manufacturer's instructions, before measuring GCase activity.

## 2.5.12 Delivery of loaded-EVs *in vitro*

### *2.5.12.1 Delivery of luciferase enzyme to cells of visceral origin*

To establish the ability of EVs loaded with luciferase to deliver functional enzyme to cells, the luciferase assay kit (Promega) was used according to the manufacturer's instructions. A 96 well plate was seeded with 50 000 HEK293T cells overnight and an increasing volume of loaded-EVs (10, 20, 40 µl of EV preparation with a concentration of 1 x $10^{12}$ particles/ml) was added before the

plate was incubated for 1 hour at 37 °C. The media was removed, the cells washed twice with PBS, lysed by adding 20 µl of lysis buffer (CCLR), and then being mixed gently and left at room temperature for 5 minutes to ensure complete lysis. 100 µl of the luciferase assay reagent was added to each sample, and mixed gently by pipetting up and down 2-3 times. Bioluminescence images were taken using an IVIS® Lumina Series III *in vivo* imaging system 5 minutes after addition of the substrate to the cells. Luminescence was also measured using a luminometer (GLOMAX 20/20, Promega). This was repeated following addition of 10 µl of loaded-EV preparation (1 x $10^{12}$ particles/ml) or controls (naïve EVs of concentration ca. 1x $10^{12}$ particles/ml or PBS) to cells and incubation for 6 hours at 37 °C, in the same manner as above. Similarly, Luminescence of the luciferase enzyme reaction in transduced HEK293T cells was assayed and used as positive control.

#### *2.5.12.2 Delivery of eGFP to primary neurons*

The following stock reagents were prepared prior to the assay: a) 1X Tris buffered saline (TBS): 6.04 g Trizma, 8.5 g NaCl, 3.2 ml 1M HCl (Sigma-Aldrich), $dH_2O$ to final volume of 1 l; b) 1X TBS with Triton X-100 (TBS-T), which is made up of 1X TBS and 0.3 % Triton X-100 (Sigma-Aldrich).

Mouse primary embryonic neuronal cells (mixed culture) from wild type CD1 mice were kindly provided by Dr. Laura Poupon. Following extraction from embryos of a pregnant female at embryonic day 13.5–15.5, cells were grown on a cover glass in 6 well plates for 7 days in complete neuron-basal medium. Complete neurobasal medium was prepared by supplementing Neurobasal medium (Gibco) with 2 %v/v B27 (Gibco), 1 %v/v streptomycin / amphotericin B (Gibco), glutamine (Gibco) to a final concentration of 300 µM, and β-mercaptoethanol (Gibco) to a final concentration of 25 µM.

Micro-cover slips were transferred to 24 well plates and incubated with 500 µl of complete growth media. 20 µg of loaded-EVs (containing luciferase, derived from sorted-transduced HEK293T cells) were added to two wells and incubated for 1 and 3 hours at 37 °C. 20 µg of naïve EVs from non-transduced

HEK293T cells was added a third well, to serve as a negative control, and the plate was incubated for 3 hours at 37 °C. Following incubation, the media was removed, cells washed twice with PBS, fixed with 2 %v/v paraformaldehyde (in PBS, pH 7.4) for 10 minutes, and permeabilized with 0.1 %v/v Triton X-100 (Sigma) in PBS for 5 minutes. Following blocking with TBS-T containing 5 %w/v BSA and 3 %v/v goat serum for 30 minutes, cells were incubated with anti-Lamp1 antibody overnight at 4°C, under very gentle agitation. The cells were then washed with TBS and incubated with AlexaFluor 546 goat anti-rabbit IgG for 2 hours at room temperature, in the dark and under gentle agitation. To stain cell nuclei, cells were incubated in 4′,6-diamidino-2-phenylindole (DAPI, Sigma-Aldrich) at 1 in 5000 dilution in TBS-T, for 10 minutes in the dark. Accumulation of EVs in neurons was then visualised using confocal microscopy (Zeiss LSM 710). Image analysis was conducted using the Zen™ software.

#### *2.5.12.3 Delivery of GCase to cells of visceral origin*

To establish the ability of EVs loaded with GCase to deliver functional enzyme to cells, a fluorometric assay using 4-MUβGlu as a GCase enzyme substrate was used. A 96 well plate was seeded with either 20 000 or 40 000 HEK293T cells overnight and 50 µl of loaded-EVs (concentration 1 x $10^{12}$ particles/ml) were added, and the plate incubated at 37°C for 15 minutes, 1, 3, 6 hours (for which wells were seeded with 40 000 cells) and 24 hours (wells seeded with 20 000 cells). As a control, cells were incubated with 50 µl of naïve EVs (concentration ~ 1 x $10^{12}$ particles/ml) for the same time periods. The media was then removed, cells washed twice with PBS and GCase extracted. Activity was evaluated as detailed in **Section 2.5.11**. The percentage increase in GCase activity following incubation with GCase loaded-EVs in comparison to control cells incubated with naïve EVs at each time point was calculated.

## 2.6 *In vivo* biodistriubtion studies

### 2.6.1 Animals

Wild-type CD1 mice were used for all *in vivo* biodistribution studies. All listed procedures were conducted under Professor Rahim's project licence (PPL PCC436823) and have been approved by the UK Home Office (Animal Scientific Procedures Act, 1986), and by the ethical review committees of University College London. The Animal Research Reporting of *In Vivo* Experiments (ARRIVE) guidelines were followed.

### 2.6.2 EV administration

To evaluate the biodistribution of loaded-EVs (derived from sorted-transduced HEK293T cells) *in vivo*, experiments were performed in which they were administered via different routes in both neonate and adult wild type CD1 mice (Table 2.5). The concentration of eGFP in the loaded-EVs was first determined (using ELISA as described in **Section 2.5.10**). Animals were also injected with naïve EVs derived from non-transduced HEK293T cells to serve as a negative control. One limitation of this *in vivo* biodistribution study comes from the fact that it was carried out in wild type mice rather than the specific Gaucher animal disease model. Thus the obtained tissue distribution profiles may not be entirely representative of that seen in diseased mice.

**Table 2.5:** Administration schedule of loaded-EVs derived from HEK293T cells

| ***Route of administration*** | ***Volume (µl)*** | ***Time point (hours)*** |
|---|---|---|
| ***P0-1 * Neonates (n=4 for each route)*** | | |
| **Intracerebroventricular *(ICV)*** | *10* | *1,6,24* |
| ***Intravenous (IV)*** | *40* | *1,6,24* |
| ***Intranasal (IN)*** | *40* | *1* |
| ***Intraperitoneal (IP)*** | *20* | *1,6,24* |
| ***P30 Adults (n=4 for each route)*** | | |
| **Intracerebroventricular *(ICV)*** | *20* | *1,6* |
| ***Intravenous (IV)*** | *200* | *1,6* |
| ***Intraperitoneal (IP)*** | *200* | *1,6* |

**P0-1 neonates are those injected on the same day they are born (P0) or the day after (P1),** P30 are adult mice 30 days of age.*

A similar biodistribution study was conducted using loaded-EVs from SH-SY5Y cells, but only in neonate mice (Table 2.6). Injections were performed by Dr. M. Hughes or Miss A. Geard, UCL School of Pharmacy.

**Table 2.6:** Administration schedule of loaded-EVs derived from SH-SY5Y cells

| ***Route of administration*** | ***Volume (µl)*** | ***Time point (hours)*** |
|---|---|---|
| ***P0-1 * Neonates (n=4 for each route)*** | | |
| **Intracerebroventricular *(ICV)*** | *10* | *1* |
| ***Intravenous (IV)*** | *40* | *1* |
| ***Intranasal (IN)*** | *40* | *1* |
| ***Intraperitoneal (IP)*** | *20* | *1* |

**P0-1 neonates are those injected on the same day they are born (P0) or the day after (P1).*

### *2.6.2.1 ICV route (neonates)*

EVs were administered via bilateral intracerebroventricular (ICV) injection, targeting the anterior horn of the lateral ventricle as previously described [144]. Injection sites were identified at 2/5 of the distance directly from the lambda

suture to the eye. Pups were cryo-anesthetised for 1 minute after which a loaded 33-gauge needle (Hamilton) with syringe was inserted perpendicular to the surface of the skull at a depth of 3 mm from the tip of the needle to slowly administer 5 µl of EV suspension. Following a brief pause the needle was carefully withdrawn and the contralateral ventricle was injected with the same volume. The pups were warmed up to allow recovery and returned to the dam.

#### *2.6.2.2 IV route (neonates)*

Pups were anesthetised on ice for 30-60 seconds, moved under a microscope and intravenous injections of 40 µl of EV suspension were performed via the superficial temporal vein using a 33-gauge needle (Hamilton) [145]. A 15 second pause was observed before withdrawing the needle slowly, and gentle pressure was applied to the injection site. The pups were then warmed up to allow quick recovery and once fully recovered returned to the dam.

#### *2.6.2.3 IN route (neonates)*

Pups were held in a vertical position with the head immobilized and then using a micropipette a 5 µl droplet was placed at the nasal opening. The animal was allowed to inhale the droplet and the process repeated with the other nostril, until a total of 20 µl was administered. Again the pup was allowed to fully recover before returning it to the dam.

#### *2.6.2.4 IP route (neonates and adults)*

Mice were restrained and positioned ventral to expose the abdomen, with head pointing downward at a 30° angle to allow intestines to fall forward. An injection of the relevant volume was then given into the peritoneal cavity using a 29-gauge insulin needle. Neonates were cryo-anesthetised before injections. Following the procedure the mice were returned to the cage.

#### *2.6.2.5 IV route (adult)*

Prior to injections mice were warmed up at in a heat chamber set to 37 °C and then anaesthetised using a constant flow of isoflurane. Mice were then injected into the lateral tail vein using a 29-gauge insulin needle [146].

#### *2.6.2.6 ICV route (adults)*

Animals were anesthetized with a 50/50 injection solution of hypnovel+fentanyl (0.1 mL/10 g of body weight, IP). The head of the animal was shaved, and the animal placed in a stereotaxic frame with a constant flow of isoflurane. The skin of the skull was disinfected with iodine and incised. Stereotaxic coordinates of the injection site were selected by first aligning the 33-gauge needle (Hamilton) on the bregma and then moved 0.5 mm posterior to the bregma, 1.1 mm right of the midline. The site of injection was marked with a disinfected pen, the site of injection drilled carefully without damaging the brain, the needle introduced and injection of the EV suspension started at 3 µl/min. One minute after the injection was finished the needle was removed slowly. The wound was closed with tissue adhesive and two clips, and disinfected with iodine. Finally, a 0.5 ml injection of saline was given and the animal warmed up to 37 °C before being returned to the cage.

### 2.6.3 Harvesting of tissues

Mice were euthanised by transcardial perfusion using PBS while under terminal isofluorane anaesthesia, and organs were subsequently harvested. Brains and visceral organs were extracted and either fixed in PBS with 4 % paraformaldehyde (PFA) for immunohistochemistry or snap frozen on dry ice and stored at -80 °C for further protein extraction and analysis. After 48 hours of fixation in 4 % PFA, tissues were transferred into 30 % sucrose (Sigma-Aldrich) in PBS for cryoprotection.

## 2.7 Histological analysis of tissues

### 2.7.1 Coating of slides

Microscope slides (Superfrost, VWR) were double coated with gelatine to allow adhesion of tissues and allow downstream washes. The gelatine solution was prepared from 2.5 g of gelatine (VWR) and 0.25 g of chromium (III) potassium sulphate 12-hydrate (VWR) in 500 ml of $dH_2O$ preheated to 45 °C. The slides were immersed in the gelatine solution (maintained at 45 °C) for a few seconds and left to dry at 56 °C overnight. This process was repeated a

second time to produce double coated microscope slides, which were used for immunohistochemistry studies.

### 2.7.2 Cryosectioning of tissue samples

Prior to cryosectioning: 1000 ml of 1X TBSAF was prepared, this is composed of 545 ml of 1XTBS, 5 ml sodium azide (10 %), (VWR), 150 g sucrose and 300 ml of ethylene glycol

To cut the fixed organs, they were first embedded in specimen matrix (Thermo Scientific) and frozen. All organs were cut to 40 µm thickness slices at a constant temperature of -20 °C with a Leica CM3050 cryostat (Leica Biosystems). Coronal brain sections were sliced starting from the front of the olfactory bulbs to the cerebellum and brain stem. Slices were stored at 4 °C in TBSAF in 96-well plates (NUNC).

### 2.7.3 Immunohistochemistry

3,3'- diaminobenzidine (DAB, Sigma-Aldrich) mediated immunohistochemistry was used to analyse eGFP tissue distribution following EV administration. A series of representative sections were transferred to six-well plates and washed with 3 ml of 1X TBS. Endogenous peroxidase activity was depleted with 1 % hydrogen peroxide ($H_2O_2$, Sigma-Aldrich) in 1X TBS for 30-60 minutes under gentle agitation. Slices were then washed three times with 1X TBS, followed by incubation with 15 % v/v normal serum (Sigma-Aldrich) in 1X TBS-T for 30 minutes under gentle agitation, to block any non-specific binding. Sections were again washed three times with 1X TBS before adding 3 ml of GFP primary antibody (ab290, ABCAM) diluted 1:10 000 with 10 %v/v normal serum in TBS-T and incubating at 4 °C overnight under gentle agitation.

The following day, slices were washed three times with 1X TBS and incubated for 2 hours at room temperature with the secondary antibody diluted with 10 %v/v normal serum in TBS-T. Sections were again washed before being incubated for 2 hours with 1:1000 avidin-biotin reagent (Vectastain Elite ABC kit, Vector Labs). Sections were washed and incubated with 0.05 % DAB solution containing 0.001 % $H_2O_2$ to visualise the staining. This DAB solution was prepared by first dissolving one DAB tablet in 20 ml of TBS, filtering

through a 0.45 µm membrane (Milipore) and adding 6 µl of 30 % $H_2O_2$. The plate was covered with foil and kept under agitation for a few minutes. The reaction was stopped by adding ice-cold 1X TBS. After three washes in 1X TBS, sections were mounted on chrome-gelatine coated slides (as prepared in Section 2.9.1) and left to air-dry overnight. Slides were dehydrated in ethanol, cleared in Histo-clear (National Diagnostic) for 30 minutes and DPX mountant (Fisher Scientific) used to coverslip the slides.

### 2.7.4 Microscope imaging

Light bright-field images were taken with a Nikon DS-Fi1 camera (Nikon, Tokyo, Japan) attached to a Nikon Eclipse E600 microscope. Representative images of the full brain section were taken at 1X magnification. Higher magnification pictures of discrete areas of the sections were taken with 10X/0.25 and 40X/0.65 objectives (CFI Achromat, Nikon).

## 2.8 Protein analysis

### 2.8.1 Protein concentration measurement from tissues

The total protein concentration of tissue lysates was determined using the Pierce BCA Protein Assay Kit (ThermoFisher Scientific) according to the manufacturer's instructions. Prior to quantification, 100 to 200 mg of tissues was homogenized using an Ultra-Turrax TP (IKA Labortechnik) on ice in 0.5-1.0 ml of 1X Cell Extraction Buffer PTR (provided in the GFP ELISA kit detailed in **Section 2.5.10**). Homogenates were incubated on ice for 20 minutes before being centrifuged at 13 600 g for 30 minutes at 4 °C. The supernatant was transferred to 1.5 ml microcentrifuge tubes and stored at –80 °C.

### 2.8.2 GFP ELISA on frozen tissue

eGFP content in each tissue was quantified using the GFP ELISA as detailed in **Section 2.5.10.** Prior to the ELISA, the protein content of all tissues was normalised by diluting in sample buffer, such that 200 µg of protein was added to each pre-coated ELISA wells.

## 2.9 Formulation of EVs and stability testing

### 2.9.1 Freeze drying

EVs isolated from non-transduced HEK293T cells were characterised using:

- NTA for size and concentrations
- BCA for total protein content
- Western blot for EV marker validation
- TEM for morphology

All of the above tests were performed as described in earlier sections of this chapter.

Following characterisation, EVs were aliquoted into 50 µl volumes in labelled microcentrifuge tubes and mixed with 50 µl of trehalose (Pfanstiehl) solutions to give final concentrations of 0.5, 2 and 4 % w/v. Samples were then snap frozen on dry ice before being lyophilised under vacuum overnight using a VirTis AdVantage freeze dryer (SP Scientific). Lyophilised EVs (cake form) were stored under different conditions for 4 weeks (Table 2.7) to evaluate the stability of the samples with different concentration of cryoprotectant. Additionally, non-lyophilised EVs were stored at 4, 20 and -80°C in parallel, to serve as controls. The experiment was conducted with three independent repeats.

Once the optimal concentration of cryoprotectant was established, the experiment was repeated but with luciferase-eGFP loaded-EVs.

**Table 2. 7**: EV formulations and storage conditions

| Type of EVs | Concentration of trehalose (%w/v) | Storage temperature (°C) | Time points |
|---|---|---|---|
| **Naïve HEK293T derived EVs** | 0, 0.5, 2, 4 | 4, 20 | 1 day, 1 week, 2 weeks and 4 weeks |
| **Luciferase-eGFP loaded EVs** | 0.5, 2 | 4, 20 | 1 week and 2 weeks |

### 2.9.2 Evaluation of lyophilised EVs

At each time point, EVs were carefully re-suspended in deionised milliQ water to the original volume and vortexed for 30 s to ensure complete re-dispersion. This was followed by NTA (**Section 2.5.1**), TEM (**Section 2.5.2**), BCA (**Section 2.5.3**), Western blot analysis (**Section 2.5.5**), and luciferase assay **(Section 2.5.9**).

## 2.10 Statistical analysis

All statistical analysis was performed with the GraphPad Prism software (v 8). Data are presented as average values (mean) ± standard deviation (SD) unless otherwise stated. T-test, one-way ANOVA (analysis of variance) and two-way ANOVA tests were performed where appropriate. Significance was taken to be where $p < 0.05$, and is denoted as follows: * $p < 0.05$, ** $p \leq 0.01$, *** $p \leq 0.001$, **** $p < 0.0001$.

# Chapter 3: Production, optimisation and validation of loaded-EVs

## 3.1 Introduction

Over the past decade, extracellular vesicles (EVs) have received great attention in the scientific community and many high-impact journal articles have detailed their potential in both therapeutics and diagnostics. However, to date there is still a lack of standardisation of protocols in terms of sample collection, isolation and characterisation [86].

### 3.1.1 Isolation of EVs

Currently, there is no standardised method to isolate and/or purify EVs, and the choice of method to use depends on (a) the specific scientific question asked and (b) the downstream applications envisaged [147]. One of the main reasons why it has been difficult to obtain a standardised method is the heterogeneous nature of EVs. They can vary significantly in size, shape, and source, and there considerable overlap in size and phenotype between different subpopulations of EVs (e.g. exosomes formed in multivesicular endosomes and vesicles released directly from the membrane such as microvesicles) [85,147]. EVs can be extracted from a range of tissue culture supernatants and body fluids, and concomitantly present in solution are a wide spectrum of components of similar size and shape that can impact the isolation of a pure EV subpopulation. As a result, it is difficult to compare data from different studies and establish an optimal isolation protocol [148,149].

Nonetheless, a large variety of EV purification methods have been explored in the literature. They can be broadly divided into five groups. These are ultracentrifugation based techniques, size-based approaches, immunoaffinity capture-based techniques, EV precipitation, and microfluidics-based techniques [148,150,151]. A brief overview of these techniques as well as some of their advantages and disadvantages are presented in Table 3.1.

**Table 3.1:** Overview of most common isolation methods for EVs

| Isolation Technique | Isolation principle | Advantages | Disadvantages | Ref. |
|---|---|---|---|---|
| **Ultracentrifugation-based techniques** | Sequential separation of components based on density, size, and shape | ***Differential ultracentrifugation:*** Large capacity and yields of EVs. Reduced cost per run. Lack of contamination risk with separation reagents. | High equipment cost, time-consuming, labour-intensive. Low portability - not available at point of-care. High speed centrifugation may damage EVs. Co-isolation of non-EV components. | [152,153] |
| | | ***Density gradient centrifugation:*** Higher separation efficiency, thus resulting in greater purity of EV subpopulations | Lower yield. Complex method, and time-consuming. Highly user intensive and not suitable for high-throughput applications. | [154,155] |
| **Size-based techniques** | Isolation is exclusively based on the size difference between EVs and other components, by using filter membranes or gel chromatography columns | ***Ultrafiltration:*** Fast, does not require special equipment. Good portability. No limit on sample processing capacity. Low equipment cost | . Moderate purity of isolated EV subpopulations. Shear stress induced deformation of EVs. Possibility of clogging and vesicle trapping. Loss of EVs in membranes. | [156,157] |
| | | ***Size-exclusion chromatography:*** High-purity and uniform size of samples. Gravity flow preserves the integrity and biological activity. Superior reproducibility. | Moderate equipment cost. Requires dedicated equipment. Not trivial to scale up. Long run time. Low extraction volume. | [158,159] |
| **Immunoaffinity capture based techniques** | Isolation is based on specific interaction between membrane-bound antigens (receptors) of EVs and immobilized antibodies (ligands) on beads | Enables the isolation of specific EV subpopulations. Highly pure samples. | High reagent cost. Low capacity and yields. Difficult to elute the EVs from the beads. Reagents used can affect biological activity of EVs. Only possible when working with cell-free samples. | [160–162] |

| | | | | |
|---|---|---|---|---|
| **Precipitation-based techniques** | Isolation is based on precipitating EVs through use of water excluding polymers and pelleting at low centrifugal speeds | Easy to use.<br>Does not require specialized equipment.<br>Enables high EV recoveries. | Precipitation of other non-EV contaminants.<br>Polymer retention in final product.<br>Residual polymer could affect downstream analysis and Quantification. | [163,164] |
| **Microfluidics-based techniques** | Isolation based on a variety of properties of EVs like immunoaffinity size, and density but at the microscale | Fast and low cost.<br>Easy automation and integration. High portability<br>High efficiency. | Lack of standardization and large scale tests on clinical samples.<br>Lack of method validation.<br>Moderate to low sample capacity. | [165,166] |

Ultracentrifugation is currently regarded to be the “gold standard” method for isolation of EVs, and the majority of published studies use a variation of this method [148]. Fundamentally, particle separation through centrifugation involves spinning a sample of heterogeneous particles around an axis and relying on the fact the different components will have different buoyant densities and so will sediment at different speeds and times, thus allowing them to be sequentially isolated. Bigger and more dense particles will sediment faster and at lower speeds, whereas smaller and less dense particles require higher speeds and longer times to sediment [167]. EVs are always isolated by differential ultracentrifugation. A typical protocol as first described by Théry *et al*. [153] is shown in Fig. 3.1

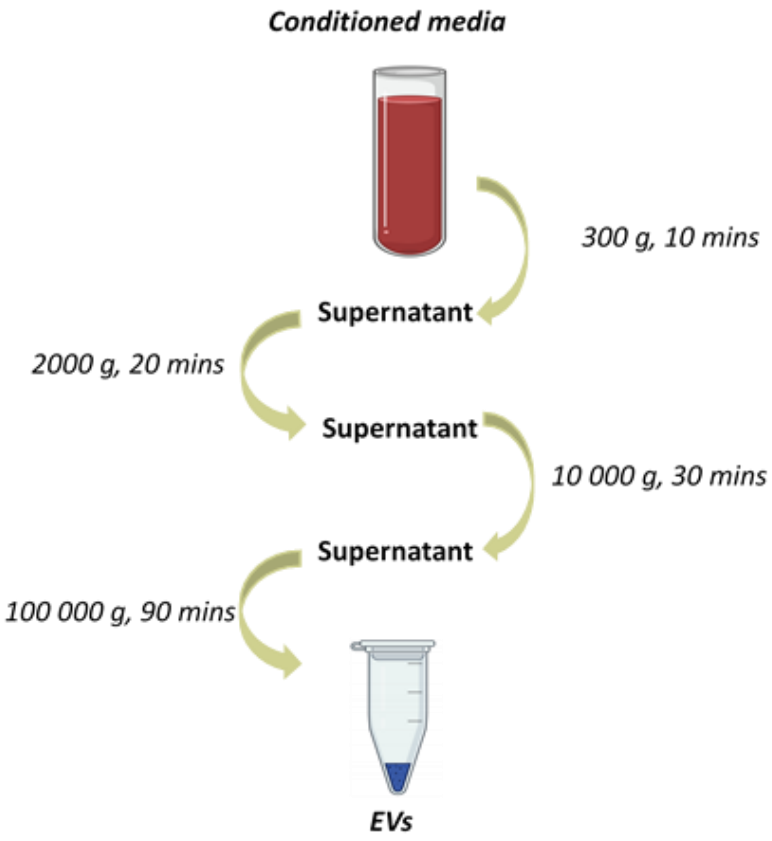


**Figure 3.1:** Illustration of a typical isolation protocol for EVs as developed by Théry *et al*. [153]

In this protocol, the starting biological fluid is conditioned cell culture media, which is complex in nature and contains a mixture of components from cells, cell debris, EVs, etc. Therefore, to ensure that only EVs are isolated in the final product and prevent co-sedimentation of particles, successive rounds of centrifugation are employed before the final ultracentrifugation round that aims to pellet particles of same size and density as EVs. The 300 g step aims to pellet and remove the majority of viable cells, the 2000 g step to remove dead cells, and the 10 000 g step should remove cell debris and the other structures with buoyant density higher than that of EVs. EVs present in the resulting supernatant are finally pelleted by ultracentrifugation at 100 000 g. After this, the pellet is re-suspended in an appropriate medium such as phosphate buffered saline (PBS). To successfully isolate a relatively pure sample of EVs from a biological fluid using ultracentrifugation, several factors have to be considered and iterated to optimise the isolation protocol.

The viscosity of the biological fluid from which EVs are to be isolated is one important factor to be considered when optimising an isolation protocol. Viscosity can also be defined as the “the resistance to flow”, and the higher the viscosity of a fluid the higher the resistance to flow will be. This ultimately means slower sedimentation rates will be seen during centrifugation [168]. Different biological fluids such as serum, plasma and cell culture media have different chemical and biological composition and hence have different viscosities. Therefore, it is only logical to assume that if these media were to be spun under the same conditions the yield and purity of EVs isolated would differ significantly. This was demonstrated by Momen-Heravi *et al*. [168], who measured the viscosity of different biological fluids and then subjected them to same isolation protocol and evaluated the yield of EVs obtained. Recovery of EVs was lower in more viscous media when spun for a specific time at a given speed [168], but dilution of more viscous media with PBS prior to ultracentrifugation could eliminate this problem [153].

Another factor to take into account is the type of the rotor to be used and its characteristics. These parameters can influence the time needed for pelleting as well as the characteristics of the isolated EV population [169]. Two rotors are commonly used: swing bucket (SW) or fixed angel (FA). An SW-rotor is horizontal relative to the rotation axis with the component to be pelleted gradually forced to the bottom of the tube, whereas a FA-rotor is fixed at a certain angle to the rotation axis and the component to be pelleted is deposited against the wall of the tube. Hence, the component to be pelleted in a SW-rotor needs to travel further than in a FA-rotor, which could mean longer centrifugation times are needed and result in lower sedimentation efficiency with SW-rotors [149,169]. The time (t) required to pellet a certain component during centrifugation depends on two factors. One is the k-factor of the rotor used and the second is the sedimentation coefficient (s) of the component or particle to be pelleted (Equation 3.1) [169]. The k-factor of a rotor is a measure of its pelleting efficiency at maximum rotational speed, and the sedimentation coefficient of a particle describes its migration through a medium based on Stokes’ law [169,170].

**(Equation 3.1)**

$$t = \frac{K}{S}$$

Despite these complexities, multiple research groups often use the same original protocol as reported by Thery *et al*. or make minor modifications [153,171–174], without considering the above factors. This is likely to be a major reason that has led to inconsistencies in the reproducibility and repeatability of the reported data in EV research, highlighting the need for standardisation of isolation protocols and increasing sedimentation efficiency. Moreover, for separation using differential ultracentrifugation to work effectively, the sedimentation coefficients of the particles to be distinguished need to differ significantly (by orders of magnitude) [169]. As the compositions of the biological fluids from which EVs are extracted are very complex, this often means that the final product contains a heterogeneous mixture of EVs rather than purely exosome subpopulations. Taking this consideration into account, from this point onwards all isolated pellets will be referred to as comprising extracellular vesicles (EVs).

## 3.1.2 Characterisation of EVs

As previously discussed it is relatively difficult to isolate a totally pure EV subpopulation, which is why characterisation of EVs also still lacks standardisation. However, in 2014 the International Society for Extracellular Vesicles (ISEV) released a set of guidelines with a minimal set of biochemical, biophysical and functional standards that should be used to attribute any specific biological cargo or functions to EVs. These were updated in 2018 [86,147]. The aim of these guidelines, which are briefly summarized below, are to help the EV research community work towards standardisation of minimal experimental requirements needed to demonstrate the presence of EVs. Standardisation of EV characterisation is essential as we move towards their use in the clinic [175].

To begin with, it is recommended that, when isolating EVs from cell culture media, if media supplements such as foetal bovine serum (FBS) are used they

should be pre-depleted of EVs. Protocols that are recognised to sufficiently deplete EVs include ultracentrifugation (at 100 000 g) for at least 18 hours, tangential flow filtration or other forms of ultrafiltration [86]. However, shorter centrifugation times at around 100 000 g are deemed inefficient in depleting all EVs from FBS [86,153,176]. Alternatively, commercial "EV-depleted" serum and other supplements may be used, but not prior to confirming the product is genuinely "EV-free".

Another recommendation is with regard to the protein markers expected to be found on EVs. At least two positive protein markers (that are typically enriched in EVs) and one negative protein marker (that are not found in EVs) should be measured in a semi-quantitative or quantitative way. As all EVs are vesicles bounded with a lipid bilayer it is essential that the isolated product contains at least one transmembrane or GPI-anchored protein such as CD63, CD81 and CD9 [86]. Furthermore, to prove that the particles enclose cytosolic material from the originating cell line and are not just open cell membrane fragments, at least one cytosolic/periplasmic protein with lipid or membrane protein-binding ability must be shown. Examples of such proteins include TSG101, ALIX and Flotillins I and II [86]. Finally, to exclude the presence of subcellular compartments that may have the same size as EVs and can co-sediment with them, it is essential to demonstrate the lack of proteins typically present in such compartments. Examples of proteins that should be absent include Calnexin and GM130 [86]. Common methods that can be used for quantification include western blots (WB) [177], flow cytometry [178] and enzyme-linked immunosorbent assay (ELISA) [179].

It is also recommended that at least two different but complementary technologies are used to characterise individual EVs within the final product, as this will provide an indication of the heterogeneity of the EV population [86,147]. For example, two complementary techniques could be one that generates high-resolution images of single EVs (such as electron microscopy or atomic-force microscopy (AFM)), and the one that relies on the biophysical features of EVs to measure their size (such as resistive pulse sensing electric field displacement, or nanoparticle tracking analysis (NTA, which relies on light scattering properties)). It is essential to combine techniques that rely on

biophysical properties to provide particle size distributions (but cannot distinguish membrane vesicles from co-isolated non-membranous particles of similar size), with techniques that show single EVs and their topology. Thus, a powerful combination of methods often used in the literature employs NTA for size distribution analysis of EVs in the bulk sample, and transmission electron microscopy (TEM) to provide high-resolution images of single EVs and wide-field images encompassing multiple EVs in a small aliquot.

Finally, recommendations on functional analysis of EVs were also provided by ISEV [86]; however, these were specific to individual scenarios. The general aim of these ISEV recommendations is to ensure that appropriate controls are used in experiments assessing the functional performance of EVs.

The recommendations highlighted by the ISEV guidelines were considered when establishing the methodology for isolating and characterising EVs in this Chapter.

### 3.1.3 Loading of EVs

EVs have been demonstrated to be very promising delivery vectors for therapeutic agents, owing to their biocompatibility among other factors [180]. As detailed in Fig. 3.2, loading of EVs with a therapeutic agent can be divided into two main approaches: a) before isolation ("*in-situ*) or b) after isolation ("*ex-situ*"). In the "*in-situ*" approach, the desired agent is incorporated first into the producer cells using e.g. transfection with a plasmid or transduction with viral vectors to cause the cells to overexpress a certain protein or messenger RNA (mRNA). The latter is consequently incorporated into EVs during their biogenesis [181]. The *ex-situ* approach is divided into active (Fig. 3.2b:1-4) or passive encapsulation (Fig. 3.2b:5). The loading efficiency and stability of the loaded-EVs differs between these approaches [180].

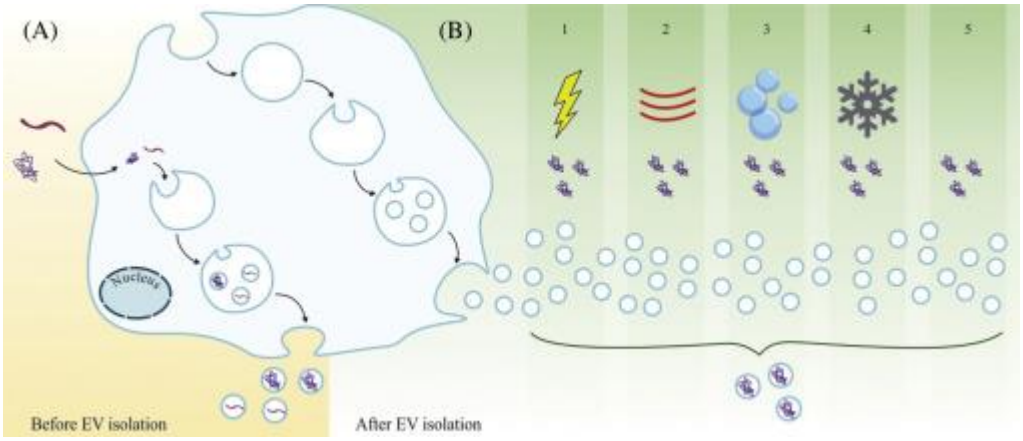


**Figure 3.2:** Overview of extracellular vesicle loading strategies. (A) *In-situ* and (B) *ex-situ* loading methods. The latter include electroporation (1), sonication (2), saponin-treatment (3), freeze-thaw cycles (4) and incubation at room temperature (5). Reproduced from Halder *et al*. [182], with permission from Elsevier Books.

The *ex situ* loading category can further be split into active or passive loading. Passive loading involves the incubation of EVs at room temperature with hydrophobic membrane-permeable molecules such as curcumin [183] or Paclitaxel [184]. This method relies on the hydrophobic cargo in diffusing into EVs and the main disadvantage is that it often results in low loading efficiency [180]. Active loading on the other hand involves permeabilization of the EV membrane using electroporation, sonication, saponin-treatment or repeat freeze-thaw cycles to allow entry of the component to be encapsulated [185] . The loading efficiency and stability of the resultant EVs varies between the different methods[185].

Electroporation is the most frequently reported method in the "*ex-situ*" category, especially for hydrophilic membrane-impermeable components such as a biological cargo [182]. In this approach a small electrical field is applied to EVs suspended in a solution of the desired cargo. This disturbs the phospholipid bilayer of the EVs and forms temporary pores. The therapeutic agent to be loaded then diffuses into the EVs via these pores, and the latter are closed upon recovery of the membrane during an incubation period at 37 °C. This method is widely used for loading silencing RNA (siRNA) or micro RNA (miRNA) into EVs, because these nucleotides are relatively large and cannot diffuse into the EVs spontaneously [180]. Several groups have shown that it is possible to use electroporation to successfully incorporate siRNA into

EVs, and that the RNA-loaded EVs then showed inhibitory effects both *in vitro* and *in vivo* [108,186,187].

Despite reported successes using electroporation to incorporate cargo into EVs, it has several limitations. These include the lack of standardisation of experimental parameters for loading (in terms of EV source, concentration to be used, the cargo molecules to be incorporated (miRNA, siRNA, or plasmids) and the applied electroporation time and voltage) [181]. Moreover, electroporation has been shown to cause both RNA and EV aggregation, resulting in a lower loading efficiency than often reported. More importantly, the effect on the EV membrane and its integrity is not well understood, and may negatively impact the efficacy of these engineered EVs [188]. Additionally, the final product contains loaded-EVs, unloaded-EVs and excess un-incorporated therapeutic agent, which needs to be removed in a subsequent purification step. A classical purification step would involve further ultracentrifugation at 120 000 g for 70 minutes [189]. From prior personal research experience, this does not successfully remove the majority of the residual solution drug cargo, which can affect the measurement of loading efficiency as well as functional performance assays.

The *in-situ* strategy has been more extensively used to load EVs with biological cargos such RNA [190,191] and enzymes [126,192]. It is the preferred strategy because EVs are natural carriers of such material, and loading of the therapeutic cargo can be achieved by making use of the natural EV biogenesis process [181,193]. This simplifies the loading process, as transfected producer cells that overexpress a certain therapeutic cargo will produce EVs containing this. There is no need for any additional purification step after the standard EV isolation protocol. This results in no consequent loss of material, and no detrimental effects on membrane stability and biological activity.

Targeting EVs to specific tissues can also be achieved through this *in-situ* loading strategy. This is typically executed by creating a plasmid construct containing two sequences fused together. The first sequence is responsible for targeting a specific tissue, and the second sequence codes for a component that is enriched in EVs (such as CD63 or

glycosylphosphatidylinositol (GPI)-anchored proteins) [109]. When this plasmid construct is consequently used to transfect EV producer cells, the component that is enriched in EVs results in the concomitant expression of the tissue targeting moiety on EVs during their biogenesis [109]. This has been demonstrated by multiple research groups; for example, Alvarez-Erviti *et al*. [108] genetically modified producer cells with a vector containing a fusion of lysosome-associated membrane protein 2 (Lamp2b, found abundantly in EV membranes) with the rabies viral glycoprotein (RVG) peptide. This led to the production of EVs with Lamp2b-RVG on their surface as seen in Fig. 3.3.

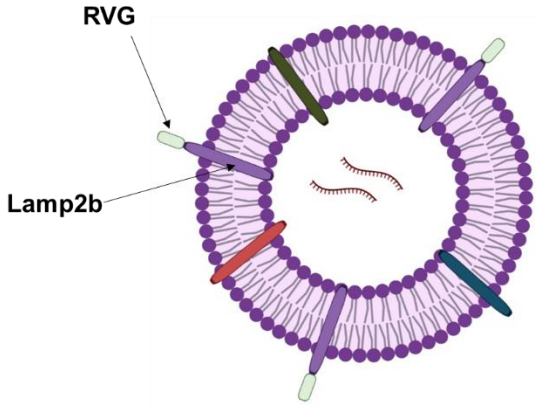


**Figure 3.3**: Illustration of EVs with Lamp2b-RVG fusion on their surface. Created using Biorender.com

The RVG peptide in this case provided targeting to the central nervous system following systemic injection in mice, because RVG binds specifically to the acetylcholine receptors on neurons, oligodendrocytes and microglia. These EVs delivered the siRNA cargo incorporated in them primarily to neurones, microglia and oligodendrocytes, where they resulted in significant knockdown of complementary mRNA. Another targeting example was developed by Kooijmans *et al*. [194]. Here, a plasmid construct containing a sequence coding for nanobodies that specifically target the epidermal growth factor receptor (EGFR) were fused to a sequence coding for GPI-anchored peptides enriched in EVs. The EVs produced displayed GPI-linked nanobodies on their surface and during *in vitro* uptake assays showed improved binding to EGFR-expressing tumour cells than EVs without this targeting property.

Thus far, the genetic modification of producer cells to produce EVs loaded with a therapeutic cargo or targeting moieties has almost exclusively been achieved by transfection of the cells with plasmids. Here, the expression of the gene of interest is transient, as the plasmid is not incorporated into the genome of the cells and exists episomally. Hence, the overall levels of expression reduce every time the cells divide as the plasmid becomes diluted out. This means that to generate loaded or targeted EVs in a reproducible manner the cells have to be transfected prior to every harvest. As a result, the process is laborious and also not assuredly reproducible. An alternative strategy that could circumvent this problem is the use of lentiviral vectors to deliver the desired genes to producer cells. In this case, the lentiviral vector can integrate a gene of interest into a cell's genome. Therefore, all subsequent progeny cells will carry a copy of the gene. This enables the generation of a "factory" of genetically modified producer cells that constantly produce loaded-EVs as they grow and divide. This is the strategy we will employ here when producing loaded-EVs.

## 3.2 Aims and objectives

The underlying aim of this chapter is to produce EVs loaded with marker genes for the enhanced Green Fluoroscent Protein (*eGFP*) and luciferase. Two lentiviral vectors (VSV.G.CMV.eGFP.WPRE and VSV.G.SFFV.LUC.2A.eGFP.WPRE) will be produced and used to transduce HEK-293T and THP-1 cell lines, and also bone marrow mesenchymal stem cells (BMSCs). Cells with the highest transduction efficiency will be taken forward for production of loaded-EVs, which will be characterised for size, concentration, eGFP content and luciferase activity.

## 3.3 Results and discussion

### 3.3.1 Lentiviral production and titration

As explained in **Section 2.3**, lentiviral vectors are produced through triple transfection of HEK293T cells with a packaging plasmid, a transfer plasmid that contains the gene of interest and an envelope plasmid. Fig. 3.4 shows the expression cassette in the transfer plasmids used to make the two lentiviral

vectors produced in this study. The first plasmid was used to make the VSV.G.SFFV.LUC.2A.eGFP.WPRE lentiviral vector (Fig. 3.4a). Here the ubiquitous spleen focus forming virus (SFFV) promoter was used to drive the expression of the luciferase gene (Luc) and the downstream enhanced green fluorescent protein (*eGFP*) gene. The 2A element is a self-cleaving linker and when this is translated it results in an 18–22 amino acid long peptide that induces ribosomal skipping during translation [195]. As a result, no peptide bond is formed between eGFP and luciferase. The exact mechanism of skipping not known but its presence between luciferase and eGFP allows both genes to be expressed from the same SFFV promoter [195]. The second plasmid was used to make the VSV.G.CMV.eGFP.WPRE lentiviral vector (Fig. 3.4b). This contained the mammalian cytomegalovirus (CMV) promoter driving the expression of eGFP. The presence of the woodchuck hepatitis virus post-transcriptional regulatory element (*WPRE*) in both constructs is to stabilise mRNA expression and enhance gene expression, as previously reported [196].

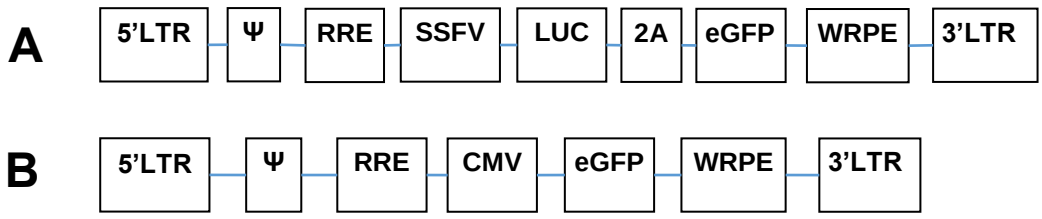


**Figure 3.4** A schematic of the lentiviral transfer plasmids used to make vectors that deliver a) luciferase and eGFP genes or b) eGFP gene only. 5' and 3'LTRs - long terminal repeats, Ψ - psi packaging sequence, RRE - rev response element, SSFV - spleen focus forming virus, CMV - cytomegalovirus, LUC - luciferase, 2A - self cleaving element, eGFP - enhanced green fluorescent protein and WPRE - woodchuck hepatitis virus posttranscriptional regulatory element.

Lentiviral titer was obtained by quantification of the viral envelope protein p24 using the p24 assay. This revealed high titres of 1.1 x $10^9$ vp/ml for VSV.G.SFFV.LUC.2A.eGFP.WPRE and 2.8 x $10^9$ vp/ml for VSV.G.CMV.eGFP.WPRE.

### 3.3.2 Gene delivery to HEK293T and THP-1 cells

First, we sought to determine the transduction efficiency of HEK293T, THP-1 and BMSC [197]. Thus, only HEK293T and THP-1 cells were transduced with

the lentiviral vector at different MOIs. The two lentiviral vectors were explored because sometimes when *eGFP* is the second gene in the vector (as in VSV.G.SFFV.LUC.2A.eGFP.WPRE), it does not get expressed well in cells. Thus, a second vector containing *eGFP* only was prepared (VSVG.CMV.eGFP.WPRE) to serve as a control. Different MOIs were used to determine the optimal ratio for transduction. To confirm successful transduction, fluorescence microscopy was employed to visualise eGFP expression, and flow cytometry performed to quantify the percentage of eGFP expressing cells.

#### *3.3.2.1 Fluorescence microscopy*

72 hours post transduction of HEK293T and THP-1 cell lines, eGFP expression was visualised using fluorescence microscopy (Fig. 3.5a-b and Fig. 3.6a-b). Generally, eGFP expression was observed both in the cytoplasm and nucleus of the cells, indicating that the HEK293T and THP-1 cells had been effectively transduced (Fig. 3.5a-b and Fig. 3.6a-b). No eGFP expression could be seen in control non-transduced HEK293T cells (Fig. 3.5ai, 3.5bi), and as the MOI increased, the levels of eGFP expression in the cells also increased (Fig. 3.5aii-iv and 3.5bii-iv). The strongest fluorescence was obtained when an MOI of 100 was used (Fig. 3.5aiv and 3.5biv).

Similar results were observed for THP-1 cells (Fig. 3.6a-b), although non-transduced THP1 cells were slightly autofluoroscent (Fig. 3.6ai and Fig. 3.6bi). All cells looked healthy and continued to divide and grow post transduction. No distinguishable difference in eGFP expression can be observed in the microscopy images of cells transduced with either of the two lentiviral vectors

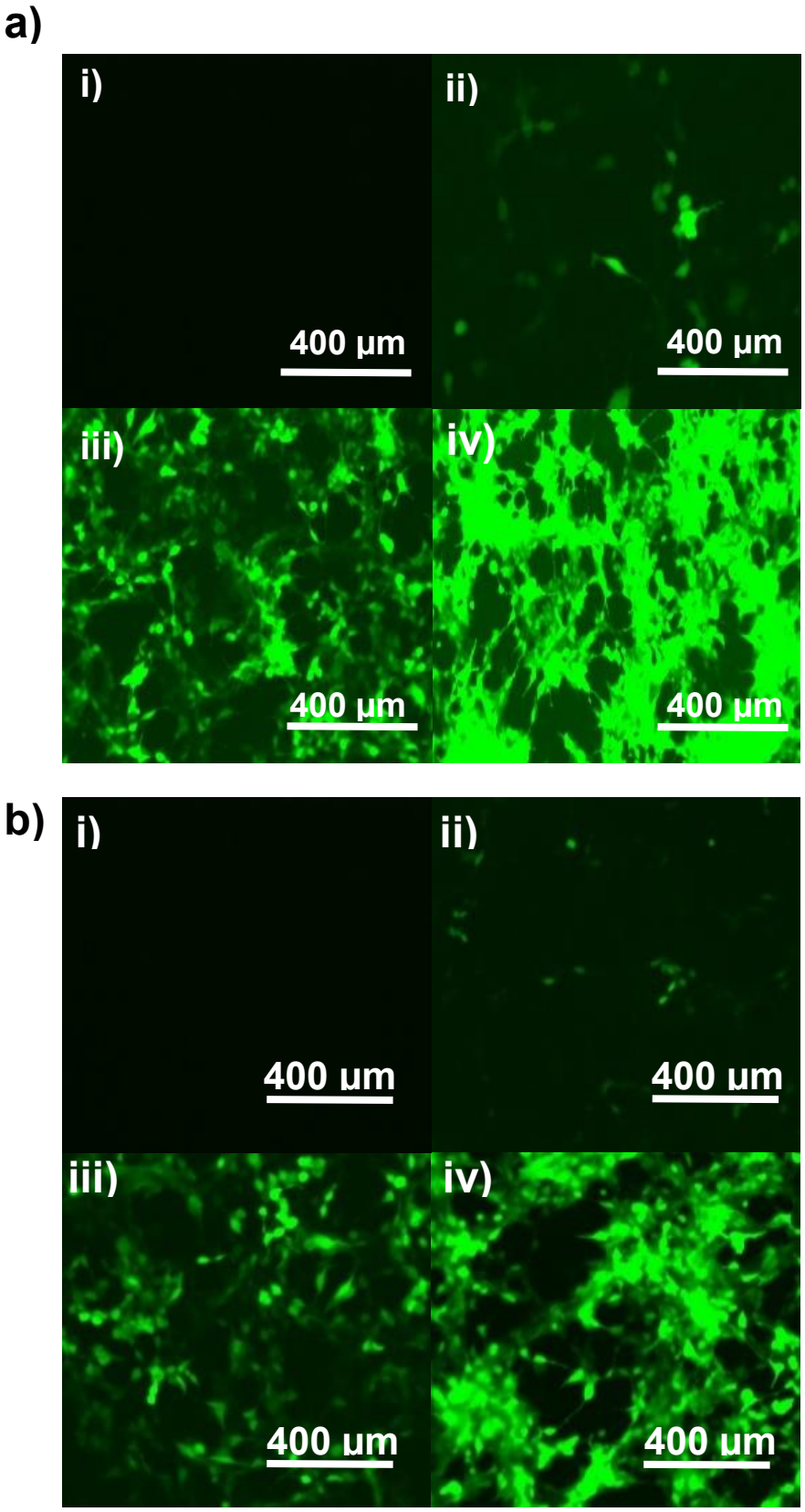


**Figure 3.5:** Representative images showing eGFP expression in HEK293T cells 72 h post transduction with a) VSV.G.SFFV.LUC.2A.GFP.WPRE and b) VSV.G.CMV.eGFP.WPRE. Panels: i) control non-transduced cells, and ii-iv) cells transduced at MOI of 1, 10 and 100 respectively.

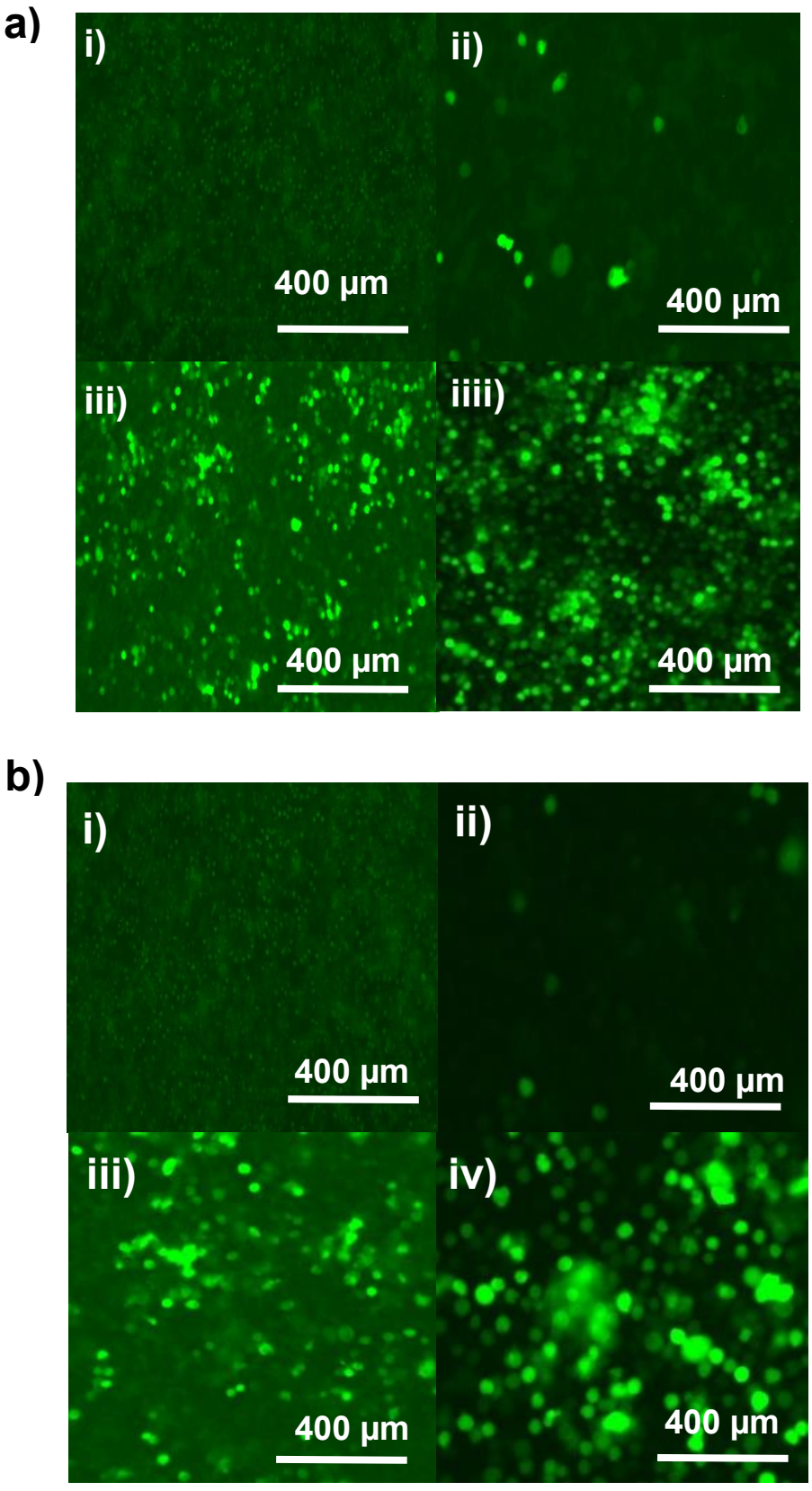


**Figure 3.6:** GFP expression in THP-1 cells 72 h post transduction with a) VSV.G.SFFV.LUC.2A.GFP.WPRE and b) VSV.G.CMV.eGFP.WPRE. Panels: i) control non-transduced cells, and ii-iv) cells transduced at MOI of 1, 10 and 100 respectively.

### *3.3.2.2 Flow cytometry*

To quantify the percentage of cells that were successfully transduced using the flow cytometer, first non-transduced cells were run through the machine to establish background fluorescence and enable gates to be set for data acquisition. This is illustrated in Fig. 3.7. A gate or threshold is set to the right of the peak corresponding to non-fluorescent and non-transduced cells, and any cells that lie beyond this threshold are registered as fluorescent or eGFP positive.

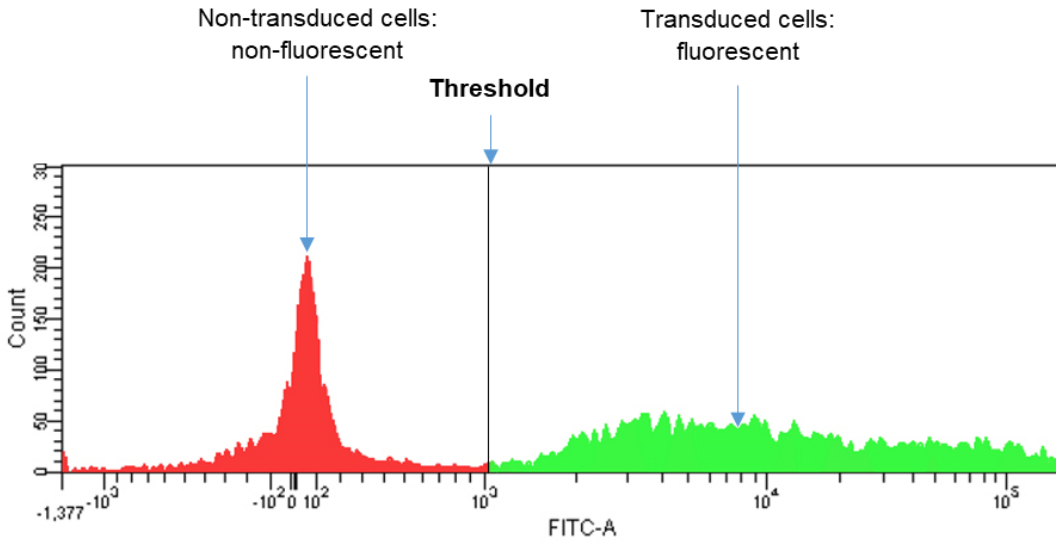


**Figure 3. 7:** An example of a histogram generated using the MACSQuantify software, showing non-transduced/non-fluorescent cells and transduced/fluorescent cells with an appropriate threshold/gate.

Fig. 3.8 shows the transduction efficiency of HEK293T and THP-1 cells after treatment with the VSV.G.CMV.eGFP.WPRE lentiviral vector. The flow cytometry data confirm the earlier fluorescence microscopy findings. A higher MOI results in a greater percentage of eGFP positive HEK293T and THP-1 cells. Moreover, Fig. 3.8 reveals that at all MOIs the percentage of eGFP positive HEK293T cells is significantly higher than that of eGFP positive THP-1 cells. The percentage of eGFP positive HEK293T cells at an MOI of 100 is 94 ± 3 % whereas for THP-1 cells this value is 78 ± 1 %. Thus, we can conclude that with the VSV.G.CMV.eGFP.WPRE lentiviral vector HEK 293T cells have a higher transduction efficiency than THP-1 cells.

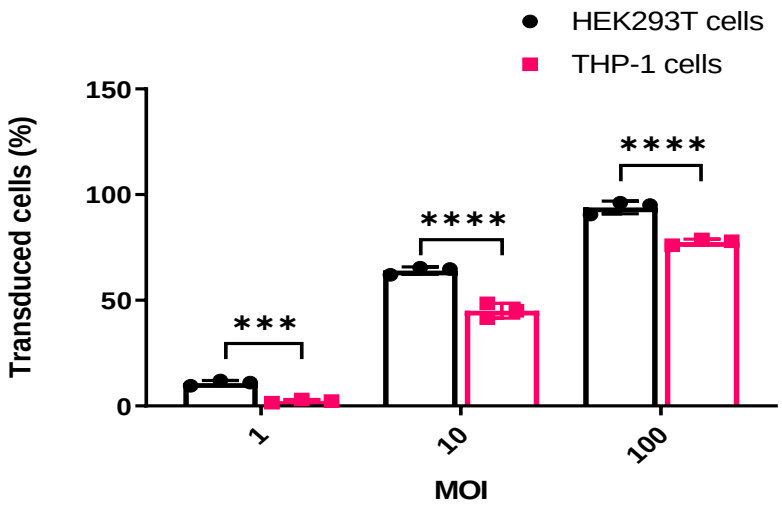


**Figure 3.8:** Transduction efficiency of HEK293T and THP-1 cells treated with the VSV.G.CMV.eGFP.WPRE lentiviral vector at different MOIs. Three independent experiments were performed and data are presented as mean ± SD. Statistical analysis: two-way ANOVA, Tukey's multiple comparisons test, ***p ≤ 0.001, ****p < 0.0001.

The transduction efficiency of HEK293T cells treated at MOI100 with the VSV.G.SFFV.LUC.2A.eGFP.WPRE lentiviral vector was next measured. As can be seen from Fig. 3.9 there is no significant difference between the transduction efficiency with the two vectors. Therefore, we chose to proceed with HEK293T cells transduced with VSV.G.SFFV.LUC.2A.eGFP.WPRE at MOI100 for further experiments, as this will allow us to produce EVs loaded with both luciferase and eGFP. This choice was based on the higher trandsuction efficiency of HEK293T cells, but also on the fact that they give high yields of EVs in the size range of 40-150 nm (See **Appendix I**) and are easy to handle (relative to THP-1 cells where it is more difficult to determine if they have reached confluence, given they grow in suspension) for mass production of EVs. Moreover, published data support their use for the production of EVs that can be isolated, characterised efficiently, and employed for the delivery of a variety of biomolecules (e.g. mRNA) [198,199]. Finally, the immunogenicity of HEK293T cell-derived EVs has been shown to be minimal both *in vivo* [110] and *in vitro* [46]. In contrast, with THP-1 EVs there are contradictory data on whether they induce an inflammatory response [200,201].

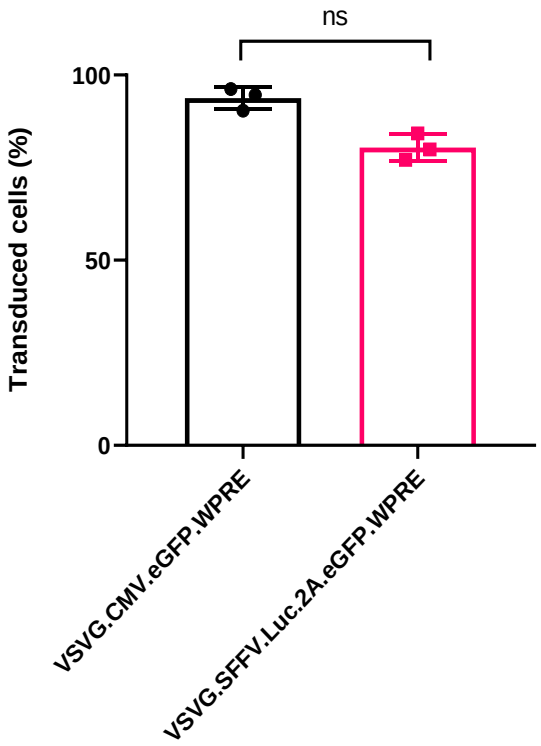


**Figure 3.9:** Transduction efficiency of HEK293T cells with the two lentiviral vectors at MOI100. Three independent experiments were performed and data are presented as mean ± SD. Statistical analysis: Mann Whitney test, ns denotes $p > 0.05$.

### *3.3.2.3 Cell sorting to enrich eGFP in loaded EVs*

FACs analysis was used to select cells with the highest expression of eGFP and sort them into single cell colonies. As can be seen from Fig. 3.10 single cells from the P3 population where cells express a high amount of eGFP were sorted into single cell colonies in a 96 well plate. A colony was then propagated to give appropriately high cell numbers for EV production.

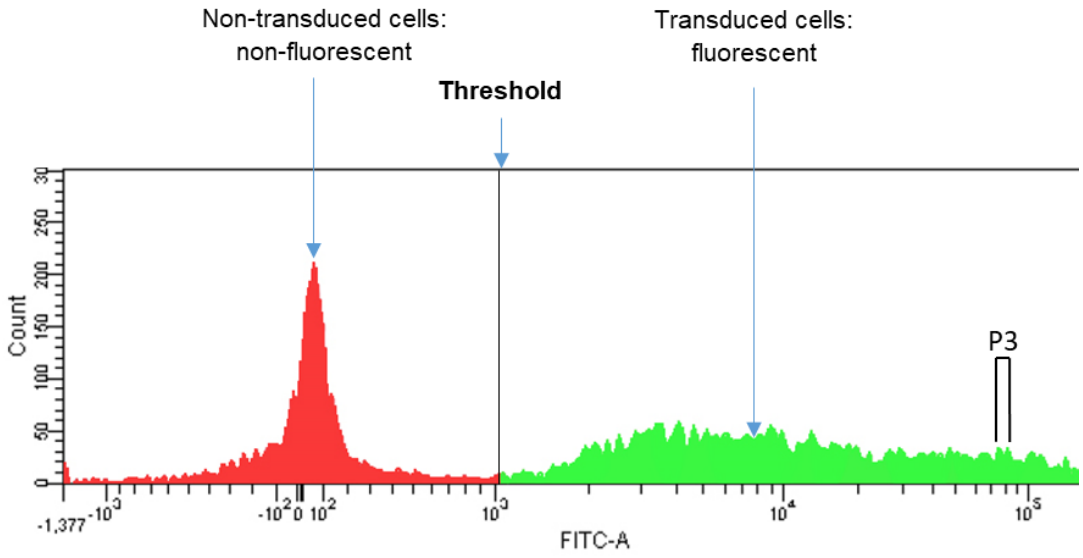


**Figure 3. 10**: An example of a histogram generated using the MACSQuantify software, showing non-transduced/non-fluorescent cells and transduced/fluorescent cells with an appropriate threshold/gate, where P3 represents the population from which cells were sorted into single cell colonies.

Cell sorting in this case ensures that all the progeny used in the production of EVs are genetically identical, express a high amount of eGFP, and thus results in reproducible EV product. As can be seen from fluorescent microscopy images (Fig. 3.11), cells derived from the sorted cells have much higher eGFP expression than non-sorted cells. It is thus expected that these cells will also produce EVs with a higher eGFP content. From here onwards, unless otherwise stated, loaded-EVs are those that have been produced and isolated from sorted HEK293T cells transduced with VSV.G.SFFV.LUC.2A.eGFP.WPRE at MOI100. These loaded-EVs should contain both luciferase and eGFP. Also, unless otherwise stated, naïve EVs are those produced and isolated from non-transduced HEK293T cells.

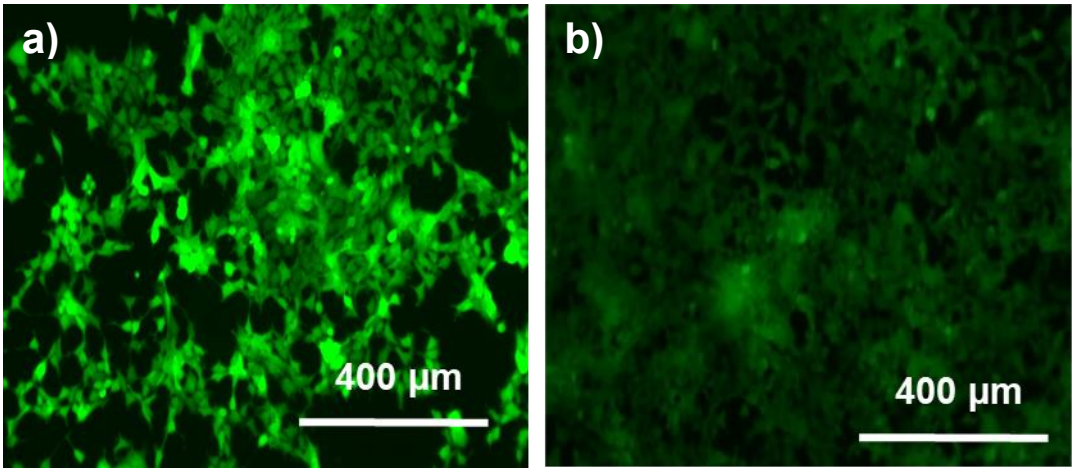


**Figure 3.11:** Fluorescent microscopy images of HEK293T cells transduced with VSV.G.SFFV.LUC.2A.eGFP.WPRE at MOI of 100: a) sorted cells, b) non-sorted cells.

## 3.3.3 Production of EV-free media

### *3.3.3.1 Depletion of EVs from FBS*

When isolating EVs from conditioned cell culture media there are a series of experimental requirements that must be considered. An important issue is the abundant presence of EVs in the FBS that is typically used to supplement cell culture media [147,202]. This means that the pellet from any downstream EV isolation will contain a proportion of EVs derived from FBS, as has been observed by various groups working in the field [152,153]. As shown by Lötvall *et al*. [176], FBS-derived EVs can also influence cell phenotype; thus, to avoid eventual contamination of the final product, with FBS-derived EVs, several options have been proposed in the literature. Three of these are evaluated to establish the optimal route for the cells used in this study (Fig. 3.12).

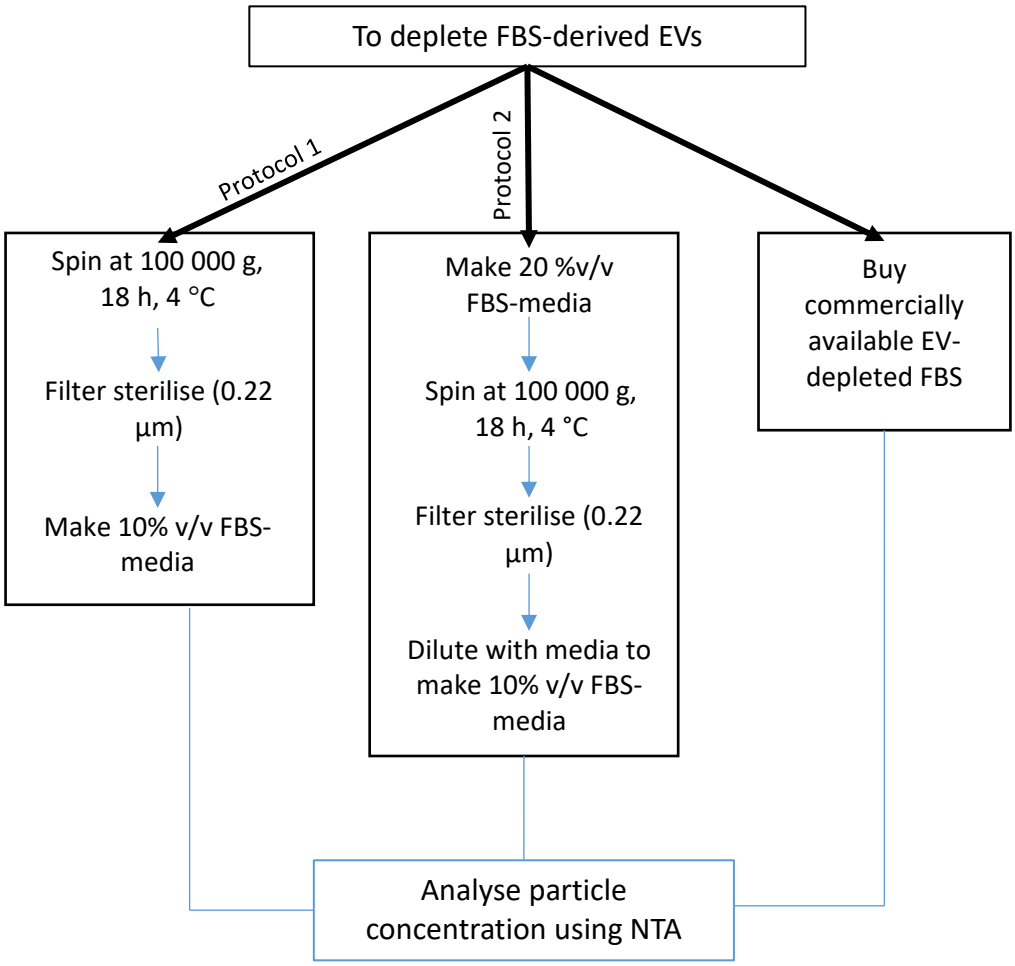


**Figure 3.12:** Illustration of the different routes explored to obtain EV-depleted FBS media.

Fig. 3.13 shows the size distribution of particles in the different media, as measured by NTA. Standard media with 10 % v/v FBS contains a large number of particles in the size range of 50-200 nm, whereas the media obtained from protocols 1 and 2 have considerably fewer particles. Freshly opened, non-augmented, cell culture medium also contains a small number of particles that resemble EVs in size.

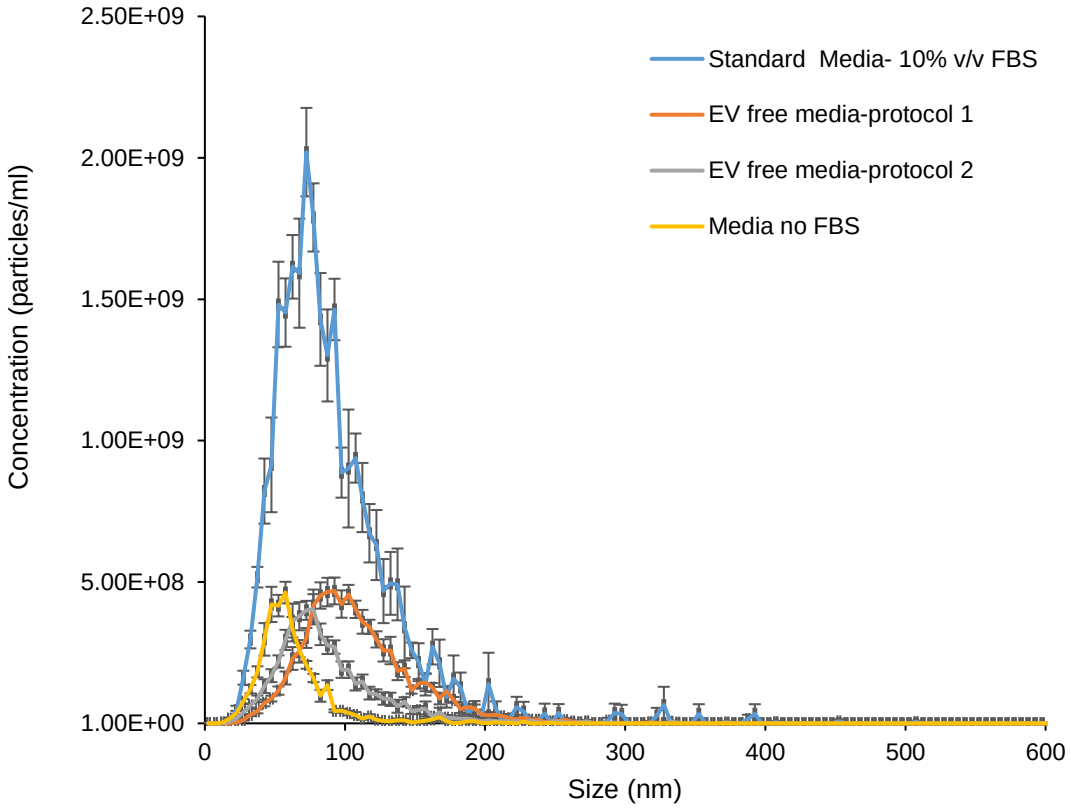


**Figure 3.13:** NTA profiles obtained with different media, showing the size distribution of particles and their relative frequency in standard 10 % v/v FBS media, EV-free media produced using protocol 1 and 2 and media with no FBS. Data presented as mean ± SD, N=5.

From Fig. 3.14 we can conclude that using protocol 1 for depletion results in media that has 77 % fewer particles, whereas using protocol 2 results leads to 90 % fewer particles in comparison to standard 10 % v/v FBS-media. These results are consistent with the literature [153,176]. Although both protocols result in media with significantly fewer particles ($p<0.0001$) in comparison to standard media, they are time consuming and laborious; therefore, using commercially available EV-free FBS was considered as a possible alternative.

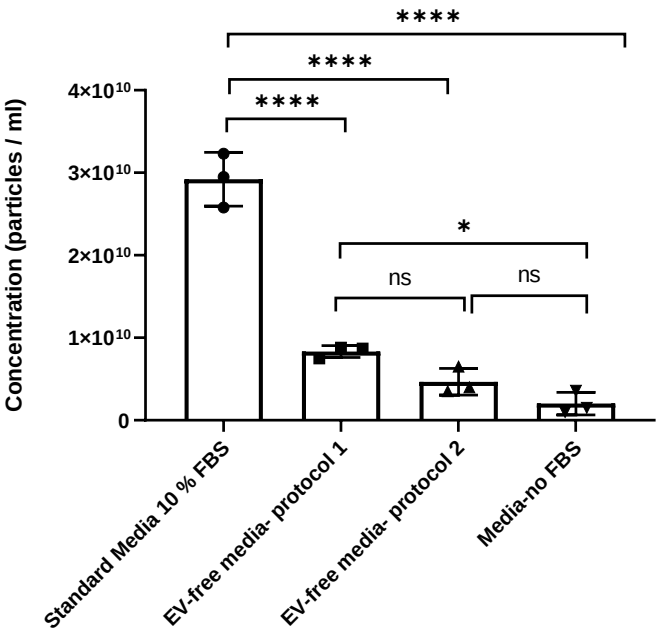


**Figure 3.14:** Particle concentrations in the different media as measured by NTA. Data presented as mean ± SD. Statistical analysis: one-way ANOVA, Tukey's multiple comparisons test; ns $p > 0.05$, *$p < 0.05$, ****$p < 0.0001$.

However, upon analysis of this commercial EV-free FBS it was revealed (Fig. 3.15) that there are a significant number of particles in the size range of EVs. This may be an isolated incident where the FBS supplied was contaminated, but highlights the importance of confirming the presence of EV-sized particles in such products. The commercial EV-free FBS was hence not taken forward.

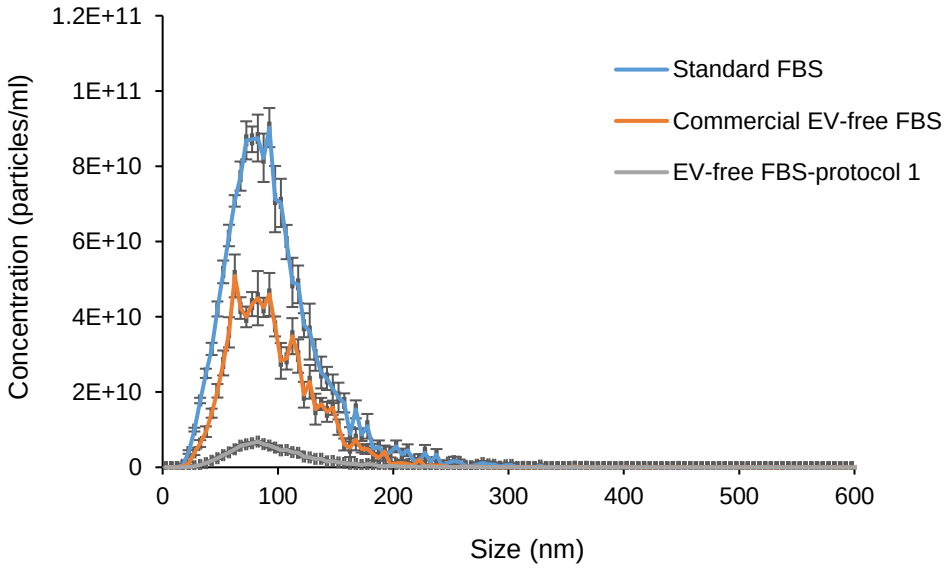


**Figure 3.15:** NTA profiles for different media, showing the size distribution of particles and their relative frequency. Data presented as mean ± SD, N=5.

### *3.3.3.2 Cell viability*

The cell viability of HEK293T cells grown in media supplemented with 10 % v/v FBS from differences sources was measured using the CellTiter-Glo® luminescent cell viability assay. This assay relies on the generation of a luminescent signal proportional to the amount of ATP. Since the amount of ATP is proportional to the number of metabolically active cells present in culture, the luminescent signal can be used as an indicator of cell viability. As can be seen from Fig. 3.16, the viability of transduced HEK293T cells after 48 hours incubation in EV-free media prepared using protocol 2 is similar to that of cells grown in standard 10 % v/v FBS media, but significantly higher ($p<0.05$) than that of cells grown in EV-free media prepared using protocol 1. A plausible explanation for this is that when raw FBS is subject to centrifugation the high viscosity of FBS will cause the elimination of many components such as proteins, which will pellet as aggregates that have been suggested to negatively affect the cell viability [153]. The viability of both transduced and non-transduced cells grown without FBS is significantly reduced (Fig. 3.16), which is as expected for adherent cells: FBS provides major functions in cell culture such as hormone factors for cell growth and proliferation, essential nutrients, trace elements, adherence and extension factors [203]. Non-transduced cells grow faster than transduced cells in all conditions, which could be due to the high lentiviral MOI used to deliver the reporter genes.

Overall, the EV-free FBS produced using protocol 2 gives the best results and thus will be taken forward for use to produce EVs.

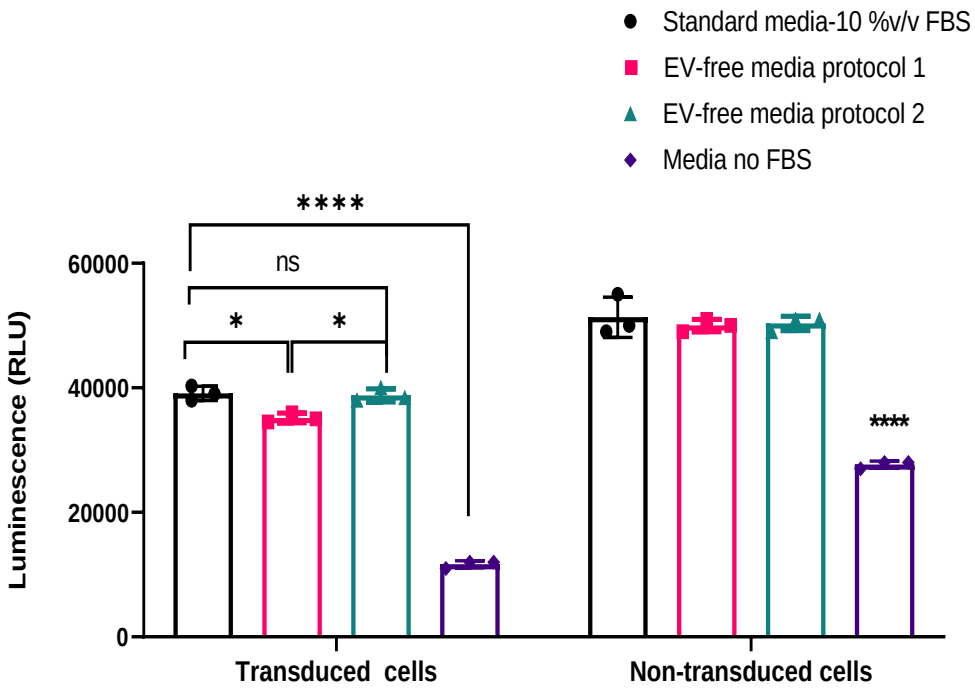


**Figure 3.16:** The cell viability assay of sorted-transduced and non-transduced HEK293T cells gown in media with different sources of FBS. Three independent experiments were performed and data presented as mean ± SD. Statistical analysis: two-way ANOVA, Tukey's multiple comparison test, ns $p > 0.05$, *$p < 0.05$.

### 3.3.4 Isolation of EVs

As previously explained, EVs represent only a small fraction of the components present in culture medium. As differential ultracentrifugation is the most widely used method for isolation of EVs, and the impact of high centrifugal forces on EV size and integrity has been proven to be negligible [204]. Different isolation protocols were explored and the concentration, modal and mean size of the final EV product obtained following each isolation protocol was determined using NTA, as described in **Section 2.5.1**. The NTA camera captures a video file of the particles moving under Brownian motion. Each individual particle is identified and tracked by the software, which allows for determination of its mean squared displacement that is in turn used to calculate its theoretical hydrodynamic diameter using the Stokes-Einstein equation (Equation 3.1) [205].

**(Equation 3.1)**

$$d_H = \frac{kT}{3\pi \eta D}$$

Equation 3.1: The Stokes-Einstein equation, used to calculate the hydrodyanamic size of EVs moving under Brownian motion. dH –hydrodynamic diameter (m), k-Boltzmann constant (J/K=kg·m2 /s2 ·K), T- temperature (K), ŋ – solvent viscosity (kg/m·s) and D – diffusion coefficient (m2 /s).

From this the software then generates a summary file with the mean and modal size of particles in the sample analysed. The mean size of the particles given by the software is equal to the average size of all particles in the sample whereas the modal size is the most common particles size observed in the sample analysed [205]. Moreover, as the sample volume analysed is known, this allows the software to determine the concentration of particles in the suspension [205].

Fig. 3.17 shows the different isolation protocols evaluated. Protocol 1 is most commonly used in isolation of EVs and we explored different variations of this protocol to establish one with the highest efficiency of isolating vesicles within the size range of EVs. Protocols 2-4 resulted in isolation of EV pellets with a mean size higher than 150 nm, and were thus abandoned early on. The final protocol 5 however resulted in pellets with mean sizes less than 150 nm and was further explored in detail.

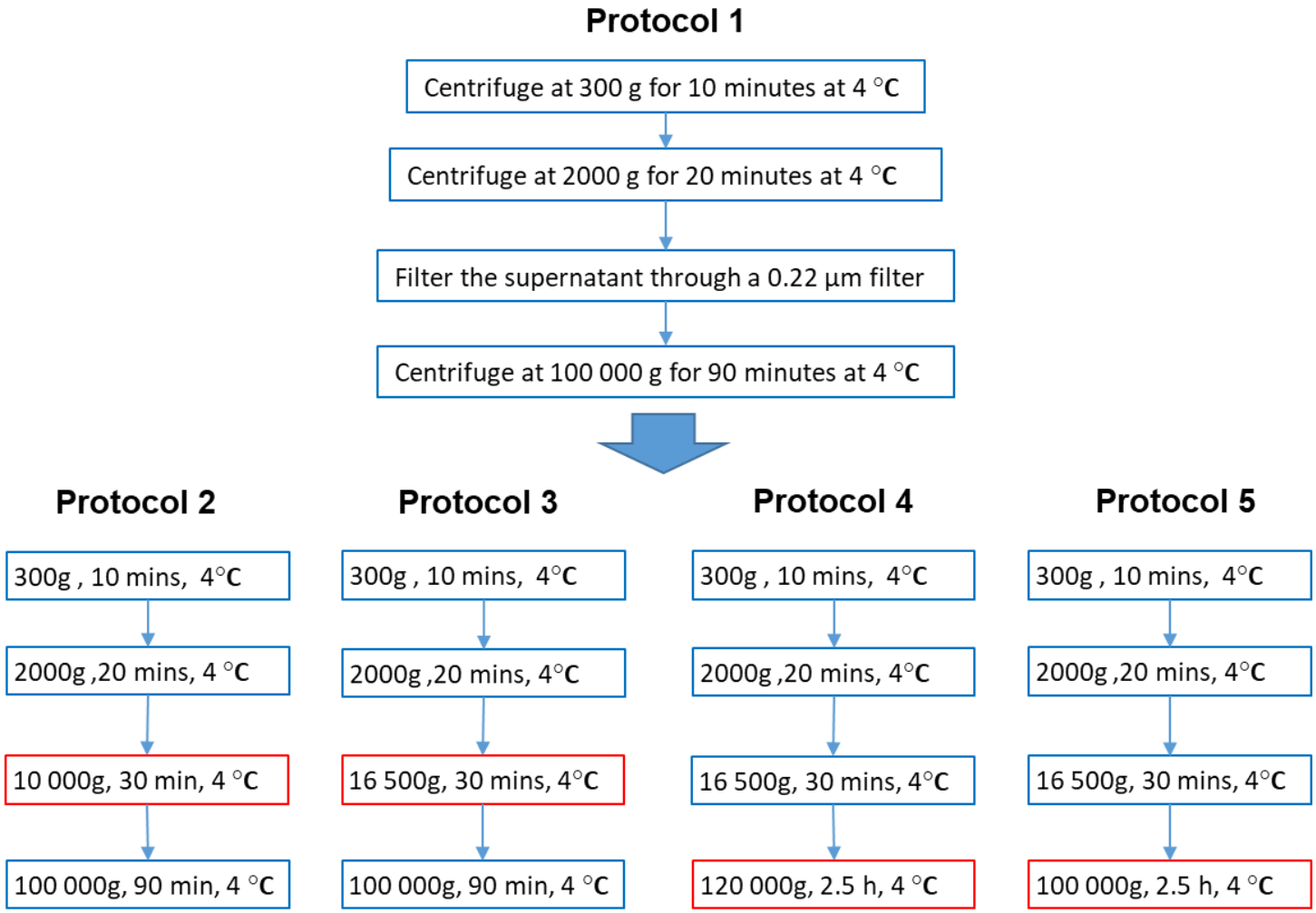


**Figure 3.17:** Schematic describing the isolation protocols explored. Stepwise alternations to the initial protocol 1 were executed to reach the final protocol 5

### *3.3.4.1 Isolation of EVs using protocol 5*

As can be seen from Fig. 3.18a there is a stepwise reduction in the mean size after the different centrifugation steps. The mean size of particles in the final EV pellet is significantly smaller than that in the starting media. Similar results are observed in Fig. 3.18b, which shows the modal size of particles.

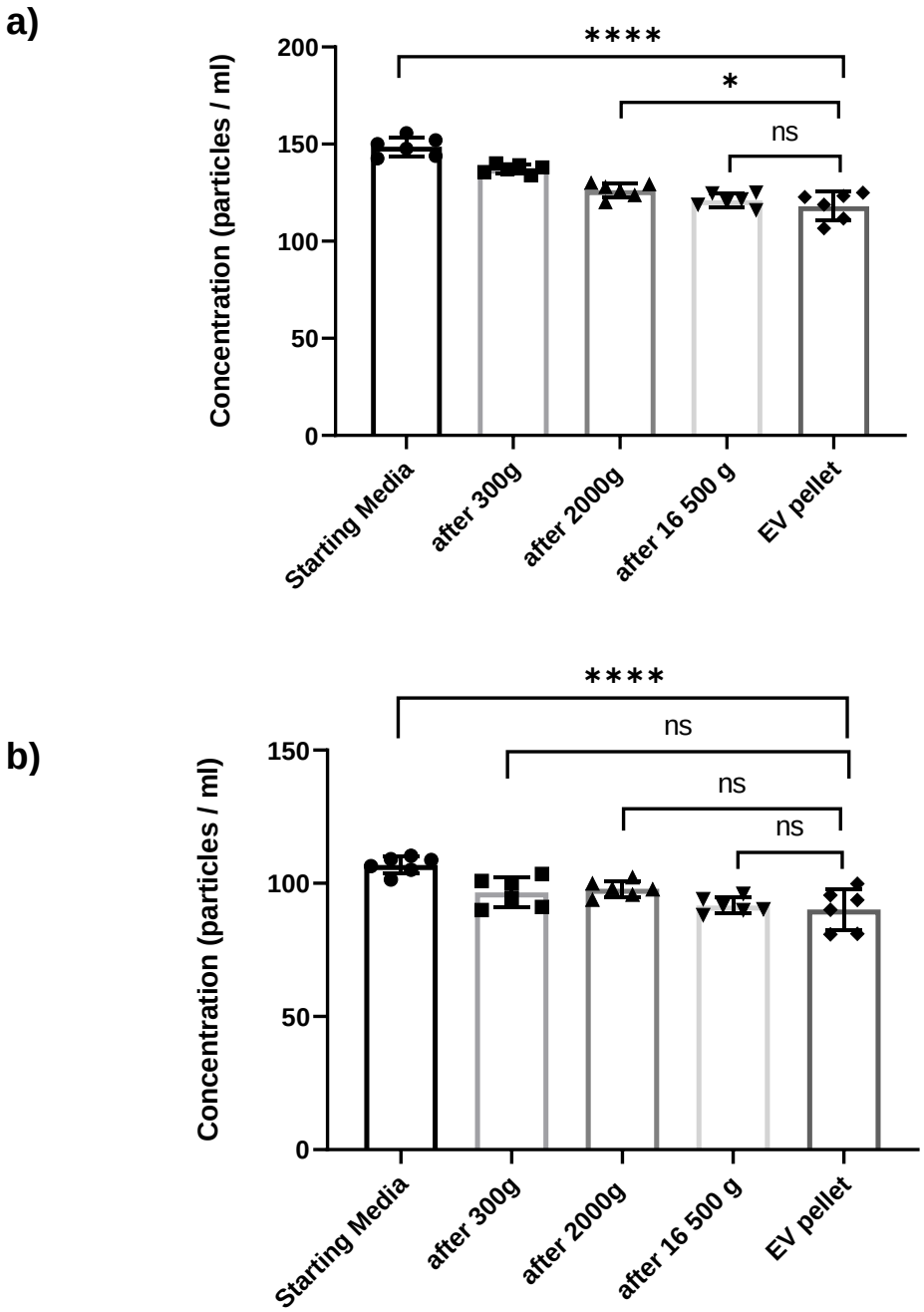


**Figure 3. 18:** The mean (a) and modal sizes (b) of particles in the starting media, supernatant following subsequent centrifugation steps and in the final EV pellet. Six independent experiments were performed and data presented as mean ± SD. Statistical analysis: one-way ANOVA, Tukey's multiple comparison test; ns $p > 0.05$, *$p < 0.05$, ****$p < 0.0001$.

The EV pellets obtained using protocol 5 have a significantly smaller mean size in comparison to those isolated using protocol 1 (115 nm and 130 nm, respectively, Fig. 3.19). Similar results are observed in terms of the modal sizes of these pellets (90 nm and 100 nm, respectively). One potential reason leading to these differences is replacement of the filtration step (through a 0.22 µm membrane filter) with a centrifugation step at 16 500 g.

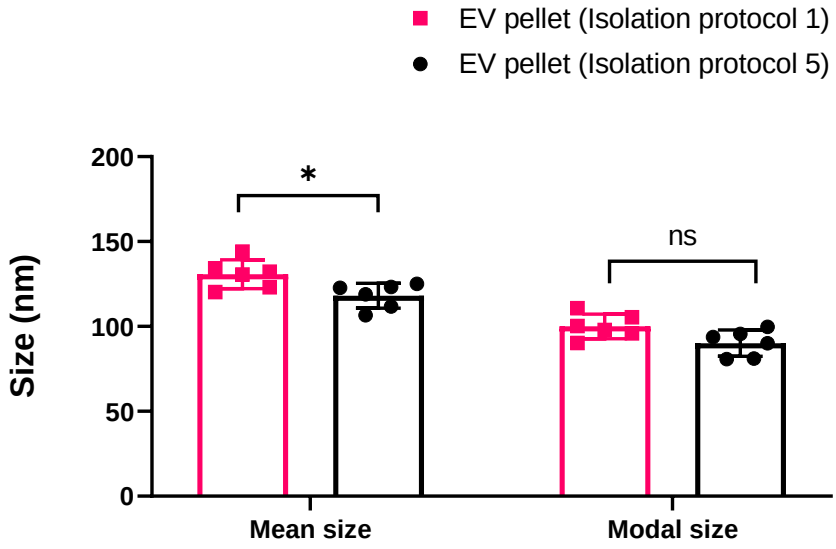


**Figure 3.19:** The mean and modal size of particles in the final EV pellet isolated using protocol 1 and protocol 5, as measured by NTA. Six independent experiments were performed and data presented as mean ± SD. Statistical analysis: two-way ANOVA, Tukey's multiple comparison test; ns $p > 0.05$ and *$p < 0.05$.

In addition to the improvement in mean and modal size obtained using isolation protocol 5 instead of protocol 1, a small but significant increase in the concentration of EVs in the pellet isolated using protocol 5 is observed (Fig 3.20). This is probably due to the longer centrifugation time (2.5 hours instead of just 90 minutes). Therefore, we decided to proceed with protocol 5 for all future EV isolations, as this protocol enabled the isolation of an EV pellet with a small mean and modal size and high particle concentration.

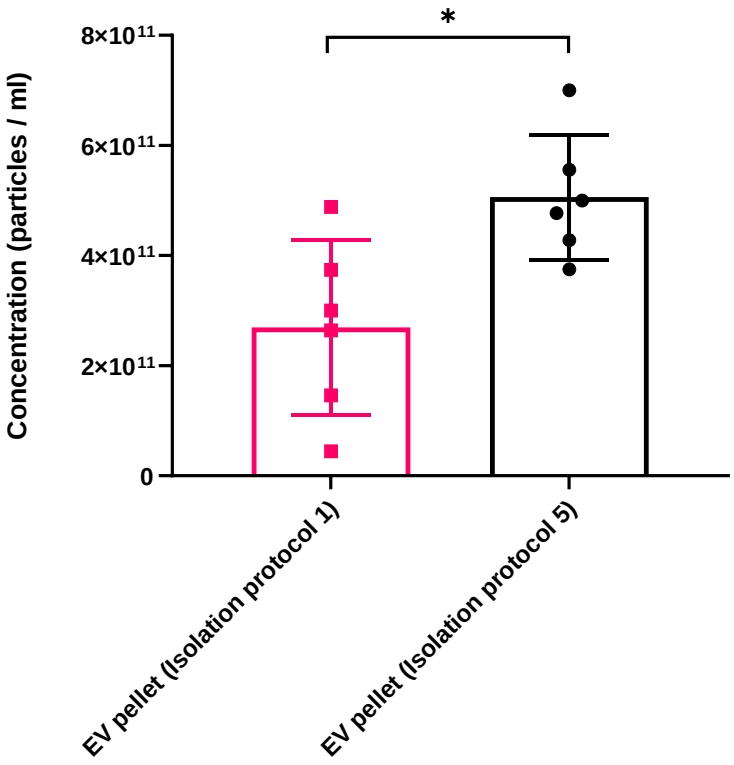


**Figure 3.20:** The concentration of particles as measured by NTA in in the final EV pellets isolated using protocol 1 and 5 following re-suspension in 100 µl of PBS. Six independent experiments were performed and data are presented as mean ± SD. Statistical analysis: unpaired t-test, Welch's correction; *p < 0.05.

### *3.3.4.2 Concentration and further purification of EVs*

To concentrate EVs further, pellets isolated using protocol 5 were pooled together and centrifuged a second time at 100 000 g for 2.5 hours at 4 °C. The concentration and size of the resultant EV pellet was then analysed**.** It was expected based on the literature that this additional ultracentrifugation step would result in a more concentrated EV suspension that was also further purified [153]. However, we were unable to obtain such results reproducibly, and the isolated pellets often did not have higher concentrations and smaller mean size, and complete loss of the pellet was also observed. Similar results were observed by Webber and Clayton [206], who demonstrated that washing the EV pellet using a second ultracentrifugation step decreased the EV yield. These losses were attributed to the incomplete sedimentation and aggregation in the pellet during this step; correspondingly, the fraction isolated does not significantly differ in its purity from that obtained without additional washing.

Thus to obtain a suspension with a higher concentration of EVs we resorted to suspending 6 isolated pellets in the 300 µl of PBS, instead of suspending each pellet separately in 100 µl of PBS.

## 3.3.5 Characterisation of loaded-EVs

### *3.3.5.1 Size and concentration*

Following establishment of the optimal isolation protocol, the size and concentration of loaded-EVs derived from sorted cells were characterised and compared to naive EVs and loaded-EVs from non-sorted transduced HEK293T cells (Fig. 3.21).

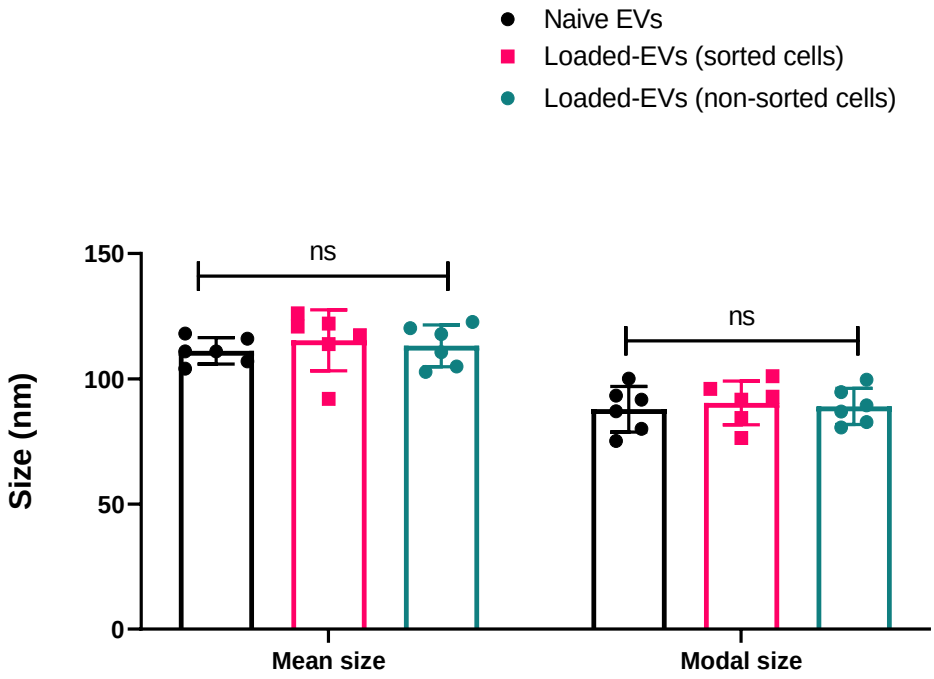


**Figure 3.21:** The mean and mode size of particles in different EV pellets. Six independent experiments were performed and data are presented as mean ± SD. Statistical analysis: two-way ANOVA, Tukey's multiple comparison test; ns denotes $p > 0.05$.

Both the mean and mode size of naive EVs appear smaller than those of the loaded-EVs. However, this difference is not statistically significant. Both mean and mode for all EV preparations are below the 150 nm upper size limit normally considered for EVs. The concentration of naive EVs in the pellet is higher than that of loaded-EVs (Fig. 3.22), but again this is not statistically significant.

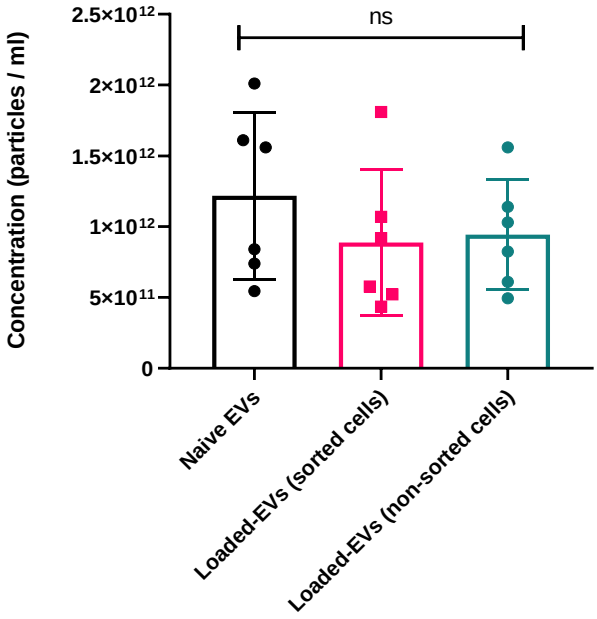


**Figure 3.22**: The concentration of particles in different EV pellets following re-suspension in 300 µl of PBS. Six independent experiments were performed and data are presented as mean ± SD. Statistical analysis: one-way ANOVA, Tukey's multiple comparison test; ns denotes $p > 0.05$

### *3.3.5.2 TEM*

As previously stated (**Section 3.1.2**) at least two different but complementary techniques should be used to characterise EVs. Therefore, in addition to NTA we also preformed TEM analysis. Conventional TEM (whole-mount negative staining method) was used in this study. This results in dehydration of EVs and hence cup-shaped membrane vesicles are observed (Fig. 3.23) [41,207–209] instead of the round-shapes seen in cryo-TEM (which does not dehydrate the EVs) [208,210,211] . The vesicles observed in the TEM images in Fig. 3.23 display a diameter in the range of 40-100 nm, corresponding to that expected for EVs, and in agreement with the size observed by NTA analysis.

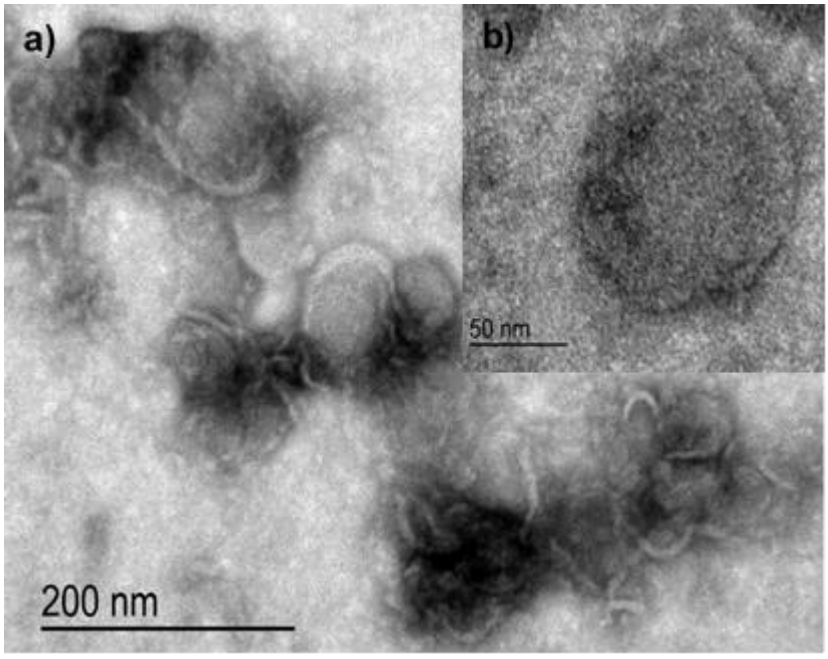


**Figure 3.23:** Representative TEM images of loaded-EVs. Magnification for image a - 20 000X and magnification for image b – 40 000X.

### *3.3.5.3 Evaluation of EV protein content*

*Protein analysis using western blot*

During the initial stages of this study, traditional western blot analysis was used to evaluate the presence of markers enriched in EVs. The quality of the results obtained was variable. Therefore, the simple western method was used instead. This technology is completely automated and eliminates several factors (such as process variability, blot transfer and manual analysis) that can often negatively impact the reproducibility and quality of the data [212,213]. Moreover, the fact that very small volumes of antibodies (10 µl) are used in simple western enabled us to use very low dilutions of primary antibodies and hence increase the sensitivity of the blot.

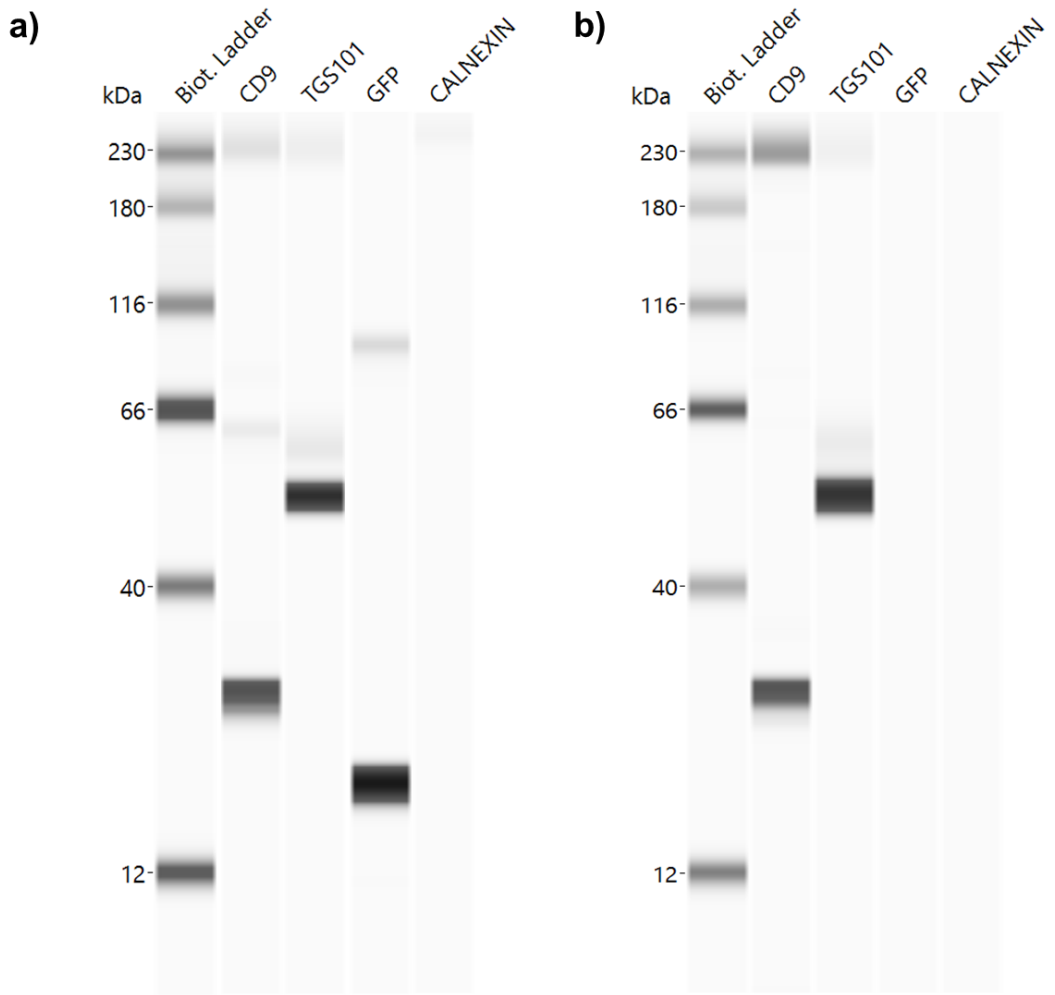


**Figure 3.24:** Detection of the EV targets CD9 and TSG101, eGFP, and the endoplasmic reticulum vesicle marker Calnexin as analysed by simple western blotting of a) loaded-EVs and b) naïve EVs derived from HEK293T cells.

Fig. 3.24 gives a representative Western blot obtained for loaded-EVs and naïve EVs. The presence of the transmembrane protein CD9 in both preparations analysed is diagnostic for the lipid bilayer of EVs, and the presence of cytosolic TSG101 confirms that these lipid bilayer structures enclose intracellular material [86]. Fig. 3.24a also shows a positive band for eGFP in the loaded-EVs which is not visible for naïve EVs (Fig. 3.24b). We also note the absence of Calnexin in both EV preparations, which would appear as a band at approximately 90 kDa. This observation signifies that there are no contaminating vesicles from the endoplasmic reticulum (which are sometimes co-isolated with EVs).

*Quantification of eGFP content in loaded-EVs*

GFP ELISA was used to quantify the eGFP content of EVs derived from transduced and sorted, transduced and non-sorted, and naïve HEK293T cells (see Fig. 3.25). The eGFP concentration in EVs derived from transduced and sorted cells is significantly higher (0.17 ng/$10^9$ particles) than that in EVs derived from transduced non-sorted cells (0.013 ng/$10^9$ particles). Naïve EVs contained no eGFP, as expected given it is not an intrinsic mammalian protein.

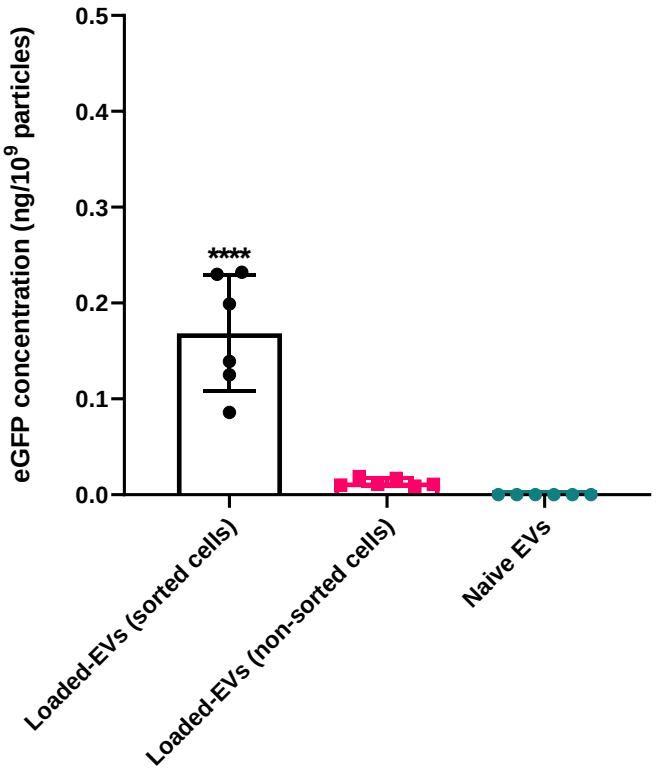


**Figure 3.25:** eGFP concentration in different EV preparations from HEK293T cells. Six independent experiments were performed and data are presented as mean ± SD. Statistical analysis: one-way ANOVA, Tukey's multiple comparisons test; ****p<0.0001.

The fluorescence microscopy images presented earlier (Fig. 3.11) revealed that the sorted cells have much higher eGFP expression than non-sorted cells. In the latter case, even when an MOI of 100 was used the transfected cells have a wide distribution of virus integration events. Thus, the mean amount of eGFP per EV in the non-sorted cells is correspondingly low. The use of sorted cells to produce EVs will also ensure homogeneity of EV populations, as all producer cells will have been derived from that same single cell colony.

### *3.3.5.4 Total RNA isolation*

Recent studies have demonstrated that EVs are not only specifically targeted to recipient cells to exchange proteins and lipids or to trigger downstream signaling events, but also to deliver specific nucleic acid cargos for cell communication purposes. They have been shown to be natural carriers of coding and noncoding RNA, including miRNA, with the ability to induce *de novo* transcriptional and translational changes in target cells [56,73,214,215]. For example, Valadi *et al*. [56] demonstrated that MC/9 and human mast cell line-1 cells secrete EVs that contain mRNA from approximately 1300 genes and small RNAs, including 121 unique miRNAs. The transfer of EVs to a donor cell showed that at least some mRNAs were full-length, as they were translated in the recipient cell. Therefore, we set out to confirm whether overexpression of eGFP genes in the cell line leads to the production of EVs that contain eGFP mRNA as well as the protein. The results are given in Fig. 3.26.

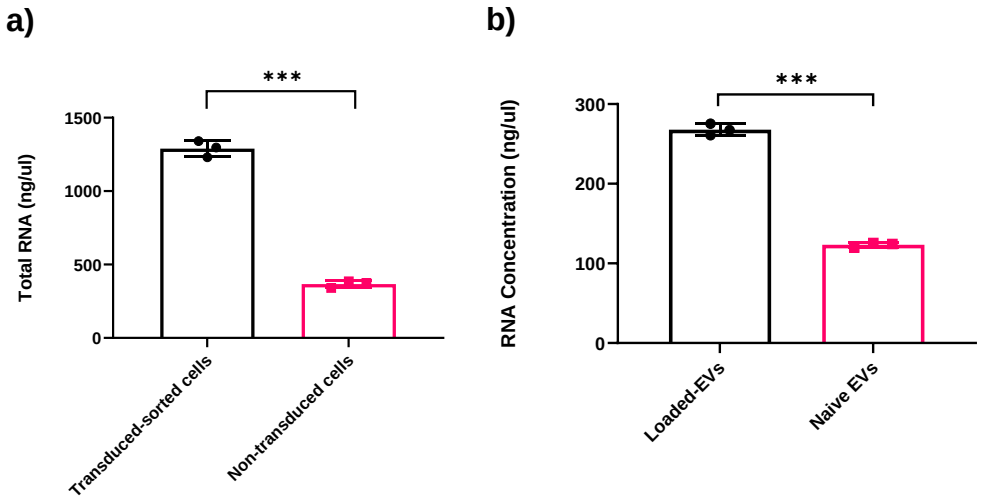


**Figure 3. 26:** RNA concentration in a) transduced-sorted and non-transduced HEK293T cells, and b) loaded EVs and naïve EVs. Three independent experiments were performed and data are presented as mean ± SD. Statistical analysis: unpaired t-test, Welch's correction; ***p<0.001.

From Fig. 3.26a it can be observed that the RNA content in sorted-transduced cells is three times that of non-transduced cells (p<0.001). This was expected, since the overexpression of the eGFP gene will ultimately result in much greater RNA levels. Moreover, the total RNA levels in EVs derived from sorted-transduced cells are more than double those in EVs from non-transduced cells (Fig. 3.26a, p<0.001). This led us to question whether the

increased RNA level could be due the presence of eGFP specific mRNA. This would be of significant importance to the ultimate aim of this project, because it could mean that not only can we deliver the therapeutic enzyme of interest but also the mRNA for that enzyme, which can then be translated into a functional enzyme in the recipient cell. Since the size of the eGFP mRNA is 720 bp long, we proceeded to quantify only the RNAs larger than 200bp (Fig. 3.27).

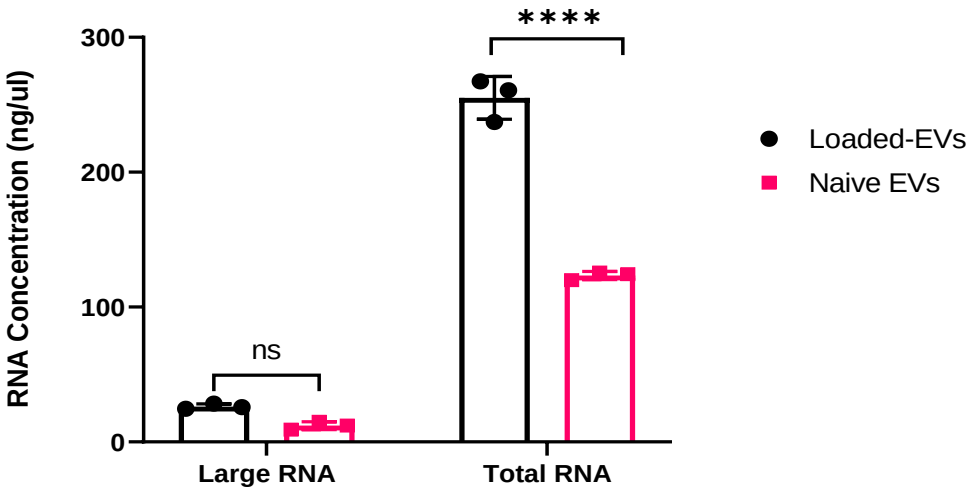


**Figure 3.27:** Large and total RNA concentration in loaded-EVs and naïve EVs. Three independent experiments were performed and data are presented as mean ± SD. Statistical analysis: two-way ANOVA, Sidak's multiple comparison test; ns $p>0.05$, ****$p<0.0001$.

Although the concentration of total RNA is significantly higher in loaded-EVs than in naïve EVs, this is not mirrored in the concentration of large RNAs. The latter is slightly higher in loaded than in naïve EVs, but this difference is not statically significant ($p>0.05$). A plausible assumption is that EVs are more enriched in miRNA and to a lesser extent with mRNA owing to the small size of EVs and numerous other incorporated components. However, to be able to reliably verify whether the above assumption is correct an alternative RNA isolation method than the one used in this study would need to be explored. The RNA isolation method used in the study does not enable isolation of miRNA but only large RNA. Overall, it is not certain whether the overexpression of eGFP genes in transduced cells leads to the incorporation of eGFP mRNA into EVs.

### *3.3.5.5 RT and q-PCR analysis*

To specifically detect for eGFP mRNA, RT and q-PCR were used. Here two different eGFP primers were used in the amplification of eGFP genes, as depicted in Fig. 3.28**.** Primer set 1 and 2 result in amplification of 200 and 100 bp fragements, respectively.

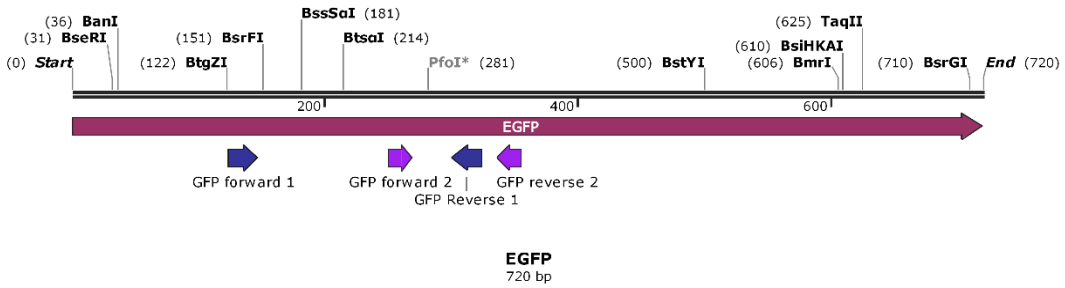


**Figure 3.28:** An illustration of the binding and amplification of eGFP genes using the primer sets 1 and 2. Illustration was generated using the Snap Gene software.

Fig. 3.29a-b show the Ct (cycle threshold) values for the q-PCR analysis of RNA sequences isolated from HEK293T cells and their EVs (the q-PCR amplification plots can be seen in Apendix I Fig. A.I.2). In a q-PCR assay a positive reaction is detected by accumulation of a fluorescent signal. The Ct is defined as the number of cycles required for the fluorescent signal to cross the threshold (i.e. exceed the background level). Ct levels are inversely proportional to the amount of target nucleic acid in the sample (i.e. the lower the Ct level, the greater the amount of target nucleic acid in the sample). Generally, a Ct value of above 30 is considered to signify unsuccessful amplification. The Ct values for the amplification reactions in samples from transduced cells are lower than 30, and signficantly lower than those in naïve cells (Ct value ~30, $p<0.0001$). This shows that the two primers chosen can be used to amplify the eGFP gene without non-specific reactions.

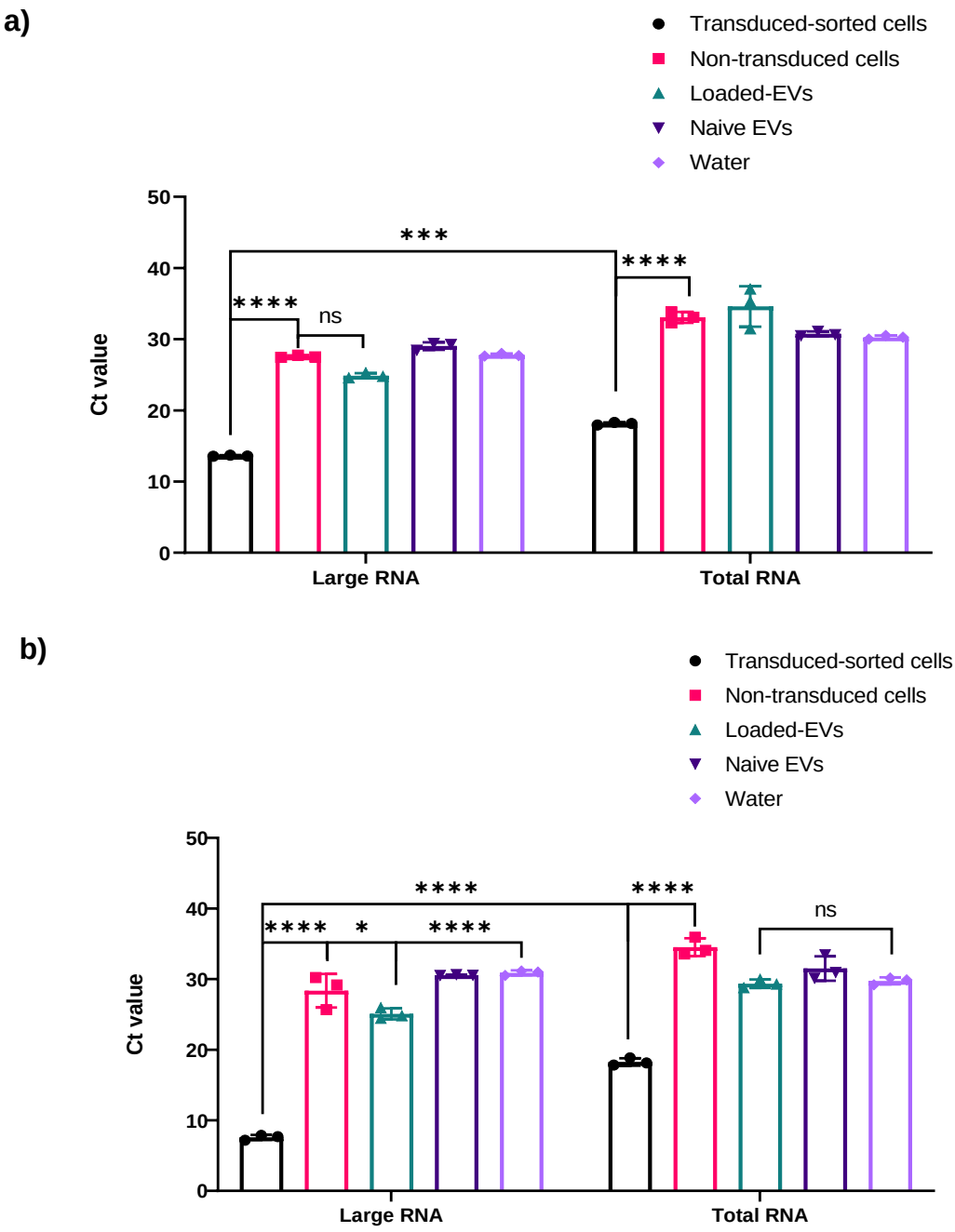


**Figure 3.29:** Ct values of eGFP amplification reactions using a) primer set 1 and b) primer set 2. Two different RNA sources were used: large and total RNA, extracted from sorted-transduced and non-transduced HEK293T cells, EVs derived from the two respective cell sources, and water. Three independent experiments were performed and data presented as mean ± SD. Statistical analysis: two-way ANOVA, Tukey's multiple comparisons test; ns>0.05, *p < 0.05, ***p ≤ 0.001, ****p < 0.0001.

The Ct values for eGFP gene amplification in samples from transduced cells are significantly higher ($p < 0.0001$) when using large RNA as the source for cDNA than when using total RNA, for both primer sets. This can probably be explained because the Ct value is inversely proportional to the amount of target nucleic acid in the sample and so, when using total RNA (which includes

miRNA and mRNA), we are effectively diluting the amount of mRNAs (such as eGFP mRNA) available for amplification. When primer set 1 is used (Fig. 3.29a), the Ct value for samples from loaded-EVs is either not significantly different or higher than that for reactions in non-transduced cell samples that do not have the eGFP gene. This indicates that there is no specific amplification of eGFP genes and hence no eGFP mRNA. When comparing the same Ct values for the amplification reactions but using primer set 2 (Fig. 3.29b), the outcome is slightly different. The Ct value for reactions in samples from loaded-EVs is significantly smaller ($p<0.05$) than that for non-transduced cells, but only when using large RNA as a source for cDNA production. This suggests that that there may be some eGFP mRNA incorporated in the loaded-EVs.

#### *3.3.5.6 Quantification of ATP content in loaded-EVs*

The loaded-EVs are expected to contain both eGFP and luciferase. Before establishing the luciferase activity in these loaded-EVs we needed to establish whether the EVs contain ATP. Currently, there is no published information on whether EVs contain ATP or not. The ATP levels in loaded-EVs need to be established here because ATP is one of the co-factor requirements for the reaction of luciferase enzyme and luciferin substrate (Fig. 3.30).

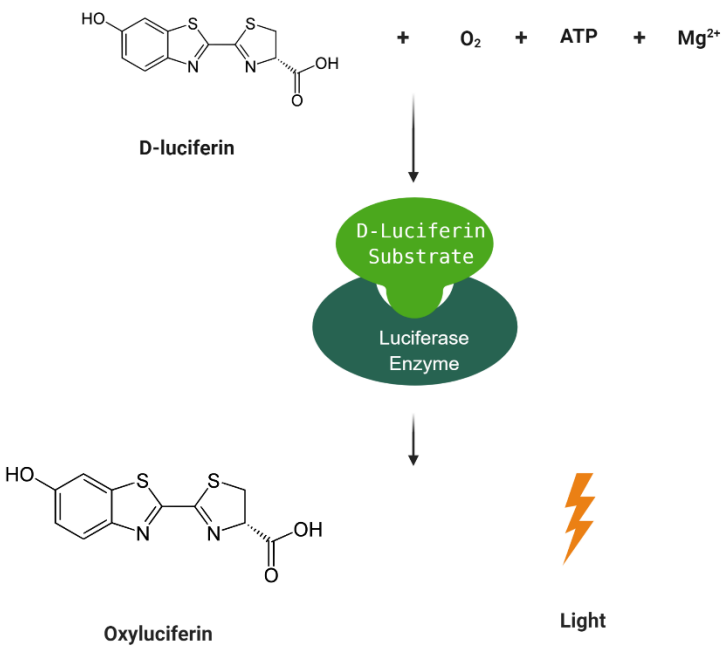


**Figure 3.30:** The bioluminescence reaction of firefly luciferase enzyme and luciferin, in the presence of cofactor requirements (ATP, $O_2$ and $Mg^{2+}$). Created using BioRender.com

The ATP content of EVs was measured and compared to that of cells using the CellTiter-Glo® luminescent cell viability assay, where a linear relationship between luminescence and ATP concentration exists. Fig. 3.31 shows the relative luminescence of EVs compared to that of cells. It can be concluded that there is no ATP in EVs as there is no significant difference in comparison to the negative control, which is the D-luciferin solution. This means that it will be necessary to include ATP when measuring the luciferase content in EVs using a luminescence dependent assay.

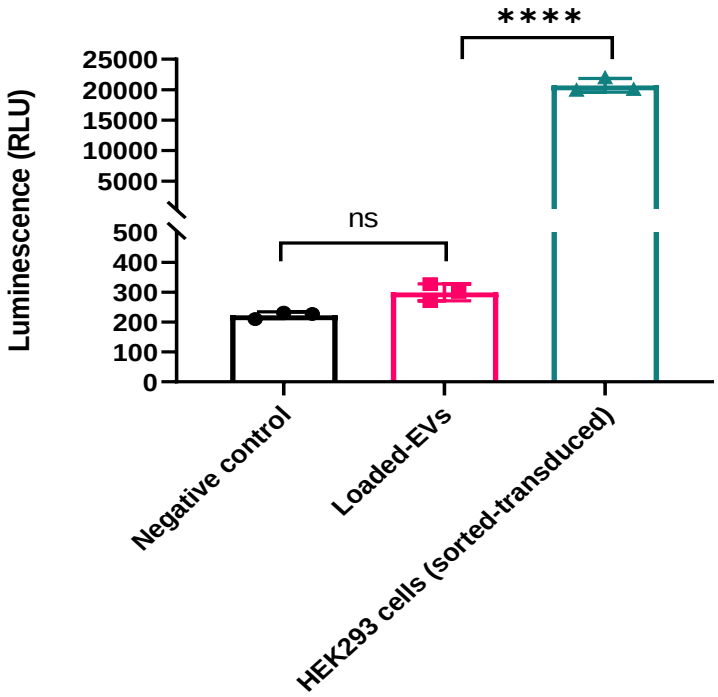


**Figure 3.31:** Luminescence of a negative control, loaded-EVs, and sorted-transduced HEK293T cells as measured using the CellTiter-Glo® assay. Three independent experiments were performed and data are presented as mean ± SD. Statistical analysis: one-way ANOVA; Tukey's multiple comparisons test, ns= $p>0.05$, **** $p<0.0001$.

### *3.3.5.7 Analysis of luciferase content in loaded-EVs*

As briefly described in **Section 3.3.5.6** (Fig. 3.30) the luciferase enzyme converts the substrate luciferin to the luminescent product oxyluciferin in the presence of the co-factors ATP, molecular oxygen and $Mg^{2+}$ ions. This allows for both live imaging of emitted light and also analysis of the luminescence signal using a luminometer. Fig. 3.32 shows the luminescence signals obtained using lysed and non-lysed loaded-EVs and naïve unloaded EVs in the presence of ATP. The luminescence signal measured following lysis of the EVs is significantly higher than that measured without prior lysis. This could be because the luciferin substrate and/or ATP experience difficulty in entering the intact EVs, or the luminescent signal is partially reduced by the EV membrane.

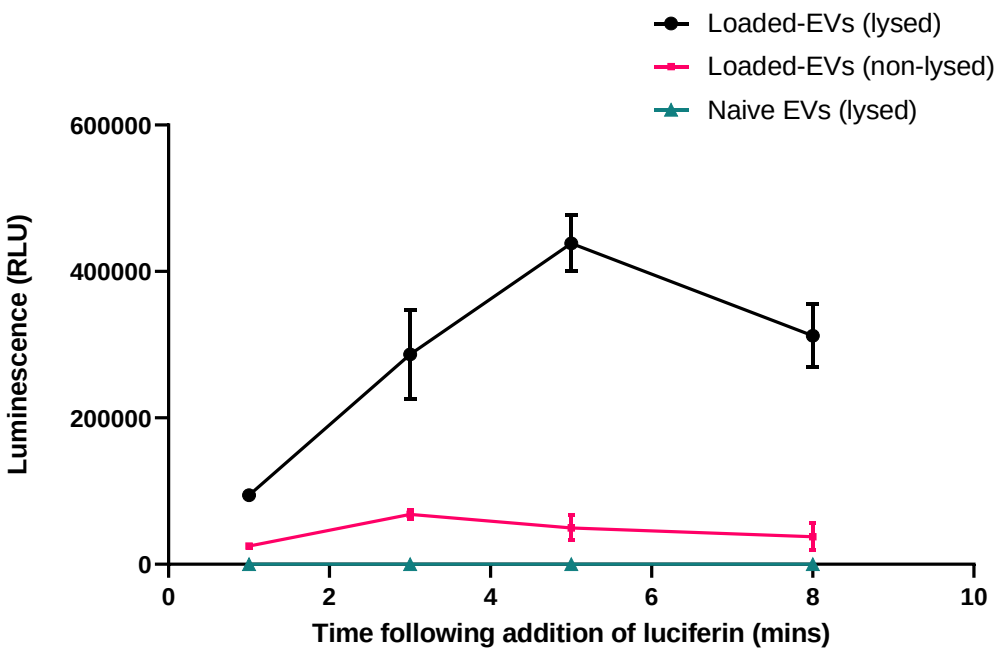


**Figure 3.32:** Luminescent signals of EV samples. Three independent experiments were performed and results are presented as mean ± SD.

These results are very promising and suggest that genetic engineering of HEK293T cells using lentiviral vectors is successful strategy in loading derived EVs with active luciferase enzyme as well as eGFP.

## 3.4 Conclusions

Two lentiviral vectors VSV.G.SFFV.LUC.2A.eGFP.WPRE and VSV.G.CMV.eGFP.WPRE were used to transduce HEK293T, THP1 and BMSC cells. Of these, HEK293T cells had the highest transduction efficiency with the VSV.G.CMV.eGFP.WPRE vector at an MOI 100. There was no significant difference between the eGFP transduction efficiency of HEK293T cells at MOI 100 using both viral vectors. As a result, HEK293T cells transduced with VSV.G.SFFV.LUC.2A.eGFP.WPRE at an MOI of 100 were chosen as producer cells for loaded-EVs containing both eGFP and luciferase. These cells were sorted to ensure high and homogenous eGFP expression. An EV isolation protocol was then optimised. Using this, loaded-EVs were isolated and characterised. They were found to be in the size range of EVs, contain eGFP protein, be positive for the EV markers CD9 and TSG101 and contain active luciferase enzyme. EVs produced from sorted-transduced cells contained a higher amount of eGFP in comparison to non-sorted cells. In conclusion we have successfully developed a platform of cellular factories to produce EVs loaded with a high content of eGFP and active luciferase enzyme. These results are very promising because this platform has the potential to be used to load EVs with various desired cargo. The next chapter will explore ability of these loaded-EVs to deliver cargo *in vitro* and *in vivo*.

# Chapter 4: In vitro and in vivo delivery of cargo by loaded-EVs

## 4.1 Introduction

A large number of studies can be found in the literature to demonstrate that EVs can be used as therapeutics for a variety of conditions, with some studies showing the pathways by which EVs are internalised by cells [95,114,199,216–219]. However, few reports have evaluated EV pharmacokinetics (PK) and tissue distribution following exogenous administration [113,220–222]. These are important parameters to understand because they are crucial to therapeutic efficacy and toxicity [181]. Moreover, as EVs have an extensive biological content (ranging from proteins, RNA, DNA and lipids) that varies depending on cellular source, PK and tissue distribution properties are also likely to vary with the source as well as how the EVs are isolated and purified [43]. It is therefore important to assess whether the HEK293T-derived EVs intended for the purpose of treatment of Gaucher disease Type 2 can be internalised by cells of visceral origin, such as HEK293T cells, primary neurons, and how they are trafficked *in vivo*.

### 4.1.1 Cellular internalisation of EVs

It is widely accepted that EVs can enter cells and deliver biological cargo to serve different functions [56,214,223,224]. Fig. 4.1 shows the possible mechanisms through which EVs can be internalised [225]. Several groups have used specific agents to block individual pathways and study EV internalisation in greater detail [224,226–229]. These studies indicated that the main mechanism through which EVs are internalised is endocytosis. This can be divided into several sub-pathways, such as clathrin-mediated endocytosis, macropinocytosis and phagocytosis. In addition to endocytosis, EVs can also be internalised via direct fusion of the EV membrane with the cell plasma membrane [74,230]. However, the extent at which EVs are internalised through this mechanism is uncertain and requires further evaluation.

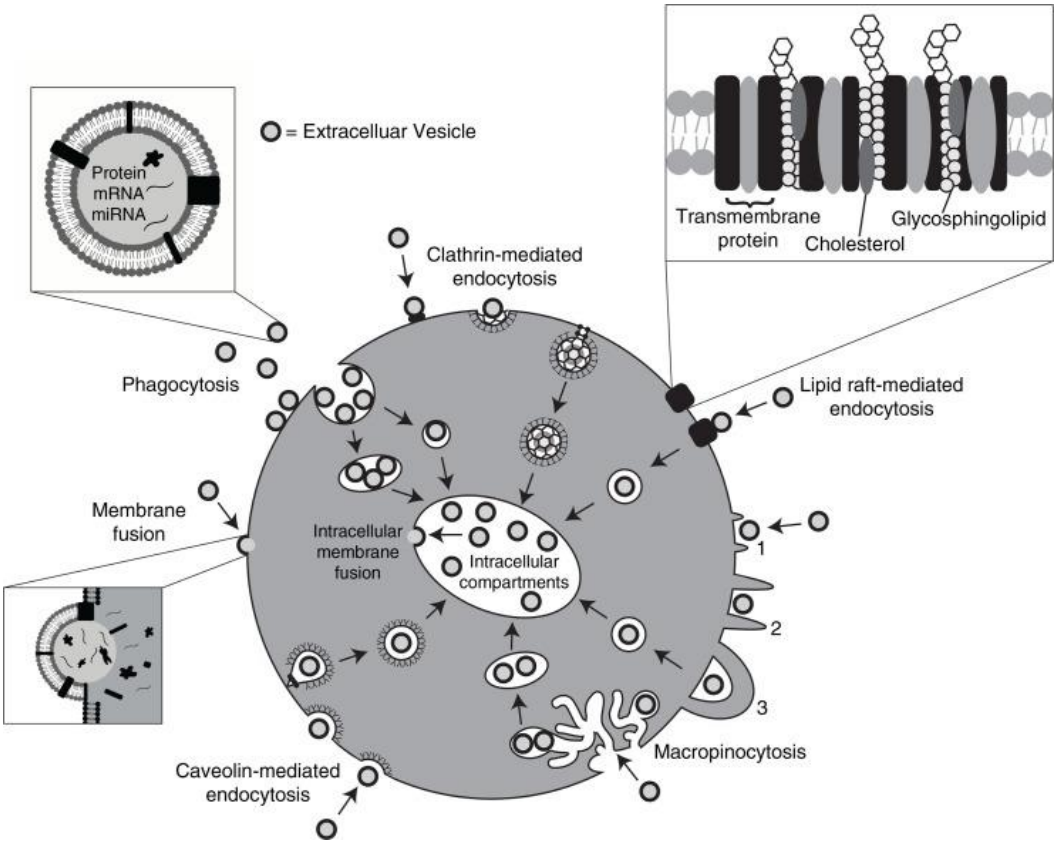


**Figure 4.1:** The routes by which EVs can be internalised by target cells. Taken from Mulcahy *et al*. [225] (Open access journal with Attribution-NonCommercial 3.0 Unported license type, allowing use in this thesis).

No general consensus has been reached on which internalisation mechanism is most significant for EVs, owing to the heterogeneity of the reported results. The differences between the various studies are expected to arise from factors such as the type of EVs, the protein on the EV membrane, and the type of recipient cells used in the study. Different EVs have varied compositions, and internalisation is at least in part governed by the proteins present on the EV surface (e.g. tetraspanins [231], integrins [226] and lectins [224]), which can facilitate uptake via protein-protein interactions. Likewise, internalisation pathways are likely to vary between target cells. Moreover, owing to the lack of standardisation in EV isolation and characterisation, most studies use EV samples with a degree of heterogeneity.

There are at present few studies that evaluate the fate of EVs and incorporated cargo once internalised and the possible underlying mechanisms. Some reports have shown that uptake of EVs occurs in a time and concentration

dependent manner where uptake is first detectable after 3-6 hours, plateauing and attenuating at around 12-24 hours [126,219,232]. Over times, EVs are first found co-localised in endosomes in perinuclear regions, then with the lysosome, possibly where they are degraded [126].

### 4.1.2 *In vivo* biodistribution of EVs

To further the advancement of EVs as therapeutic delivery vehicles, in addition to a better understanding of how they are internalised by target cells we also need to consider PK and tissue distribution. Such information will shed further light on the efficacy and safety of EVs *in vivo*. A limited number of studies have been published in this area, in part because there is a lack of methods to quantitatively evaluate EVs *in vivo* [135]. Almost all studies have been performed using adult mice, and a recent review by Yi *et al*. [222] found that the intravenous route has been most widely explored (Fig. 4.2).

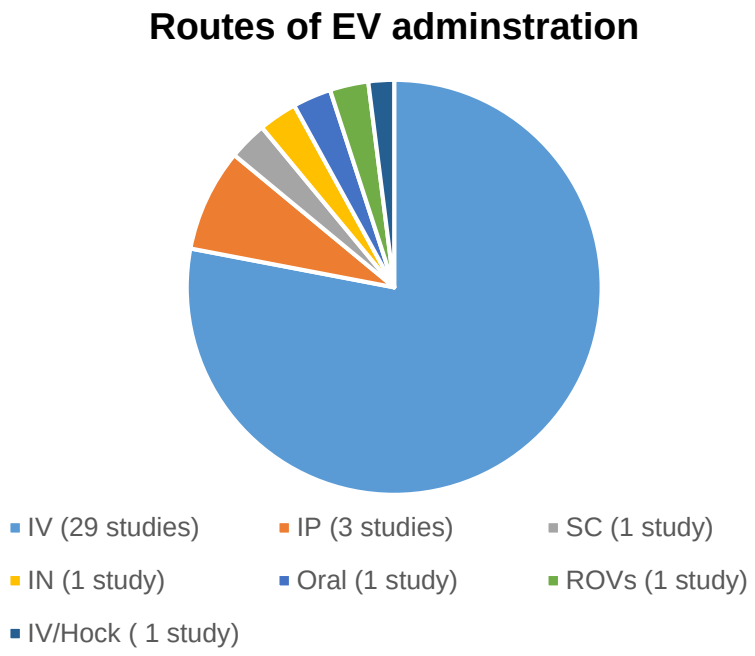


**Figure 4.2:** Routes of administration of EVs in juvenile-adult mice in published studies where IV: intravenous, IP: intraperitoneal, SC: subcutaneous, IN: intranasal and ROVs: retro-orbital venous sinus. Adapted and redrawn from Yi *et al*. [222].

A common observation among all these biodistribution studies is that following intravenous administration EVs will preferentially accumulate in the liver, lung,

spleen and kidney [113,135,222,233]. It is suggested that, in the liver, Kupffer cells (a type of macrophages) are responsible for the majority of uptake and clearance of EVs, with some EVs also being taken up by hepatocytes [234]. EVs being present in the spleen is most likely due to their uptake by circulating lymphocytes in the blood and macrophages, followed by their migration to the spleen [234]. EVs trafficked to the kidney are likely to have been internalised for subsequent excretion in the urine [235], but the reasons underlying their accumulation in the lung are not yet clear [236]. Tissue distribution can also depend on the disease state of the subject [43]. Although the studies discussed above could not demonstrate that EVs make their way to the brain, there is some evidence that EVs are capable of delivering RNA cargo to the brain[108,237].

In contrast to the general consensus on the tissue distribution of EVs, studies detailing the PK of EVs show conflicting results. Some studies have suggested that half-life of EVs following IV administration ranges from 30 to 60 minutes, with complete clearance by 4 hours [135–137,238]. However, others find that EVs are retained in the liver and spleen even 24 hours after administration [199,239]. This variation between the findings is likely a result of differences in the study protocols, such as dose of EVs administered, EV producer cells, and the types and size of the EVs in the final isolate. All these factors can affect internalisation by tissues [109,113,181,236].

## 4.2 Aims and objectives

In Chapter 3, it was shown that EVs loaded with high levels of luciferase and eGFP could be generated via lentiviral transduction of HEK293T cells. This chapter now seeks to evaluate EVs' ability to deliver their cargo *in vitro and in vivo*. *In vitro* bioluminescence assays were used to measure uptake of the loaded-EVs in HEK293T cells, and immunohistochemistry performed to evaluate uptake in primary neurons. To evaluate *in vivo* performance, loaded-EVs were delivered to both neonate and adult mice, using different routes of administration, and the pharmacokinetics and tissue distribution were assessed at different time points.

## 4.3 Results and discussion

### 4.3.1 Delivery of luciferase enzyme to cells of visceral origin

The luminescence of HEK293T cells transduced with the VSV.G.SFFV.LUC.2A.eGFP.WPRE lentiviral vector at MOI100 and subsequently sorted was first assayed using the IVIS® Lumina Series III *in vivo* imaging system. These cells were used to produce loaded-EVs. The luciferase gene is incorporated into the genome of the cells and is continuously transcribed and translated into active luciferase enzyme. Thus, during live imaging of the cells using the IVIS system, when the substrate for the enzyme is added the luminescence signal can be measured. The signal from these cells was extremely high and so the cells could only be imaged for a minimal amount of time (1 second) to prevent signal saturation (Fig. 4.3a). No signal was detectable in control non-transduced cells (Fig. 4.3b) or cell growth media (Fig. 4.3c). These results confirmed successful incorporation of the luciferase gene into HEK293T cells, and that this imaging system can be used to detect luminosity generated by the luciferase enzyme reaction following addition of substrate.

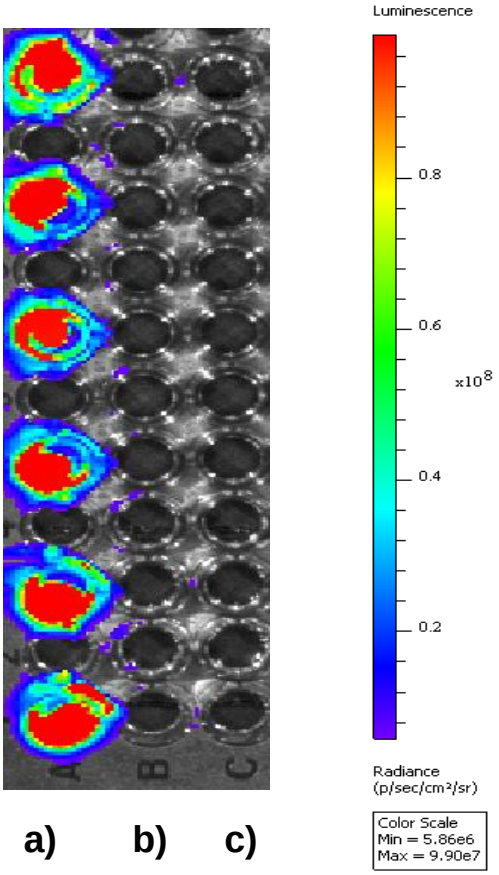


**Figure 4.3**: Bioluminescence image showing luciferase activity in a) sorted-transduced HEK293T cells, b) control non-transduced HEK293T cells and c) the cell growth media. The bioluminescent signal is expressed in photons per second and displayed as an intensity map.

Following establishment of positive control signals (sorted-transduced cells) and negative control signals (non-transduced cells), we analysed the uptake of different volumes (10, 20, 40 µl; concentration 1 x $10^{12}$ particles/ml) of loaded-EVs by HEK293T cells after one hour of incubation. As can be seen from Fig. 4.4a, as the volume of loaded-EVs added increases there is a rise in the luminescence signal observed after 1 minute of imaging. This is expected because as the volume of loaded-EVs added increases, so does the amount of luciferase enzyme delivered to the target cells. Addition of naïve EVs or PBS does not result in a luminescence signal (Fig. 4.4b-c). Further, as the incubation time increases from 1 to 6 hours, the luminescence signal increases by almost 3-fold (Fig. 4.4d, e respectively), whereas incubation of naïve EVs for 6 hours still does not result in any luminescent signal (Fig.4.4f). This rise is due to the greater extent of internalisation of EVs over time, which has been reported by other studies [225,240].

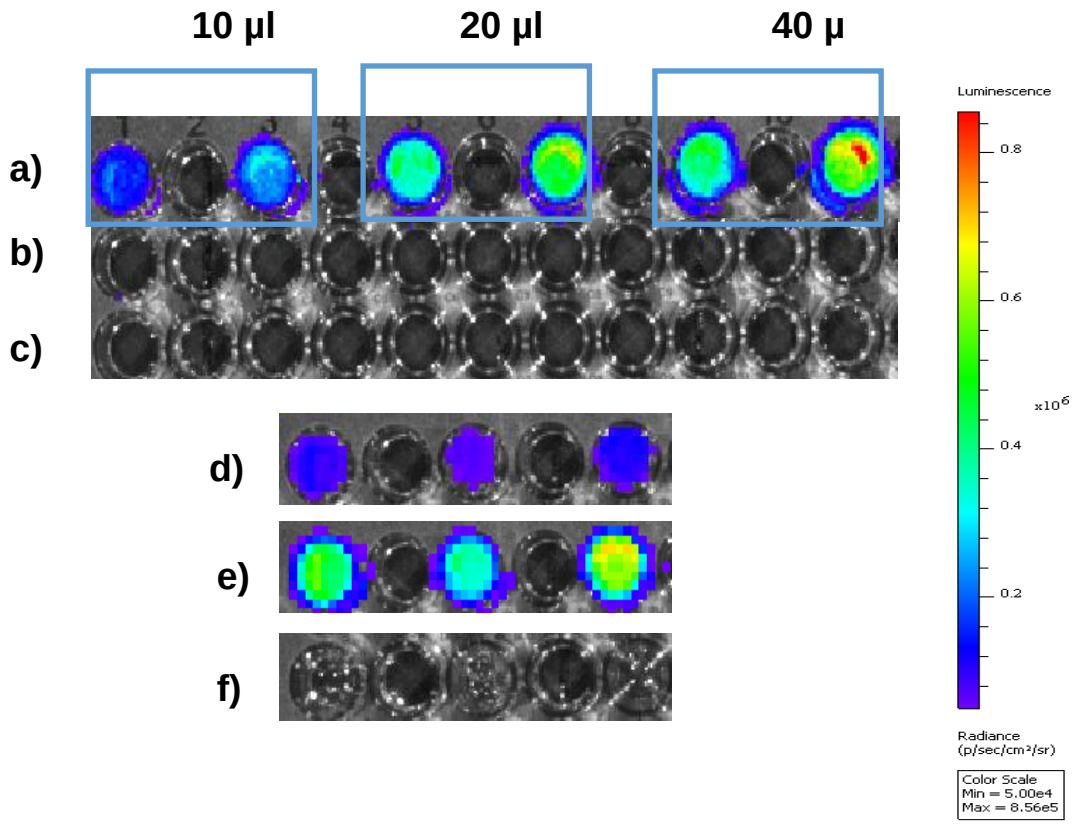


**Figure 4.4**: Bioluminescence images showing luciferase activity in HEK293T cells following 1 hour incubation with 10, 20 and 40 µl a) of loaded-EVs (concentration 1 x $10^{12}$ particles/ml), b) naïve EVs ( concentration 1 x $10^{12}$ particles/ml), c) PBS, d) following 1 h incubation with 10 µl of loaded-EVs, e) following 6 hours incubation with 10 µl of loaded-EVs and f) following 6 hours incubation with 10 µl of naive EVs. The bioluminescent signal was measured 5 minutes after addition of the luciferin substrate and is expressed in photons per second, displayed as an intensity map.

After 24 hours of incubation the luminescent signal was greatly reduced, such that it was no longer detectable. These results suggest that uptake of loaded-EVs is first detectable after 1 hour, with an increase over time until 6 hours. The signal is diminished at 24 hours, suggesting that EVs and cargo have degraded considerably.

### 4.3.2 Delivery of eGFP to primary neurons

Scanning confocal microscopy was used to investigate the ability of EVs to interact with primary neuronal cells, co-localise with the lysosome and deliver an eGFP cargo. 50 µl of loaded-EVs (representing 6 ng of eGFP) were incubated with primary neuronal cells for 3 hours. Naïve EVs served as a negative control. DAPI was used as a nuclear and chromosome counterstain

for identifying nuclei. It selectively binds to DNA and shows little to no background staining of the cytoplasm (blue channel). Anti-LAMP1 and Alexa Fluor 546 (red) were used to visualise the lysosome in the red channel. Finally, the green channel was used to visualise the fluorescence from any incorporated eGFP in EVs.

As seen from Fig. 4.5a, nuclei are seen in in blue, positive lysosomal staining seen in red channel (Fig. 4.5b) and green fluorescence is observed in the perinuclear region of primary neurons (Fig. 4.5c) , suggesting that loaded-EVs containing eGFP have been taken up by neurons. Moreover the co-localisation between the green and red channels manifested in an orange colour (Fig. 4.5d), indicates that EVs are co-localised with lysosomes. This co-localisation is further confirmed by the weighted co-localisation of the green and red channel is as calculated by the Zen software displayed in Fig. 4.5e.

The results from the control experiment are displayed in Fig. 4.6. Here the nuclei are seen in blue channel (Fig. 4.6a), no signal observed in the red channel as primary Anti-LAMP1 antibody was excluded to ensure that any red signal observed is not due the background from non-specific binding of Alexa Fluor 546 (red). Moreover, no green signal is seen in Fig. 4.6c as these cells were incubated with the naïve EVs that do not contain any eGFP. This confirms that any green fluorescencent signal seen previously in the channel in Fig. 4.5c observed is due to eGFP in the loaded-EVs. Fig. 4.6d which the merge only shows the blue staining positive for nuclei.

This results are encouraging for the ultimate goal of this project, which is to deliver GCase-loaded EVs to the lysosomes of both neurones and cells in the visceral organs as a treatment for Gaucher Disease Type 2. As discussed in **Section 4.1.1**, EVs have the ability to interact with target cells as their surface is rich with proteins such as tetraspanins and integrins that facilitate attachment to and eventual internalisation by target cells [153,231]. Our findings are in agreement with results in the literature which show that the internalized EVs ultimately migrate to lysosomes following internalisation [126] .

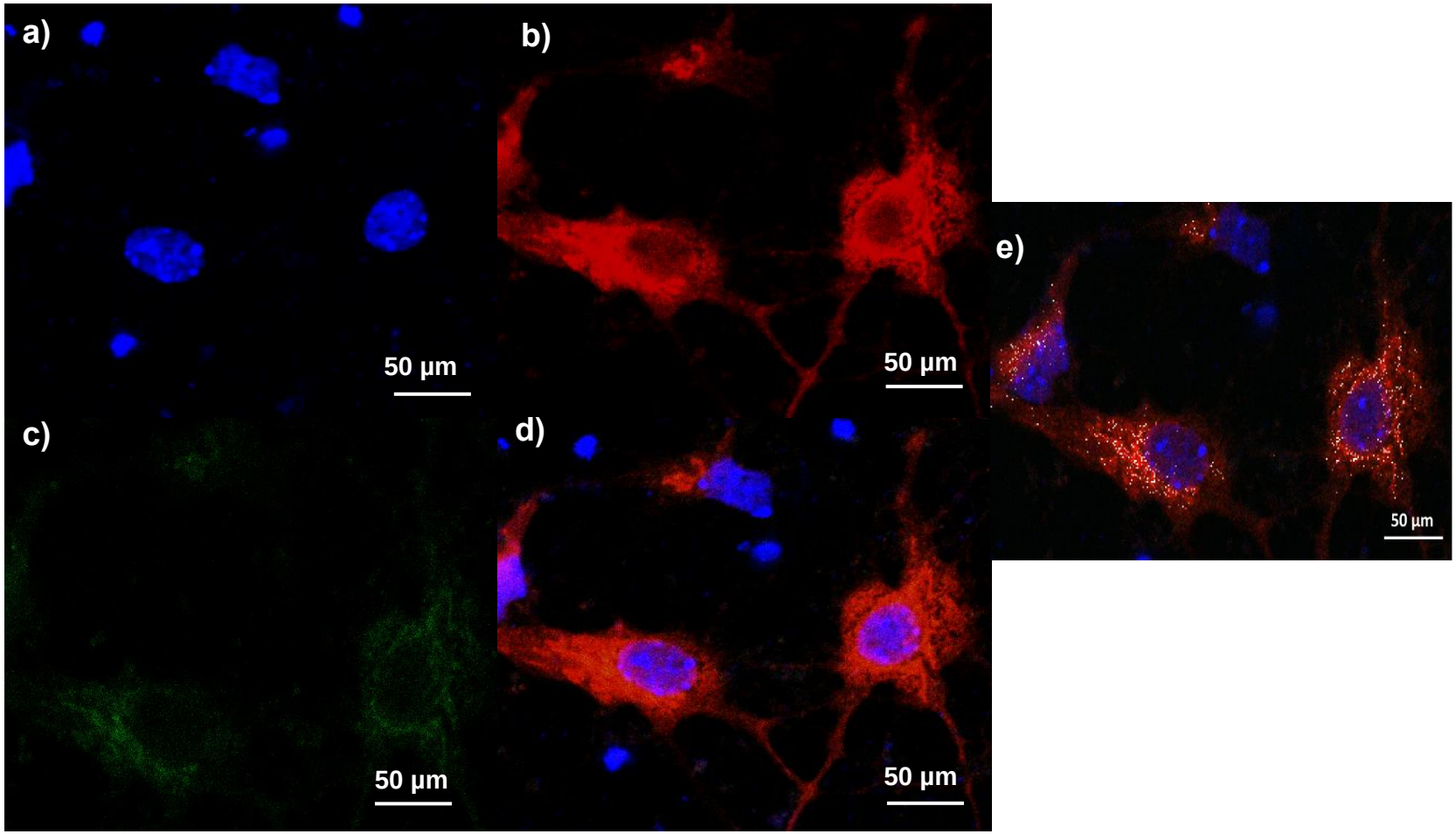


**Figure 4. 5:** Intracellular localization of loaded-EVs in primary neuronal mixed culture, following 3 hours' incubation. Images show a) DAPI for nuclei staining (blue), b) antibodies to LAMP1 lysosomal marker (+ Alexa Fluor 546, red), c) eGFP from loaded-EVs, d) a merged image showing co-localization of eGFP (green) in EVs and lysosomal staining (red) manifested in an orange colour and e) merged image showing the weighted co-localisation of the eGFP (green) in EVs and lysosomal staining (red) manifested in an orange colour as calculated by the Zen™ software.

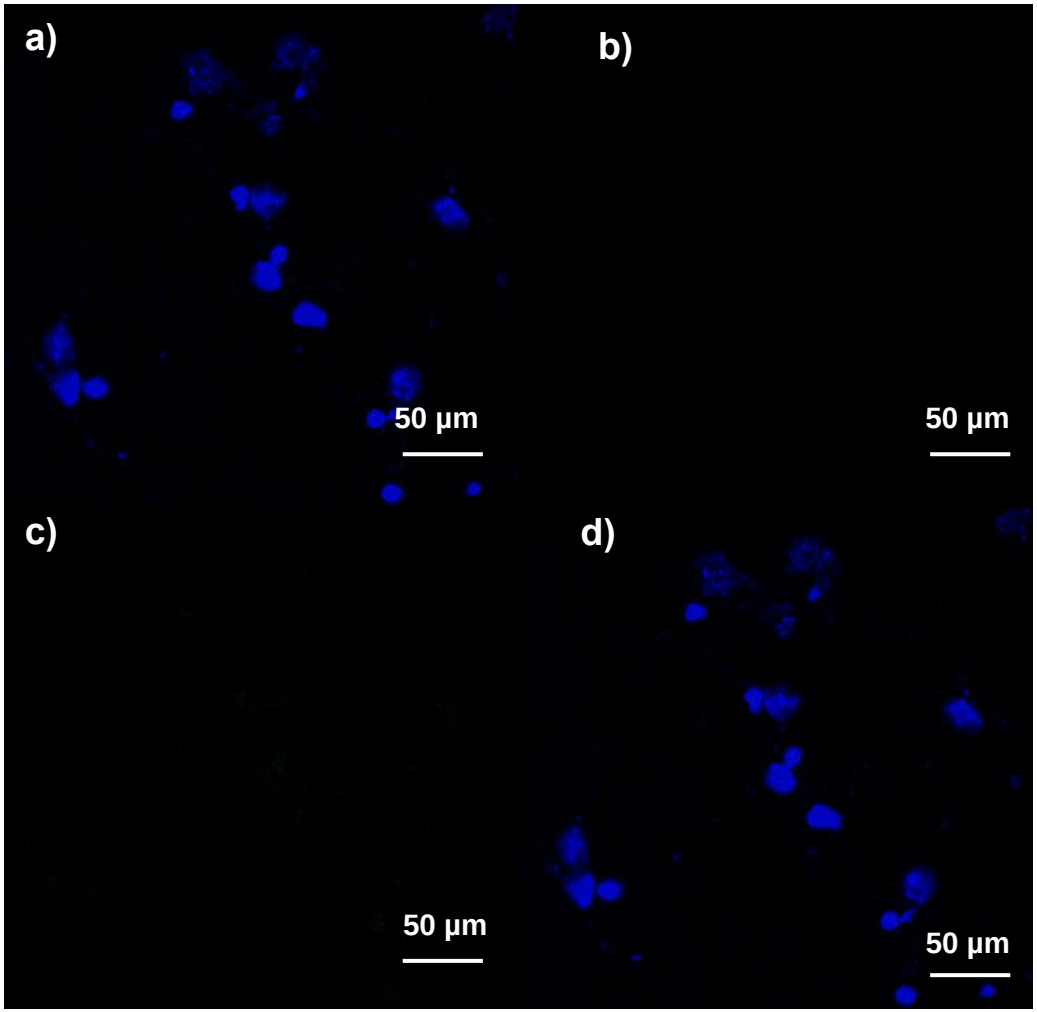


**Figure 4.6**: Intracellular localization of naïve EVs in primary neuronal mixed culture following 3 hours incubation with naive EVs. Images show a) nuclei stained with DAPI (blue), b) antibodies to LAMP1 lysosomal marker (- Alexa Fluor 546, red), c) eGFP from naïve EVs and d) a merged image.

### 4.3.3 *In vivo* biodistribution study

Despite the great increase in research activities involving EVs, very few publications can be found that detail the biodistribution of EVs *in vivo*. An understanding of this, how it varies between different routes of administration, and the EV half-life is crucial for the advancement of EVs to the clinic. As the *in vivo* biodistribution can vary depending on the source of EVs and the isolation/characterisation protocols, it is important to establish this for our specific EV product [113]. Furthermore, the vast majority of *in vivo* EV biodistribution studies in the literature were performed using adult mice (with the exception of some studies evaluating the intranasal route in neonates)[222]. The ultimate aim of this project is to evaluate the use of EVs loaded with therapeutic enzymes for paediatric diseases, and thus the biodistribution in neonates is particularly important here. The administration schedule, routes of administration and time points (as reported in **Section 2.6.2**, Table 2.5) was designed with all of the above considerations in mind. The dose of EVs to be injected in adult and neonatal mice were determined by the maximum concentration that could be obtained for loaded-EVs and maximum permissible volume to be injected via each route. The reason for this was to, to reduce the risk of achieving non-detectable levels of eGFP when using ELISA for analysis.

Loaded-EVs were produced at a large scale using 10 layer Cell Factories as described in **Section 2.4.5**. Isolated EV pellets were pooled together and characterised for size and concentration (by NTA and TEM, **Section 2.5.1** and **2.5.2** respectively), EV markers by western blot (**Section 2.5.5**), and eGFP content (by GFP ELISA, **Section 2.5.10**). The eGFP concentration of loaded-EVs was normalised to 100 ng/ml with a corresponding EV concentration of ~5 x$10^{11}$ EVs/ml, ensuring homogenous dosing throughout the study. Naïve EVs to be used as negative controls in this study were also prepared and characterised in the same manner, and concentration normalised to the approximately the same concentration as loaded-EVs. A summary of the characterising data is presented in Fig. 4.7. All the data agree with the small-scale data from Chapter 3, and confirm the successful generation of loaded-EVs.

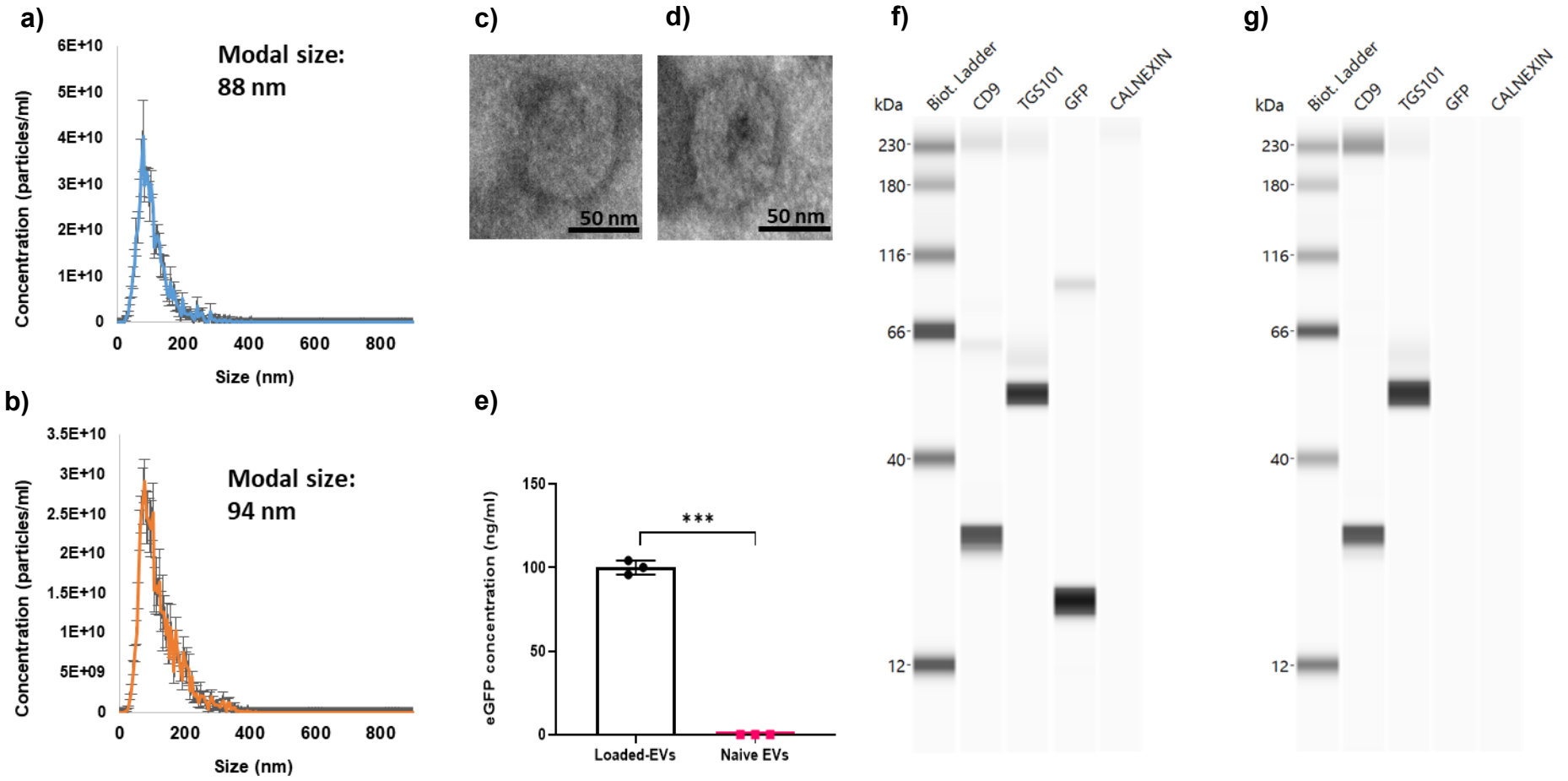


**Figure 4.7:** Characterisation of naive EVs and loaded-EVs produced at large scale, NTA profiles of a) naïve EVs and b) loaded-EVs; TEM images of c) naïve EVs and d) loaded-EVs; e) eGFP content in both loaded-EVs and naïve EVs and Western blots of f) naïve EVs and g) loaded-EVs

### *4.3.3.1 Neonatal ICV route*

CD1 neonates were injected with 10 µl of either loaded-EVs or naïve EVs through the ICV route and sacrificed after 1, 6, or 24 hours. The brain, liver and heart were harvested, proteins extracted, and eGFP content measured using GFP ELISA (Fig. 4.8). eGFP can still detected in the brain 1 and 6 hours after injection, but is much diminished after 24 hours.

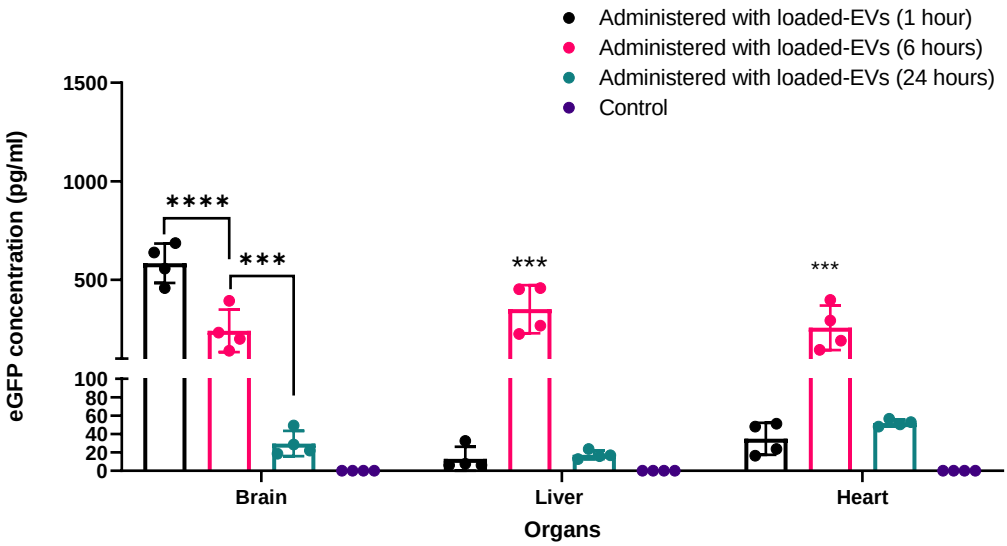


**Figure 4.8:** The eGFP content in the brain, liver and heart of neonatal mice 1, 6, and 24 hours after 10 µl ICV injections with loaded-EVs and 1-6 hours after 10 µl ICV injections with naïve EVs as control. N=4 for each group of injections. Data are presented as mean ± SD. Statistical analysis: one-way ANOVA, Tukey's multiple comparisons test; ns $p > 0.05$, *$p < 0.05$, ***$p \leq 0.001$.

In contrast, the content in the liver one hour following injection is negligible. This increases over time to become detectable at 6 hours and then decreases again at 24 hours. The eGFP content in the liver six hours following ICV injection is significantly higher ($p<0.001$) than that in control animals injected with naïve EVs. Similar results are observed in the heart, where some eGFP is observed one hour after injection. This increases at six hours and decreases to a negligible amount at 24 hours. The eGFP content in the heart at 6 hours is again significantly higher ($p<0.001$) than that in the control group. These findings demonstrate that some of the EVs injected into the brain are slowly drained into the visceral organs as the cerebrospinal fluid (CFS) is rapidly absorbed into the peripheral bloodstream [241].

### *4.3.3.2 Neonatal IV route*

Fig. 4.9 shows the eGFP concentration following injection of 40 µl of loaded-EVs though the IV route. The eGFP concentration after 1 h is highest in the liver (as expected for the IV route), with some reaching the brain and the heart. However, the concentration in the heart is not significantly higher than the control ($p>0.05$). At 6 h, the eGFP concentration in all organs is not significantly different to that in the control group. This signifies that EVs have a short half-life after IV injection, and are almost completely cleared within six hours.

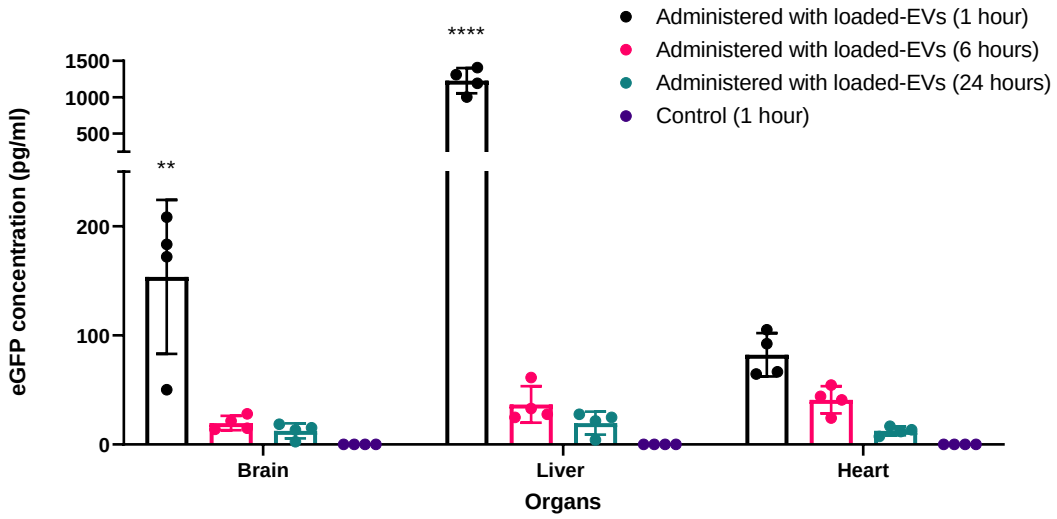


**Figure 4.9:** The eGFP content in the brain, liver and heart of neonatal mice 1, 6, and 24 hours following 40 µl IV injections with loaded-EVs and 1 hour following 40 µl of IV injection with naïve EVs (control). N=4 for each group of injections and data are presented as mean ± SD. Statistical analysis: one-way ANOVA, Tukey's multiple comparisons test; **p ≤ 0.01, ****p < 0.0001.

The most interesting observation here is that some of the loaded-EVs are reaching the brain following IV injection. This is in agreement with work by other groups [108,242,243] . This is very important from a therapeutic point of view, since although the IV route can provide direct access to the blood brain barrier (BBB) about 98 % of small molecule drugs and almost all bio-macromolecules have very poor bioavailability in the brain [241,244]. This is because it is inherently difficult to cross the BBB. The BBB is composed of two membranes in series, the luminal and abluminal membranes of the brain capillary endothelium [245]. The BBB is selectively permeable with high resistance tight junctions that

greatly limit paracellular or transcellular transport. Therefore, for molecules in the general circulation to enter the brain interstitial fluid (ISF) they must be small (<400 Da) and lipophilic enough to diffuse through the BBB, or their transport must be either carrier or receptor mediated [244,246]. It is clear that EVs are able to cross the BBB to some extent, which is promising for the intended application of this work, but the route by which they do so remains unclear.

Some research has been conducted to evaluate how EVs can cross the BBB and gain access to the brain. Chen *et al*. [240] investigated the interactions between HEK293T derived luciferase-loaded EVs and brain microvascular endothelial cells (BMECs) in an *in vitro* model. It was shown that the majority of EVs cross the BBB through the transcellular route, where they are first internalised through endocytosis, followed by multivesicular body (MVB) formation and release of EVs on the other side of the BMEC monolayer. The main endocytic routes through which EVs were internalised were clathrin-dependent and caveolae-dependent endocytosis. It was also shown that few EVs cross by passive diffusion. Since the crossing of the BBB by EVs is dependent on specialised receptors, EVs from different sources might potentially cross the BBB differently.

#### *4.3.3.3 Neonatal IP route*

Fig. 4.10 depicts the eGFP concentration in the different organs following injection of 40 µl of loaded-EVs though the IP route. Here we can see that the at one hour post injection, the liver has the highest concentration of eGFP followed by the brain and heart. The eGFP concentration in all three organs at this 1 hour post-injection time point is significantly higher than the control ($p<0.0001$). However, as seen following IV injection, the eGFP concentration in all three organs at the 6 hour time point is not significantly higher than that in control organs, demonstrating that EVs are cleared significantly within six hours following IP injection.

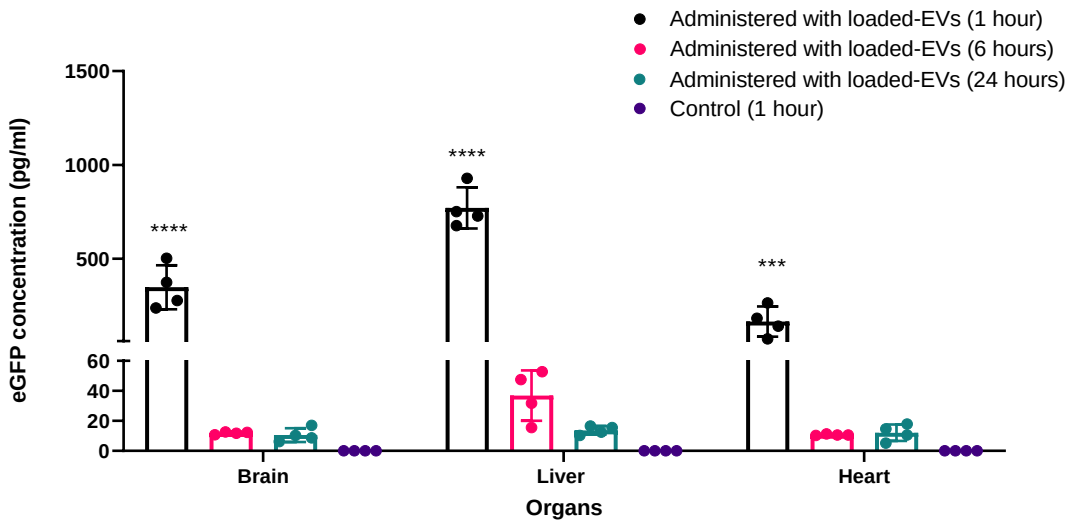


**Figure 4.10:** : The eGFP content in the brain, liver and heart of neonatal mice 1, 6, 24 hours following 40 µl IP injections with loaded-EVs and 1 hour following 40 µl of IP injection with naïve EVs (control). N=4 for each group of injections and data are presented as mean ± SD. Statistical analysis: one-way ANOVA, Tukey's multiple comparisons test; ****p < 0.0001.

In comparison to the IV route, after IP injection the eGFP concentration after 1 h is lower in the liver (1260 pg/ml with IV vs. 720 pg/ml IP). In contrast, the eGFP concentration in the heart increases from 82 pg/ml (IV) to 152 pg/ml (IP) and the concentration in the brain from 150 pg/ml (IV) to 347 pg/ml (IP). This difference in biodistribution between the two routes is probably because IP injection avoids the issue of first pass metabolism in the liver, and hence more EVs are available to reach other organs. There is clearly a wider distribution of EVs through the IP route in comparison to the IV route, where the majority ends up in the liver. The amount of loaded-EVs that reach the brain following IP injection is significantly higher ($p<0.05$) than that achieved through the IV route (Fig. 4.10).

The ICV route is by far the most effective route to get EVs in the brain (see Fig. 4.11). Even reducing the dose 4-fold, the eGFP concentration in the brain 1 hour after ICV injection is significantly higher than that achieved by the two other routes. This is logical since an ICV injection is delivering the payload straight to the brain. However, overall the findings suggest that the IP route could be a suitable and less invasive route of administration in neonates to target both the brain and visceral organs.

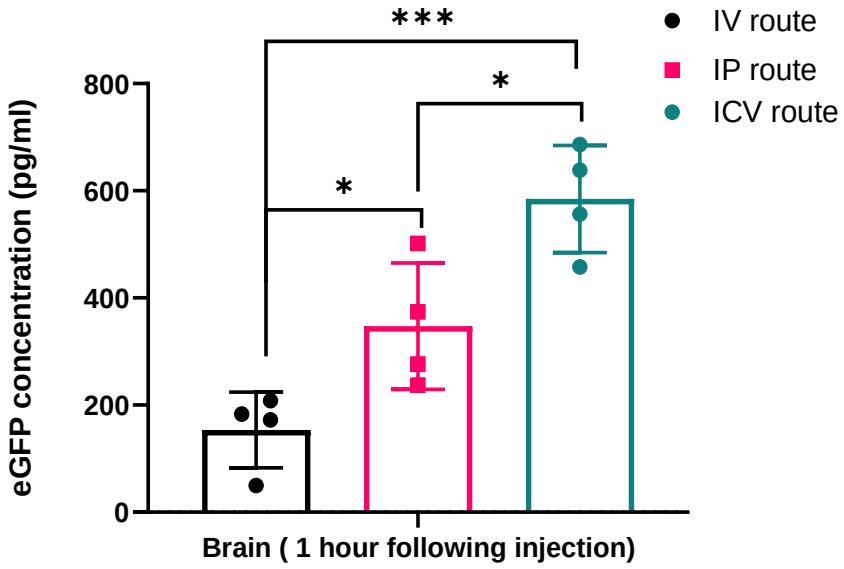


**Figure 4.11:** The eGFP content in the brain of neonatal mice one hour following injection with loaded-EVs through the IV, IP and ICV routes. N=4 for each group of injections, and data are presented as mean ± SD. Statistical analysis: one-way ANOVA, Tukey's multiple comparisons test; *p < 0.05, ***p ≤ 0.001.

The percentage dose that is available in the brain 1 hour after ICV administration is compared to the percentage dose that has crossed the BBB following IV and IP administration at the same time point (Fig. 4.12). The dose in the brain after systemic administration is lower than aimed for (4 % for IP and 1.8 % for IV administration). This indicates that EVs are crossing the BBB following systemic administration, but either this occurs at lower levels than desired or they have a very short half-life and the amount that has crossed the BBB is eliminated quickly within the hour. Thus, to facilitate the advancement of EVs as delivery vectors of GCase enzyme in the treatment of Gaucher Disease Type 2 further development is needed to increase the amount of loaded-EVs delivered to the brain as well as the half-life in the visceral organs.

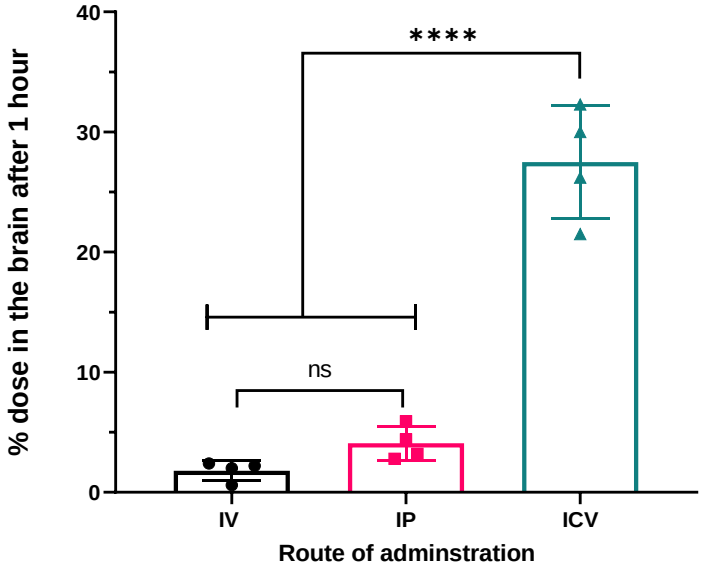


**Figure 4.12:** Percentage dose available in the neonatal brain 1 hour after IV, IP and ICV administration of loaded-EVs. N=4 for each group of injections, and data are presented as mean ± SD. Statistical analysis: one-way ANOVA, Tukey's multiple comparisons test; ns denotes $p > 0.05$ ****$p < 0.0001$.

### *4.3.3.4 Neonatal IN route*

Owing to the success of recent studies that have shown EV delivery to the brain through the intranasal (IN) route, we evaluated the ability of loaded-EVs derived from HEK293T cells to be delivered IN [247–250]. It is hypothesised that IN administered EVs can enter the brain through the a) the systemic pathway, whereby EVs absorbed through the nasal cavity into the systemic circulation first cross the BBB and enter the brain; or, b) the olfactory route, whereby EVs are directly delivered to the brain through the olfactory region situated at the top of the nasal cavity, thereby bypassing the BBB altogether [251]. Since neonate mice are obligatory nose breathers [252], IN administration can be achieved easily by placing small drops of loaded-EV suspensions on each nostril and allowing the pup to breath in, repeating this stepwise until 20 µl has been delivered. The results of these experiments are depicted in Fig. 4.13.

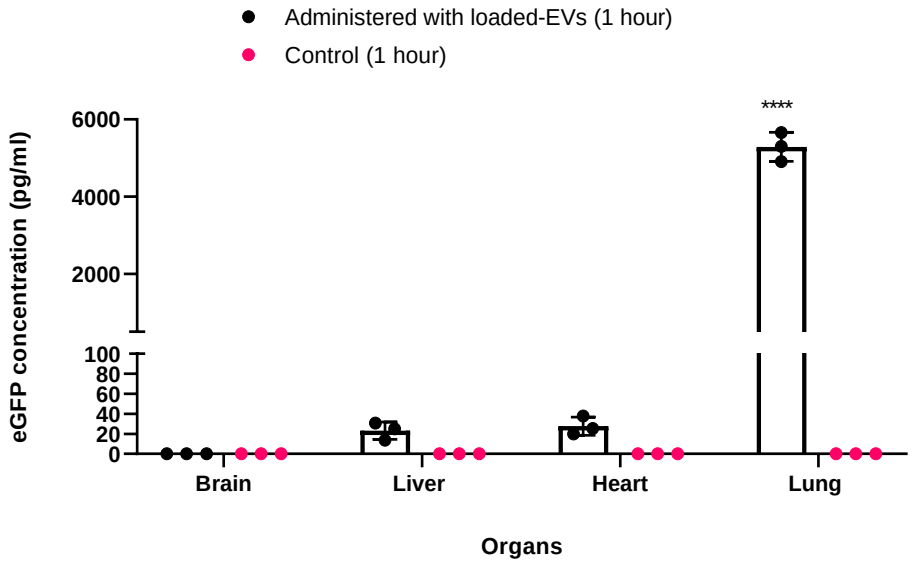


**Figure 4.13**: The eGFP content in the brain, liver, heart and lung of neonatal mice one hour following intranasal administration of 20 µl of loaded-EVs or 20 µl of naïve EVs (control). N=4 for each group and data are presented as mean ± SD. Statistical analysis: one-way ANOVA, Tukey's multiple comparisons test; ****p < 0.0001.

The eGFP concentration in the lung is significantly higher with the loaded-EVs than the control ($p<0.0001$), suggesting that the majority of loaded-EVs reach the lung with negligible amounts in other organs. The percentage dose that remains in the lung 1 hour after administration is 45 %. Particles smaller than 3 µm are typically deposited in the alveoli, after which they become available systemically [253]. As the mechanism by which EVs can be transported from the lung to the brain is not determined, we can only propose potentially plausible reasons for the non-detectable levels of eGFP in the brain. Such reasons include the possibility that once EVs are deposited in the alveoli they are slowly absorbed into the systemic circulation, and thus at 1 hour after administration very low levels were available for absorption by the other organs. In addition, as shown by Wiklander *et al*. [113], the biodistribution of EVs is dependent on cell source: thus, EVs may display an intrinsic homing pattern to cells of similar origin to the parental producer cell line. This homing pattern can be attributed to the fact that EVs will have a similar repertoire of surface receptors as their parent cell, facilitating their binding and uptake. The EVs used here are derived from HEK293T cells, which are of visceral origin, and as such will not have any intrinsic homing ability to neuronal cells in the brain [113].

The eGFP concentration in the lung (~5200 pg/ml) following IN administration is the highest achieved in any organ through all routes explored, and thus this could be a viable route for lung-specific delivery. This represents a potential therapeutic strategy for the treatment of lung diseases such as pulmonary fibrosis, because of ease of administration, and the observation of local delivery to the lungs without any distribution to other organs that could result in unwanted side-effects.

#### *4.3.3.5 Adult ICV route*

The eGFP concentration in the organs of adult mice 1 and 6 hours after ICV injection are presented in Fig. 4.14. It can be seen that the eGFP concentration in the adult brain after one hour is significantly higher after administration of loaded-EVs than in the control brain. However, this concentration is much smaller (~ 100pg/ml) than in neonate brains (~ 600 pg/ml) at the same time point.

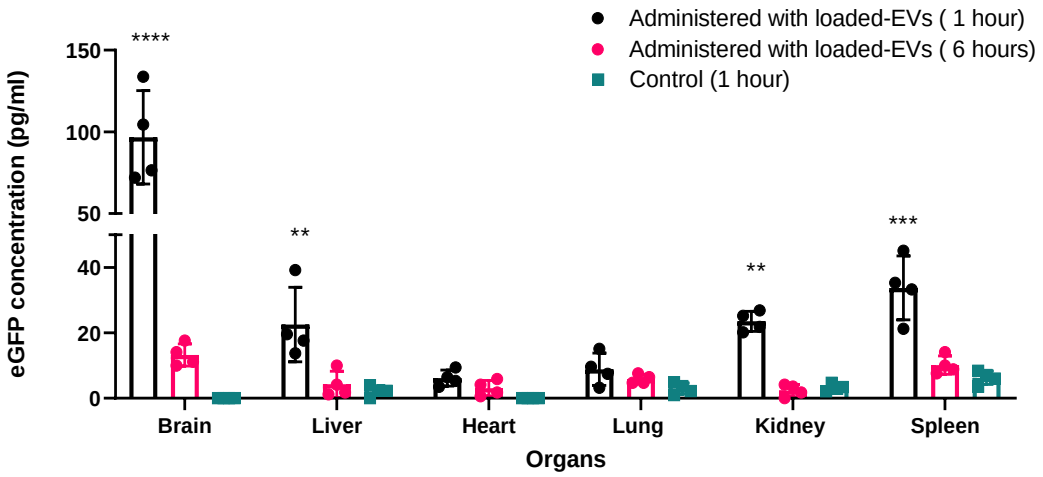


**Figure 4.14:** The eGFP content in the brain, liver, heart, lung, kidney and spleen of adult mice 1 and 6 hours following 20 µl ICV injections with loaded-EVs or one hour after ICV injection with naïve EVs (control). N=4 and data are presented as mean ± SD. Statistical analysis: two-way ANOVA, Tukey's multiple comparisons test; **p ≤ 0.01, ***p ≤ 0.001 ****p < 0.0001.

The eGFP concentration in the adult brain decreases to negligible levels six hours after ICV injection. This is different to the neonate brain, where the eGFP persists for 6 h. The lower overall distribution of eGFP in adult brains in comparison to that in neonates at both 1 hour and 6 hours can probably be

explained by the fact that the dose of eGFP/body weight given to the adult animals is significantly lower than that with the neonates (10 µl was administered to neonate mice with a body weight of around 1 g and 20 µl into adults with body weight of around 15 g). Moreover, some drainage of eGFP from the brain to other organs is seen with the adult mice. Although the eGFP concentration in the liver, kidney and spleen is higher than the control (liver $p<0.01$, kidney $p<0.01$, and spleen $p<0.001$) it is still lower than desired. This could be due to faster clearance by the adult brain, which could lead to more rapid drainage to the other organs. Since the half-life of these EVs has been shown to be low, it is possible that they have already been degraded or cleared to undetectable levels 1 hour after administration.

#### *4.3.3.6 Adult IV route*

Fig. 4.15 shows the eGFP concentration in adult organs one and six hours following 200 µl injections of loaded-EVs or naïve EVS through the IV route. One hour following IV administration the eGFP concentration in the brain and the heart is not significantly different to the control, and almost non-detectable for the brain. The highest eGFP concentration is observed in the liver, followed by the spleen, lung and kidney. This tissue distribution is in agreement with the findings of previous studies exploring the distribution of HEK293T derived EVs following IV administration in adult mice [113]. EVs are generally cleared from the system by macrophages, which are prevalent in the spleen, lung, liver and kidneys [135,234]. This was demonstrated in the literature by reductions in the clearance of EVs in animals depleted of macrophages [254]. This preferential tissue accumulation can be harnessed for the treatment of visceral manifestations in Gaucher Disease, where the liver, spleen and lungs are affected [7].

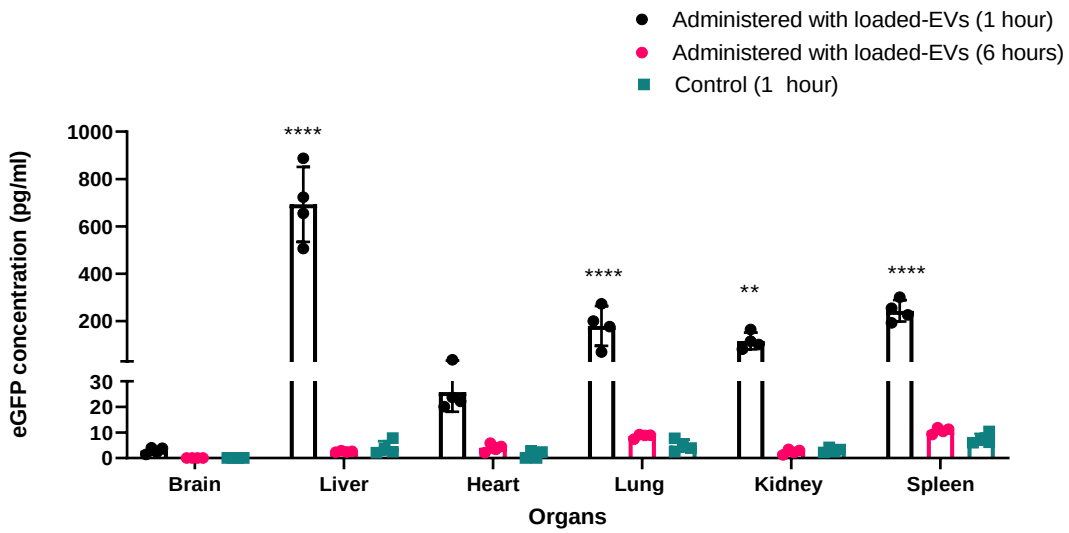


**Figure 4.15:** The eGFP content in the brain, liver, heart, lung, kidney and spleen of adult mice one and six hours following 200 µl injections of loaded-EVs and one hour following IV injection with naïve EVs (control). N=4 and data are presented as mean ± SD. Statistical analysis: two-way ANOVA, Tukey's multiple comparisons test; **p ≤ 0.01, ****p < 0.0001.

Six hours following IV administration, the eGFP concentration in all organs is not significantly different to the control, which highlights the short half-life of EVs given IV. This too can again be attributed to the rapid clearance of EVs by macrophages, and is in agreement with literature reports showing that the half-life of EVs is very short (ranging from 2 to 30 minutes [135]) and they are mostly cleared by 6 hours [136] .

#### *4.3.3.7 Adult IP route*

The eGFP concentration in the different organs following 200 µl injection through the IP route is given in Fig. 4.16. Similar to the IV injection results, the highest concentration of eGFP is seen in the liver. However, the value obtained is smaller (~ 320 pg/ml) than that seen following IV administration (~ 690 pg/ml). The eGFP concentrations in the lung, kidney and spleen are also significantly higher than those seen in the negative control one hour post-administration. Although the brain eGFP concentration seen IP is higher than that seen following IV administration, it is not significantly different to the negative control.

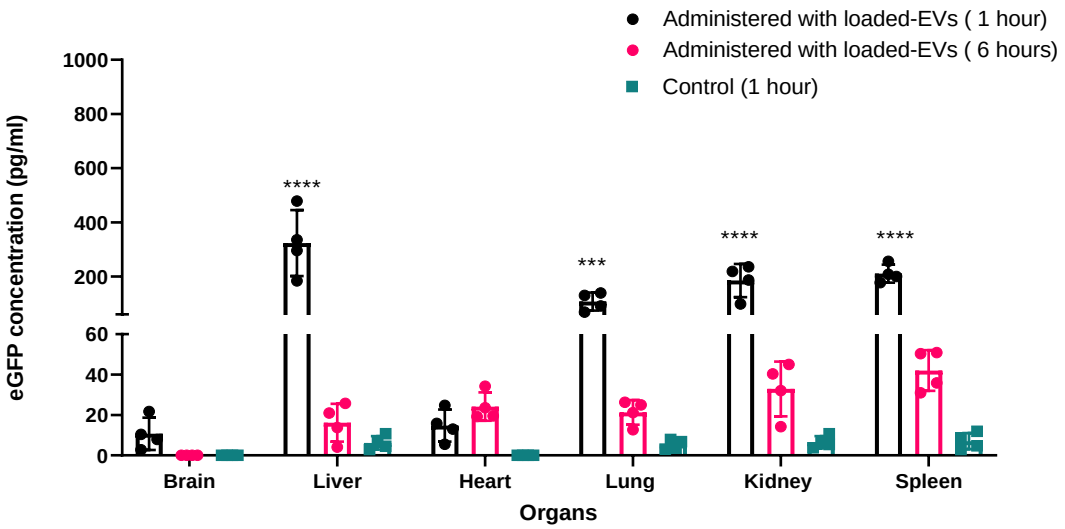


**Figure 4.16:** The eGFP content in the brain, liver, heart, lung, kidney and spleen of adult mice 1 and 6 hours following IP injections with loaded-EVs and one hour following ICV injection with naïve EVs (control). N=4 and data are presented as mean ± SD. Statistical analysis: two-way ANOVA, Tukey's multiple comparisons test; ***p ≤ 0.001 ****p < 0.0001.

The eGFP concentration in all organs is negligible six hours after administration. This confirms the short half-life of EVs, as has been observed by other research groups. Systemically injected EVs are swiftly taken up by the liver, lung, kidney spleen and then hepatically and renally excreted within 1-6 hours [136,238] .

### 4.3.3.8 Immunocytochemistry

In addition to the ELISA data presented above, immuno-peroxidase-based immunohistochemistry was used to analyse eGFP tissue distribution following EV administration. This staining was not quite successful and we could only see noteworthy differences in liver sections of mice injected IV with loaded-EVs in comparison to mice injected IV with naïve EVs (data not shown here). The livers in animals injected IV with loaded-EVs had the highest concentration of eGFP from all the organs of mice injected by the various routes. This is consistent with these organs being the only ones to show differences in the staining data. Considering that the loaded-EVs contained only 0.17 ng of eGFP per $10^9$ EV particles, it was not unexpected that their tissue distribution would be difficult to visualise in this manner. Thus this staining protocol will need to be improved as part of future work.

## 4.4 Conclusion

The *in vitro* uptake and *in vivo* biodistribution of loaded-EVs containing both eGFP and luciferase enzyme was investigated in this chapter. *In vitro* bioluminescence assays were conducted to evaluate the uptake of loaded-EVs and delivery of functional luciferase enzyme to HEK293T cells. These experiments confirmed that loaded-EVs can be internalised by HEK293T cells and successfully deliver functional luciferase enzyme. An increase in the incubation time from 1 to 6 hours led to an increase in the uptake of EVs. Immunohistochemistry experiments using primary neurones confirmed that loaded-EVs can be taken up primary neurones, and co-localise with the lysosome. This is very promising for the use of EVs as therapeutic delivery vectors of lysosomal enzymes.

*In vivo* biodistribution studies in neonates showed that all routes of administration except the IN route can deliver eGFP cargo to both the brain and visceral organs. The IP route is potentially the most appropriate method, since it can deliver cargo to both the brain and visceral organs in a relatively non-invasive manner (in comparison to ICV injection). The IN route failed to deliver any eGFP to the brain, in contradiction to the findings of some previous studies in the literature. However, this could be due to the fact that because organs were harvested 1 hour after administration EVs deposited in the alveoli were slowly absorbed into the systemic circulation, and thus at 1 hour after administration very low levels were available for absorption by the other organs. In comparison to neonates, in adult mice only ICV administration delivered cargo to the brain. IV and IP administration resulted in eGFP being present only in the visceral organs (liver, lung, kidney and spleen). The pharmacokinetics following IV and IP routes of adminstration in both adults and neonates are in agreement, showing that eGFP in loaded-EVs is eliminated within 6 hours.

The results in this chapter indicate that EVs derived from HEK293T cells can potentially be used as delivery vectors of GCase enzyme for the treatment of Gaucher Disease Type 2. However, these EVs seem to be more efficient in delivering cargo to visceral organs than the brain, and display a short half-life.

These parameters must be addressed to facilitate the advancement of the EVs for their intended use.

# Chapter 5: Use of neuronal SH-SY5Y cells to produce loaded-EVs for targeting to the CNS

## 5.1 Introduction

Recent research has demonstrated that EVs may have a natural homing ability to the same cell type as those that produce them [48,231,255,256]. For example, Hood *et al*.[256] demonstrated that EVs derived from melanoma cells have specific homing ability to sentinel lymph nodes, where they proceed to promote tumour metastasis. Another example was shown by Tran *et al*.[257], where EVs were isolated from HT29 (human colorectal adenocarcinoma cells) and MDA-MB-231 (metastatic breast cancer cells), loaded with aspirin, and the cytotoxicity of each EV preparation on the two cell lines was evaluated. This showed that the loaded-EVs had greater cytotoxicity to their parent cells than the other cancer cell line, indicating a homing effect. The same homing effect was also demonstrated by Hazan-Halevy *et al*.,[255] who used co-cultures of different cell lines (mantel cell lymphoma, T-cell leukaemia and bone marrow stromal cell lines) and demonstrated that EVs derived from mantel lymphoma cells were predominantly internalised by the parent cells over the other two cell lines.

This cell specific homing property of EVs is based on the fact that EVs contain a similar biological cargo and lipid composition to the producer cells. As internalisation of EVs relies to some extent on the surface markers, this makes them naturally designed to be preferentially taken up by cells similar to those from which they are produced [48,258]. Although the specific mechanism of this homing effect is yet to be established some studies suggest that the interaction of molecules on the surface of EVs with integrins on the cell surface may be in part responsible for this homing effect [226,259–261]. Denzer *et al*.[259] showed that the homing effect of B-cell derived EVs to follicular dendritic cells was mediated by the interaction of tetraspanin proteins CD37, CD53, and CD82 on EVs with integrins on the cell surface. Considering all of the above, it was hypothesised that EVs derived from neurons will naturally have a homing ability to neurons, and will hence be better equipped to deliver a cargo specifically to the CNS than EVs derived from non-neuronal cell lines.

## 5.2 Aims and objectives

In Chapter 4, it was shown that loaded-EVs from HEK293T cells can be used to deliver a biological cargo both *in vitro* and *in vivo*. However, the percentage of HEK293T-derived loaded-EVs that could cross the blood brain barrier (BBB) was lower than desired. In this chapter we evaluate the ability of loaded-EVs from the SH-SY5Y neuronal cell line to deliver eGFP to the brain. To do this, loaded-EVs were produced, administered to neonate mice via the same routes of administration as those used in Chapter 4, and the pharmacokinetics and tissue distribution assessed.

## 5.3 Results and discussion

### 5.3.1 Gene delivery to SH-SY5Y cells

Here we sought to use parameters already optimised in Chapter 3 **(Section 3.3.2)** to transduce and determine the transduction efficiency of SH-SY5Y cells with VSV.G.SFFV.LUC.2A.eGFP.WPRE at different MOIs. Again, to confirm successful transduction fluorescence microscopy was employed to visualise eGFP expression, and flow cytometry performed to quantify the percentage of eGFP expressing cells. This was followed by fluorescence activated cell sorting (FACS) to select single cell colonies with the highest eGFP expression. These were then propagated to give appropriately high cell numbers for EV production.

#### *5.3.1.1 Fluorescence microscopy*

72 hours post transduction with VSV.G.SFFV.LUC.2A.eGFP.WPRE at different MOIs, eGFP expression in the SH-SY5Y cells was visualised using fluorescence microscopy (Fig. 5.1).

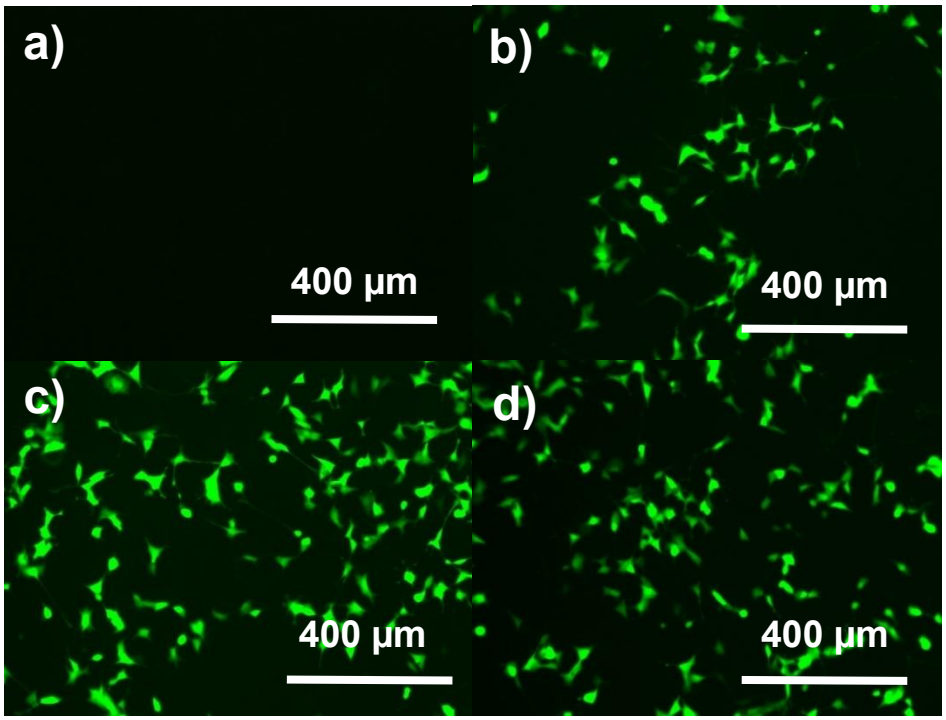


**Figure 5.1:** eGFP expression 72 h post transduction of SH-SY5Y cells with VSV.G.SFFV.LUC.2A.eGFP.WPRE, showing a) control non-transduced cells, and cells transduced at MOI of b) 25, c) 40 and d) 50. Representative images of one in three independent experiments is shown here.

As can be seen in Fig. 5.1, SH-SY5Y cells were effectively transduced at all three MOIs, with eGFP expression being observed both in the cytoplasm and nucleus of the cells. No eGFP expression could be seen in control non-transduced SH-SY5Y cells (Fig. 5.1a). No distinguishable differences in eGFP expression can be observed between the microscopy images of cells transduced at different MOIs (Fig. 5.1 b-d). All cells looked healthy and continued to divide and grow post transduction.

#### *5.3.1.2 Flow cytometry*

Although no differences in eGFP expression could be seen in fluorescent microscopy between cells transduced at the different MOIs, flow cytometry was used to quantify the transduction efficiency at each MOI. The flow cytometry data confirm the fluorescence microscopy findings (Fig. 5.2). The transduction efficiency of SH-SY5Y cells at all MOIs is 100 %. Thus we chose

to proceed with cells transduced at an MOI of 25, as we can achieve the highest transduction efficiency with the lowest amount of virus.

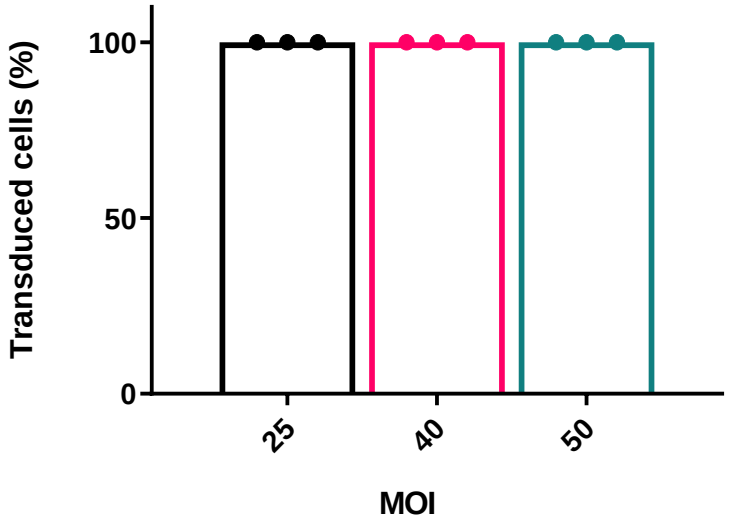


**Figure 5.2:** Transduction efficiency of SH-SY5Y cells transduced with VSV.G.SFFV.LUC.2A.eGFP.WPRE at MOI of 25, 40 and 50. Three independent experiments were performed and data are presented as mean ± SD.

Fig. 5.3 compares the transduction efficiency of SH-SY5Y cells at MOI 25 to that of HEK293T cells at MOI 100. The transduction efficiency of SH-SY5Y is higher than that of HEK293T cells, but this is not statistically significant ($p>0.05$).

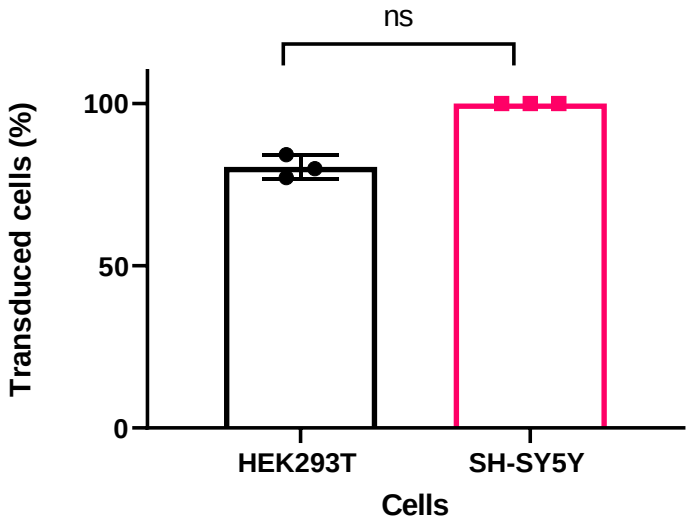


**Figure 5.3**: Transduction efficiency with VSV.G.SFFV.LUC.2A.eGFP.WPRE in SH-SY5Y cells at MOI 25 and HEK293T cells at MOI 100. Three independent experiments were performed. Statistical analysis: Mann Whitney test, ns denotes $p > 0.05$.

#### *5.3.1.3 Cell sorting to enrich eGFP in loaded EVs*

In Chapter 3 (**Section 3.3.2.2**), it was seen that the transduction efficiency of HEK293T cells with VSV.G.SFFV.LUC.2A.eGFP.WPRE at MOI 100 is 80 ± 3 %, meaning that some cells remain non-transduced. Thus cell sorting was performed to ensure that only cells with the highest expression of eGFP were selected for EV production. In the case of the SH-SY5Y cells, all cells in the sample were transduced and hence sorting is not likely to be of great benefit. Nonetheless, transduced SH-SY5Y cells were sorted in the same manner as HEK293T cells to ensure homogeneity of results and allow for comparison. As can be seen from Fig. 5.4 no visible differences are seen between the eGFP expression levels in sorted and non-sorted transduced cells. However, cell sorting means that all cells used for EV production originate from a single progenitor with the same level of virus integration and eGFP expression, which in turn should result in a more homogenous EV sample. From here onwards, unless otherwise stated, loaded-EVs are those that have been produced and isolated from sorted SH-SY5Y cells transduced with VSV.G.SFFV.LUC.2A.eGFP.WPRE at MOI 25. Also, unless otherwise stated, naïve EVs are those isolated from non-transduced SH-SY5Y cells.

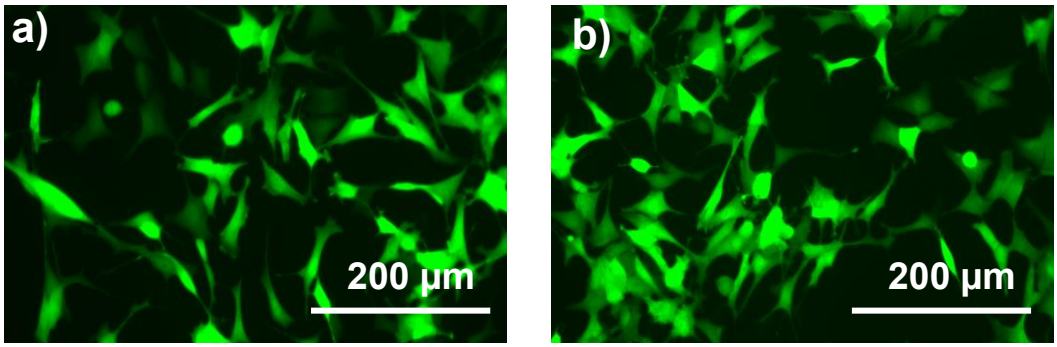


**Figure 5.4:** eGFP expression of SH-SY5Y cells transduced with VSV.G.SFFV.LUC.2A.GFP.WPRE at an MOI of 25, showing a) sorted and transduced cells, and b) transduced cells without sorting. Representative images of one in three independent experiments are shown.

### 5.3.2 Characterisation of loaded-EVs

#### *5.3.2.1 Size and concentration*

EVs from SH-SY5Y cells were isolated in the same manner as those from HEK293T cells. Fig. 5.5 shows the mode and mean sizes of particles in EV

pellets derived from both transduced and non-transduced SH-SY5Y cells and HEK293T cells. The modal size of loaded-EVs and naïve EVs derived from SH-SY5Y cells is within the size range of EVs (89 ± 4 nm and 100 ± 4 nm, respectively) and although the modal size of the latter is slightly bigger this difference is not statistically significant. The modal and mean sizes of naïve EVs derived from SH-SY5Y and HEK293T cells are not significantly different, and the same is true for loaded-EVs derived from the two cell lines. In comparison to HEK293T-derived EVs, where the mean size of the loaded-EVs and naïve EVs were not significantly different, SH-SHY5Y-drived EVs show a significant difference between mean size of loaded-EVs and naïve EVs. This could possibly be attributed the higher payload incorporated in SH-SY5Y-derived loaded-EVs, which is expected because SH-SY5Y cells show a better transduction efficiency and thus greater expression of eGFP.

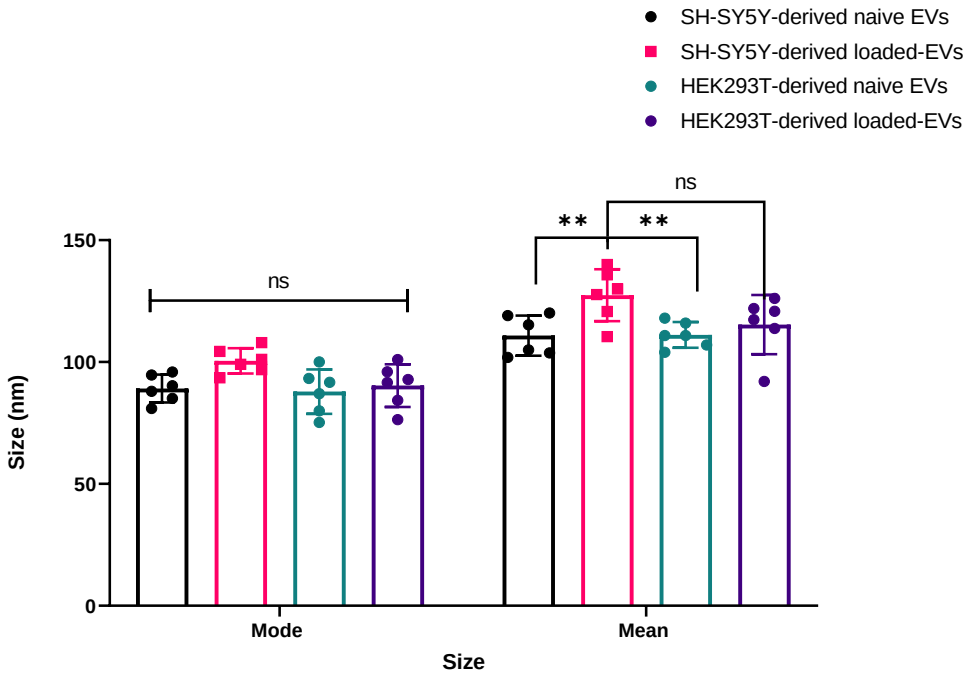


**Figure 5.5**: The mean and mode size of particles in different EV pellets. Six independent experiments were performed and data presented as mean ± SD. Statistical analysis: two-way ANOVA, Tukey's multiple comparison test; ns denotes $p > 0.05$, ** $p \leq 0.01$.

The concentrations of EVs in pellets isolated from the different cell samples, re-suspended in the 300 µl of PBS buffer, is depicted in Fig. 5.6. It can be observed that the concentration of naïve EVs derived from non-transduced SH-SY5Y cells and HEK293T cells is higher than for the yields of loaded-EVs

derived from the two sorted-transduced cell lines. This can be attributed to the fact that the high viral load in transduced cells causes them to grow more slowly than non-transduced cells (as was demonstrated by the cell viability assay for HEK293T cells in Chapter 3, **Section 3.3.3.2**), and hence produce fewer EVs. However, this difference is not statistically significant, and the concentrations of loaded-EVs derived from both cell lines are very similar.

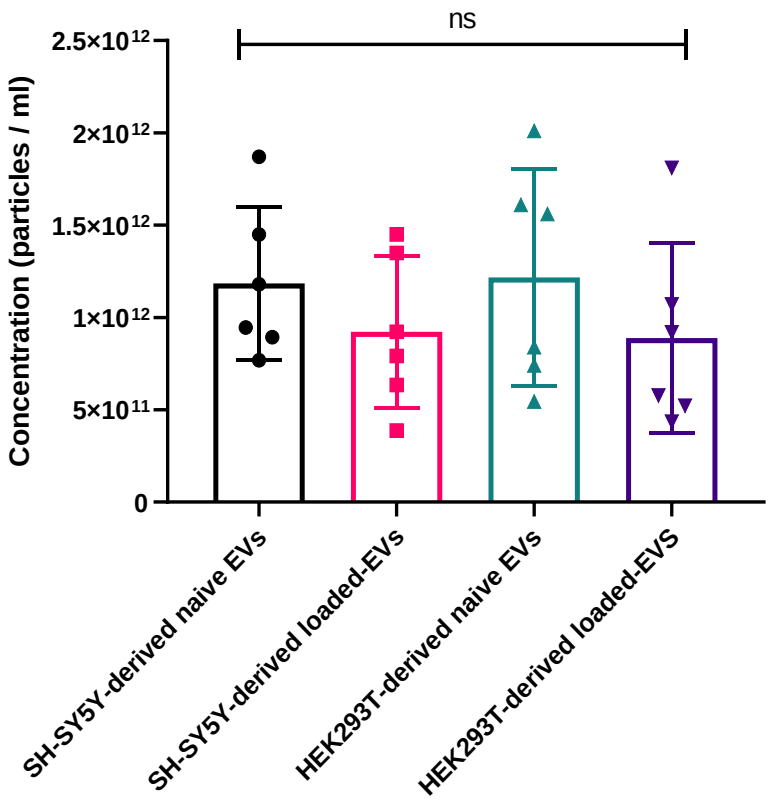


**Figure 5.6:** The concentrations of EV in pellets following resuspension in 300 µl of PBS isolated from both non-transduced and sorted-transduced SH-SY5Y and HEK293T cells. Six independent experiments were performed and data presented as mean ± SD. Statistical analysis: one-way ANOVA, Tukey's multiple comparison test; ns denotes $p > 0.05$.

### *5.3.2.2 TEM*

In addition to NTA analysis of size, TEM was also performed to characterise loaded-EVs from SH-SY5Y cells. Fig. 5.7a-b display cup-shaped, negative stained vesicles characteristic of literature reports for EVs analysed using TEM [207–209]. It can be estimated from Fig. 5.7 that the diameter of the vesicles is around 90 nm, which is consistent with the size observed by NTA analysis. The size determined by TEM is slightly less than that shown by NTA, which

arises because NTA gives the hydrodynamic size of hydrated EVs present in suspension, whereas dry conditions were used for the TEM analysis[147].

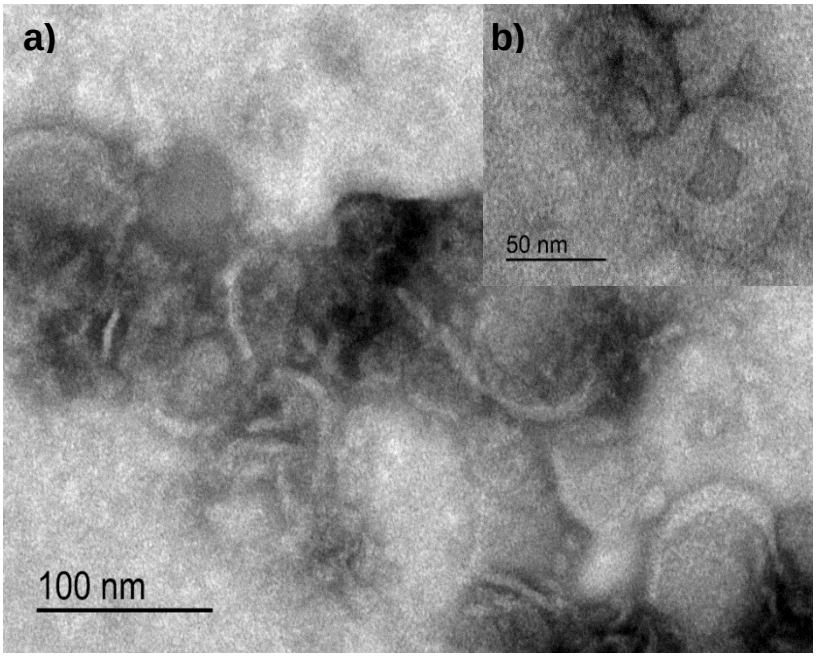


**Figure 5.7:** Representative TEM images of loaded-EVs from sorted-transduced SH-SY5Y (image a: magnification 20 000x and image b: magnification 40 000x).

### *5.3.2.3 Evaluation of EV protein content*

*Protein analysis using western blot*

Fig. 5.8 shows a representative western blot obtained for loaded-EVs and naïve EVs derived from SH-SY5Y cells. The presence of the transmembrane protein CD9 in both preparations is consistent with the lipid bilayer of EVs, and the presence of cytosolic TSG101 confirms that these lipid bilayer structures enclose intracellular material [86]. Fig. 5.8a also shows a positive band for eGFP in the loaded-EVs which is not visible for the naïve EVs (Fig. 5.8b). We also note the absence of Calnexin in both EV preparations, which would appear as a band at approximately 90 kDa. This observation signifies that there are no contaminating vesicles from the endoplasmic reticulum (these are sometimes co-isolated with EVs).

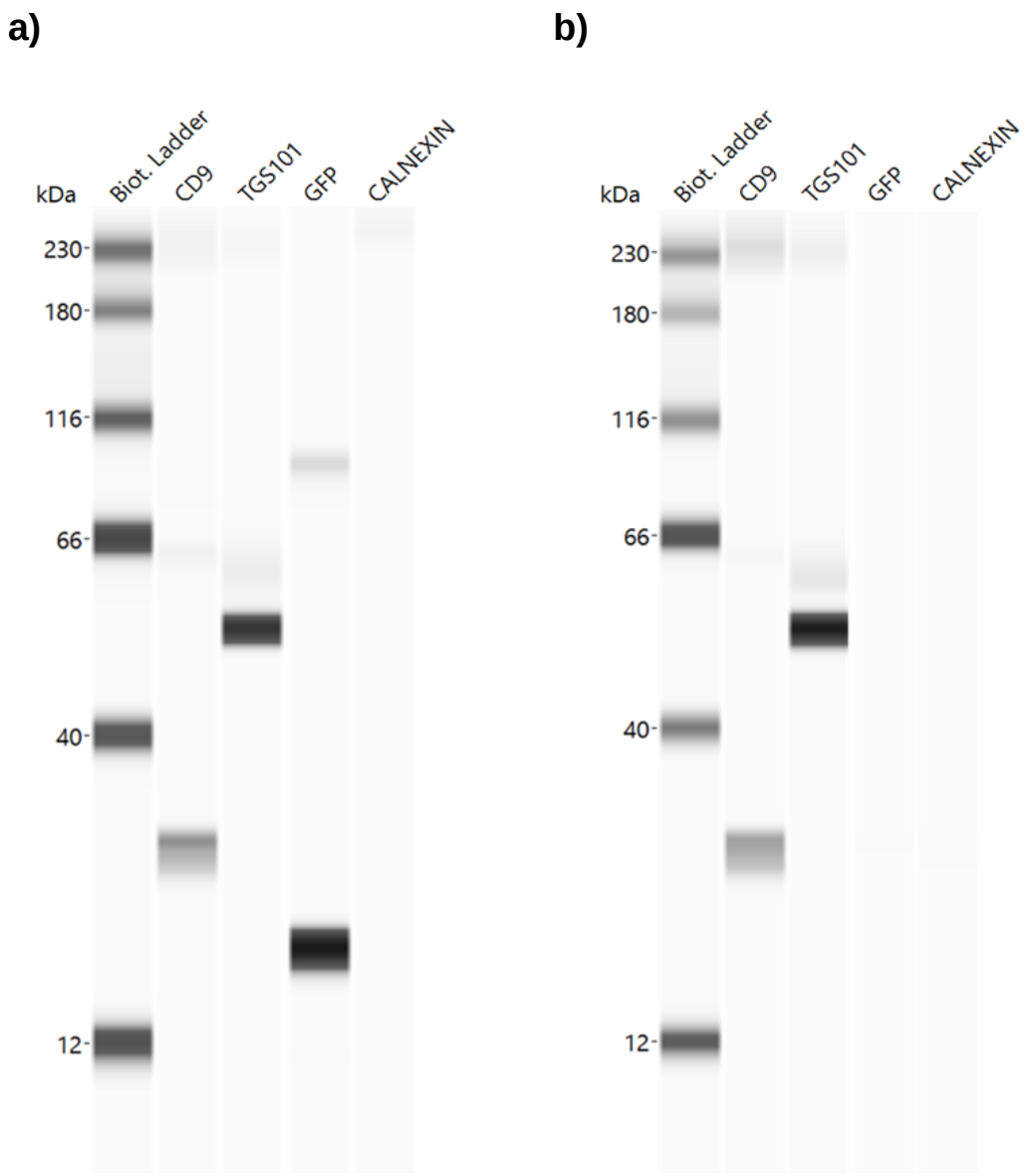


**Figure 5.8:** Detection of EV target proteins (CD9, TSG101), incorporated eGFP, and the endoplasmic reticulum vesicle marker Calnexin, as analysed by simple western blotting of a) loaded-EVs and b) naïve EVs derived from SH-SY5Y cells.

*Quantification of eGFP content in loaded-EVs*

GFP ELISA was used to quantify the eGFP content of loaded-EVs and naïve EVs derived from SH-SY5Y cells (Fig. 5.9). The eGFP concentration in loaded-EVs from SH-SY5Y cells is significantly higher than that of loaded-EVs from HEK293T cells (0.53 and 0.17 ng/$10^9$ particles, respectively). This difference can be attributed to the fact that the SH-SY5Y cells have greater transduction efficiency than HEK293T cells, as seen by the 100 % transduction efficiency at MOI 25 compared to 80 % at MOI 100 in HEK293T cells (Fig. 5.3). This probably also means that the level of virus integration into the genome of SH-

SY5Y cells is higher than with HEK293T cells and hence there is a higher level of eGFP expression in the producer cells themselves. Moreover, naïve EVs contained no eGFP, as expected given it is not an intrinsic protein in non-transduced SH-SY5Y and HEK293T cells.

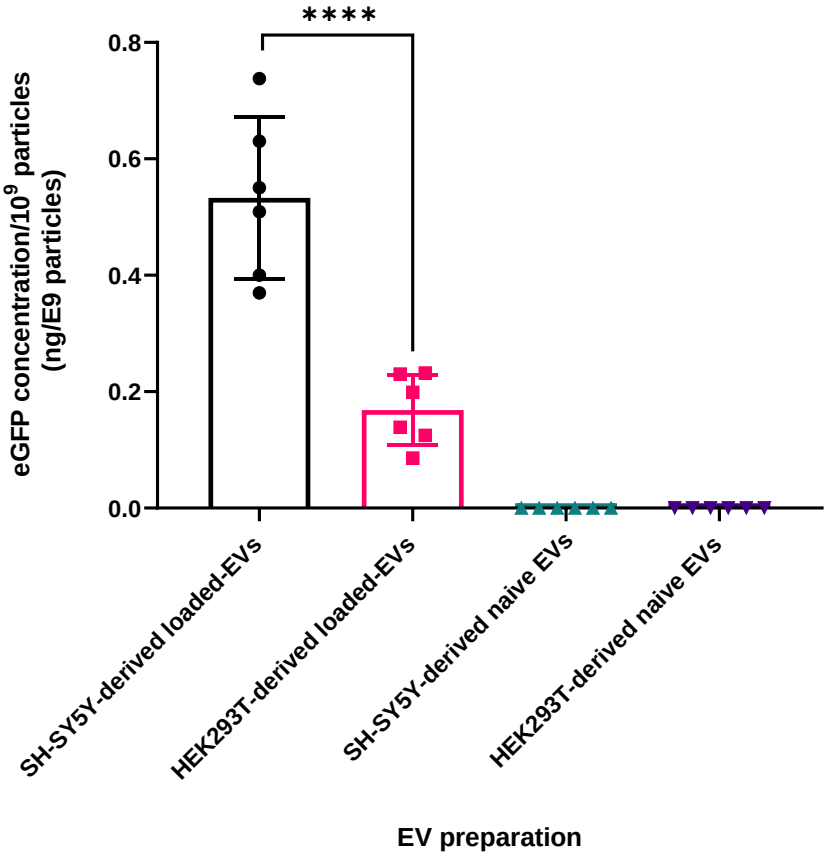


**Figure 5. 9**: eGFP concentration in different EV preparations derived from HEK293T and SH-SY5Y cells. Six independent experiments were performed and data are presented as mean ± SD. Statistical analysis: one-way ANOVA, Tukey's multiple comparisons test; ****p < 0.0001.

### 5.3.3 *In vivo* biodistribution study

The key aim of this chapter is to evaluate whether loaded-EVs derived from a neuronal cell line can deliver a higher payload to the CNS than EVs from HEK293T cells. The loaded-EVs from SH-SY5Y cells have a similar size, concentration and presence of protein markers as EVs from HEK293T cells, but contain a higher amount of incorporated eGFP. Therefore, they seemed like a promising candidate to deliver eGFP to the CNS as well as other organs. A biodistribution study in neonates was conducted using the same protocols

as with loaded-EVs from HEK293T cells (see **Section 2.6.2**, Table 2.6 for the administration schedule, routes of administration and time points).

The eGFP concentration of loaded-EVs was normalised to 300 ng/ml, with a corresponding EV concentration of ~5.5 x $10^{11}$ EVs/ml, to ensure homogenous dosing throughout the study. Naïve EVs were used as negative controls in this study. The concentration was normalised to the approximately the same as for the loaded-EVs. The administration schedule and routes of administration (as reported in **Section 2.6.2**, Table 2.6) were designed such that the highest volume of loaded-EVs permissible via each route was injected, to reduce the risk of achieving non-detectable levels of eGFP when using ELISA for analysis. As EVs have been shown to have a short half-life with non-detectable levels observed 6 hours after administration, a one hour time point was used in this study.

#### *5.3.3.1 eGFP content in the brain*

Fig 5.10 shows the eGFP content in the brain one hour following injection of loaded-EVs derived from either SH-SY5Y or HEK293T cells using different routes of administration. The eGFP concentration in the brain is significantly higher with loaded-EVs from HEK293T cells than that achieved following administration of loaded-EVs from SH-SY5Y cells, through all routes studied: ICV ($p < 0.01$), IV ($p < 0.05$) and IP ($p < 0.0001$). This is despite the fact that loaded-EVs from SH-SY5Y cells had a higher concentration of eGFP than those from HEK293T cells.

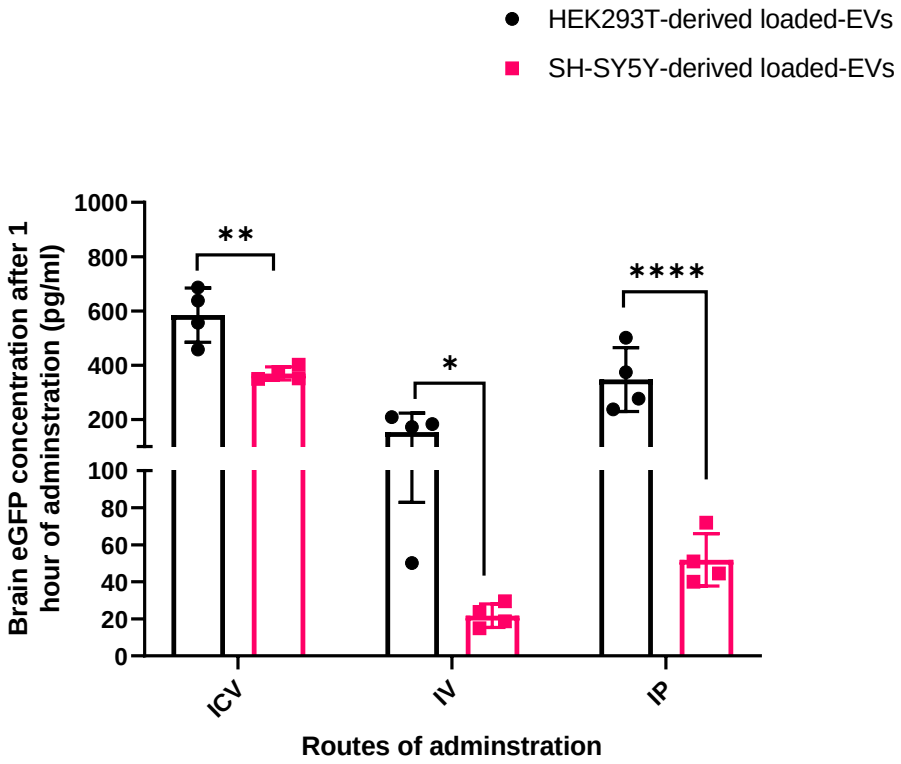


**Figure 5.10**: The eGFP content in the brain of neonatal mice one hour following administration of loaded-EVs from HEK293T or SH-SY5Y cells through ICV, IV and IP routes. N=4; data presented as mean ± SD. Statistical analysis: two-way ANOVA, Tukey's multiple comparisons test; *p < 0.05, **p ≤ 0.01, ****p < 0.0001

A similar trend in tissue distribution is seen with loaded-EVs from both SH-SY5Y and HEK293T cells. The highest concentration of eGFP in the brain is attained via the ICV route, followed by IP and then IV administration. Fig. 5.11 depicts the percentage of loaded-EVs from both preparations that have crossed the BBB and are present in the brain one hour following IV and IP administration. We can see that the percentage of HEK293T loaded-EVs administered via the IP route is significantly higher than that with SH-SY5Y EVs (4.2 % and 0.6 %, respectively, $p < 0.001$). However, the difference between the two EV preparations administered via the IV route is not significant (1.8 % and 0.3 %, respectively, $p > 0.05$). There is also no significant difference between the percentage of loaded-EVs from SH-SY5Y cells that have crossed the BBB following IP and IV administration ($p > 0.05$).

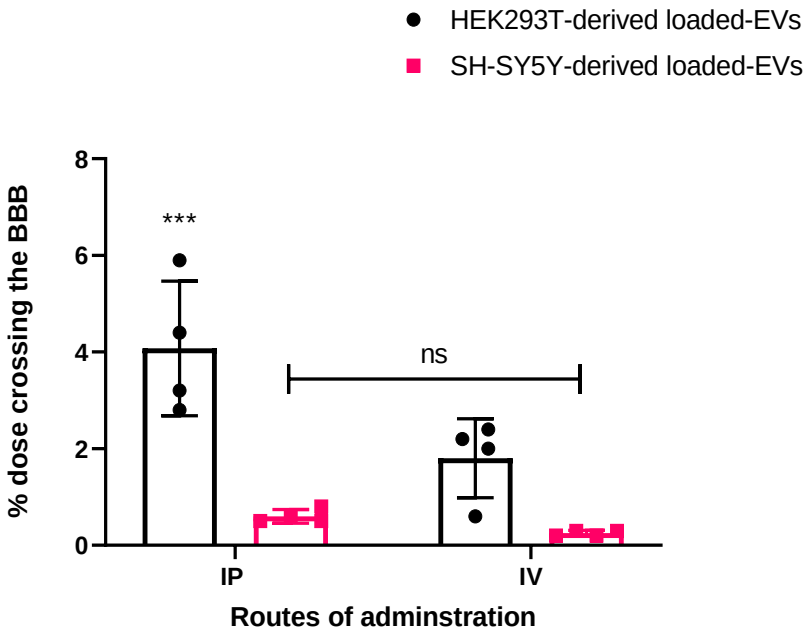


**Figure 5.11:** The percentage of loaded-EVs derived from HEK293T and SH-SY5Y cells that have crossed the BBB 1 hour after IP and IV administration. N=4 and data presented as mean ± SD. Statistical analysis: one-way ANOVA, Tukey's multiple comparisons test; ***p ≤ 0.001.

The reduced presence of EVs in the brain following administration of loaded-EVs from SH-SY5Y cells could be attributed to multiple factors, for instance faster elimination and a shorter half-life. This is despite the fact that EVs derived from SH-SY5Y cells have a higher load of eGFP than those from HEK293T cells (0.53 and 0.17 ng/$10^9$ particles, respectively). The observation that eGFP levels are lower with SH-SY5Y than HEK293T EVs even after ICV injections, where EVs are delivered directly to the brain without having to cross the BBB, suggests that the lower eGFP levels in the brain are not simply due to the SH-SY5Y EVs being less able to cross the BBB, but rather faster clearance. If the levels of eGFP achieved in the brain following ICV injections of the two EV preparations were similar but reduced amounts were seen with the SH-SY5Y EVs delivered through the other routes, then this would indicate an inability of SH-SY5Y EVs to cross the BBB, but this is clearly not the case. Alternatively, it might be that the two sets of EVs display different surface receptors, resulting in different levels of internalisation. Since little is known about how EVs are internalised, cleared, and what composition is responsible for such features, it is difficult to draw a definitive conclusion. However, these

results seem to suggest that EVs derived from neuronal cell lines do not necessarily have a natural homing ability to neurons.

### *5.3.3.2 eGFP content in the liver*

The eGFP content in the liver one hour following injection of loaded-EVs derived from the two cell lines could allow us to evaluate whether the lower brain distribution of SH-SY5Y-derived loaded-EVs is simply due to more extensive trafficking to the liver. These data are presented in Fig. 5.12.

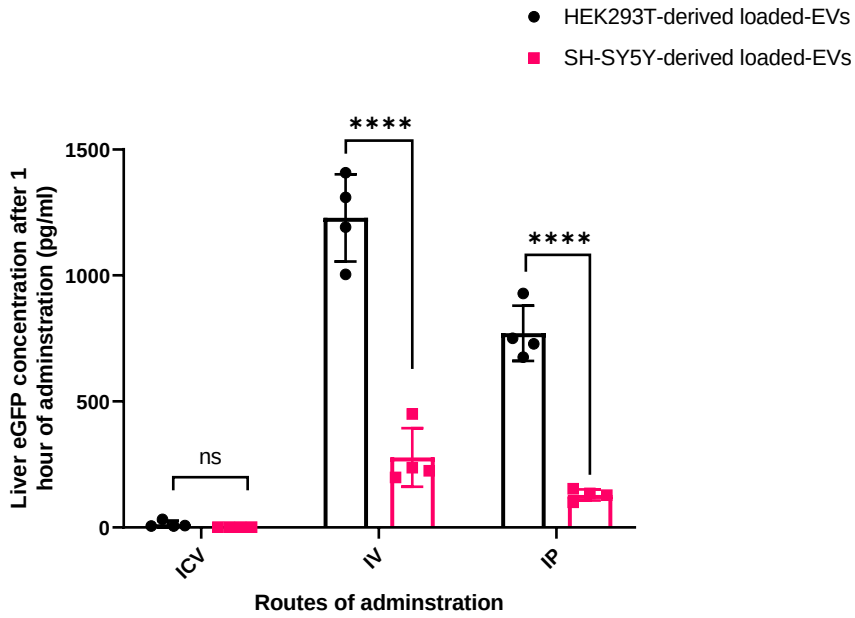


**Figure 5.12**: The eGFP content in the liver of neonatal mice one hour following administration of loaded-EVs from HEK293T or SH-SY5Y cells through ICV, IV and IP routes. N=4 and data presented as mean ± SD. Statistical analysis: two-way ANOVA, Tukey's multiple comparisons test; ns denotes $p > 0.05$, ****$p < 0.0001$.

A similar trend in distribution to the liver is seen following injections of both EV preparations via the different routes. The eGFP concentration in the liver following ICV injection is non-detectable for both EV preparations, higher following IP administration, and highest after IV administration. There is no significant difference between the liver eGFP concentrations following ICV administration of either EV preparation. However, the eGFP concentration is significantly higher following both IV and IP administration of HEK293T-derived loaded-EVs ($p < 0.0001$). The fact that the eGFP concentration in the liver is lower following IV and IP administration of SH-SY5Y-derived loaded-

EVs could mean that this EV preparation might have a faster elimination rate in comparison to EVs from HEK293T cells, or that they simply have a different distribution profile.

#### *5.3.3.3 eGFP content in the heart*

Finally, the eGFP concentration in the heart following administration of the EV preparations was quantified, as depicted in Fig. 5.13.

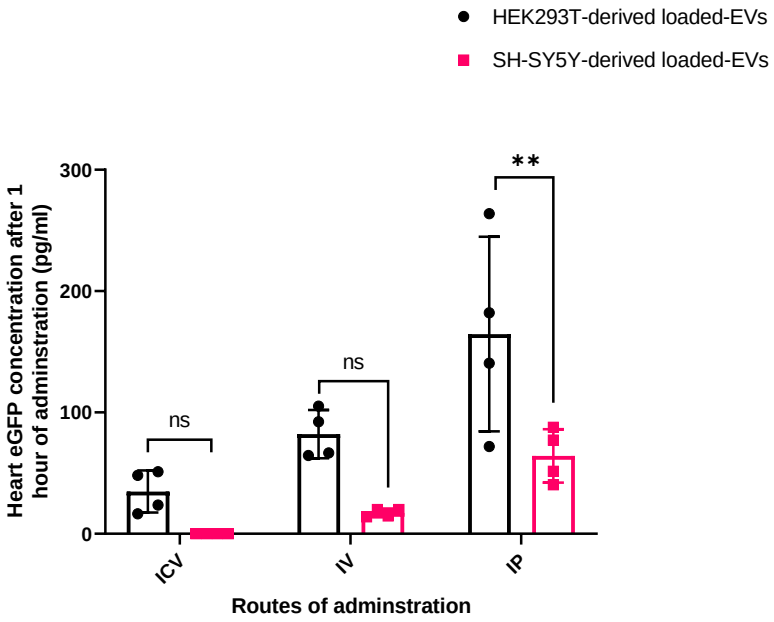


**Figure 5.13:** The eGFP content in the heart of neonatal mice one hour following administration of loaded-EVs from HEK293T or SH-SY5Y cells through ICV, IV and IP routes. N=4 and data presented as mean ± SD. Statistical analysis: two-way ANOVA, Tukey's multiple comparisons test; ns denotes $p > 0.05$, **$p \leq 0.01$.

The highest heart eGFP concentration is achieved following IP injections, followed by IV, and then ICV administration. There is no significant difference in the levels achieved in the heart via administration via the ICV and IV route. The eGFP concentration in the heart following IP injection of HEK293T EVs is significantly higher than that with SH-SY5Y EVs. This tends to agree with the previous datasets, and indicates that the SH-SY5Y EV preparation might have a faster elimination rate than EVs derived from HEK293T cells.

Overall the findings in this chapter suggest that simply using a neuronal cell line to produce EVs does not necessarily result in EVs that display neuron targeting properties *in vivo*. This targeting has previously been reported *in*

*vitro,* as found by some studies discussed in **Section 5.1**, but the *in vivo* targeting capability remains to be verified and seems to be more complex than initially expected.

## 5.4 Conclusion

SH-SY5Y cells were used to successfully produce loaded-EVs with similar characteristics (mean and mode size, concentration and surface markers) as those previously produced from HEK293T cells. The SH-SY5Y-derived loaded-EVs had a higher concentration of incorporated eGFP than those produced from HEK293T cells (0.53 and 0.17 ng/$10^9$ particles, respectively).

The *in vivo* biodistribution profiles of SH-SY5Y-derived loaded-EVs in neonate mice were assessed and compared to those of loaded-EVs derived from HEK293T cells, following the same routes of administration. These studies demonstrated that SH-SY5Y-derived loaded-EVs can deliver cargo to both the brain and visceral organs via the different routes of administration (IV, IP and ICV). The tissue distribution of SH-SY5Y-derived loaded-EVs followed the same pattern as that of HEK293T EVs. However, the eGFP concentrations achieved in the brain, heart and liver following injections of SH-SY5Y loaded-EVs were lower than when HEK293T loaded-EVs were given by the same route. This suggests a faster relative clearance of SH-SY5Y-derived EVs, which means that to be able to verify whether these EVs have a homing ability to neurons the biodistribution must be evaluated sooner than 1 hour after administration. Such a short half-life is likely to be problematic when it comes to therapeutic applications, however, and thus HEK293T cells appear to be more suitable for further exploration. Overall, it seems that alternative strategies to increase the levels of cargo delivered to the brain must be evaluated. This is important for our ultimate aim of delivering GCase loaded-EVs to both the brain and visceral organs for the treatment of Gaucher Dissease Type 2. A potential strategy could be to further optimise HEK293T-derived EVs such that they incorporate a higher amount of the desired cargo, since they were shown in Chapter 4 to be able to cross the BBB following systemic administration.

The next chapter will use the platform of cellular factories for the production of loaded-EVs developed in Chapter 3 and in this case the EVs will be loaded with GCase enzyme to be evaluated as a potential treatment for Gaucher Disease.

# Chapter 6: Production of therapeutic GCase-loaded EVs

## 6.1 Introduction

In Chapter 4, it was determined that loaded-EVs from HEK293T cells were able to cross the blood brain barrier (BBB) following IV and IP administration, although the percentage dose remaining in the brain 1 hour after administration was only 4 % following IP administration. Subsequently, in Chapter 5 it was revealed that targeting of loaded-EVs to the brain was not improved through the use of a neuronal cell line as producer cells for loaded-EVs, and EVs from HEK293T cells delivered a higher eGFP cargo to the brain as well as the visceral organs. Thus, in this chapter we aimed to increase the amount of cargo incorporated into EVs derived from HEK293T cells, such that when these EVs cross the BBB they can deliver a higher cargo load to the brain.

Some strategies have been evaluated in the literature to increase the targeting of cellular cargo to EVs. One relies on first creating a lentiviral construct where a gene of interest is fused to the N-terminal of the C1C2 domain of lactadherin. This vector is then used to transduce the EV producer cell line, and EVs produced contain the chimeric protein. The lactadherin C1C2 domain is a lipid binding domain that was initially found to mediate the secretion of lactadherin in EVs in non-mammillary gland derived cell lines [262]. Further studies revealed that the fusion of proteins (including soluble and intracellular proteins) to the C1C2 domain of lactadherin results in their almost exclusive presence in the inside of EVs and that they are no longer found intracellularly [263–266]. Deletion of the C1C2 domain results in elimination of this targeting to EVs [262]. The underlying mechanisims behind this highly specific targeting to EVs is still undefined but it is established that N-terminal fusion of the C1C2 domain is essential to this targeting to the EV compartment [262]. Studies on the three-dimensional structure of coagulation factors V and VIII, which contain a C1C2 domain related to that in lactadherin, suggest that the sizes of and the distances between the grooves present in the C1 and C2 domains of lactadherin, which mediate binding and docking of membrane lipids, favour binding to membranes of specific lipid content as found in EVs [267–269].

A similar strategy fusing the gene of interest to the transmembrane protein of vesicular stomatitis virus GP (VSVG), has also been used to target proteins to EVs [126]. As previously explained in **Section 1.7.1** VSVG is often used for pseudotyping of lentiviral vectors, which is the process whereby VSVG protein is incorporated into the envelope of the lentiviral vector. Once the VSVG is incorporated into the envelope of the vector it warrants broad tropism and high efficacy in transduction, due to its ability to bind to receptors on a wide range of cells. [129,133,134]. VSVG incorporation occurs during the budding of microdomains at the plasma membrane, the same domains involved in the formation of endosomes and EVs [270]. Meyer *et al*. demonstrated that this pseudotyping approach can result in the targeting of protein payloads such as green fluorescent protein (eGFP), red fluorescent protein (RFP) and luciferase to EVs [271].

Both of the above approaches have promise, but also drawbacks since the underpinning mechanisms are not known. An alternative route relies on the genetic fusion of the protein ubiquitin, and here the mechanism by which proteins are targeted to EVs is relatively better understood [272]. To understand how addition of ubiquitin tag to a protein can influence targeting to EVs, we must revisit the biogenesis of EVs detailed in Chapter 1 (**Section 1.4**). During biogenesis, first intraluminal vesicles (ILVs) are formed in multivesicular bodies (MVBs) through the invagination of the endosomal membrane. MVBs then fuse with the plasma membrane releasing EVs [39,57,58]. Protein cargo is sorted into MVBs using the endosomal sorting complex required for transport (ESCRT) machinery [59,62,273]. It has been shown that ESCRT-0 is involved in this sorting, which is mediated by ubiquitin-interacting motifs on the protein complexes. ESCRT-0 thus clusters ubiquitinated proteins for delivery into MVBs [273]. Some studies have demonstrated that fusion of ubiquitin to a soluble protein such as eGFP, mycobacterial proteins or the tumour antigenic protein nHer2 can increase targeting to EVs [272,274–276]. It was also determined that fusion of the gene of interest to the N-terminal of ubiquitin provides better targeting results, with concentrations of desired protein increasing by 10-fold in comparison to samples lacking the ubqiutin fusion tag [274].

Thus, in this chapter we aimed to create a lentiviral construct containing the therapeutic *GBA1* gene fused to the N-terminal of the ubiquitin tag to ensure that GCase enzyme is targeted to EVs. A lentiviral construct containing the *GBA1* gene without the ubiquitin tag will also be investigated. The ultimate aim is to evaluate the use of these GCase loaded-EVs for the treatment of Gaucher disease Type 2.

## 6.2 Aims and objectives

In Chapter 5, it was shown that loaded-EVs derived from HEK293T cells led to higher eGFP concentrations than SH-SHY5Y EVs *in vivo* one hour after administration, and hence HEK293T cells will be used to produce EVs loaded with the therapeutic GCase enzyme. Further optimisation of the loading capacity of these EVs will also be attempted, using the ubiquitin tag to facilitate targeting of GCase to EVs. Firstly, cloning will be used to produce a lentiviral vector containing the *GBA1Ub* insert, followed by subsequent transduction of HEK293T cells. These will then be used to produce loaded-EVs containing GCase. Loaded-EVs will be characterised for size and concentration, surface markers and GCase activity, and finally their ability to deliver and upregulate GCase levels in HEK293T cells will be evaluated.

## 6.3 Results and discussion

### 6.3.1 Cloning

To make a lentiviral construct containing the *GBA1Ub* gene, cloning using double enzyme digest followed by subsequent ligation was performed (Fig. 6.1). A plasmid containing the *GBA1Ub* gene was obtained from ThermoFisher and the plasmid with lentiviral backbone was kindly provided by Dr. Michael Hughes (Fig. 6.1a). *BamH*I and *Mlu*I restriction enzymes were used to remove the *GBA1Ub* gene from the pGBA1Ub construct, and the same enzymes were also used to remove IRES.eGFP from the construct with the lentiviral backbone (pSFFV.IRES.eGFP.WPRE) and generate compatible sticky ends (Fig. 6.1b). The product of each digestion reaction underwent gel electrophoresis. The results of this are presented in Fig. 6.1c, where in lane 1

a band at around 1.9 kb corresponding to the *GBA1Ub* gene and another band for the rest of the plasmid are observed. In lane 2, a band at around 1.5 kb corresponds to IRES.eGFP and a second band at 10 kb to the rest of the template construct (the lentiviral backbone). The 1.9kb *GBA1Ub* insert and the 10 kb lentiviral backbone were then extracted from the gel, purified, and ligated at a molar ratio of 1:3 backbone to insert, to produce pSFFV.GBA1Ub.WPRE (Fig. 6.1d).

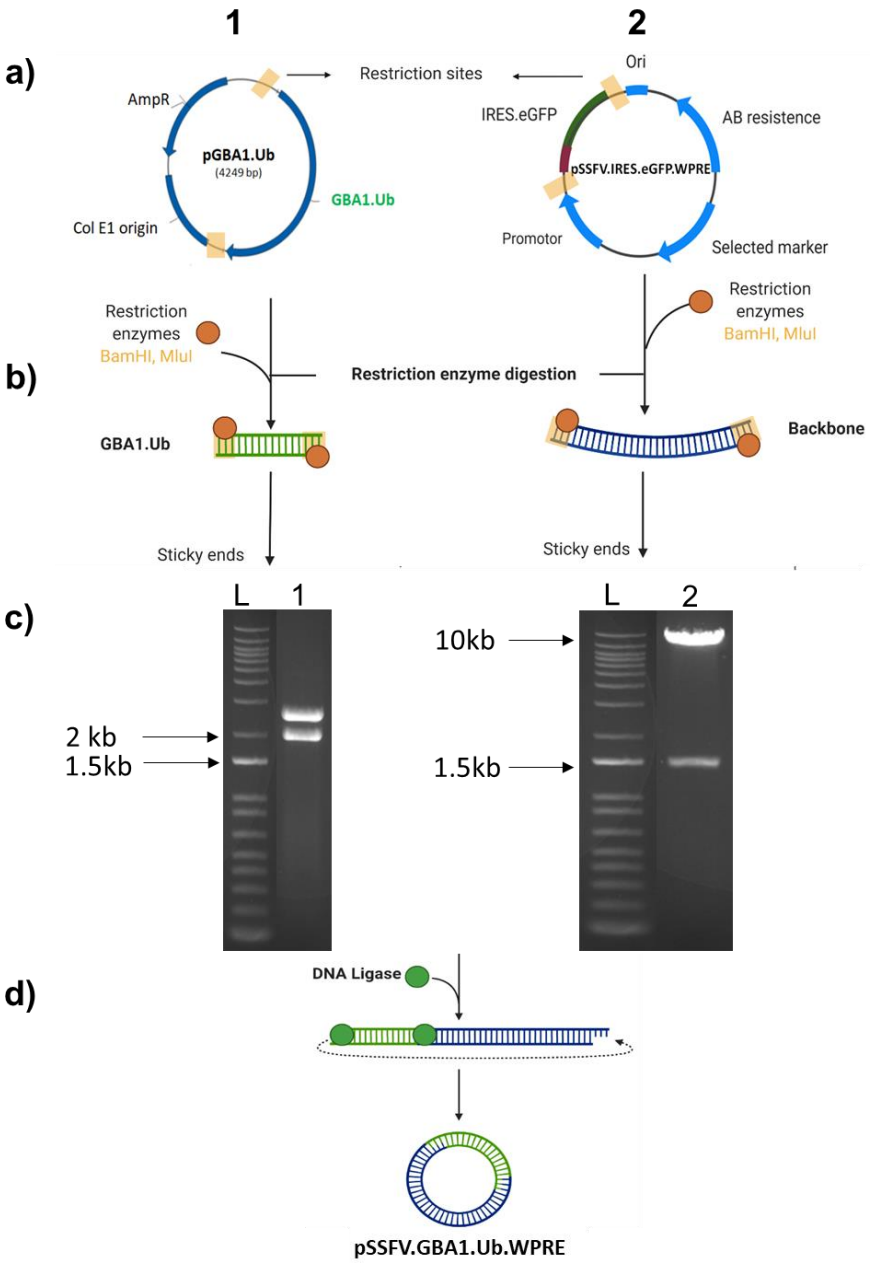


**Figure 6.1:** Cloning the *GBA1Ub* gene into a lentiviral construct. a) Illustrations of pGBA1Ub (1) and lentivral construct pSSFV.IRES.eGFP.WPRE (2); b) digestion using *BamHI* and *MluI* restriction enzymes to obtain *GBA1Ub* and remove IRES.eGFP from the lentivial construct; c) gel electrophoresis results of *BamH*I and *Mlu*I double digests of 1- pGBA1Ub, 2-

pSFFV.IRES.eGFP.WPRE, L-ladder; and, d) ligation of sticky ends to generate pSSFV.GBA1Ub.WPRE. Illustrations created with BioRender.com

Incorporation of the insert was confirmed by a *BamH*I and *Mlu*I restriction enzyme digest and agarose gel electrophoresis, which revealed the predicted bands at 1.9 kb and 10 kb corresponding to *GBA1*Ub and the lentiviral backbone respectively (Fig. 6.2). Automated Sanger sequencing (outsourced to SourceBiosciences) of the plasmid was performed to confirm the successful introduction of the *GBA1* gene into the lentiviral construct. The sequence obtained was compared to the expected SFFV.GBA1Ub sequence, which revealed the successful incorporation of *GBA1Ub* instead of IRES.eGFP.

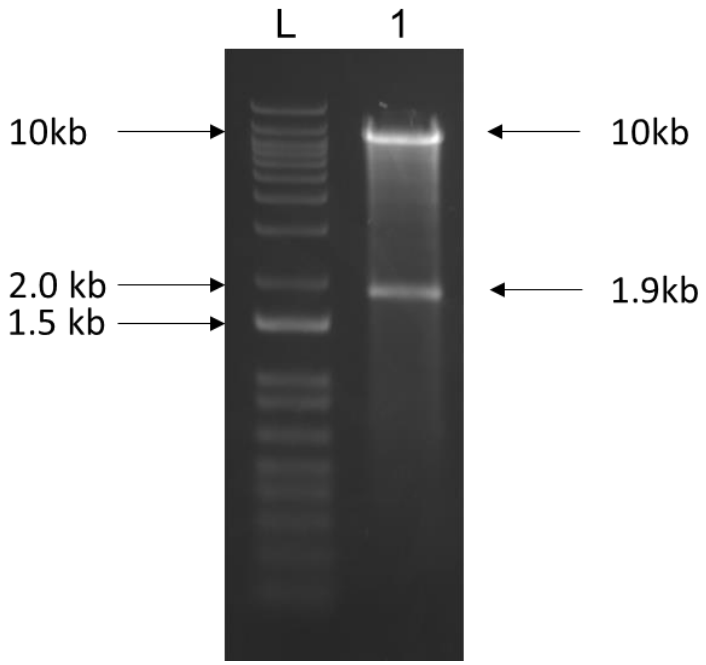


**Figure 6.2:** Image of confirmation digest of pSSFV.GBA1Ub.WPRE, where in lane 1 the band at 1.9 kb corresponds to *GBA1Ub* and the band at 10 kb to the lentiviral backbone.

We also aimed to produce a lentiviral plasmid construct with the *GBA1* gene but without the ubiquitin tag, by cloning out the IRES.eGFP in the pSFFV.GBA1.IRES.eGFP.WPRE plasmid to obtain pSFFV.GBA1.WPRE. This plasmid would be used as a control to ensure that the addition of the ubiquitin tag does not negatively affect the GCase enzyme activity, and that it enables the targeting of GCase to EVs. However, this cloning was not successful within the timeframe of the project. Therefore we decided to proceed with *GBA1Ub* while relying on previous literature that proved addition

of the ubiquitin tag does not negatively affect biological activity of tagged cargo, and enables targeting of this cargo to EVs [272,274,276–279].

Finally we attempted to generate the lentiviral plasmid pSFFV.GBA1.2a.eGFP.WPRE (Fig. 6.3). The aim here was to transduce HEK293T cells with this lentiviral vector, utilise the fluorescence provided by eGFP expression in these cells to sort the transduced cells, and select those with the highest expression of eGFP (and consequently GBA1) for subsequent use to produce loaded-EVs, in the same manner as detailed in **Section 3.3.2.3**. However, again this cloning was not successful despite numerous attempts.

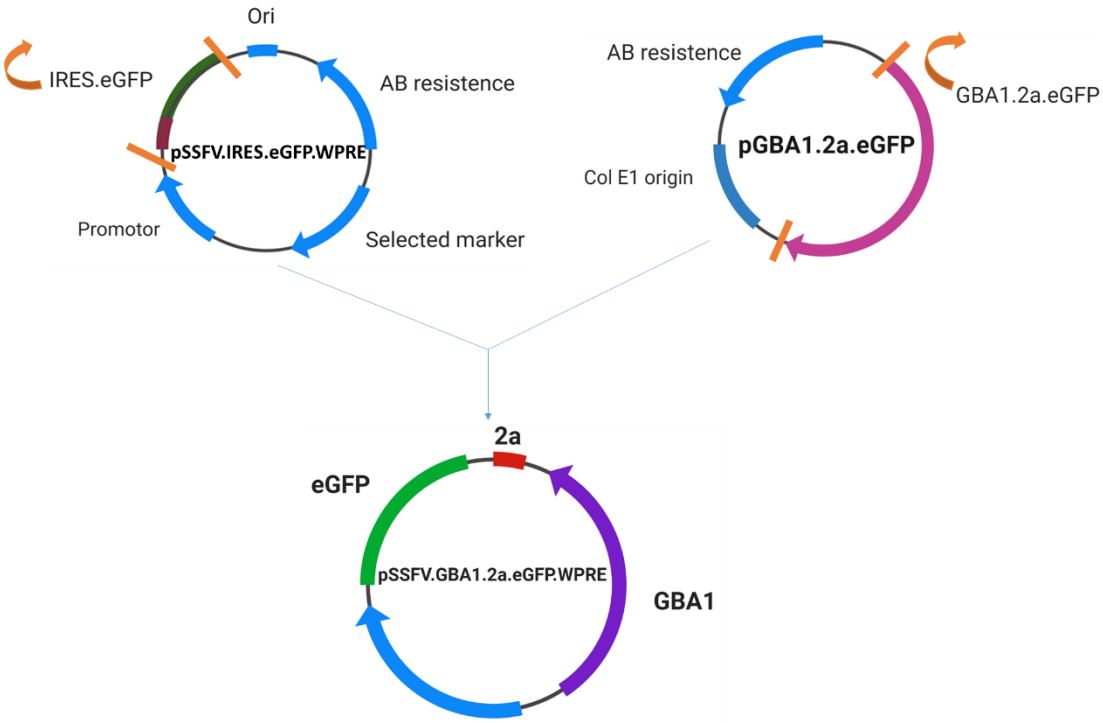


**Figure 6.3:** Illustration of cloning steps to generate a pSSFV.GBA1.2a.eGFP.WPRE lentiviral vector. Created using Biorender.com

## 6.3.2 Lentiviral production and titration

Following successful cloning of the *GBA1Ub* gene into a lentiviral plasmid construct, triple transfection of HEK293T cells was performed to make the lentivirus vector. Lentiviral titer was then obtained by quantification of the viral envelope protein p24 using the p24 assay. This revealed high titres of 4.15 $x10^8$ vp/ml.

### 6.3.3 *GBA1Ub* gene delivery to HEK293T cells

HEK293T cells were transduced with the lentivirus containing *GBA1Ub* at MOI of 100, since this enabled the highest transduction efficiency of VSV.G.SFFV.LUC.2A.eGFP.WPRE virus. To confirm successful transduction, GCase activity was determined by a fluorometric assay that relies on using 4-methylumbelliferyl-β-D-glucopyranoside (*4-MUβGlu)* as a substrate as detailed in **Section 2.4.5.3**. As can be seen from Fig. 6.4, transduced cells had significantly higher (11x) GCase enzyme activity than non-transduced cells. This confirms successful overexpression of GCase gene in the transduced cells. The GCase enzyme is intrinsic to all cells, which is why there is still some enzyme activity in non-transduced cells.

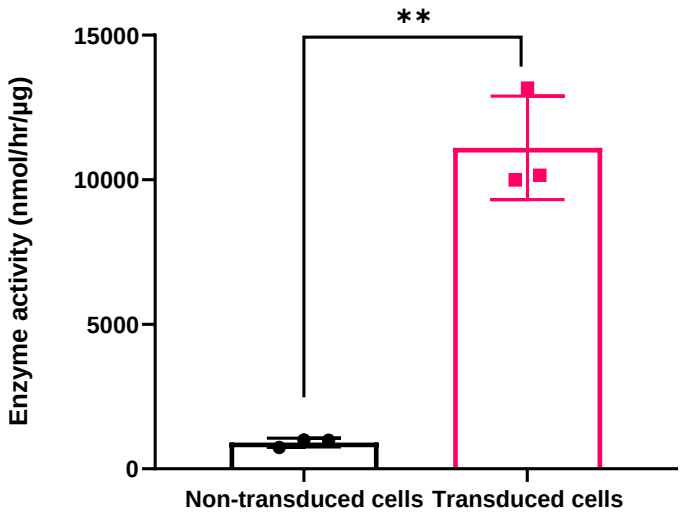


**Figure 6.4:** GCase activity for non-transduced and transduced HEK293T cells. Three independent experiments were performed and results are presented as mean ± S.D. Statistical analysis: unpaired t-test, Welch's correction, **p ≤ 0.01.

### 6.3.4 Characterisation of GCase-loaded EVs

#### *6.3.4.1 Size and concentration*

EVs from transduced HEK293T cells were then produced and isolated in the same manner as in Chapter 3. Fig. 6.5 shows the modal and mean sizes of particles in EV pellets derived from non-transduced cells and those transduced with VSV.G.SFFV.LUC.2A.eGFP.WPRE and SSFV.GBA1Ub.WPRE. All pellets displayed sizes within the size range expected for EVs. The modal

sizes of the loaded-EVs and naïve EVs showed no significant differences. In contrast, the mean size of loaded-EVs containing GCase was significantly smaller than those containing luciferase-eGFP. The reason for this is not understood.

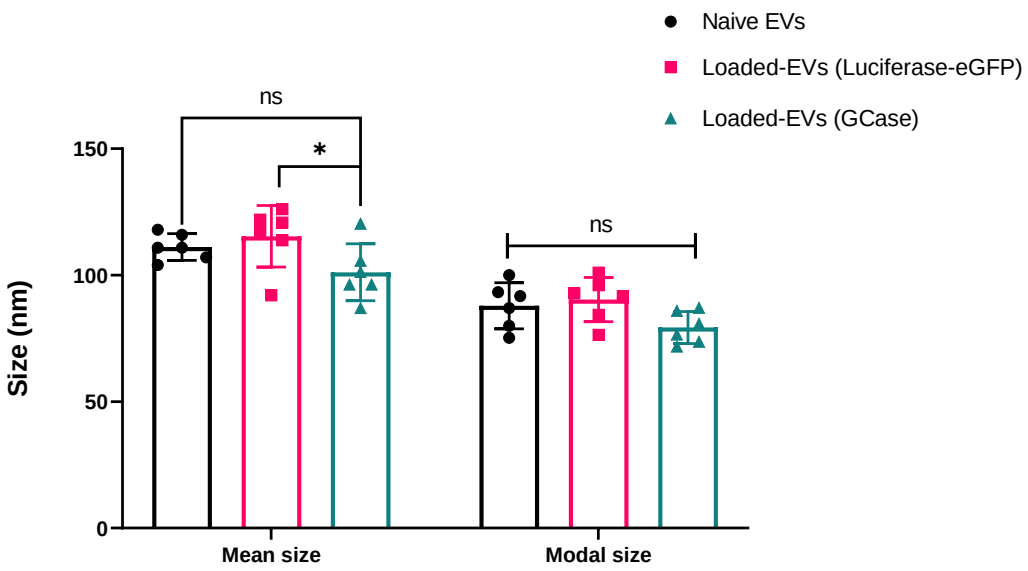


**Figure 6.5:** The mean and modal size of particles in different EV pellets. Six independent experiments were performed and data presented as mean ± SD. Statistical analysis: two-way ANOVA, Tukey's multiple comparison test; ns denotes $p > 0.05$, * $p \leq 0.05$.

The concentrations of EVs in the pellets following resuspension in 300 µl of PBS are compared in Fig. 6.6, which shows that there is no statistically significant difference between the three different EV samples.

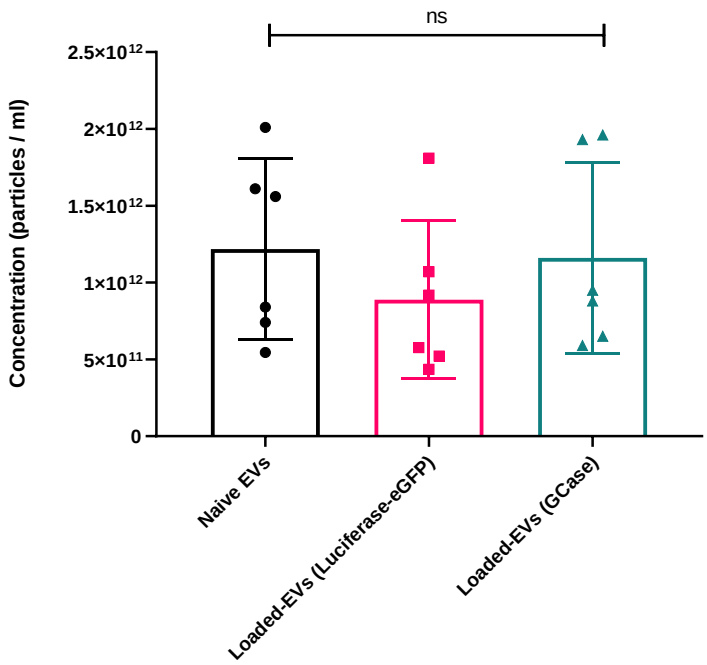


**Figure 6.6:** The concentrations of EVs in pellets following re-suspension in 300 µl of PBS, isolated from non-transduced HEK293T cells, sorted-transduced HEK293T cells (Luciferase-eGFP lentivirus) and transduced HEK293T cells (*GBA1Ub* lentivirus). Six independent experiments were performed and data are presented as mean ± S.D. Statistical analysis: one-way ANOVA, Tukey's multiple comparison test; ns denotes $p > 0.05$.

### *6.3.4.2 TEM*

TEM was also performed to characterise the GCase-loaded-EVs. The images in Fig. 6.7 depict cup-shaped, negative stained vesicles characteristic of literature reports for EVs analysed using TEM [207–209]. The vesicles had a diameter ranging from 50 - 150 nm, which is in agreement with the size observed by NTA analysis. The size determined by TEM is typically less than that shown by NTA because EVs in suspension are hydrated [147].

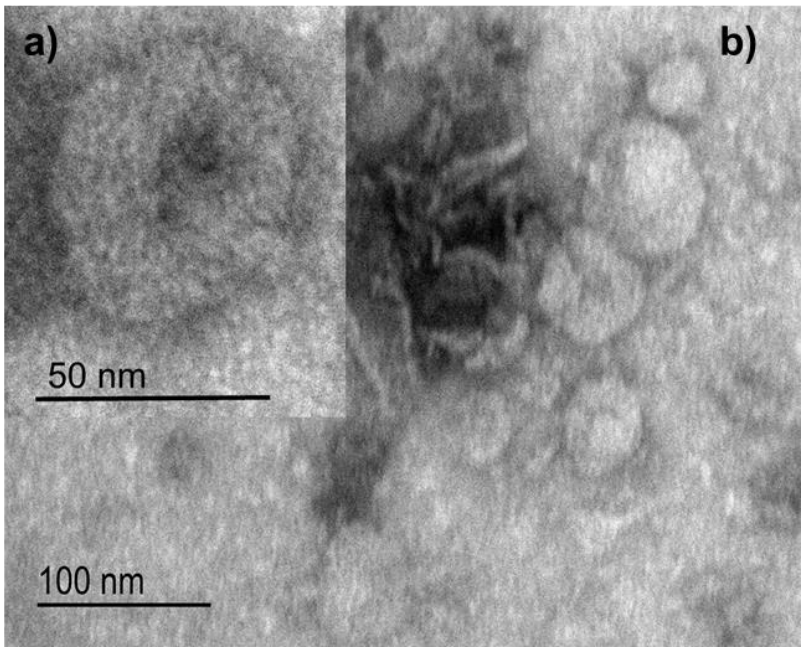


**Figure 6. 7:** Representative TEM images of GCase-loaded-EVs from transduced HEK293T cells (image a: magnification 40000x and image b: magnification 20 000x).

### *6.3.4.3 Protein analysis using western blot*

Fig. 6.8 depicts a representative western blot obtained for GCase-loaded-EVs and naïve EVs from non-transduced HEK293T cells. The presence of the transmembrane protein CD9 in both preparations is consistent with the lipid bilayer of EVs, and the observation of cytosolic TSG101 confirms that these enclose intracellular material [86]. We also note the absence of Calnexin in both EV preparations (this would appear as a band at approximately 90 kDa). This observation signifies that there are no contaminating vesicles from the endoplasmic reticulum (which are sometimes co-isolated with EVs). Fig. 6.8b also shows a positive band for GBA1UB in the loaded-EVs, which is not visible for the naïve EVs (Fig. 6.8a).

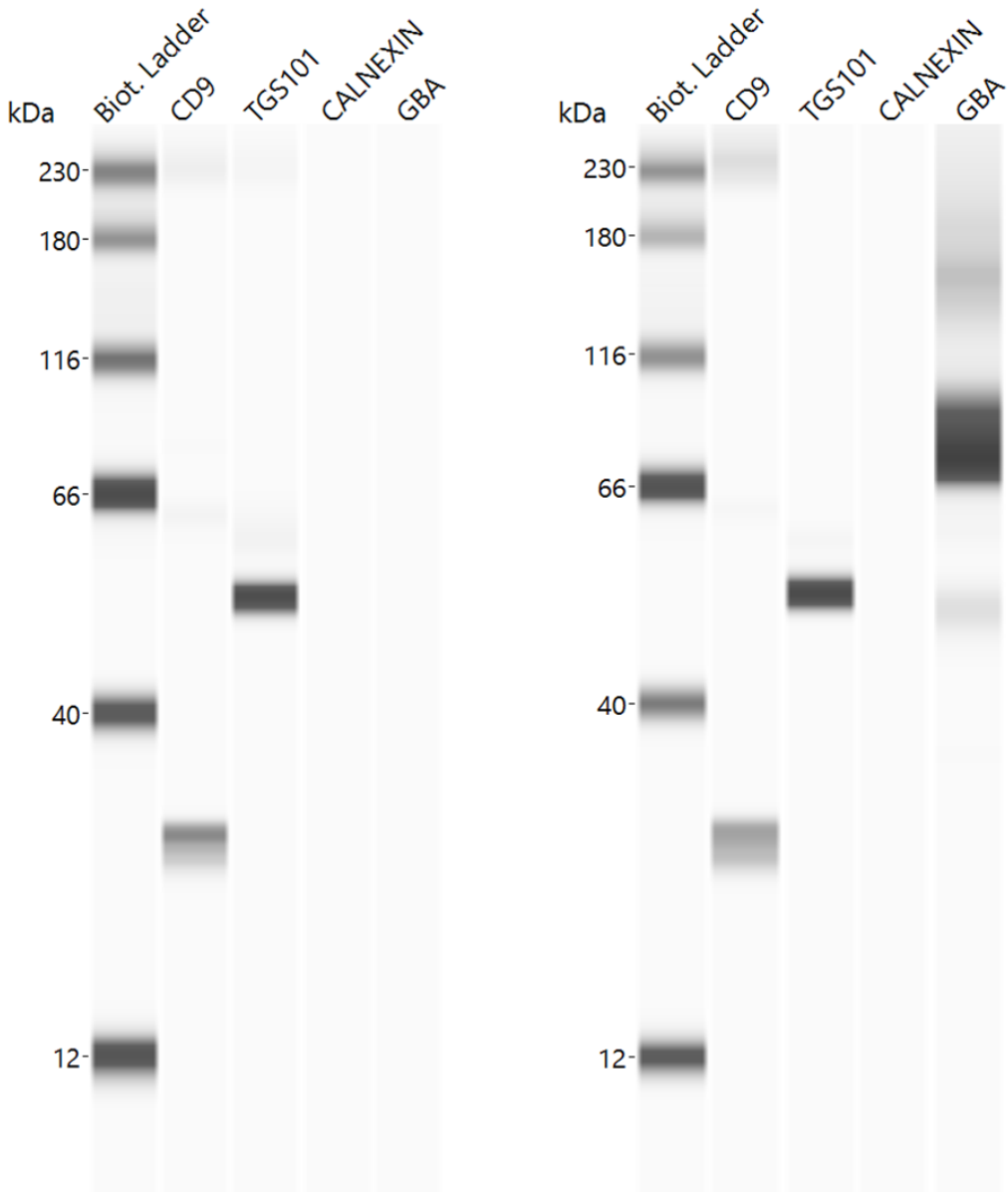


**Figure 6.8:** Analysis of the EV marker proteins CD9 and TSG101, GBA1, and the endoplasmic reticulum vesicle marker Calnexin, as analysed by simple western blotting of a) naïve EVs and b) GCase-loaded-EVs.

### *6.3.4.4 Analysis of GCase activity in loaded-EVs*

The activity of GCase in loaded-EVs was assessed using the GCase assay and compared to that in transduced cells, non-transduced cells and naïve EVs. As can be seen from Fig. 6.9, loaded-EVs have significantly (100-fold) higher enzyme activity than naive EVs ($p < 0.001$) and non-transduced cells ($p < 0.01$), which show non-detectable levels of activity. This is in agreement with the western blot results obtained above, where there are no bands corresponding to GCase in the naïve EV sample. Moreover, this suggests that

the ubiquitin tag might have facilitated trafficking of the GCase enzyme to EVs but we cannot be certain until we can determine GCase enzyme activity in loaded-EVs derived from cells transduced with the *GBA1* gene but without the ubiquitin tag.

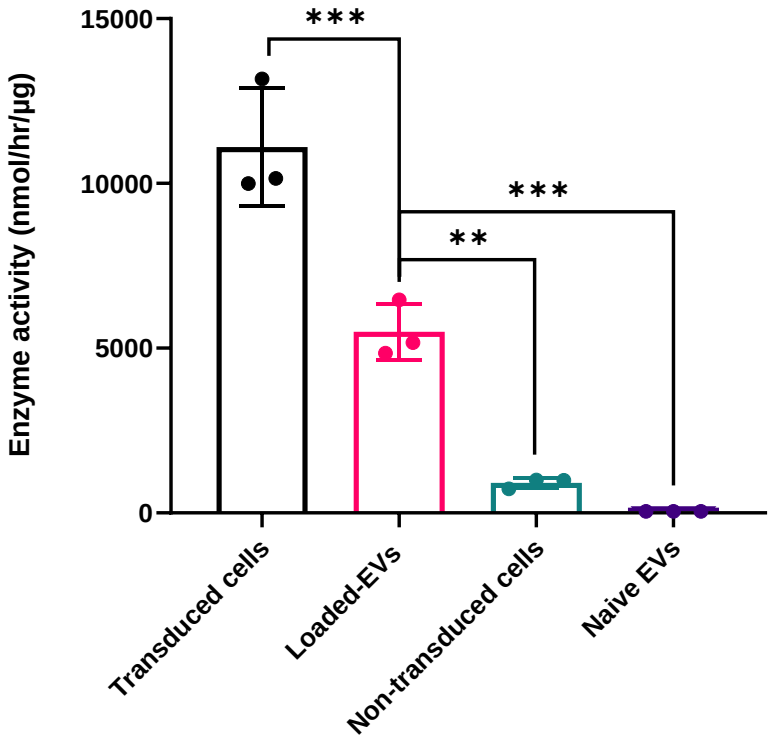


**Figure 6.9:** GCase activity in transduced and non-transduced HEK293T cells, and EVs derived from each. Three independent experiments were performed and results are presented as mean ± SD. Statistical analysis: one-way ANOVA, Tukey's multiple comparisons test; **p ≤ 0.01 and ***p ≤ 0.001.

### *6.3.4.5 Evaluation of uptake of GCase loaded-EVs by cells*

The ability of GCase loaded-EVs to upregulate GCase activity in HEK293T cells was determined and compared to control naïve EVs. As can be seen from Fig. 6.10, after 15 minutes incubation there is no significant difference in activity between cells incubated with GCase loaded-EVs and the control cells. This is followed by a gradual increase in activity over 1, 3 and 6 hours, at which time the increase relative to the control is significant. However, again at 24 hours this difference is no longer significant. These results suggest that loaded-EVs are internalized by cells and that they are slowly trafficked into the lysosome, where the GCase is active in the acidic environment [1]. This trend in uptake is similar to that seen for luciferase-eGFP loaded-EVs in **Section 4.3.1**.

Although these results are promising, confirmation of upregulation of GCase activity in GBA deficient primary neurons *in vitro* is essential for further development of the loaded-EVs. Additionally, the upregulation of GCase activity *in vitro* appears to be short lived, which could negatively impact the clinical translatability of these EV therapies. Therefore, this experiment should be repeated with a higher number of replicates as well as use of wider range of concentrations of GCase-loaded EVs to be incubated with cells.

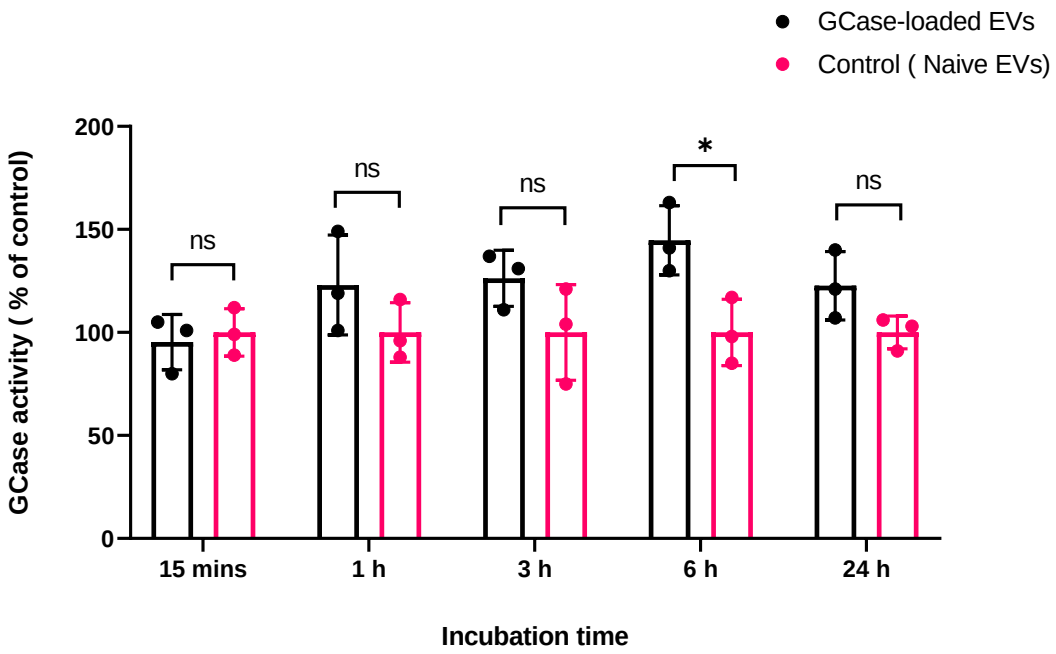


**Figure 6.10:** GCase enzyme activity in HEK293T cells following 15 minutes, 1, 3, 6, and 24 hours incubation with equal amounts of GCase loaded-EVs or naïve EVs (control). Three independent experiments were performed and results are presented as mean ± SD. Statistical analysis: two-way ANOVA, Tukey's multiple comparisons test; ns denotes $p > 0.05$ and *$p < 0.05$.

## 6.4 Conclusion

The *GBA1Ub* gene was successfully cloned into a lentiviral plasmid construct, and this was then used to generate a SFFV.GBA1Ub.WPRE lentivirus. Following transduction of HEK293T cells with this virus, GCase enzyme activity was determined to be 11x higher than that in non-transduced cells. The transduced cells could be used to produce GCase-loaded-EVs with similar characteristics (mean and modal size, concentration and surface markers) as EVs previously produced from HEK293T cells. Naïve EVs showed non-detectable GCase enzyme activity, but loaded-EVs showed 100x higher activity. Furthermore, the GCase loaded-EVs were shown to upregulate GCase enzyme levels *in vitro*. This suggests that the EVs can deliver a GCase cargo to target cells, and the enzyme is then transported to the lysosome where it becomes activated. These results are very promising for future translation of EVs as potential treatments of Gaucher disease but also other lyosomal storage disorders caused by a defect or lack of a lysosomal hydrolase.

# Chapter 7: Freeze-drying of EVs for long term storage

# 7.1 Introduction

## 7.1.1 Storage of EVs

As frequently noted in this thesis, over the last decade EV research has demonstrated that they can potentially be used in the treatments of various diseases [107,182,280–282]. EVs are generally stored suspended in phosphate buffered saline (PBS) at - 80 °C, as agreed upon by most studies and by the international EV research community [147,283]. Storage at -80 °C has been found to preserve size, concentration and biological activity of EVs over the long term more efficiently than storage at higher temperatures such as -20, 4 and 20 °C [284]. EVs can suffer from aggregation, flocculation or degradation, and these processes occur more rapidly at -20, 4 and 20 than at -80 °C [141]. For example in a study conducted by Lőrincz *et al*. [285] it was demonstrated that EVs derived from human neutrophilic granulocytes and loaded with an antibacterial agent (Zymozan A particles) exhibit a decrease in both their concentration and antibacterial activity as soon as after one day at either 20 or 4 °C. Storage at -20 °C did not have any significant effect on EV concentration but it resulted in a shift in the EV size distribution curve to higher sizes, signifying aggregation during storage. Moreover, a gradual loss of antibacterial activity was noted, with almost no residual activity after day 28 of storage. However, storage at -80 °C did not cause any significant changes to either concentration or size, though the antibacterial function exhibited a gradual (but not significant) reduction over the duration of the 28 day study.

In another study partially detailed in a patent owned by Capricor Therapeutics [286] on producing stable cardiosphere cell derived-EV formulations, nanoparticle tracking analysis (NTA) was used to show that the concentration and size of EVs remained stable over one week of storage at 4 or -20 °C. This is in contrast to the EVs' miRNA content which reduces in concentration over the same period of time, reaching less than 50 % of the original content at 1 month of storage and showing continual reduction over 3 months. The patent does not show any results for the size and concentration of EVs under these storage temperatures. In contrast, the size, yield and miRNA content of EVs stored at - 80 °C did not exhibit any significant changes over 3 months.

Despite the fact the above studies are not in exact agreement in terms of the effect of storage at 4 or -20 °C on EV physical characteristics, they both stipulate that the ideal storage temperature to maintain EV characteristics and function is -80 °C. However, for EV based therapeutics to be produced on a large scale for evaluation in clinical studies, alternative approaches must be developed as storage at -80 °C is resource intensive, costly and is not always feasible for handling or transportation [175,284]. One potential solution is lyophilisation, which could enable storage at higher temperatures without detrimental impacts on size, yield or biological activity.

### 7.1.2 Lyophilisation

Lyophilisation is a procedure that is commonly used in the biopharmaceutical industry to ensure that thermo-liable biological products such as proteins, peptides, enzymes and vaccines can be stored at temperatures higher than -80 °C while retaining a satisfactory shelf life [287–290]. Simplistically, lyophilisation is a preservation method involving the freeze-drying of typically thermolabile biological products such as proteins in the presence of a lyoprotectant. The freeze-drying process is comprised of primary drying, in which the majority of water is sublimed, followed by secondary drying, whereby any water adsorbed on the surface is desorbed (Fig. 7.1) [291]. Excipients termed lyoprotectants are added to the formulation, and can serve different purposes such as acting as tonicity modifiers, pH stabilisers or stabilising agents, to ultimately protect the biological activity of the product during the freeze-drying process.

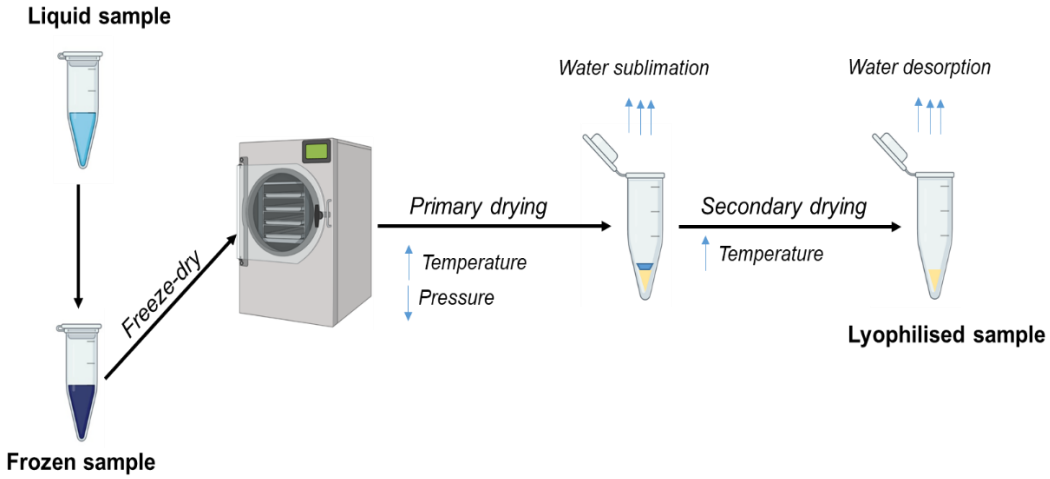


**Figure 7. 1:** Schematic of the process of freeze-drying. Created using BioRender.com

The freeze-dried solid material is amorphous in nature, giving it high solubility and meaning it can be easily reconstituted with pure water just prior to use [292]. A lyophilized product is typically much less bulky than the original solution, allowing more convenient storage. More importantly, freeze-drying ensures greater stability of thermo-labile biological products in comparison to aqueous state storage[289,291,293]. This is because when proteins are in solution they are more susceptible to various physical reactions (such as aggregation or precipitation) and deleterious chemical reactions involving the side chains of amino acid residues in which water is a direct participant [293–295]. These processes can in turn lead to loss of biological activity. Thus, a freeze dried solid material where water is removed is more stable because the protein is "locked" in place, reducing the chances of e.g. aggregation. In addition, as water is removed undesirable chemical reactions are less likely [293].

As outlined earlier, EVs are thermo-labile, in particular in terms of their biological cargo, and thus lyophilisation could be a suitable option for formulation to enable storage at higher temperatures and facilitate ease of handling [292,296]. Recently, a small number of studies have evaluated the lyophilisation of EVs and determined that freeze-dried EVs can be stored at higher temperatures such as 4 and 20 °C for up to 14 days, without significant loss of biological function in comparison to control samples stored at standard

-80 °C [286,297–299]. These studies additionally evaluated the use of trehalose as a lyoprotectant during the freeze-drying of EVs.

Trehalose is a disaccharide that acts as a stabilising agent. It is one of the most effective lyoprotectants used with proteins, liposomal products and EVs [141,284]. It is hypothesised that its stabiliser function is conveyed through water replacement and vitrification during the drying process. In the vitrification hypothesis, when trehalose is freeze-dried it forms an amorphous sugar glass that immobilises EVs and any protein content. In the water replacement theory, trehalose acts through the replacement of the hydration sphere around EVs and proteins by hydrogen bonding, interacting with phospholipid head groups to maintain the native conformation and prevent fusion of products or protein destabilization [284,300]. Moreover, trehalose is a natural and non-toxic sugar that is widely used by both the food and drug industries, and has been validated as a stabilising agent for thermo-labile proteins, vaccines, and liposomes, as well as cells and organs for transplant [301].

Although there is some knowledge of the effect of lyophilisation on EVs, the literature is limited. The studies reported to date used specific types of EVs, and it is not clear whether EVs from different cell sources can be lyophilised in the same way while achieving similar results. This is because EVs from different cell sources will have different surface lipid and protein compositions, as well as varied biological cargos, all of which have a role in their biological activity [284]. Moreover, different isolation methods were used in the published studies. Since it is known that the isolation method can impact the concentration, purity, and integrity of EVs it is also critical to evaluate the effect of lyophilisation of EVs isolated using a specific method, to ensure reproducible results [283,302,303].

## 7.2 Aims and objectives

In this chapter, we aimed to evaluate the long-term stability of HEK293T-derived EVs under different storage temperatures (20, 4 and -80 °C). The effect of lyophilisation of EVs in the presence or absence of trehalose was assessed, to determine if this can enable storage at higher temperatures

without deleterious effects on size, concentration, protein content, surface markers and incorporated enzyme activity.

# 7.3 Results and discussion

## 7.3.1 Evaluation of stability of naïve non-lyophilised EVs

### *7.3.1.1 Concentration and modal size*

Prior to the formulation of EVs using lyophilisation, we set out to evaluate the impact of long-term storage at -80, 4 and 20 °C on naïve non-formulated EVs. NTA was used to evaluate the concentration and modal size over a period of 4 weeks. Given that the size distribution of isolated EVs falls over a large range, modal size was evaluated rather than mean particle size.

As can be seen from Fig. 7.2, there is a general decrease in EV concentration over time during four weeks of storage at all three temperatures. When EVs are stored at -80 °C (Fig. 7.2a) this decline in concentration is only significant after 4 weeks of storage. Similarly the modal particle size (Fig.7.2a) remains stable over a period of two weeks at -80 °C but is significantly increased following four weeks ($p < 0.001$) of storage. The fact that the modal size and concentration remain stable for the first two weeks indicates that EVs are structurally stable at this temperature and do not undergo decomposition into smaller particles or degradation. The increase in modal size, accompanied with a decrease in concentration, after four weeks signifies that EVs are undergoing aggregation or fusion. Similar results were also observed by Maroto *et al*. [304] who noted an increase in EV diameter attributed to aggregation during storage at -80 °C.

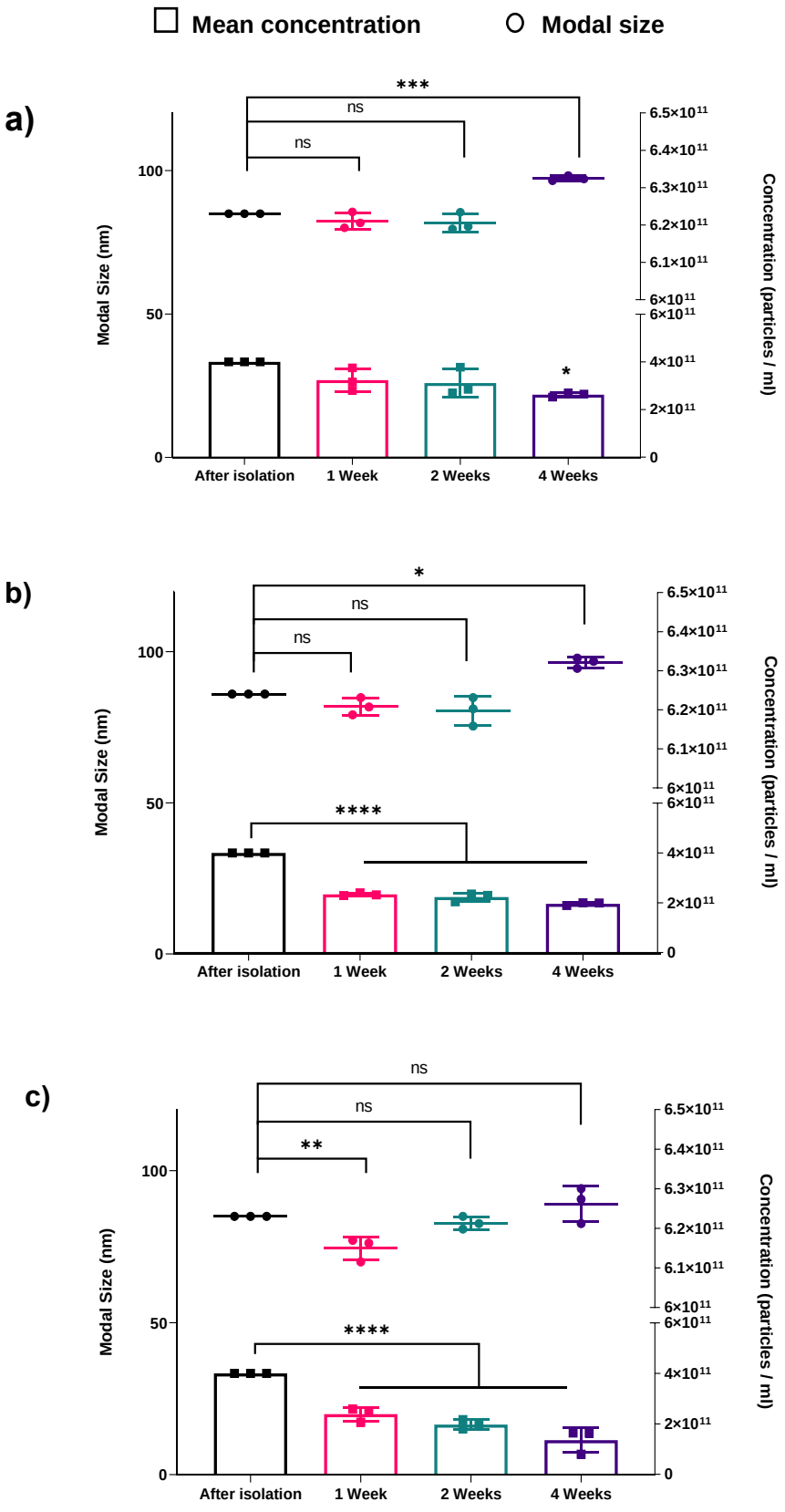


**Figure 7.2:** Mean concentration and modal particle size measured by NTA on naïve EVs derived from HEK293T cells over the course of one month under different storage conditions: (a) -80°C, (b) 4°C and (c) 20°C. N=3 and data are presented as mean ± SD. Statistical analysis: one-way ANOVA followed by Dunnett's multiple comparisons test versus control (after isolation); ns denotes $p > 0.05$, *$p < 0.05$, **$p \leq 0.01$, ***$p \leq 0.001$, ****$p < 0.0001$.

Storage at 4 °C (Fig. 7.2b) also results in a decline in concentration with time, with the decline being significant after one week ($p < 0.0001$). The modal size remains stable over two weeks, but increases significantly following four weeks of storage ($p < 0.05$). The fact that the modal size remains stable while the concentration decreases signifies that EVs are not aggregating or decomposing into smaller particles but rather degrading [140].

As seen from Fig. 7.2c, storage at 20 °C also results in a significant decline in particle concentration following one week of storage ($p < 0.0001$), accompanied by a significant decline in modal size ($p < 0.01$). This reduction in both concentration and modal size indicates that EVs are both decomposing into smaller particles and degrading. The modal size starts to increase following 2 and 4 weeks' storage, suggesting aggregation or fusion of EV particles. The precise mechanisms of storage induced changes (degradation, aggregation, decomposition or fusion) to EVs have not been studied and remain unclear. Nonetheless, it can be confirmed that the optimal temperature for storage of EVs derived from HEK293T cells is -80 °C, where they are stable for a duration of at least two weeks in terms of both structure and concentration. EVs stored at 4 °C are only relatively morphologically stable for two weeks. EVs stored at 20 °C are not stable in terms of either structure or concentration after one week.

#### *7.3.1.2 Total protein concentration*

The BCA protein assay was used to evaluate the total protein content of EVs stored at -80, 4 and 20 °C. The total protein concentration exhibits a decline over 4 weeks of storage (Fig. 7.3), but this is not statistically significant at -80 and 4 °C. However, for samples stored at 20 °C, the decline in total protein concentration is significant after one week. This can be attributed to the fact that at 20 °C EVs are decomposing (as seen by the decline in modal size), so the incorporated protein is released and is no longer protected by the surrounding phospholipid bilayer. Proteins are thermo-labile and at 20 °C will start to degrade[287,305]. These results, together with the data on storage effects on concentration and modal size, allow us to conclude that storage at a

temperature of -80 °C is optimal and has the least damaging effect on the EV characteristics evaluated.

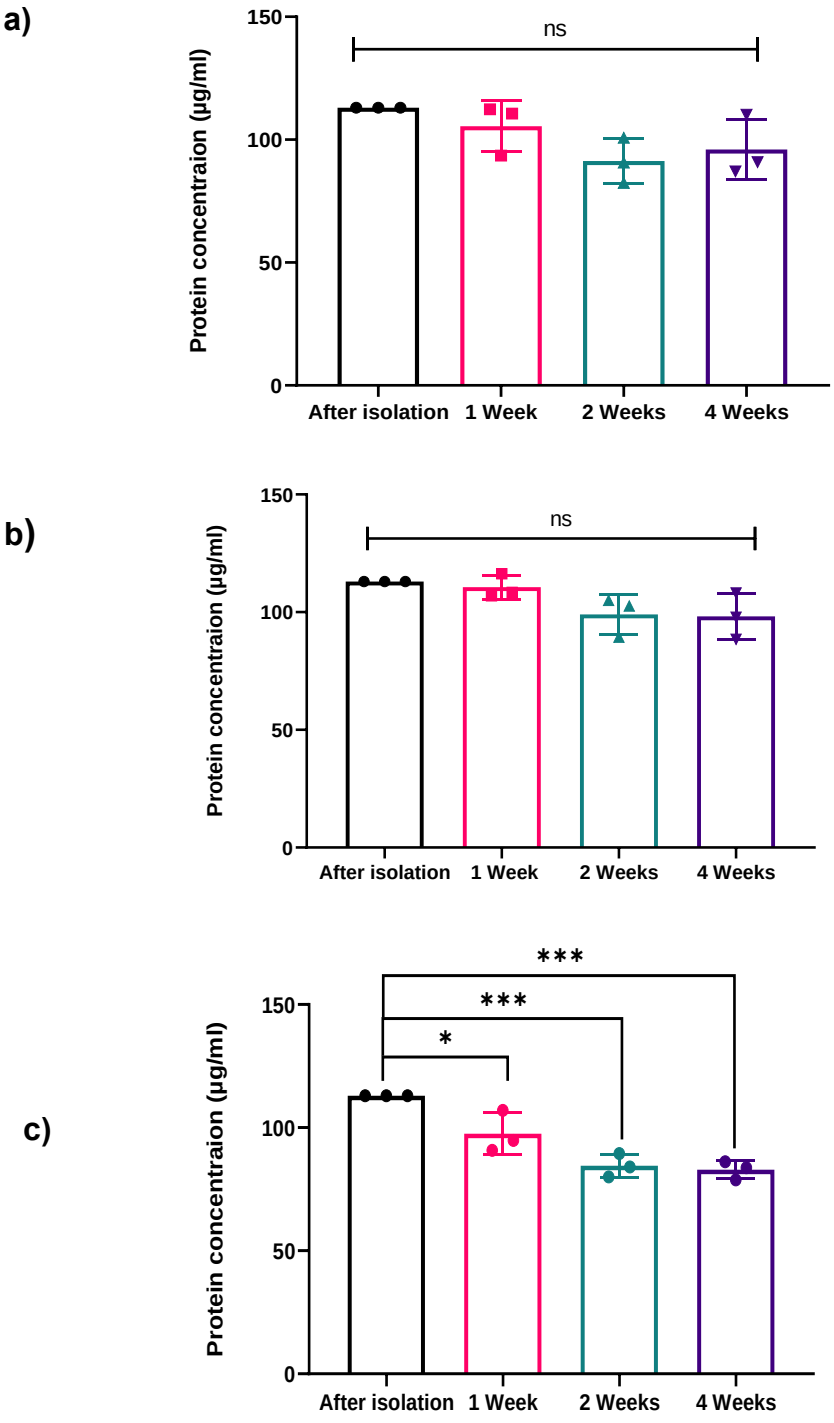


**Figure 7. 3:** Total protein concentration of HEK293T-derived EVs over the course of four weeks under different storage conditions: (a) -80°C, (b) 4°C and (c) 20°C, as measured by BCA. N=3 and data presented as mean ± SD. Statistical analysis: one-way ANOVA followed by Dunnett's multiple comparisons test versus control (after isolation); ns denotes $p > 0.05$, * $p < 0.05$, and ***$p \leq 0.001$.

## 7.3.2 Evaluation of stability of lyophilised naïve EVs

HEK293T-drived EVs were lyophilised under vacuum with a primary drying step overnight (16 hours at -25 °C) and shorter secondary drying step (2 hours at 20 °C). Experiments were undertaken in the presence of different concentrations of the lyoprotectant trehalose (0.5, 2 and 4 % w/v), and without any lyoprotectant (i.e. just EVs resuspended in PBS). This range of trehalose concentrations was chosen because it has been previously determined to be effective during lyophilisation of EVs [298]. Following lyophilisation, the EV cake/pellet was stored at 4 or 20 °C for a period of four weeks. The concentration, modal size, protein concentration and surface markers were evaluated over the four weeks. At the point of measurement, the cake was reuspended in millliQ water immediately prior to analysis. The EV particle concentration for each measurement was normalised to the average particle concentration of EV samples (in suspension) stored at -80 °C. This is because -80 °C was previously established to be the optimal temperature for storage of the EVs (**Section 7.3.1**) and we sought to determine how lyophilised samples compare to this baseline. The simple western system (WES) was used to obtain Western blots of the EV markers CD9 and TSG10 and the compass software used to quantify the level of each marker in each sample, which was normalised to the amount of total protein added.

### *7.3.2.1 Concentration modal size of lyophilised EVs stored at 4°C*

As can be seen from Fig. 7.4a, following one week of storage at 4 °C EVs lyophilised in the presence of 0.5-4 %w/v trehalose do not have significantly different particle concentrations to non-lyophilised EVs stored at -80 °C. EVs lyophilised in the presence of 2 %w/v trehalose had the highest concentration out of all three lyophilised samples after one week. In contrast, non-lyophilised EVs stored at 4 °C for one week had a significantly lower particle concentration than control samples at -80 °C. EVs lyophilised without a lyoprotectant (in PBS alone) had an even lower particle concentration. This suggests that EVs have experienced degradation caused by the freeze-drying process when this is performed without a lyoprotectant. The presence of trehalose during freeze-drying ensures that water is osmotically “pressed” out of the EVs and avoids

the potentially destructive formation of ice crystals inside the vesicles [141,306]. Moreover, as can be seen from Fig. 7.4b the modal size of all samples after one week of storage remains stable, with less than 10 % variation in comparison to samples stored at -80 °C, indicating that the EVs are structurally stable and are not decomposing into smaller particles.

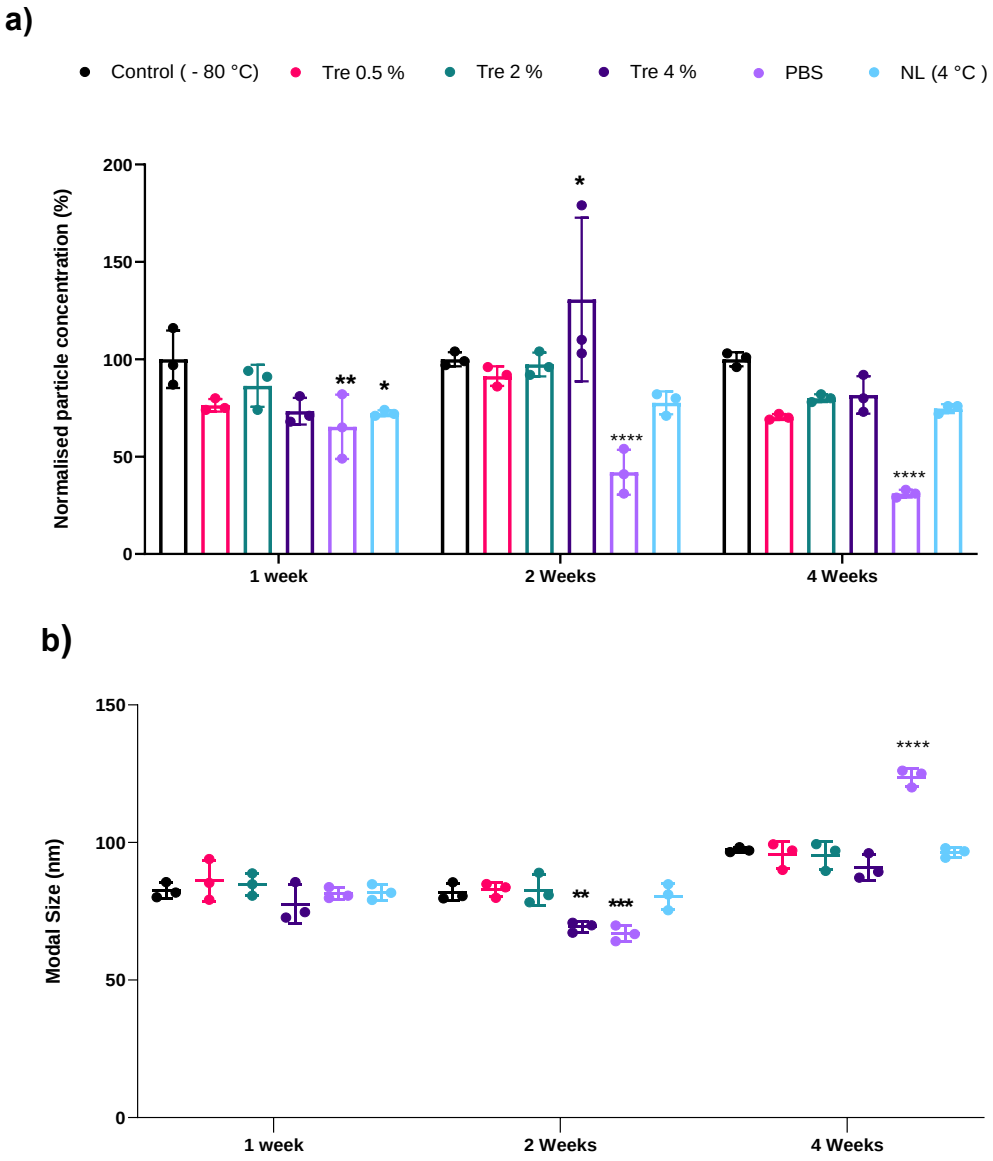


**Figure 7.4:** a) Particle concentration and b) modal size of naive HEK293T-derived EVs stored for four weeks at -80 °C, or at 4 °C after lyophilisation with 0-4 %w/v of trehalose. For each experiment, the particle concentration was normalised to the average particle concentration at −80 °C. N=3 and data presented as mean ± SD. Statistical analysis: two-way ANOVA followed by Dunnett's multiple comparisons test versus control (–80 °C); *p < 0.05, **p ≤ 0.01, ***p ≤ 0.001 and ****p < 0.0001

Following two weeks of storage the particle concentration and modal size in the presence of 0.5 and 2 % w/v trehalose remained stable, and was not significantly different to at the -80 °C control sample (Fig. 7.4). This indicates that stability is comparable over all these conditions. However, samples lyophilised in the presence of 4 % w/v trehalose have a significantly higher particle concentration than non-lyophilised samples at -80 °C, which can be attributed to the decomposition into smaller particles; this idea is supported by the significantly lower modal size (Fig. 7.4b). However, as the SD for the concentration data is quite large it is not possible to conclude whether this is an artefact or a negative effect of using 4 % w/v trehalose on the structure of EVs during freeze-drying and storage. Higher concentrations of trehalose can lead to crystallisation of the disaccharide during the sublimation step of freeze-drying, which prevents the formation of the hydrogen bonding needed to establish the protective hydration sphere around EVs [301]. Again, following two weeks of storage lyophilised samples without a lyoprotectant exhibit a significant decline in both concentration and modal size, indicating that EVs in these samples are both decomposing and degrading.

Following four weeks of storage there is no significant difference between the particle concentration of all three samples lyophilised with a cryoprotectant, non-lyophilised samples stored at 4 °C and control samples stored at – 80 °C (Fig. 7.4a). Hence, these samples stored at 4 °C have similar stability to control samples stored at -80 °C following four weeks of storage (NB: some degradation is seen upon storage at -80 ºC). The concentration of samples lyophilised without trehalose is significantly lower than the control samples stored at -80 °C. The modal size of all samples exhibits an increase following four weeks of storage, with this being greatest for lyophilised samples without lyoprotectant. This trend where the modal size is decreased following one and two weeks of storage followed by an increase in modal size following four weeks is similar to that seen for non-lyophilised samples stored at 20, 4 and – -80 °C seen in Fig. 7.2a-c. This was attributed to some aggregation, which seems to be most prevalent in the absence of a lyoprotectant, as reported by some studies in the literature [141,307].

In conclusion, we find that following 1 week of storage at 4 °C EV samples lyophilised in the presence of 0.5 and 2 %w/v trehalose had particle concentrations and modal sizes comparable to control samples stored at -80 °C, while non-lyophilised samples stored at 4 °C displayed significantly more degradation in concentration. Thus, it seems that lyophilisation may be beneficial in offsetting deleterious effects of storage at higher temperatures for 1 week but not longer. Maybe better to say offers a benefit for the first week

### *7.3.2.2 Total protein concentration of lyophilised EVs stored at 4°C*

The BCA protein assay was used to evaluate the total protein content of the EVs over the four week storage period (Fig. 7.5). The total protein concentration of samples stored at 4 °C exhibits a gradual but slight decline over the four weeks of storage, although this is not significantly different than that measured for control samples stored at -80 °C. The total protein concentration in non-lyophilised and samples lyophilised without lyoprotectant consistently have the lowest total protein concentration, but again significance is not attained. Overall, we can conclude that lyophilisation does not have a negative effect on the total protein concentration in EV samples.

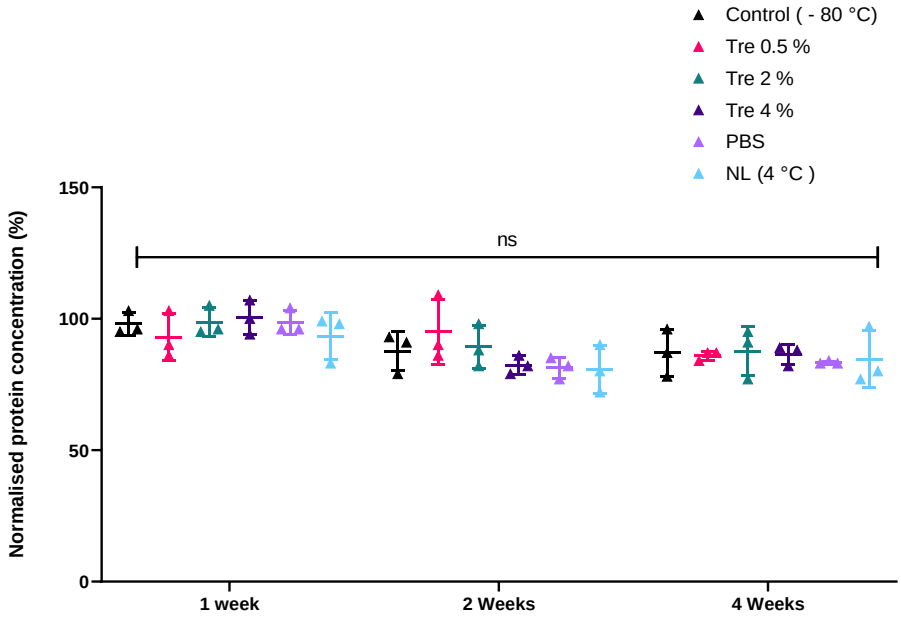


**Figure 7.5:** Total protein concentration of naive HEK293T-derived EVs stored for four weeks at -80 °C, or at 4 °C after lyophilisation with 0-4 %w/v of trehalose. For each measurement, the total protein concentration was measured by BCA assay and normalised to that before storage. N=3 and data presented as mean ± SD. Statistical analysis: two-way ANOVA followed by Dunnett's multiple comparisons test versus control (-80 °C), ns denotes $p > 0.05$.

### *7.3.2.3 EV surface markers of lyophilised EVs stored at 4°C*

Representative Western blots for the EV markers CD9 and TSG10 can be seen in the **Appendix II** (Fig. AII.1-2). The levels of each marker in the different samples are plotted in Fig. 7. 6a-b. The CD9 levels after one week of storage are highest for the lyophilised samples with 4 % w/v trehalose, followed by non-lyophilised samples stored at 4 °C and those stored at -80 °C (Fig. 7.6a). Similar results are observed for the TSG101 marker (Fig. 7.6b).

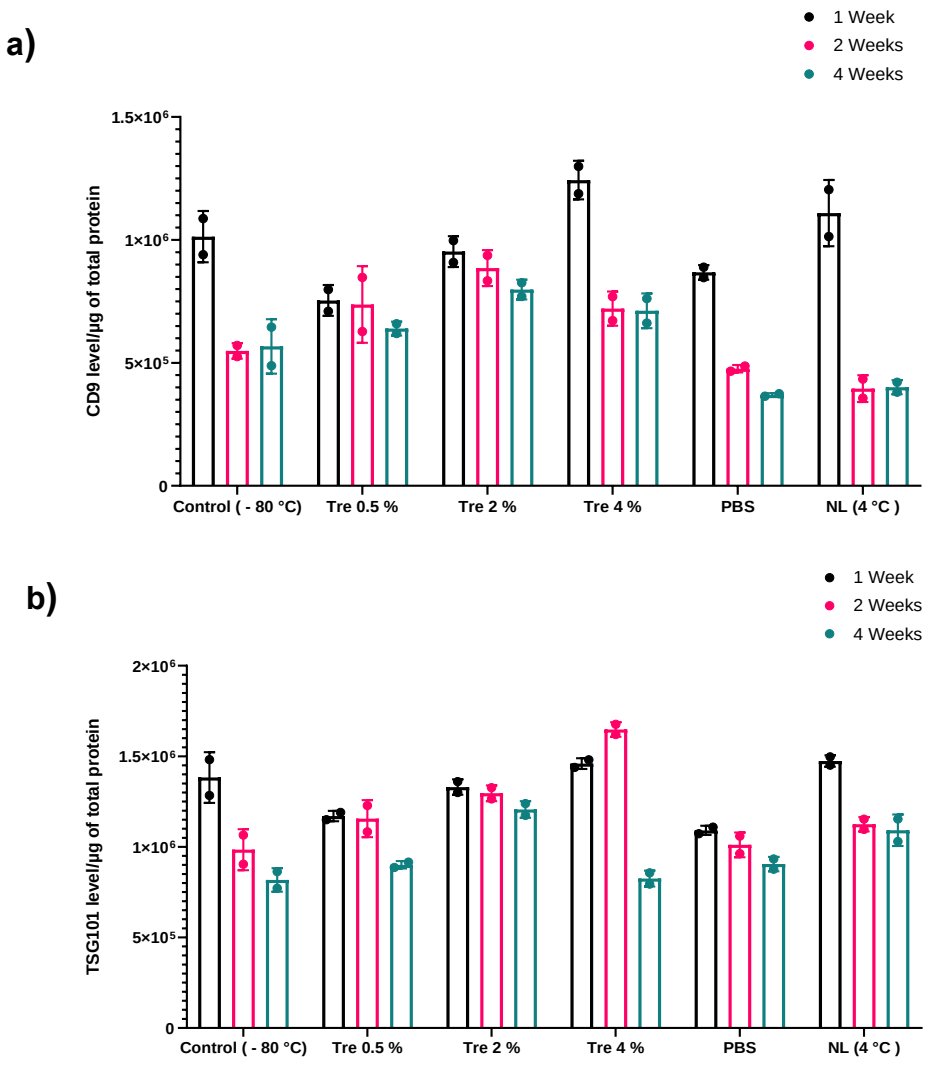


**Figure 7.6:** Levels of the EV surface markers a) CD9 and b) TSG101 in different samples of naive HEK293T-derived EVs stored for four weeks at -80 °C, 4 °C, and after lyophilisation with 0-4 %w/v trehalose. N=2 and data presented as mean ± SD

The fact that CD9 and TSG101 levels are slightly lower for samples stored at -80 °C in comparison to 4 °C is because freeze-thawing of the former samples contributes to degradation of these surface markers [140]. The CD9 and TSG101

levels exhibit a pronounced drop after two weeks of storage, with this being most marked for non-lyophilised samples stored at -80 °C or 4 °C and lyophilised samples with 4 %w/v trehalose or without trehalose. The CD9 levels in all three lyophilised samples stored at 4 °C are higher than that in control -80 °C samples and non-lyophilised samples stored at 4 °C after two and four weeks of storage, which showcases the protective effect of lyophilisation on this marker. In contrast, only samples lyophilised in the presence of 2 %w/v trehalose display TSG101 levels higher than control -80 °C samples and non-lyophilised samples stored at 4°C. Overall, lyophilised samples with 2 %w/v trehalose exhibited the smallest changes not only in surface marker levels but also size and concentration over the four week storage period, indicative of the higher stability of EVs in these samples.

#### *7.3.2.4 Concentration and modal size of lyophilised EVs stored at 20°C*

The concentration and modal size of lyophilised EVs stored at 20 °C are displayed in Fig. 7.7. After one week of storage samples lyophilised with 0.5 %w/v trehalose exhibited a significant decline in particle concentration but no decline in modal size. In comparison, EVs lyophilised in the presence of 2 %w/v trehalose had particle concentrations and modal sizes comparable to samples stored at -80°C. EVs lyophilised with 4 %w/v trehalose show a significant decline in particle concentration. Thus, compared to storage at 4 °C, a higher storage temperature of 20 °C causes more damaging effects on EV sample size and concentration.

EVs lyophilised without a lyoprotectant have a significantly lower particle concentration and modal size in comparison to the -80°C control, not only for the first week but the entire four week period (Fig. 7.7a). This further confirms the effectiveness of trehalose as a stabilising agent during freeze-drying. In fact non-lyophilsed samples stored at 20 °C have a slightly higher particle concentration than those lyophilised without lyoprotectant. This further confirms that lyophilisation process without lyoprotectant has some degradative effect on EVs. However, the benefit of lyophilisation in terms of size and concentration of EVs 1 week after storage at 20 °C is not visible. This is because the size and concentration of EVs in sample lyophilised with

trehalose is not significantly different to that in non-lyophilised samples stored 20 °C.

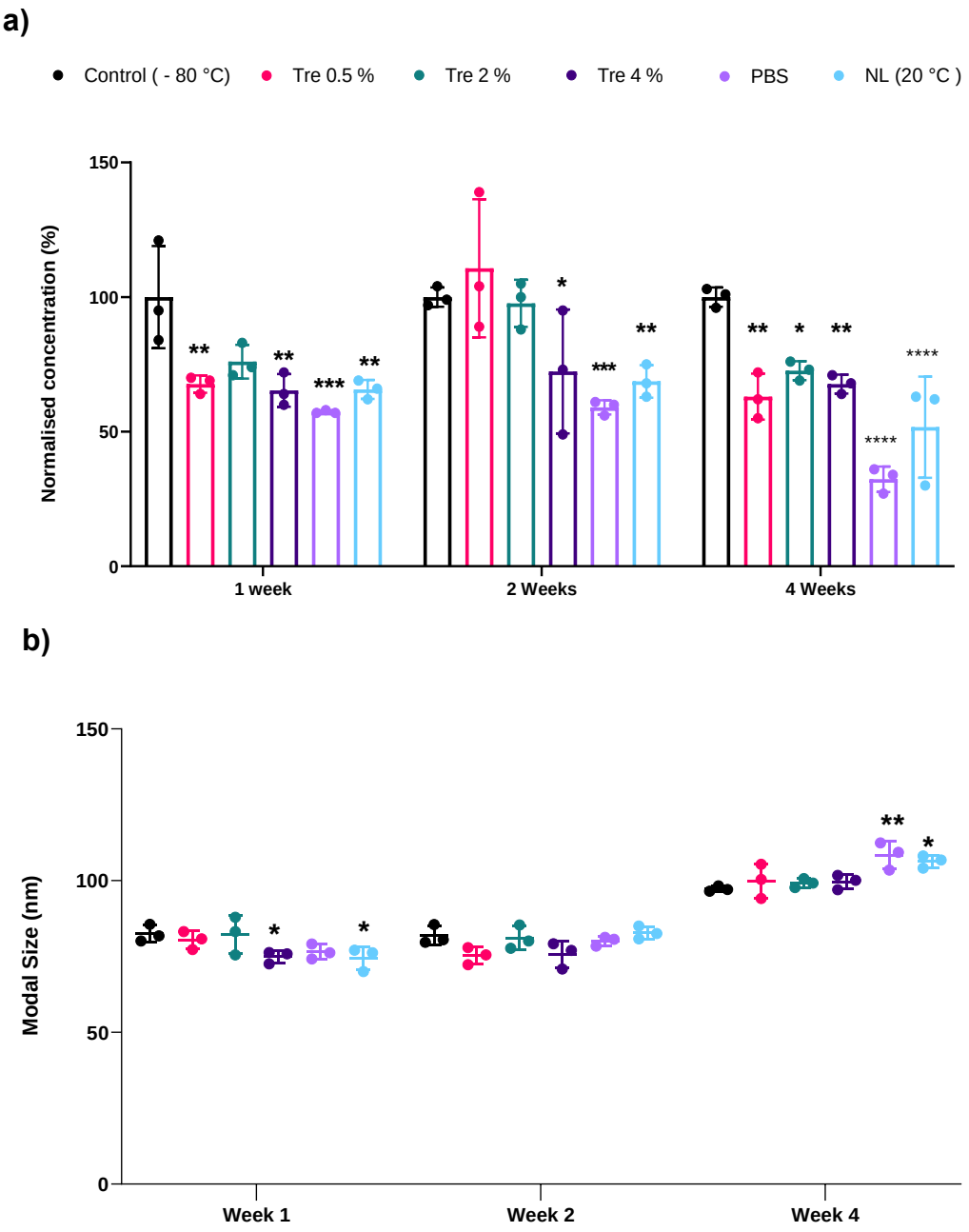


**Figure 7.7:** a) Particle concentration and b) modal size of naive HEK293T-derived EVs stored for four weeks at -80 °C, 20 °C and after lyophilisation with 0-4 %w/v of trehalose. For each measurement, the particle concentration was normalised to the average particle concentration at −80 °C. N=3 and data presented as mean ± SD. Statistical analysis: two-way ANOVA followed by Dunnett's multiple comparisons test versus control (–80 C); *p < 0.05, **p ≤ 0.01, ***p ≤ 0.001 and ****p < 0.0001.

Following two weeks of storage the particle concentration and modal particle size of EVs lyophilised in the presence of 0.5 and 2 %w/v trehalose remained

stable and not significantly different to the control samples stored at –80 °C (Fig. 7.7). The particle concentration of these lyophilised samples is also significantly higher than non-lyophilised EVs stored at 20 °C (two-way ANOVA, Tukey's multiple comparisons test, $p < 0.05$). In contrast to storage at 4 °C, stability of the lyophilised EV samples following two weeks' storage is comparable to that of control samples stored at –80 °C, but also higher than that of non-lyophilised samples stored at 20°C. However, samples lyophilised in the presence of 4 % trehalose have a significantly lower particle concentration ($p < 0.05$) but similar modal size to the -80 °C control. This means that EVs lyophilised in the presence of 4 %w/v trehalose are degrading more rapidly than when lower amounts of sugar are added. Lyophilisation with 4 %w/v trehalose thus again appears to have a negative effect on the stability of EVs. Following four weeks of storage the modal size and concentration of EV samples stored at 20 °C follow a similar trend to that noted above for samples stored at 4 °C

Overall, at 20 °C only EV samples lyophilised in the presence of 2 %w/v trehalose had particle concentrations and modal sizes comparable to control samples stored at -80 °C, and only over a 2 week period (rather than 4 weeks at 4 °C). Moreover, although there is no significant difference between EV concentrations in 2 %w/v lyophilised samples and non-lyophilised samples after the first week of storage, this difference is significant after 2 weeks of storage ($p < 0.05$). This indicates that in the longer term lyophilisation using 2 %w/v trehalose offsets the deleterious effects of higher storage temperatures.

#### *7.3.2.5 Total protein concentration of lyophilised EVs stored at 20°C*

The total protein content of EVs over the four week storage period is displayed in Fig. 7.8. The total protein concentration of all samples exhibits a gradual but slight decline over the 4 weeks of storage, similar to the trend observed for samples stored at 4 °C. However, non-lyophilised EVs and EVs lyophilised without a lyoprotectant consistently displayed a significantly lower total protein content than lyophilised samples with trehalose and -80 °C control samples. This emphasises that lyophilisation has a protective effect on total protein concentration during storage at 20 °C.

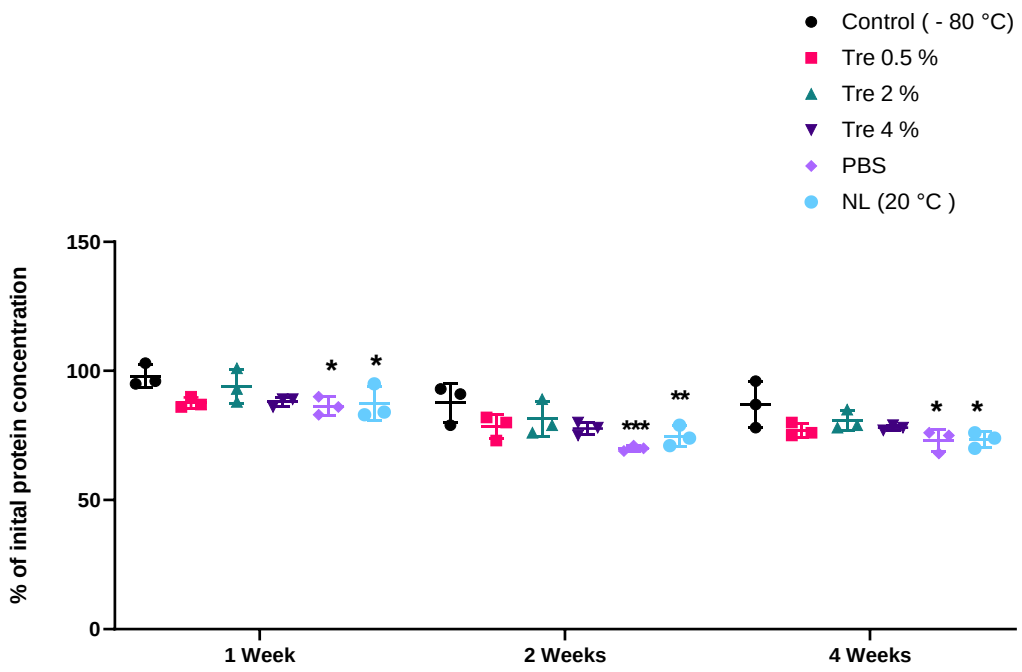


**Figure 7. 8:** Total protein concentration of naive HEK293T-derived EVs stored for four weeks at -80 °C, 20 °C and after lyophilisation with 0-4 %w/v of trehalose. For each measurement, the total protein concentration was normalised to that before storage. N=3 and data presented as mean ± SD. Statistical analysis: two-way ANOVA followed by Dunnett's multiple comparisons test versus control (–80 °C); *p < 0.05, **p ≤ 0.01, ***p ≤ 0.001.

### *7.3.2.6 EV surface markers of lyophilised EVs stored at 20°C*

Representative western blots for the EV markers CD9 and TSG10 can be seen in **Appendix II** (Fig. AII.3-4). The results are presented in Fig. 7.9a-b. In contrast to storage at 4 °C, CD9 and TSG101 levels of both lyophilised and non-lyophilised samples stored at 20 °C are lower than at -80 °C. The levels of both markers are also generally lower than in samples stored at 4 °C. This is due to the damaging effects of higher storage temperatures [140]. Moreover, the CD9 and TSG101 levels of non-lyophilised and samples lyophilised without trehalose following two and four weeks were consistently lowest. Similar to storage at 4 °C, the CD9 and TSG101 levels in lyophilised samples with 2 % trehalose exhibited the smallest changes over the four week period.

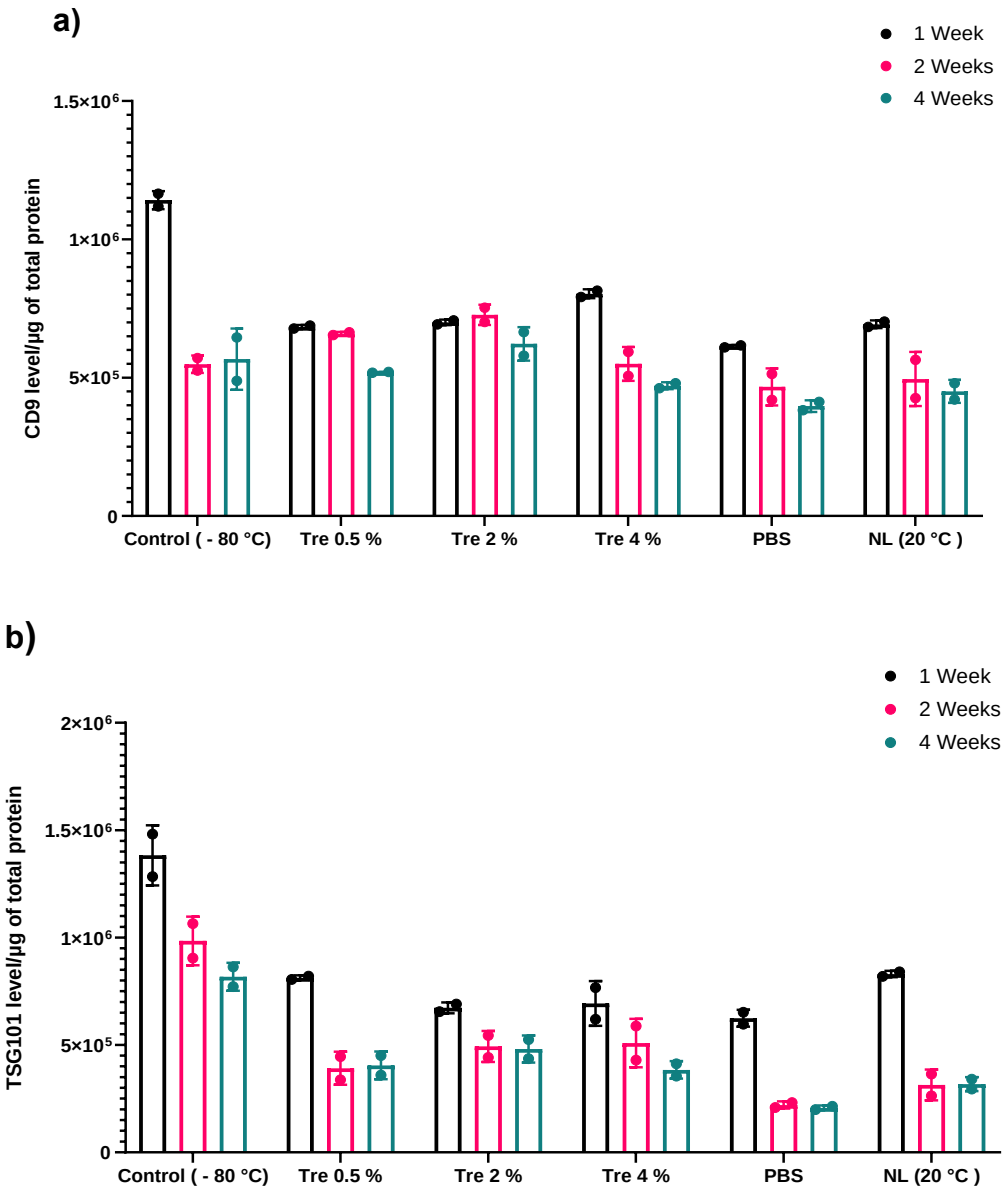


**Figure 7.9:** Levels of EV surface markers a) CD9 and b) TSG101 in different samples of naive HEK293T-derived EVs stored for four weeks at -80 °C, 20 °C and after lyophilisation with 0-4 %w/v of trehalose. N=2 and data presented as mean ± SD.

Thus far, it can be concluded that the optimal storage conditions are achieved through lyophilisation using either 0.5 or 2 %w/v trehalose and storage of the cake at 4 °C for up to four weeks. Lyophilisation using 2 %w/v trehalose could achieve similar protective effect during storage at 20 °C but for a maximum of two weeks.

### 7.3.3 Evaluation of stability of loaded-EVs containing luciferase enzyme

From the experiments detailed above we are able to determine that the use of 0.5 or 2 %w/v trehalose could potentially give the greatest protective effect on EVs during the freeze-drying process and during storage in the cake form, enabling their storage at temperatures higher than -80 °C for a maximum of two weeks. Thus, these conditions were used to lyophilise loaded-EVs derived from sorted-transduced HEK293T cells that were produced and characterised as described in Chapter 2 (**Section 2.4.5 and Section 2.5**). These EVs contain the enzyme luciferase, and we sought to evaluate the effect of lyophilisation and storage on enzyme activity as well as other parameters including particle concentration, size, total protein concentration and surface markers. The activity of the incorporated enzyme is crucial to consider alongside the stability of the EVs themselves, to ensure delivery of a potent therapeutic entity.

#### *7.3.3.1 Concentration and size of lyophilised loaded-EVs stored at 4°C*

Fig. 7.10 displays the particle concentration and modal size of lyophilised and non-lyophilised loaded-EVs stored at 4 °C. The modal size of all samples remains stable, as seen in with naïve EVs (**Section 7.3.2.1**). However, the particle concentration in samples lyophilised with 0.5 %w/v trehalose and non-lyophilised samples shows a significant decline ($p < 0.05$) over two weeks. This means that EVs in these samples are degrading at a higher rate than in control samples, and that lyophilisation with 0.5 %w/v trehalose does not provide any added protective benefit to these EVs during storage at 4 °C. On the other hand, lyophilisation with 2 %w/v trehalose appears to provide a protective effect and the particle concentration is not significantly different to control samples throughout the two week period. This is consistent with what is seen in the literature [301,308]. After two weeks of storage we can also see that lyophilised samples with 2 %w/v trehalose have signficantly higher EV concentrations than non-lyophilised samples stored at 4 °C (two-way ANOVA, Tukey's multiple comparisons test, $p < 0.05$).

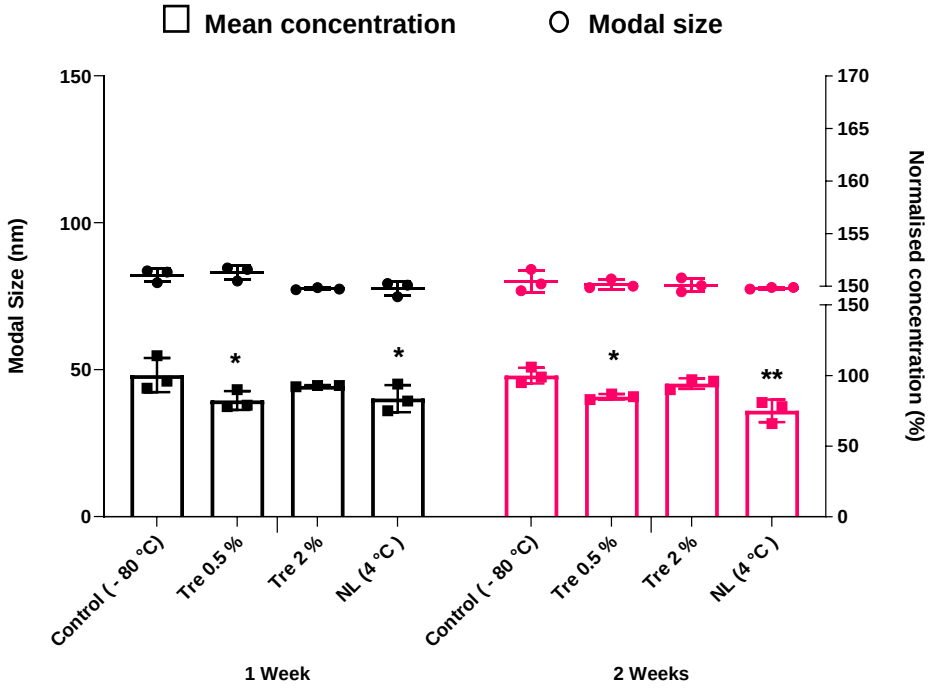


**Figure 7.10:** Particle concentration and modal size of loaded-EVs derived from sorted-transduced HEK293T cells, stored for two weeks at -80 °C, 4 °C and after lyophilisation with 0.5-2 %w/v of trehalose. For each measurement, the particle concentration was normalised to the average particle concentration of the control stored at –80 °C. N=3 and data presented as mean ± SD. Statistical analysis: two-way ANOVA followed by Dunnett's multiple comparisons test versus control (–80 C); *p < 0.05, **p ≤ 0.01, ***p ≤ 0.001 and ****p < 0.0001

### *7.3.3.2 Total protein concentration of lyophilised loaded-EVs stored at 4°C*

The total protein content of EVs over the two week storage period is displayed in Fig. 7.11. The total protein concentration of all samples exhibits a very slight decline, but this is not statistically significant in comparison to the –80 °C control. Even if the EVs start to decompose or degrade and release their protein content into solution, the proteins will likely still be stable at 4 °C for a up to 1 month [305,309]. However, this does not negate the need for lyophilisation: this has a protective effect on the structure of EVs, and free protein/enzyme in solution will not be able to cross biological membranes to deliver cargo to target cell/tissues.

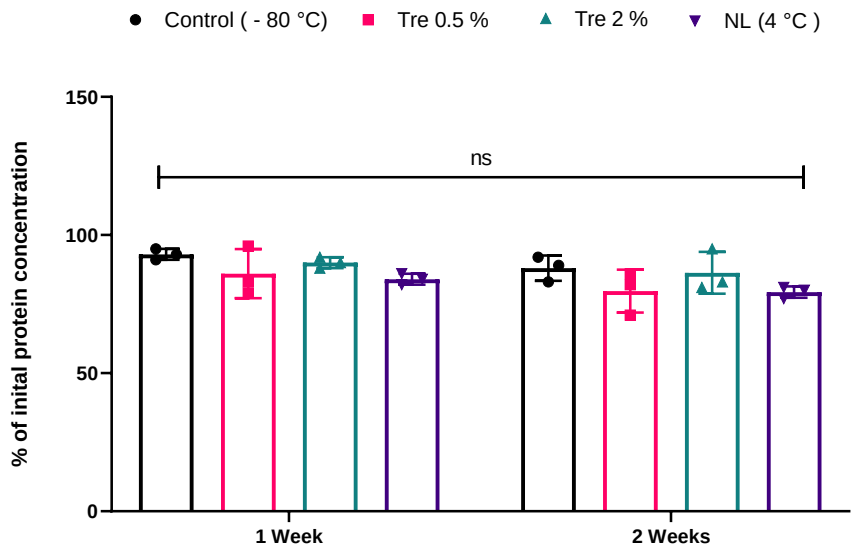


**Figure 7.11:** Total protein concentration of loaded-EVs derived from transduced-sorted HEK293T-cells, stored for two weeks at -80 °C, 4 °C and after lyophilisation with 0.5-2 %w/v of trehalose. For each measurement, the total protein concentration was measured by BCA assay and normalised to that prior to storage. N=3 and data presented as mean ± SD. Statistical analysis: two-way ANOVA followed by Dunnett's multiple comparisons test versus control (-80 °C); *p < 0.05, **p ≤ 0.01, ***p ≤ 0.001 and ****p < 0.0001

#### *7.3.3.3 EV surface markers of lyophilised loaded-EVs stored at 4°C*

Representative western blots for the EV markers CD9 and TSG10 can be seen in **Appendix II** (Fig. AII.5-6). The levels of each marker in the different samples are quantified in Fig. 7.12a-b. Similar to previous observations for naïve EVs, here also the CD9 levels after one week of storage are highest in non-lyophilised samples stored at 4 °C (Fig. 7.12a). The CD9 levels exhibit a pronounced drop after two weeks of storage, with this decline highest for non-lyophilised samples stored at 4 °C. Similar results are observed for the TSG101 marker (Fig. 7.12b). However, after one week of storage the levels of TSG101 are highest for the 2 %w/v trehalose samples. This suggests that EVs in these samples are not decomposing and releasing TSG101 (which is found on the inside of EVs). The levels of CD9 and TSG101 in both lyophilised samples are comparable to control samples stored at -80 °C, with the 2 %w/v slightly outperforming the 0.5 %w/v trehalose system. This is in agreement with results obtained in terms of particle concentration, size, and total protein content.

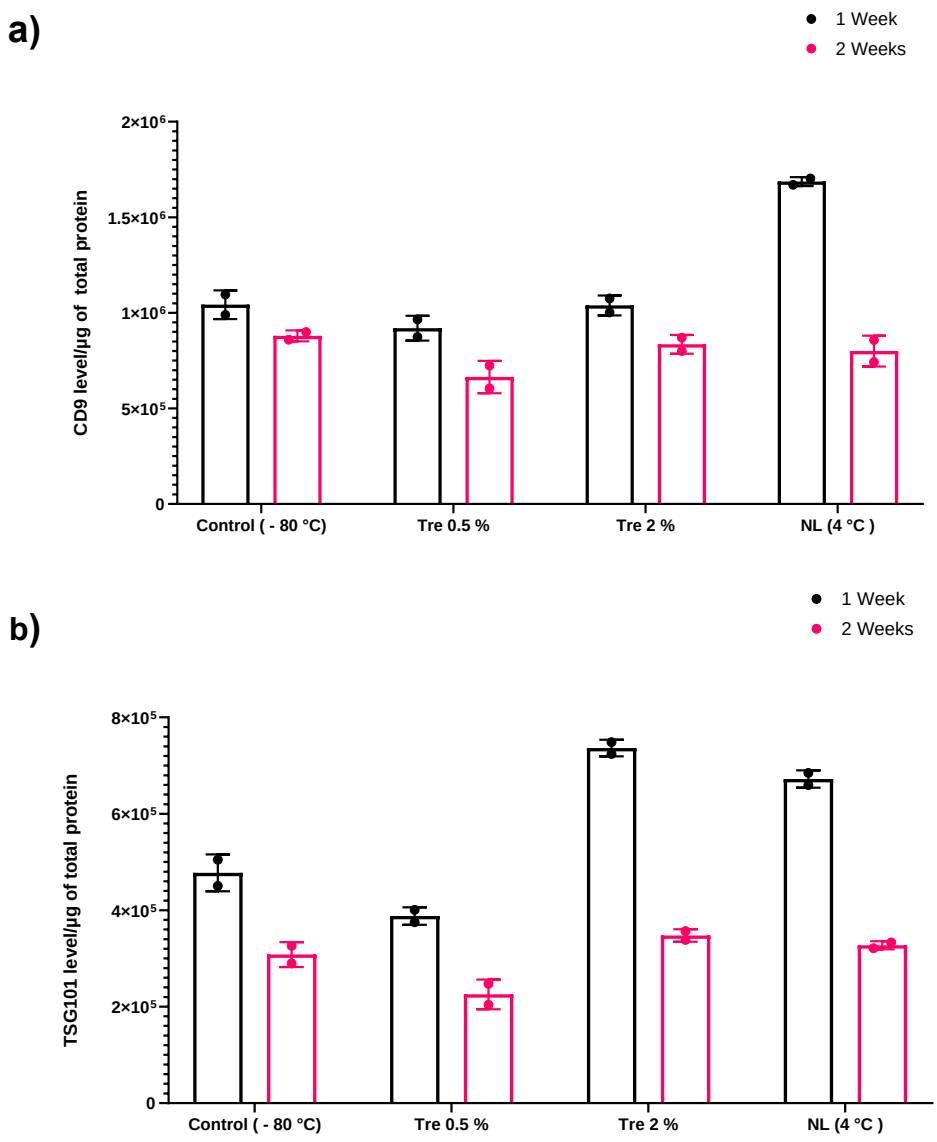


**Figure 7.12:** Levels of the EV surface markers a) CD9 and b) TSG101 in different samples of loaded-EVs derived from transduced-sorted HEK293T-cells, stored for two weeks at -80 °C, 4 °C and after lyophilisation with 0.5-2 %w/v of trehalose. N=2 and data presented as mean ± SD.

### *7.3.3.4 Luciferase enzyme activity in lyophilised loaded-EVs stored at 4 °C*

The activity of luciferase after storage is given in Fig. 7.13. The enzyme activity in all samples exhibits a slight decline over the two week storage period. Samples lyophilised with 0.5 % w/v trehalose and non-lyophilised samples stored at 4 °C show significantly less enzyme activity than control samples stored at -80 °C at both week 1 and 2. Storage of non-lyophilised EVs at 4 °C causes a greater drop in enzyme activity than storage at -80 °C from week 1 to week 2, confirming the deleterious effects of higher storage temperatures

on EVs and activity of incorporated cargo in the long term. As seen from Fig. 7.13, the EV particle concentration in samples lyophilised with 0.5 %w/v trehalose have significantly lower than that seen in control -80 °C samples, which can be attributed to the significant degradation of EVs in these samples (**Section 7.3.3.1**, Fig. 7.10). In addition, the enzyme activity in the lyophilised samples (0.5 %w/v) is not significantly different to that in non-lyophilised samples stored at 4°C (as determined following a separate two-way ANOVA, Tukey's multiple comparisons test, $p > 0.05$). However, samples lyophilised with 2 % w/v trehalose show enzyme activity comparable to those stored at -80 °C and significantly higher enzyme activity than in non-lyophilised samples stored at 4°C (two-way ANOVA, Tukey's multiple comparisons test, $p < 0.001$). In conclusion, use of 2 %w/v trehalose during lyophilisation is optimal in maintaining enzyme activity during storage at 4°C, demonstrating the advantage of lyophilisation in enhancing storage stability.

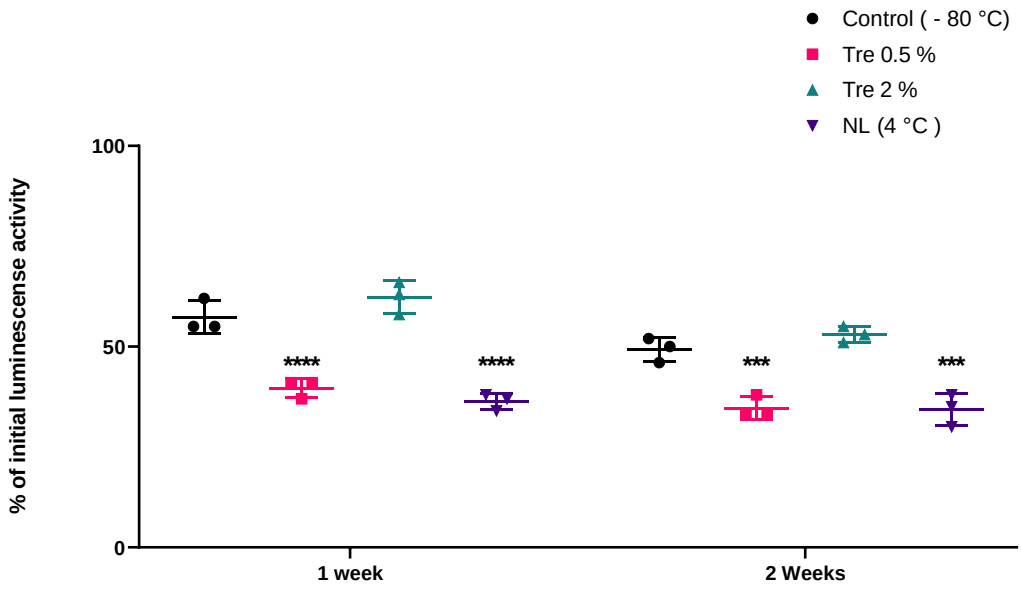


**Figure 7.13:** Luciferase enzyme activity of loaded-EVs derived from transduced-sorted HEK293T cells, stored for two weeks at -80 °C, 4 °C and after lyophilisation with 0.5-2 %w/v of trehalose. For each measurement, the total enzyme activity was normalised to that prior to storage. N=3 and data presented as mean ± SD. Statistical analysis: two-way ANOVA followed by Dunnett's multiple comparisons test versus control (-80 °C); ***$p \leq 0.001$ and ****$p < 0.0001$.

### *7.3.3.5 Concentration and modal size of lyophilised loaded-EVs stored at 20°C*

Fig. 7.14 displays the particle concentration and modal size of loaded-EVs stored at 20 °C. A similar trend is seen here to that at 4 °C, but here the non-lyophilised samples are decomposing and degrading (rather than just degradation at 4 °C). At 20 °C lyophilisation with 2 %w/v trehalose appears to provide a protective effect only for a period of 1 week (after which the particle concentration drops significantly in comparison to the –80 °C control), as opposed to two weeks at 4 °C.

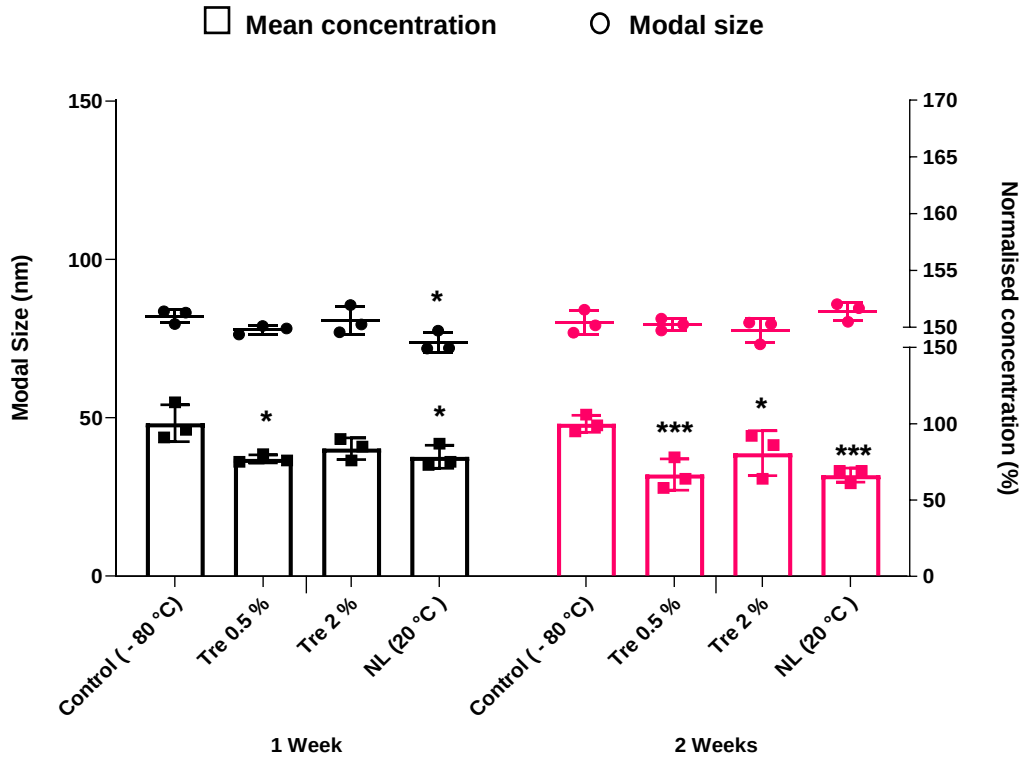


**Figure 7.14:** Particle concentration and modal size of loaded-EVs derived from transduced sorted HEK293T-cells, stored for two weeks at -80 °C, 20 °C and after lyophilisation with 0.5-2 %w/v of trehalose. For each measurement, the particle concentration was normalised to the average particle concentration of the control stored at –80 °C. N=3 and data presented as mean ± SD. Statistical analysis: two-way ANOVA followed by Dunnett's multiple comparisons test versus control (-80 °C); *p < 0.05, **p ≤ 0.01 and ***p ≤ 0.001.

### *7.3.3.6 Total protein concentration of lyophilised loaded-EVs stored at 20°C*

The total protein content determined after storage at 20 °C is displayed in Fig. 7.15. The data are similar to those obtained at 4 °C, except that the total protein concentration of samples lyophilised with 0.5 % w/v trehalose and non-

lyophilised samples are significantly lower than the –80 °C control. Lyophilisation using 2 % w/v trehalose mitigates some of the denaturing effect at 20 °C for the first week only, whereas at 4 °C this mitigates protein denaturation for a two week period.

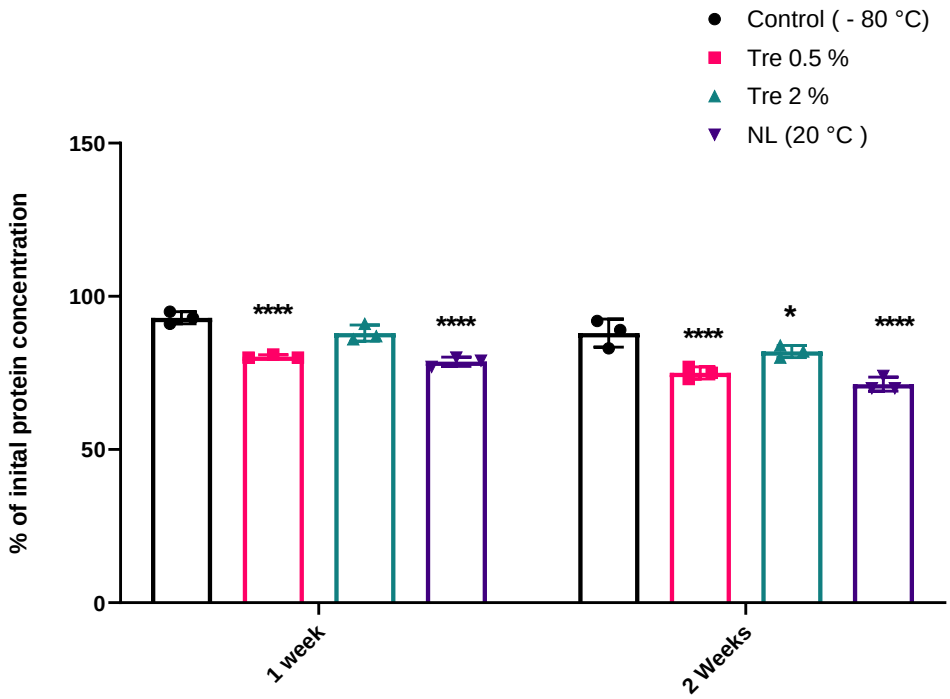


**Figure 7.15**: Total protein concentration as measured by BCA assay of loaded-EVs derived from transduced-sorted HEK293T-cells, stored for two weeks at -80 °C, 20 °C and after lyophilisation with 0.5-2 %w/v of trehalose. For each measurement, the total protein concentration was normalised to that prior to storage. N=3 and data presented as mean ± SD. Statistical analysis: two-way ANOVA followed by Dunnett's multiple comparisons test versus control (–80 ºC); ns denotes $p > 0.05$.

### *7.3.3.7 EV surface markers of lyophilised loaded-EVs stored at 20°C*

Representative western blots for the EV markers CD9 and TSG10 can be seen in **Appendix II** (Fig. AII.7-8). The levels of each marker in the different samples are seen in Fig. 7.16a-b. In comparison to storage at 4 °C, following one week of storage the CD9 and TSG101 levels of both lyophilised and non-lyophilised samples are lower at 20 °C than the –80 °C control. However, CD9 and TSG101 levels of 2 % w/v lyophilised samples are similar to the control after one week of storage, as expected given the positive effects of this treatment on EV size, concentration, and protein content.

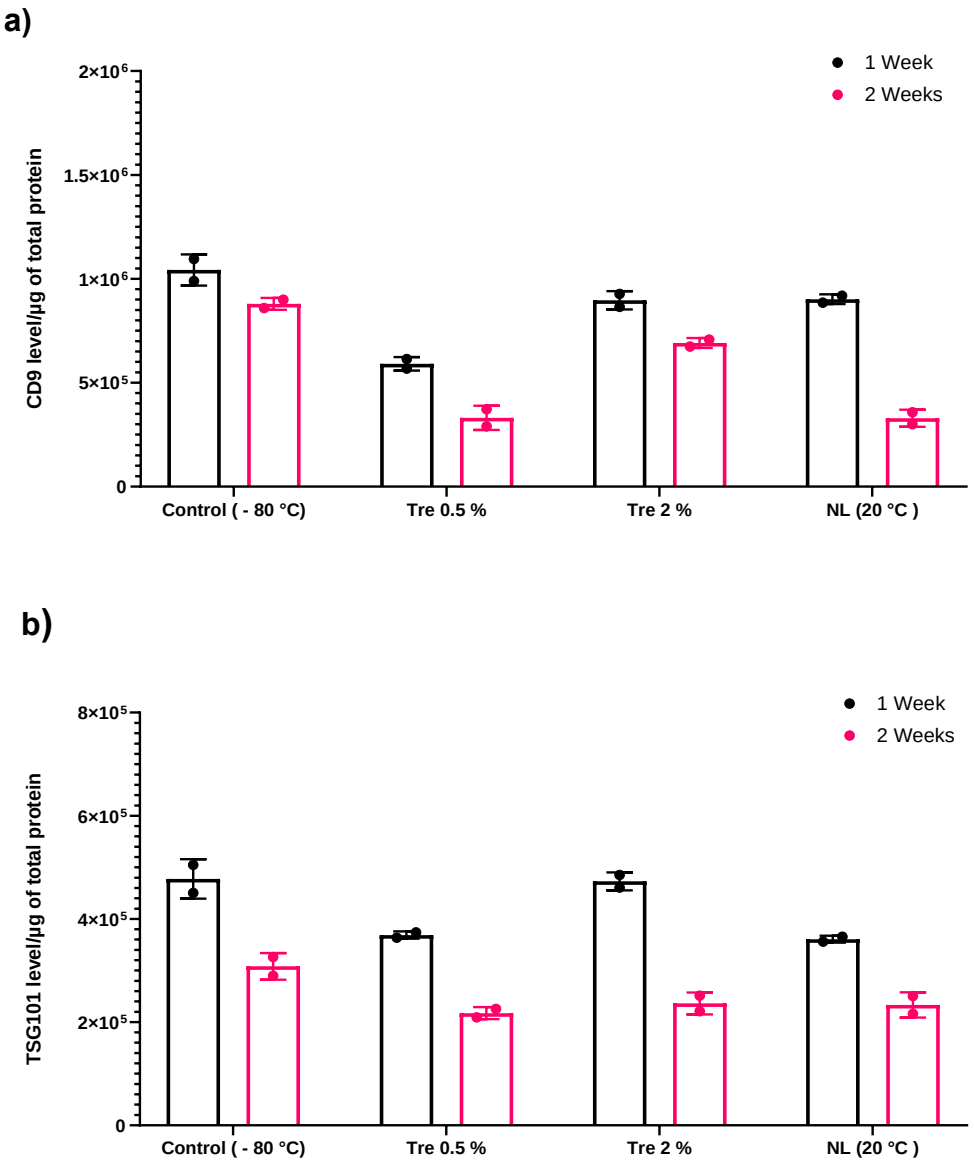


**Figure 7.16:** Levels of surface EV markers a) CD9 and b) TSG101 in loaded-EVs derived from transduced-sorted HEK293T-cells, stored for two weeks at -80 °C, 20 °C and after lyophilisation with 0.5-2 %w/v of trehalose. N=2 and data presented as mean ± SD.

### *7.3.3.8 Luciferase enzyme activity in lyophilised loaded-EVs stored at 20°C*

The activity of luciferase in the EV samples stored at 20 °C is displayed in Fig. 7.17. Again we can see that the enzyme activity declines slightly over the two week period and overall is lower than observed at 4 °C. Similar to storage at 4 °C, samples lyophilised with 0.5 %w/v trehalose and non-lyophilised EVs stored at 20 °C show significantly less enzyme activity than control samples stored at –80 °C at both timepoints. However, in contrast to storage at 4 °C,

the enzyme activity in these samples is significantly higher than that in non-lyophilised samples stored at 20 °C (two-way ANOVA, Tukey's multiple comparisons test; $p < 0.05$). Samples lyophilised with 2 %w/v trehalose show enzyme activity comparable to the -80 °C control for the first week, but this is reduced significantly after the second week of storage. The enzyme activity in these lyophilised samples is significantly higher than that in non-lyophilised samples stored at 20 °C after both week 1 and 2 (two-way ANOVA, Tukey's multiple comparisons test; $p < 0.001$).

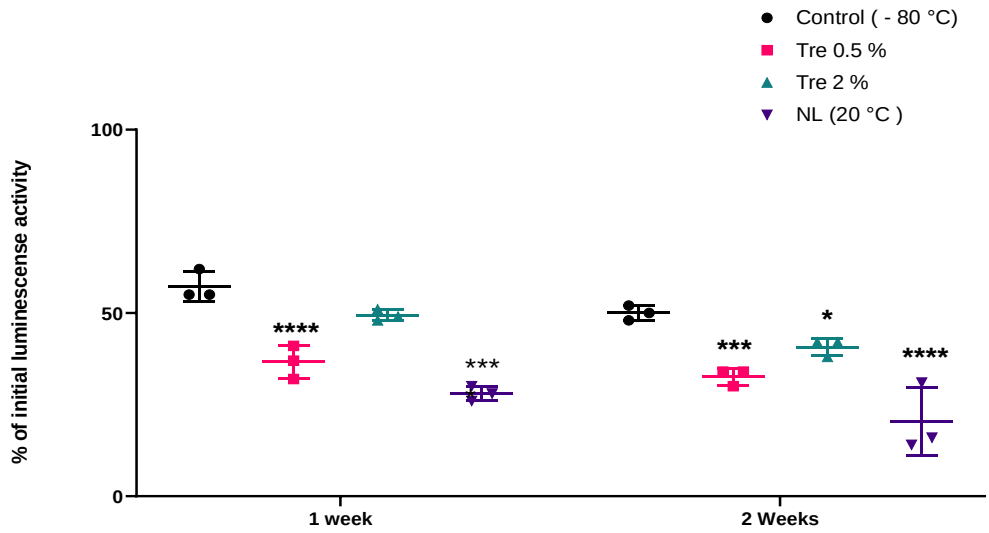


**Figure 7.17:** Luciferase enzyme activity of loaded-EVs derived from transduced-sorted HEK293T-cells, stored for two weeks at -80 °C, 20 °C and after lyophilisation with 0.5-2 %w/v of trehalose. For each measurement, the total enzyme activity was normalised to that prior to storage. N=3 and data presented as mean ± SD. Statistical analysis: two-way ANOVA followed by Dunnett's multiple comparisons test versus control (–80 °C); *$p < 0.05$, ***$p \leq 0.001$ and ****$p < 0.0001$.

It is important to point out that the enzyme activity seen in samples stored at – 80 °C, lyophilised samples stored at 4 and 20 °C is around 50 % of the initial activity, which is a greater drop in comparison to that experienced for total protein concentration. This can be explained by the fact that although the enzyme itself is not degrading the weak non-covalent interactions that hold together the three-dimensional (3D) structure required for its biological activity, are disrupted during storage at higher temperatures or during freeze-thawing [289,310]. In terms of the therapeutic potential of loaded-EVs this means that dosing would have to rely not only on the amount of EVs administered but also on the activity of incorporated enzyme.

Overall, it appears that the optimal formulation conditions for loaded-EVs are lyophilisation using 2 %w/v trehalose and storage at 4 °C. These conditions ensure that EV concentrations, size and surface markers are comparable to control non-lyophilised samples stored at the optimal -80 °C, and also allow for maintenance of significantly higher EV concentrations after two weeks (in comparison to non-lyophilised samples stored at 4 °C). More importantly, these conditions also ensure enzyme activity comparable to those stored at -80 °C and significantly higher activity than in non-lyophilised samples stored at 4°C. Lyophilisation with 2 %w/v trehalose also ensues similar protective effects on EV concentration size, surface markers and enzyme activity but only for one week at 20 °C. These findings are expected to contribute to a better understanding of the behaviour of EVs and incorporated therapeutic cargos during storage and lyophilisation, which will ultimately facilitate their development as delivery vectors for therapeutics.

## 7.4 Conclusions

The stability of EVs derived from naïve HEK293T cells at -80, 4 and 20 °C was investigated over four weeks of storage. It was established that the optimal temperature for storage is -80 °C, where the EVs can be stored for a maximum of two weeks without any deleterious effects on their properties. Following lyophilisation of naïve and loaded-EVs with the lyoprotectant trehalose, it was established that lyophilisation in the presence of trehalose at 0.5 and 2 %w/v could potentially enable storage at 4 °C while maintaining characteristics such as size and concentration at levels comparable to control samples stored at –80 °C. Only lyophilisation in the presence of 2 % w/v trehalose appeared to enable such stability enhancement during storage at 20 °C. The effect of lyophilisation on the activity of the incorporated enzyme in loaded-EVs is more substantial. Loaded-EVs lyophilised in the presence of 2 %w/v trehalose show enzyme activity comparable to those stored at -80 °C, but significantly higher enzyme activity than in non-lyophilised samples stored at 4°C, over two weeks. Similar protective effects were achieved for storage at 20 °C, but only for a duration of one week. This new understanding of EV behaviour upon lyophilisation will contribute to the advancement of EVs as therapeutic delivery vectors for preclinical or clinical settings, as it will facilitate ease of handling while maintaining biological activity and gives an idea of possible shelf-lives for EV formulations.

# Chapter 8: Discussion

## 8.1 Overview

There are a large number of inherited paediatric metabolic disorders whereby a genetic mutation leads to a lack of protein and enzyme, resulting in lethal neurovisceral manifestations and death in early childhood [2]. As these conditions are generally very rare in occurrence, often there is no effective treatment available, and hence there is an overwhelming need to develop new therapies [2]. An example of these conditions is Gaucher Disease, where mutations in the *GBA1* gene results in a defective GCase enzyme that ultimately results in three forms of the disease (Types I, II and III). Type II and Type III Gaucher disease patients exhibit both neuronal and visceral manifestations, with no available treatments for the lethal neurodegeneration.

The ultimate aim of this project is to generate a platform for the production of extracellular vesicles (EVs) loaded with GCase enzyme to be used in the treatment of Type II Gaucher disease. The rationale behind this is that EVs have been shown be deliver a desired cargo to both the visceral organs and brain, and thus if loaded with GCase enzyme could represent ideal therapies.

The results outlined in this thesis set the foundation for the development of “cellular factories” for the production of EVs loaded with a variety of biological cargo, which can be utilized as a treatment for such conditions.

## 8.2 Lentiviral vectors for generation of cellular factories for loaded-EVs

To date, almost all the studies available in the literature exploring genetic engineering of EV producer cell lines to generate loaded-EVs rely on transient transfection of producer cells with a plasmid containing a gene coding for the desired cargo to be loaded into EVs. This is laborious, time consuming and does not allow for a homogenous EV product. Therefore, to improve and facilitate clinical translation of the loaded-EV product, an alternative strategy that better streamlines the production process and ensures better homogeneity of the final therapeutic product is necessary. Lentiviral vectors, that permanently integrate a target gene into the genome of EV producer cells, were thus evaluated in Chapter 3. This removes the need for transfection of

cells prior to each isolation of loaded-EVs. In addition, sorting of transduced cells to select single cell colonies from a small range of cells showing the highest expression of the gene of interest could further optimise this process. This not only means that each single cell colony, when expanded, will contain genetically identical cells with the same level of viral integration and hence gene expression, but also will allow production of a large amount of cells that can be cryopreserved to sustain future production of loaded-EVs.

Cells transduced with viral vectors containing marker genes for eGFP and luciferase were generated, and sorted for the highest levels of gene expression before being repeatedly cultured to produce EVs loaded with luciferase and eGFP. These loaded-EVs had similar characteristics in terms of size, concentration and surface markers as naïve EVs, but in addition contained active luciferase enzyme and significant amounts of eGFP.

## 8.3 EVs can deliver cargo *in vitro* and *in vivo*

For loaded-EVs to be used as therapies for paediatric neurovisceral diseases they need to be internalised by both primary neurons and cells of visceral origin and deliver cargo *in vivo* to both the visceral organs and brain. This was evaluated in Chapter 4.

Loaded-EVs were shown to deliver active luciferase enzyme to cells of visceral origin (HEK293T cells), and eGFP to primary mouse neurons, where they co-localised with the lysosome. The fact that the EVs can co-localise with the lysosome makes them promising potential therapeutics for the large range of neurovisceral conditions classified as lysosomal storage diseases [311].

The *in vivo* biodistribution profile of EVs is minimally explored in the literature, with studies only performed in adult animals and mainly via the IV route, and no reports exploring this profile in neonates. The *in vivo* biodistribution following different routes of administration (ICV, IV, IP and IN) in both adult and neonate mice is detailed in Chapter 4. It was shown that in neonates EVs can deliver cargo to both visceral organs and the brain via the ICV, IV and IP route, although to a different extent. It was clear that EVs can cross the BBB, but to a lower extent than desired. Similar biodistribution profiles were seen in

adult mice through the different routes of administration, but here EVs were shown not to cross the BBB. The EVs appeared to have fast clearance from the system of both neonates and adult mice, indicating a short half-life. These findings are in agreement with those seen in the literature, where the reported half-life in most tissues following IV administration is < 30 minutes, with complete clearance by 6 hours [135,136].

## 8.4 Neuronal cell derived EVs do not necessarily lead to enhanced or targeted delivery to neuronal cells

In an effort to enhance overall delivery to neuronal cells of EVs to the brain a neuronal cell line (SH-SY5Y) was used in Chapter 5 to produce loaded-EVs. This was based on studies suggesting that EVs show specific tissue tropism depending on the parent cells [48,231,255,256]. Upon successful transduction of SH-SH5Y cells, they were used to produce loaded-EVs of similar characteristics as those derived from HEK293T cells, but with a higher content of incorporated eGFP. *In vivo* studies in neonates showed that the eGFP concentration in the organs (liver, heart and brain) 1 hour following injections (via the ICV, IV and IP routes) of SH-SY5Y-derived loaded-EVs was lower in comparison to similar injections of HEK293T-derived loaded-EVs. Thus it could not be established whether SH-SY5Y derived loaded-EVs showed increased targeting to the brain. This was attributed to potentially faster clearance of these EVs in comparison to HEK293T derived EVs.

## 8.5 EVs can deliver active lysosomal GCase enzyme to the lysosomal compartment

EVs loaded with the GCase enzyme were produced in Chapter 6, characterised and found to have similar properties in terms of size, concentration, and surface markers as the EVs produced in previous chapters. The activity of the GCase enzyme was evaluated and determined to be significantly higher than that in non-transduced cells and naïve EVs. Subsequent *in vitro* cell uptake assays show that GCase-loaded EVs can upregulate lysosomal GCase activity, which is in agreement with previous data

seen in Chapter 4 where EVs co-localised with the lysosome. This is promising because it suggests that the strategy can be used to load EVs with a variety of soluble lysosomal hydrolyses, essential for the treatment of various lysosomal storage diseases.

## 8.6 Lyophilisation allows for storage of EVs at higher temperatures

A storage temperature of -80 °C was determined to be optimal for maintaining the stability of EVs in Chapter 7. Lyophilisation of EVs with trehalose as a lyoprotectant allowed for storage at 4 °C for a duration of 2 weeks, or at 20 °C for 1 week, with comparable stability to -80 °C controls. These results offer a route to easier handling of EVs, which could further expand their applications and potential for development as a pharmaceutical product.

## 8.7 Study limitations and future considerations

The work presented in this thesis sets the foundation for the development of a platform of cellular factories to produce loaded-EVs for the treatment of various diseases, and in particular paediatric neurovisceral diseases. However, further investigations are necessary before these can be evaluated for therapies in the clinic.

A further improvement on the isolation method of EVs established in Chapter 3, could be beneficial. This can be done by adding an additional purification step using size exclusion chromatography columns after the final ultracentrifugation step. This could not only possibly yield a more purified batch of EVs, but could also potentially enable higher concentration EV titres. Further, the addition of a size exclusion chromatography step could allow complete separation of EVs from any incorporated protein components, and thus allow us to calculate a ratio of EV particles to protein concentration and indicate the purity of the batch of EVs. Moreover, an alternative method for faster and less laborious generation of EV-depleted FBS could be explored, such as ultrafiltration. Alternatively, other commercial EV-depleted FBS could

also be purchased and tested for EV depletion and its effect on cell viability. This will further streamline the EV production process and improve clinical translatability.

Furthermore, additional EV characterisation than that conducted in Chapter 3 is essential for future consideration, in particular characterisation of the EV cargo and specifically the increased levels of small RNAs isolated from EVs produced by transduced HEK293T cells. Microarray-based expression analysis can be used to identify the RNAs that could have been upregulated as a result of transduction. This is very important as these upregulated RNAs can have either positive or negative off target effect or even interfere with the proposed enzyme replacement therapy.

In Chapter 4, ELISA was used to determine the eGFP concentration in each harvested organ. However, as whole organs were not weighed prior to further analysis it was not possible to calculate the percentage dose of EVs in each organ. In future *in vivo* studies pre-weighing the organs could give a better indication of the percentage dose delivered. In addition, the tissues harvested were stained for eGFP and DAB in this work. We could only see eGFP in organs with the highest levels of uptake. This study limitation is imperative to resolve as it is important to analyse how EVs distribute in each tissue. Therefore, further improvements to visualise uptake in each organ such as use of a microscope capable of higher resolution imaging such as SEM should be explored.

Moreover, the in vivo distribution profiles of EVs observed in Chapter 4, although promising highlight certain limitations such as short half-life and low or negligible delivery to the brain. These aspects would need to be further investigated and improved to ensure clinical translatability of loaded-EVs. To improve tissue half-life, we need to better understand how the EVs are cleared from tissues and what factors are responsible for their rapid clearance. Furthermore, the fact that these EVs deliver higher levels of cargo to visceral organs than the brain suggest that the loaded-EVs may represent a better therapeutic treatment for diseases with less pronounced neuronal manifestations and more visceral manifestations, such as Gaucher Disease

Type I. Alternatively, the loaded-EVs may represent a suitable adjuvant to gene therapy for a given disease, such as a Gaucher Disease Type II. Most currently studied gene therapies rely on viral vectors [312–314], which cannot be given more than once as patients develop neutralising antibodies that renders repeat administration ineffective [312,315]. Thus, as gene therapy does not correct every single cell, it is expected that some symptoms will prevail post-treatment: these could be treated with subsequent and repeated EV administration. EVs from mesenchymal stem cells and HEK293T lack class I and class II human major histocompatibility complex (MHC) proteins or co-stimulatory molecules such as CD80 and CD86 and as such do not induce an immune response [110,222,316], making them promising candidates for life-long treatments.

Targeting of cargo to EVs was evaluated in Chapter 6 through the addition of an ubiquitin tag to the gene of interest, *GBA1*. However, as we were not able to successfully clone a lentiviral plasmid construct containing only the *GBA1* gene without the ubiquitin tag, we could not determine whether this addition did indeed promote targeting of cargo to EVs. Therefore, further cloning attempts should be carried out to produce such vector for comparison purposes and also to establish whether the addition of ubiquitin has an impact on the activity of the GCase enzyme. Additionally, GCase-loaded EVs were shown to upregulate GCase activity *in vitro* and although this experiments ensued promising results, it highlights two limitations one being the apparent short duration of activity and the second being that it was not tested in relevant cellular disease model. Testing the uptake and efficacy of the GCase-loaded EV therapies in the relevant cellular and animal disease models is essential to further validate their future clinical translatability for the treatment of Gaucher disease. These limitation were recognised during the project and it was our intention to test the uptake of GCase-loaded EVs by GBA deficient primary neurons from a Gaucher Type II disease mouse model, instead of uptake by HEK293T cells conducted in this Chapter. However, despite extensive efforts on returning to the lab following the COVID-19 lockdown, we could not breed the mice to generate pups from which we could isolate such primary neurons. Thus, in the future it is hoped that this experiment can be conducted to further

verify EV uptake, upregulation of GCase enzyme, and restoration of normal cellular function in the relevant cellular disease model. In addition, depending on the success of this study it was our intention to combine the *GBA1* gene therapy that has been developed in house with GCase loaded-EVs. The *GBA1* gene therapy would be administered through the ICV route to neonate mice from a Gaucher Disease Type II disease model, to correct neuronal manifestations, and the loaded-EVs would be administered subsequently at time points where the animals start showing symptoms due to visceral manifestations

The stability of EVs upon storage at different temperatures was described in Chapter 7. Here, the impact of storage on the EV concentration, size, markers and incorporated enzyme activity suggests a relatively poor commercial shelf-life of potential EV product. However, this study has two limitations, the fact that the study only lasted one month and that it did not evaluate the effect of storage on neither *in vitro* nor *in vivo* uptake of EVs. The literature has shown that a negative impact on EV characteristics such as increase in size does not necessarily alter their endogenous *in vitro* functionality [317]. Therefore, the effect of storage on *in vitro* and *in vivo* performance of EVs as well as increasing the length of the stability study, should be carried in order to better determine potential commercial shelf life. This is again important to facilitate a better clinical pathway. Moreover, the effect of lyophilisation on the stability and activity of incorporated luciferase enzyme in HEK293T-derived loaded-EVs was evaluated, but a similar study should be carried out using EVs loaded with GCase, as the enzymes may not have similar stabilities under the same formulation conditions. .

## 8.8 Conclusion

The EV research field has seen exponential growth over the last decade, with EVs being evaluated for use as therapeutic vectors in the treatment of various diseases. However, the field is still regarded to be in its infancy, and further research needs to be carried out to facilitate understanding of various aspects such as EV biogenesis, mechanisms of internalisation, and subsequent processing upon uptake, in addition to *in vivo* biodistribution profiles, half-life

and stability. All of these studies will further contribute to the development of EVs as therapeutic delivery vehicles.

The work carried out in this project included the use of lentiviral vectors to produce cellular factories of EVs loaded with either luciferase-eGFP or GCase, in addition to evaluation of the *in vitro* and *in vivo* behaviour of loaded-EVs, and the stability of EVs and incorporated enzyme cargo upon storage and lyophilisation. Its findings will contribute to the advancement of EV research not only as potential treatments for paediatric neurovisceral disease but also in terms of fundamental understanding.

# References


1. Stirnemann, J. *et al.* A Review of Gaucher Disease Pathophysiology, Clinical Presentation and Treatments. *Int. J. Mol. Sci.* **18**, 441 (2017).

2. Parenti, G., Andria, G. & Ballabio, A. Lysosomal Storage Diseases: From Pathophysiology to Therapy. *Annu. Rev. Med.* **66**, 471–486 (2015).

3. Aryani, A. & Denecke, B. Exosomes as a Nanodelivery System: a Key to the Future of Neuromedicine? *Mol. Neurobiol.* **53**, 818–834 (2016).

4. Cox, T. M. & Cachón-González, M. B. The cellular pathology of lysosomal diseases. *J. Pathol.* **226**, 241–254 (2012).

5. Iodice, A. *et al.* Infantile neuroaxonal dystrophy and PLA2G6-associated neurodegeneration: An update for the diagnosis. *Brain Dev.* **39**, 93–100 (2017).

6. Mole, S., Williams, R. & Goebel, H. *The Neuronal Ceroid Lipofuscinoses (Batten Disease)*. *The Neuronal Ceroid Lipofuscinoses (Batten Disease)* **1**, (Oxford University Press, 2012).

7. Baris, H. N., Cohen, I. J. & Mistry, P. K. Gaucher disease: the metabolic defect, pathophysiology, phenotypes and natural history. *Pediatr. Endocrinol. Rev.* **12**, 72–81 (2014).

8. Mignot, C., Doummar, D., Maire, I. & De Villemeur, T. B. Type 2 Gaucher disease: 15 new cases and review of the literature. *Brain Dev.* **28**, 39–48 (2006).

9. Goker-Alpan, O. *et al.* Phenotypic continuum in neuronopathic gaucher disease: an intermediate phenotype between type 2 and type 3. *J. Pediatr.* **143**, 273–276 (2003).

10. Gupta, N., Oppenheim, I. M., Kauvar, E. F., Tayebi, N. & Sidransky, E. Type 2 Gaucher disease: Phenotypic variation and genotypic heterogeneity. *Blood Cells, Mol. Dis.* **46**, 75–84 (2011).

11. Tylki-Szymańska, A., Vellodi, A., El-Beshlawy, A., Cole, J. A. & Kolodny, E. Neuronopathic Gaucher disease: demographic and clinical features of 131 patients enrolled in the International Collaborative Gaucher Group Neurological Outcomes Subregistry. *J. Inherit. Metab. Dis.* **33**, 339–346 (2010).

12. Sestito, S. *et al.* Neuronopathic Gaucher Disease. *J. Pediatr. Biochem.* **06**, 039–045 (2016).

13. Mignot, C., Gelot, A. & De Villemeur, T. B. Gaucher disease. in *Handbook of Clinical Neurology* 1709–1715 (2013).

14. Barneveld, R. A. *et al.* Assignment of the gene coding for human β-glucocerebrosidase to the region q21-q31 of chromosome 1 using monoclonal antibodies. *Hum. Genet.* **64**, 227–231 (1983).

15. Berg-Fussman, A., Grace, M. E., Ioannou, Y. & Grabowski, G. A.

Human acid beta-glucosidase. N-glycosylation site occupancy and the effect of glycosylation on enzymatic activity. *J. Biol. Chem.* **268**, 14861–6 (1993).

16. Grabowski, G. A., Gaft, S., Horowitz, M. & Kolodny, E. H. Acid β-Glucosidase: Enzymology and Molecular Biology of Gaucher Disease. *Crit. Rev. Biochem. Mol. Biol.* **25**, 385–414 (1990).

17. Sandhoff, K. Metabolic and cellular bases of sphingolipidoses. *Biochem. Soc. Trans.* **41**, 1562–1568 (2013).

18. Tamargo, R. J., Velayati, A., Goldin, E. & Sidransky, E. The role of saposin C in Gaucher disease. *Mol. Genet. Metab.* **106**, 257–263 (2012).

19. Hruska, K. S., LaMarca, M. E., Scott, C. R. & Sidransky, E. Gaucher disease: mutation and polymorphism spectrum in the glucocerebrosidase gene (GBA). *Hum. Mutat.* **29**, 567–583 (2008).

20. Grabowski, G. A. Gaucher disease and other storage disorders. *Hematology* **2012**, 13–18 (2012).

21. Pastores, G. M. 7 Pathological features. *Baillieres. Clin. Haematol.* **10**, 739–749 (1997).

22. Lee, R. E. The fine structure of the cerebroside occurring in Gaucher's disease. *Proc. Natl. Acad. Sci.* **61**, 484–489 (1968).

23. Aerts, J. M., Hollak, C., Boot, R. & Groener, A. Biochemistry of glycosphingolipid storage disorders: implications for therapeutic intervention. *Philos. Trans. R. Soc. London. Ser. B Biol. Sci.* **358**, 905–914 (2003).

24. Zimran, A., Altarescu, G., Rudensky, B., Abrahamov, A. & Elstein, D. Survey of hematological aspects of Gaucher disease. *Hematology* **10**, 151–156 (2005).

25. Mistry, P. K. *et al.* Pulmonary hypertension in type 1 Gaucher's disease: genetic and epigenetic determinants of phenotype and response to therapy. *Mol. Genet. Metab.* **77**, 91–98 (2002).

26. Amir, G. & Ron, N. Pulmonary pathology in Gaucher's disease. *Hum. Pathol.* **30**, 666–670 (1999).

27. Grabowski, G. A. Phenotype, diagnosis, and treatment of Gaucher's disease. *Lancet* **372**, 1263–1271 (2008).

28. Kaplan, P., Andersson, H. C., Kacena, K. A. & Yee, J. D. The Clinical and Demographic Characteristics of Nonneuronopathic Gaucher Disease in 887 Children at Diagnosis. *Arch. Pediatr. Adolesc. Med.* **160**, 603–608 (2006).

29. Bennett, L. L. & Fellner, C. Pharmacotherapy of Gaucher Disease: Current and Future Options. *P T* **43**, 274–309 (2018).

30. Aerts, J. M. F. G., Hollak, C. E. M., Boot, R. G., Groener, J. E. M. &

Maas, M. Substrate reduction therapy of glycosphingolipid storage disorders. *J. Inherit. Metab. Dis.* **29**, 449–456 (2006).

31. Cox, T. M. *et al.* Eliglustat compared with imiglucerase in patients with Gaucher's disease type 1 stabilised on enzyme replacement therapy: a phase 3, randomised, open-label, non-inferiority trial. *Lancet* **385**, 2355–2362 (2015).

32. Lukina, E. *et al.* A phase 2 study of eliglustat tartrate (Genz-112638), an oral substrate reduction therapy for Gaucher disease type 1. *Blood* **116**, 893–899 (2010).

33. Altarescu, G. *et al.* The efficacy of enzyme replacement therapy in patients with chronic neuronopathic gaucher's disease. *J. Pediatr.* **138**, 539–547 (2001).

34. Wraith, J. E. Limitations of enzyme replacement therapy: Current and future. *J. Inherit. Metab. Dis.* **29**, 442–447 (2006).

35. Lukina, E. *et al.* Improvement in hematological, visceral, and skeletal manifestations of Gaucher disease type 1 with oral eliglustat tartrate (Genz-112638) treatment: 2-year results of a phase 2 study. *Blood* **116**, 4095–4098 (2010).

36. Bellettato, C. M. & Scarpa, M. Possible strategies to cross the blood–brain barrier. *Ital. J. Pediatr.* **44**, 131 (2018).

37. Harding, C. & Stahl, P. Transferrin recycling in reticulocytes: pH and iron are important determinants of ligand binding and processing. *Biochem. Biophys. Res. Commun.* **113**, 650–658 (1983).

38. Pan, B.-T. & Johnstone, R. M. Fate of the transferrin receptor during maturation of sheep reticulocytes in vitro: Selective externalization of the receptor. *Cell* **33**, 967–978 (1983).

39. Keller, S., Sanderson, M. P., Stoeck, A. & Altevogt, P. Exosomes: From biogenesis and secretion to biological function. *Immunol. Lett.* **107**, 102–108 (2006).

40. Lai, R. C., Chen, T. S. & Lim, S. K. Mesenchymal stem cell exosome: a novel stem cell-based therapy for cardiovascular disease. *Regen. Med.* **6**, 481–492 (2011).

41. Raposo, G. & Stoorvogel, W. Extracellular vesicles: Exosomes, microvesicles, and friends. *J. Cell Biol.* **200**, 373–383 (2013).

42. Zaborowski, M. P., Balaj, L., Breakefield, X. O. & Lai, C. P. Extracellular Vesicles: Composition, Biological Relevance, and Methods of Study. *Bioscience* **65**, 783–797 (2015).

43. Yáñez-Mó, M. *et al.* Biological properties of extracellular vesicles and their physiological functions. *J. Extracell. Vesicles* **4**, 27066 (2015).

44. Théry, C., Zitvogel, L. & Amigorena, S. Exosomes: composition, biogenesis and function. *Nat. Rev. Immunol.* **2**, 569–579 (2002).

45. Momen-Heravi, F. *et al.* Current methods for the isolation of extracellular vesicles. *Biol. Chem.* **394**, 1253–1262 (2013).

46. Rosas, L. E. *et al.* In vitro immunotoxicity assessment of culture-derived extracellular vesicles in human monocytes. *J. Immunotoxicol.* **13**, 652–665 (2016).

47. Mathivanan, S., Fahner, C. J., Reid, G. E. & Simpson, R. J. ExoCarta 2012: Database of exosomal proteins, RNA and lipids. *Nucleic Acids Res.* **40**, 1241–1244 (2012).

48. Kooijmans, S. A. A., Schiffelers, R. M., Zarovni, N. & Vago, R. Modulation of tissue tropism and biological activity of exosomes and other extracellular vesicles: New nanotools for cancer treatment. *Pharmacol. Res.* **111**, 487–500 (2016).

49. Abels, E. R. & Breakefield, X. O. Introduction to Extracellular Vesicles: Biogenesis, RNA Cargo Selection, Content, Release, and Uptake. *Cell. Mol. Neurobiol.* **36**, 301–312 (2016).

50. Harding, C. V., Heuser, J. E. & Stahl, P. D. Exosomes: Looking back three decades and into the future. *J. Cell Biol.* **200**, 367–371 (2013).

51. Van Niel, G., D'Angelo, G. & Raposo, G. Shedding light on the cell biology of extracellular vesicles. *Nat. Rev. Mol. Cell Biol.* **19**, 213–228 (2018).

52. Rashed, M. H. *et al.* Exosomes: From garbage bins to promising therapeutic targets. *Int. J. Mol. Sci.* **18**, (2017).

53. Willis, G. R., Kourembanas, S. & Mitsialis, S. A. Therapeutic Applications of Extracellular Vesicles: Perspectives from Newborn Medicine. in *Extracellular Vesicles: Methods and Protocols* (eds. Kuo, W. P. & Jia, S.) 409–432 (Springer New York, 2017).

54. Buratta, S. *et al.* Lysosomal Exocytosis, Exosome Release and Secretory Autophagy: The Autophagic- and Endo-Lysosomal Systems Go Extracellular. *Int. J. Mol. Sci.* **21**, 2576 (2020).

55. Urbanelli, L. *et al.* Signaling Pathways in Exosomes Biogenesis, Secretion and Fate. *Genes (Basel).* **4**, 152–170 (2013).

56. Valadi, H. *et al.* Exosome-mediated transfer of mRNAs and microRNAs is a novel mechanism of genetic exchange between cells. *Nat. Cell Biol.* **9**, 654–659 (2007).

57. Colombo, M., Raposo, G. & Théry, C. Biogenesis, Secretion, and Intercellular Interactions of Exosomes and Other Extracellular Vesicles. *Annu. Rev. Cell Dev. Biol.* **30**, 255–289 (2014).

58. Hessvik, N. P. & Llorente, A. Current knowledge on exosome biogenesis and release. *Cell. Mol. Life Sci.* **75**, 193–208 (2018).

59. Palmulli, R. & Van Niel, G. To be or not to be... secreted as exosomes, a balance finely tuned by the mechanisms of biogenesis. *Essays Biochem.* **62**, 177–191 (2018).

60. Doyle, L. & Wang, M. Overview of Extracellular Vesicles, Their Origin, Composition, Purpose, and Methods for Exosome Isolation and Analysis. *Cells* **8**, 727 (2019).

61. Shang, M. *et al.* Extracellular Vesicles: A Brief Overview and Its Role in Precision Medicine. in *Methods in molecular biology (Clifton, N.J.)* 1–14 (2017). doi:1

62. Essandoh, K. & Fan, G.-C. Insights into the Mechanism of Exosome Formation and Secretion. in *Mesenchymal Stem Cell Derived Exosomes* **101**, 1–19 (Elsevier, 2015).

63. van Niel, G. *et al.* Dendritic Cells Regulate Exposure of MHC Class II at Their Plasma Membrane by Oligoubiquitination. *Immunity* **25**, 885–894 (2006).

64. Katzmann, D. J., Babst, M. & Emr, S. D. Ubiquitin-Dependent Sorting into the Multivesicular Body Pathway Requires the Function of a Conserved Endosomal Protein Sorting Complex, ESCRT-I. *Cell* **106**, 145–155 (2001).

65. Villarroya-Beltri, C., Baixauli, F., Gutiérrez-Vázquez, C., Sánchez-Madrid, F. & Mittelbrunn, M. Sorting it out: Regulation of exosome loading. *Semin. Cancer Biol.* **28**, 3–13 (2014).

66. Stuffers, S., Sem Wegner, C., Stenmark, H. & Brech, A. Multivesicular Endosome Biogenesis in the Absence of ESCRTs. *Traffic* **10**, 925–937 (2009).

67. Buschow, S. I. *et al.* MHC class II-associated proteins in B-cell exosomes and potential functional implications for exosome biogenesis. *Immunol. Cell Biol.* **88**, 851–856 (2010).

68. Trajkovic, K. *et al.* Ceramide Triggers Budding of Exosome Vesicles into Multivesicular Endosomes. *Science (80-. ).* **319**, 1244–1247 (2008).

69. Kajimoto, T., Okada, T., Miya, S., Zhang, L. & Nakamura, S. Ongoing activation of sphingosine 1-phosphate receptors mediates maturation of exosomal multivesicular endosomes. *Nat. Commun.* **4**, 2712 (2013).

70. Perez-Hernandez, D. *et al.* The Intracellular Interactome of Tetraspanin-enriched Microdomains Reveals Their Function as Sorting Machineries toward Exosomes. *J. Biol. Chem.* **288**, 11649–11661 (2013).

71. Mazurov, D., Barbashova, L. & Filatov, A. Tetraspanin protein CD9 interacts with metalloprotease CD10 and enhances its release via exosomes. *FEBS J.* **280**, 1200–1213 (2013).

72. van den Boorn, J. G., Daßler, J., Coch, C., Schlee, M. & Hartmann, G. Exosomes as nucleic acid nanocarriers. *Adv. Drug Deliv. Rev.* **65**, 331–335 (2013).

73. Mittelbrunn, M. *et al.* Unidirectional transfer of microRNA-loaded exosomes from T cells to antigen-presenting cells. *Nat. Commun.* **2**,

282 (2011).

74. Montecalvo, A. *et al.* Mechanism of transfer of functional microRNAs between mouse dendritic cells via exosomes. *Blood* **119**, 756–766 (2012).

75. Hergenreider, E. *et al.* Atheroprotective communication between endothelial cells and smooth muscle cells through miRNAs. *Nat. Cell Biol.* **14**, 249–256 (2012).

76. Zhang, Y. *et al.* Secreted Monocytic miR-150 Enhances Targeted Endothelial Cell Migration. *Mol. Cell* **39**, 133–144 (2010).

77. Montecalvo, A. *et al.* Exosomes As a Short-Range Mechanism to Spread Alloantigen between Dendritic Cells during T Cell Allorecognition. *J. Immunol.* **180**, 3081–3090 (2008).

78. Villarroya-Beltri, C. *et al.* Sumoylated hnRNPA2B1 controls the sorting of miRNAs into exosomes through binding to specific motifs. *Nat. Commun.* **4**, 2980 (2013).

79. Hoshino, D. *et al.* Exosome Secretion Is Enhanced by Invadopodia and Drives Invasive Behavior. *Cell Rep.* **5**, 1159–1168 (2013).

80. Sinha, S. *et al.* Cortactin promotes exosome secretion by controlling branched actin dynamics. *J. Cell Biol.* **214**, 197–213 (2016).

81. Stenmark, H. Rab GTPases as coordinators of vesicle traffic. *Nat. Rev. Mol. Cell Biol.* **10**, 513–525 (2009).

82. Heijnen, H. F. G., Schiel, A. E., Fijnheer, R., Geuze, H. J. & Sixma, J. J. Activated Platelets Release Two Types of Membrane Vesicles: Microvesicles by Surface Shedding and Exosomes Derived From Exocytosis of Multivesicular Bodies and Alpha-Granules. *Blood* **94**, 3791–3799 (1999).

83. Obregon, C., Rothen-Rutishauser, B., Gitahi, S. K., Gehr, P. & Nicod, L. P. Exovesicles from Human Activated Dendritic Cells Fuse with Resting Dendritic Cells, Allowing Them to Present Alloantigens. *Am. J. Pathol.* **169**, 2127–2136 (2006).

84. Fauré, J. *et al.* Exosomes are released by cultured cortical neurones. *Mol. Cell. Neurosci.* **31**, 642–648 (2006).

85. Van Der Pol, E., Böing, A. N., Gool, E. L. & Nieuwland, R. Recent developments in the nomenclature, presence, isolation, detection and clinical impact of extracellular vesicles. *J. Thromb. Haemost.* **14**, (2016).

86. Théry, C. *et al.* Minimal information for studies of extracellular vesicles 2018 (MISEV2018): a position statement of the International Society for Extracellular Vesicles and update of the MISEV2014 guidelines. *J. Extracell. Vesicles* **7**, 1535750 (2018).

87. Nassar, W. *et al.* Umbilical cord mesenchymal stem cells derived extracellular vesicles can safely ameliorate the progression of chronic

kidney diseases. *Biomater. Res.* **20**, 21 (2016).

88. Barry, F. P. & Murphy, J. M. Mesenchymal stem cells: clinical applications and biological characterization. *Int. J. Biochem. Cell Biol.* **36**, 568–584 (2004).

89. Phinney, D. G. & Pittenger, M. F. Concise Review: MSC-Derived Exosomes for Cell-Free Therapy. *Stem Cells* **35**, 851–858 (2017).

90. Mendt, M., Rezvani, K. & Shpall, E. Mesenchymal stem cell-derived exosomes for clinical use. *Bone Marrow Transplant.* **54**, 789–792 (2019).

91. Bagno, L., Hatzistergos, K. E., Balkan, W. & Hare, J. M. Mesenchymal Stem Cell-Based Therapy for Cardiovascular Disease: Progress and Challenges. *Mol. Ther.* **26**, 1610–1623 (2018).

92. Lou, G., Chen, Z., Zheng, M. & Liu, Y. Mesenchymal stem cell-derived exosomes as a new therapeutic strategy for liver diseases. *Exp. Mol. Med.* **49**, e346–e346 (2017).

93. Zhang, Y. *et al.* Effect of exosomes derived from multipluripotent mesenchymal stromal cells on functional recovery and neurovascular plasticity in rats after traumatic brain injury. *J. Neurosurg.* **122**, 856–867 (2015).

94. Gorabi, A. M. *et al.* The Therapeutic Potential of Mesenchymal Stem Cell–Derived Exosomes in Treatment of Neurodegenerative Diseases. *Mol. Neurobiol.* **56**, 8157–8167 (2019).

95. Burke, J. *et al.* Stem Cell-Derived Exosomes: A Potential Alternative Therapeutic Agent in Orthopaedics. *Stem Cells Int.* **2016**, 1–6 (2016).

96. Lai, R. C. *et al.* Exosome secreted by MSC reduces myocardial ischemia/reperfusion injury. *Stem Cell Res.* **4**, 214–222 (2010).

97. Gnecchi, M. *et al.* Paracrine action accounts for marked protection of ischemic heart by Akt-modified mesenchymal stem cells. *Nat. Med.* **11**, 367–368 (2005).

98. Mirotsou, M., Jayawardena, T. M., Schmeckpeper, J., Gnecchi, M. & Dzau, V. J. Paracrine mechanisms of stem cell reparative and regenerative actions in the heart. *J. Mol. Cell. Cardiol.* **50**, 280–289 (2011).

99. Wen, D., Peng, Y., Liu, D., Weizmann, Y. & Mahato, R. I. Mesenchymal stem cell and derived exosome as small RNA carrier and Immunomodulator to improve islet transplantation. *J. Control. Release* **238**, 166–175 (2016).

100. Phinney, D. G. *et al.* Mesenchymal stem cells use extracellular vesicles to outsource mitophagy and shuttle microRNAs. *Nat. Commun.* **6**, 8472 (2015).

101. Kim, D.-K. *et al.* Chromatographically isolated CD63 + CD81 + extracellular vesicles from mesenchymal stromal cells rescue cognitive

impairments after TBI. *Proc. Natl. Acad. Sci.* **113**, 170–175 (2016).

102. Lin, K.-C. *et al.* Combination of adipose-derived mesenchymal stem cells (ADMSC) and ADMSC-derived exosomes for protecting kidney from acute ischemia–reperfusion injury. *Int. J. Cardiol.* **216**, 173–185 (2016).

103. Arslan, F. *et al.* Mesenchymal stem cell-derived exosomes increase ATP levels, decrease oxidative stress and activate PI3K/Akt pathway to enhance myocardial viability and prevent adverse remodeling after myocardial ischemia/reperfusion injury. *Stem Cell Res.* **10**, 301–312 (2013).

104. Chen, Y.-S., Lin, E.-Y., Chiou, T.-W. & Harn, H.-J. Exosomes in clinical trial and their production in compliance with good manufacturing practice. *Tzu Chi Med. J.* **32**, 113 (2020).

105. Cheng, L., Zhang, K., Wu, S., Cui, M. & Xu, T. Focus on Mesenchymal Stem Cell-Derived Exosomes: Opportunities and Challenges in Cell-Free Therapy. *Stem Cells Int.* **2017**, 1–10 (2017).

106. Sengupta, V. *et al.* Exosomes Derived from Bone Marrow Mesenchymal Stem Cells as Treatment for Severe COVID-19. *Stem Cells Dev.* **29**, 747–754 (2020).

107. Haney, M. J. *et al.* Exosomes as drug delivery vehicles for Parkinson's disease therapy. *J. Control. Release* **207**, 18–30 (2015).

108. Alvarez-Erviti, L. *et al.* Delivery of siRNA to the mouse brain by systemic injection of targeted exosomes. *Nat. Biotechnol.* **29**, 341–345 (2011).

109. Murphy, D. E. *et al.* Extracellular vesicle-based therapeutics: natural versus engineered targeting and trafficking. *Exp. Mol. Med.* **51**, 32 (2019).

110. Zhu, X. *et al.* Comprehensive toxicity and immunogenicity studies reveal minimal effects in mice following sustained dosing of extracellular vesicles derived from HEK293T cells. *J. Extracell. Vesicles* **6**, 1324730 (2017).

111. Fais, S. *et al.* Exosomes: The ideal nanovectors for biodelivery. *Biol. Chem.* **394**, 1–15 (2013).

112. Zeringer, E., Barta, T., Li, M. & Vlassov, A. V. Strategies for isolation of exosomes. *Cold Spring Harb. Protoc.* **2015**, 319–323 (2015).

113. Wiklander, O. P. B. *et al.* Extracellular vesicle in vivo biodistribution is determined by cell source, route of administration and targeting. *J. Extracell. Vesicles* **4**, 1–13 (2015).

114. Kawikova, I. & Askenase, P. W. Diagnostic and therapeutic potentials of exosomes in CNS diseases. *Brain Res.* **1617**, 63–71 (2015).

115. Haney, M. J. *et al.* Exosomes as drug delivery vehicles for Parkinson's disease therapy. *J. Control. Release* (2015).

doi:10.1016/j.jconrel.2015.03.033

116. Alvarez-Erviti, L. *et al.* Delivery of siRNA to the mouse brain by systemic injection of targeted exosomes. *Nat. Biotechnol.* **29**, 341–345 (2011).

117. Cooper, J. M. *et al.* Systemic exosomal siRNA delivery reduced alpha-synuclein aggregates in brains of transgenic mice. *Mov. Disord.* **29**, 1476–1485 (2014).

118. Pusic, A. D., Pusic, K. M., Clayton, B. L. L. & Kraig, R. P. IFNγ-stimulated dendritic cell exosomes as a potential therapeutic for remyelination. *J. Neuroimmunol.* **266**, 12–23 (2014).

119. Yuyama, K., Sun, H., Mitsutake, S. & Igarashi, Y. Sphingolipid-modulated Exosome Secretion Promotes Clearance of Amyloid-β by Microglia. *J. Biol. Chem.* **287**, 10977–10989 (2012).

120. Reza-Zaldivar, E. *et al.* Mesenchymal stem cell-derived exosomes promote neurogenesis and cognitive function recovery in a mouse model of Alzheimer's disease. *Neural Regen. Res.* **14**, 1626 (2019).

121. Yang, Y. *et al.* MSCs-Derived Exosomes and Neuroinflammation, Neurogenesis and Therapy of Traumatic Brain Injury. *Front. Cell. Neurosci.* **11**, (2017).

122. Zhang, Y. *et al.* Systemic administration of cell-free exosomes generated by human bone marrow derived mesenchymal stem cells cultured under 2D and 3D conditions improves functional recovery in rats after traumatic brain injury. *Neurochem. Int.* **111**, 69–81 (2017).

123. Yun, H.-M. *et al.* Placenta-derived mesenchymal stem cells improve memory dysfunction in an Aβ1–42-infused mouse model of Alzheimer's disease. *Cell Death Dis.* **4**, e958–e958 (2013).

124. Grace, M. E., Newman, K. M., Scheinker, V., Berg-Fussman, A. & Grabowski, G. A. Analysis of human acid beta-glucosidase by site-directed mutagenesis and heterologous expression. *J. Biol. Chem.* **269**, 2283–91 (1994).

125. Sakuma, T., Barry, M. A. & Ikeda, Y. Lentiviral vectors: basic to translational. *Biochem. J.* **443**, 603–618 (2012).

126. Do, M. A., Levy, D., Brown, A., Marriott, G. & Lu, B. Targeted delivery of lysosomal enzymes to the endocytic compartment in human cells using engineered extracellular vesicles. *Sci. Rep.* **9**, 1–11 (2019).

127. Walker, J. M. *Lentiviral Vectors and Exosomes as Gene and Protein Delivery Tools*. **1448**, (Springer New York, 2016).

128. Kumar, M., Keller, B., Makalou, N. & Sutton, R. E. Systematic Determination of the Packaging Limit of Lentiviral Vectors. *Hum. Gene Ther.* **12**, 1893–1905 (2001).

129. Cronin, J., Zhang, X.-Y. & Reiser, J. Altering the Tropism of Lentiviral Vectors through Pseudotyping. *Curr. Gene Ther.* **5**, 387–398 (2005).

130. Geraerts, M., Willems, S., Baekelandt, V., Debyser, Z. & Gijsbers, R. Comparison of lentiviral vector titration methods. *BMC Biotechnol.* **6**, 1–10 (2006).

131. Cavazzana-Calvo, M. *et al.* Transfusion independence and HMGA2 activation after gene therapy of human β-thalassaemia. *Nature* **467**, 318–322 (2010).

132. Cartier, N. *et al.* Hematopoietic Stem Cell Gene Therapy with a Lentiviral Vector in X-Linked Adrenoleukodystrophy. *Science (80-. ).* **326**, 818–823 (2009).

133. Sessa, M. *et al.* Lentiviral haemopoietic stem-cell gene therapy in early-onset metachromatic leukodystrophy: an ad-hoc analysis of a non-randomised, open-label, phase 1/2 trial. *Lancet* **388**, 476–487 (2016).

134. Biffi, A. *et al.* Lentiviral Hematopoietic Stem Cell Gene Therapy Benefits Metachromatic Leukodystrophy. *Science (80-. ).* **341**, 1233158 (2013).

135. Takahashi, Y. *et al.* Visualization and in vivo tracking of the exosomes of murine melanoma B16-BL6 cells in mice after intravenous injection. *J. Biotechnol.* **165**, 77–84 (2013).

136. Lai, C. P. *et al.* Dynamic biodistribution of extracellular vesicles in vivo using a multimodal imaging reporter. *ACS Nano* **8**, 483–494 (2014).

137. Charoenviriyakul, C. *et al.* Cell type-specific and common characteristics of exosomes derived from mouse cell lines: Yield, physicochemical properties, and pharmacokinetics. *Eur. J. Pharm. Sci.* **96**, 316–322 (2017).

138. Dychter, S. S., Gold, D. A., Carson, D. & Haller, M. Intravenous Therapy. *J. Infus. Nurs.* **35**, 84–91 (2012).

139. Mazzaferro, E. M. Complications of Fluid Therapy. *Vet. Clin. North Am. Small Anim. Pract.* **38**, 607–619 (2008).

140. Cheng, Y., Zeng, Q., Han, Q. & Xia, W. Effect of pH, temperature and freezing-thawing on quantity changes and cellular uptake of exosomes. *Protein Cell* **10**, 295–299 (2019).

141. Bosch, S. *et al.* Trehalose prevents aggregation of exosomes and cryodamage. *Sci. Rep.* **6**, 36162 (2016).

142. Gardiner, C. *et al.* Measurement of refractive index by nanoparticle tracking analysis reveals heterogeneity in extracellular vesicles. *J. Extracell. Vesicles* **3**, 25361 (2014).

143. Hill, A. F. *et al.* ISEV position paper: extracellular vesicle RNA analysis and bioinformatics. *J. Extracell. Vesicles* **2**, 22859 (2013).

144. Kim, J.-Y., Grunke, S. D., Levites, Y., Golde, T. E. & Jankowsky, J. L. Intracerebroventricular Viral Injection of the Neonatal Mouse Brain for Persistent and Widespread Neuronal Transduction. *J. Vis. Exp.* 51863

(2014).

145. Gombash Lampe, S. E., Kaspar, B. K. & Foust, K. D. Intravenous injections in neonatal mice. *J. Vis. Exp.* e52037 (2014).

146. Walter, J., You, Q., Hagstrom, J. N., Sands, M. & High, K. A. Successful expression of human factor IX following repeat administration of adenoviral vector in mice. *Proc. Natl. Acad. Sci.* **93**, 3056–3061 (1996).

147. Lötvall, J. *et al.* Minimal experimental requirements for definition of extracellular vesicles and their functions: a position statement from the International Society for Extracellular Vesicles. *J. Extracell. Vesicles* **3**, 26913 (2014).

148. Gardiner, C. *et al.* Techniques used for the isolation and characterization of extracellular vesicles: Results of a worldwide survey. *J. Extracell. Vesicles* **5**, (2016).

149. Konoshenko, M. Y., Lekchnov, E. A., Vlassov, A. V. & Laktionov, P. P. Isolation of Extracellular Vesicles: General Methodologies and Latest Trends. *Biomed Res. Int.* **2018**, 1–27 (2018).

150. Li, P., Kaslan, M., Lee, S. H., Yao, J. & Gao, Z. Progress in exosome isolation techniques. *Theranostics* **7**, 789–804 (2017).

151. Momen-Heravi, F. *et al.* Current methods for the isolation of extracellular vesicles. *Biol. Chem.* **394**, 1253–1262 (2013).

152. Jeppesen, D. K. *et al.* Comparative analysis of discrete exosome fractions obtained by differential centrifugation. *J. Extracell. Vesicles* **3**, 25011 (2014).

153. Théry, C., Clayton, A., Amigorena, S., Raposo, G. & Clayton, A. Isolation and Characterization of Exosomes from Cell Culture Supernatants and Biological Fluids. *Curr. Protoc. Cell Biol.* **Chapter 3**, 1–29 (2006).

154. Cantin, R., Diou, J., Bélanger, D., Tremblay, A. M. & Gilbert, C. Discrimination between exosomes and HIV-1: Purification of both vesicles from cell-free supernatants. *J. Immunol. Methods* **338**, 21–30 (2008).

155. Kamerkar, S. *et al.* Exosomes facilitate therapeutic targeting of oncogenic KRAS in pancreatic cancer. *Nature* **546**, 498–503 (2017).

156. Cheruvanky, A. *et al.* Rapid isolation of urinary exosomal biomarkers using a nanomembrane ultrafiltration concentrator. *Am. J. Physiol. Physiol.* **292**, F1657–F1661 (2007).

157. Vergauwen, G. *et al.* Confounding factors of ultrafiltration and protein analysis in extracellular vesicle research. *Sci. Rep.* **7**, 2704 (2017).

158. Böing, A. N. *et al.* Single-step isolation of extracellular vesicles by size-exclusion chromatography. *J. Extracell. Vesicles* **3**, 23430 (2014).

159. Taylor, D. D., Lyons, K. S. & Gerçel-Taylor, Ç. Shed Membrane Fragment-Associated Markers for Endometrial and Ovarian Cancers. *Gynecol. Oncol.* **84**, 443–448 (2002).

160. Konadu, K. A. *et al.* Isolation of Exosomes from the Plasma of HIV-1 Positive Individuals. *J. Vis. Exp.* 53495 (2016).

161. Tauro, B. J. *et al.* Comparison of ultracentrifugation, density gradient separation, and immunoaffinity capture methods for isolating human colon cancer cell line LIM1863-derived exosomes. *Methods* **56**, 293–304 (2012).

162. Shih, C.-L. *et al.* Development of a magnetic bead-based method for the collection of circulating extracellular vesicles. *N. Biotechnol.* **33**, 116–122 (2016).

163. Alvarez, M. L., Khosroheidari, M., Kanchi Ravi, R. & DiStefano, J. K. Comparison of protein, microRNA, and mRNA yields using different methods of urinary exosome isolation for the discovery of kidney disease biomarkers. *Kidney Int.* **82**, 1024–1032 (2012).

164. Taylor, D. D., Zacharias, W. & Gercel-Taylor, C. Exosome Isolation for Proteomic Analyses and RNA Profiling. in *Methods in Molecular Biology* 235–246 (2011).

165. Kanwar, S. S., Dunlay, C. J., Simeone, D. M. & Nagrath, S. Microfluidic device (ExoChip) for on-chip isolation, quantification and characterization of circulating exosomes. *Lab Chip* **14**, 1891–1900 (2014).

166. Yang, D. *et al.* Progress, opportunity, and perspective on exosome isolation - efforts for efficient exosome-based theranostics. *Theranostics* **10**, 3684–3707 (2020).

167. Taylor, D. D. & Shah, S. Methods of isolating extracellular vesicles impact down-stream analyses of their cargoes. *Methods* **87**, 3–10 (2015).

168. Momen-Heravi, F. *et al.* Impact of biofluid viscosity on size and sedimentation efficiency of the isolated microvesicles. *Front. Physiol.* **3**, 162 (2012).

169. Livshts, M. A. *et al.* Isolation of exosomes by differential centrifugation: Theoretical analysis of a commonly used protocol. *Sci. Rep.* **5**, 1–13 (2015).

170. Cvjetkovic, A., Lötvall, J. & Lässer, C. The influence of rotor type and centrifugation time on the yield and purity of extracellular vesicles. *J. Extracell. Vesicles* **3**, 23111 (2014).

171. Tauro, B. J. *et al.* Comparison of ultracentrifugation, density gradient separation, and immunoaffinity capture methods for isolating human colon cancer cell line LIM1863-derived exosomes. *Methods* **56**, 293–304 (2012).

172. Pospichalova, V. *et al.* Simplified protocol for flow cytometry analysis of

fluorescently labeled exosomes and microvesicles using dedicated flow cytometer. *J. Extracell. Vesicles* **4**, 25530 (2015).

173. Greening, D. W., Xu, R., Ji, H., Tauro, B. J. & Simpson, R. J. A Protocol for Exosome Isolation and Characterization: Evaluation of Ultracentrifugation, Density-Gradient Separation, and Immunoaffinity Capture Methods. in *Methods in Molecular Biology* 179–209 (2015).

174. Jeppesen, D. K. *et al.* Comparative analysis of discrete exosome fractions obtained by differential centrifugation. *J. Extracell. vesicles* **3**, 25011 (2014).

175. Xu, R., Greening, D. W., Zhu, H.-J., Takahashi, N. & Simpson, R. J. Extracellular vesicle isolation and characterization: toward clinical application. *J. Clin. Invest.* **126**, 1152–1162 (2016).

176. Shelke, G. V., Lässer, C., Gho, Y. S. & Lötvall, J. Importance of exosome depletion protocols to eliminate functional and RNA-containing extracellular vesicles from fetal bovine serum. *J. Extracell. Vesicles* **3**, 24783 (2014).

177. Momen-Heravi, F. Isolation of Extracellular Vesicles by Ultracentrifugation. *Methods Mol. Biol.* (2017). doi:10.1007/978-1-4939-7253-1_3

178. Lässer, C., Eldh, M. & Lötvall, J. Isolation and Characterization of RNA-Containing Exosomes. *J. Vis. Exp.* 1–6 (2012). doi:10.3791/3037

179. Rhee, W. J. & Jeong, S. Extracellular Vesicle miRNA Detection Using Molecular Beacons. *Methods Mol. Biol.* (2017). doi:10.1007/978-1-4939-7253-1_23

180. Luan, X. *et al.* Engineering exosomes as refined biological nanoplatforms for drug delivery. *Acta Pharmacol. Sin.* **38**, 754–763 (2017).

181. Kim, S.-M. & Kim, H.-S. Engineering of extracellular vesicles as drug delivery vehicles. *Stem Cell Investig.* **4**, 74–74 (2017).

182. Halder, C. V. F., Fonseca, E. M. B., Faria, A. V. de S. & Clerici, S. P. Extracellular vesicles as a recipe for design smart drug delivery systems for cancer therapy. in *Drug Targeting and Stimuli Sensitive Drug Delivery Systems* 411–445 (Elsevier, 2018).

183. Sun, D. *et al.* A novel nanoparticle drug delivery system: The anti-inflammatory activity of curcumin is enhanced when encapsulated in exosomes. *Mol. Ther.* **18**, 1606–1614 (2010).

184. Saari, H. *et al.* Microvesicle- and exosome-mediated drug delivery enhances the cytotoxicity of Paclitaxel in autologous prostate cancer cells. *J. Control. Release* **220**, 727–737 (2015).

185. Luan, X. *et al.* Engineering exosomes as refined biological nanoplatforms for drug delivery. *Acta Pharmacol. Sin.* **38**, 754–763 (2017).

186. Wahlgren, J. *et al.* Plasma exosomes can deliver exogenous short interfering RNA to monocytes and lymphocytes. *Nucleic Acids Res.* **40**, (2012).

187. Didiot, M.-C. *et al.* Exosome-mediated Delivery of Hydrophobically Modified siRNA for Huntingtin mRNA Silencing. *Mol. Ther.* **24**, 1836–1847 (2016).

188. Kooijmans, S. A. A. *et al.* Electroporation-induced siRNA precipitation obscures the efficiency of siRNA loading into extracellular vesicles. *J. Control. Release* **172**, 229–238 (2013).

189. El-Andaloussi, S. *et al.* Exosome-mediated delivery of siRNA in vitro and in vivo. *Nat. Protoc.* **7**, 2112–2126 (2012).

190. Katakowski, M. *et al.* Exosomes from marrow stromal cells expressing miR-146b inhibit glioma growth. *Cancer Lett.* **335**, 201–204 (2013).

191. Ohno, S. *et al.* Systemically Injected Exosomes Targeted to EGFR Deliver Antitumor MicroRNA to Breast Cancer Cells. *Mol. Ther.* **21**, 185–191 (2013).

192. Hikita, T., Miyata, M., Watanabe, R. & Oneyama, C. Sensitive and rapid quantification of exosomes by fusing luciferase to exosome marker proteins. *Sci. Rep.* **8**, 1–14 (2018).

193. Jeppesen, D. K. *et al.* Reassessment of Exosome Composition. *Cell* **177**, 428-445.e18 (2019).

194. Kooijmans, S. A. A. *et al.* Display of GPI-anchored anti-EGFR nanobodies on extracellular vesicles promotes tumour cell targeting. *J. Extracell. Vesicles* **5**, 31053 (2016).

195. Wang, N., Rajasekaran, N., Hou, T., Lisowski, L. & Mellins, E. D. Comparison of transduction efficiency among various lentiviruses containing GFP reporter in bone marrow hematopoietic stem cell transplantation. *Exp. Hematol.* **41**, 934–943 (2013).

196. Zufferey, R., Donello, J. E., Trono, D. & Hope, T. J. Woodchuck Hepatitis Virus Posttranscriptional Regulatory Element Enhances Expression of Transgenes Delivered by Retroviral Vectors. *J. Virol.* **73**, 2886–2892 (1999).

197. Kaur, G. & Dufour, J. M. Cell lines. *Spermatogenesis* **2**, 1–5 (2012).

198. Li, J. *et al.* Identification and Characterization of 293T Cell-Derived Exosomes by Profiling the Protein, mRNA and MicroRNA Components. *PLoS One* **11**, e0163043 (2016).

199. Ohno, S. I. *et al.* Systemically injected exosomes targeted to EGFR deliver antitumor microrna to breast cancer cells. *Mol. Ther.* **21**, 185–191 (2013).

200. McDonald, M. K. *et al.* Functional significance of macrophage-derived exosomes in inflammation and pain. *Pain* **155**, 1527–1539 (2014).

201. Osada-Oka, M. *et al.* Macrophage-derived exosomes induce inflammatory factors in endothelial cells under hypertensive conditions. *Hypertens. Res.* **40**, 353–360 (2017).

202. Szatanek, R., Baran, J., Siedlar, M. & Baj-Krzyworzeka, M. Isolation of extracellular vesicles: Determining the correct approach (review). *Int. J. Mol. Med.* **36**, 11–17 (2015).

203. Fang, C.-Y., Wu, C.-C., Fang, C.-L., Chen, W.-Y. & Chen, C.-L. Long-term growth comparison studies of FBS and FBS alternatives in six head and neck cell lines. *PLoS One* **12**, e0178960 (2017).

204. Sokolova, V. *et al.* Characterisation of exosomes derived from human cells by nanoparticle tracking analysis and scanning electron microscopy. *Colloids Surfaces B Biointerfaces* **87**, 146–150 (2011).

205. Wright, M. Nanoparticle tracking analysis for the multiparameter characterization and counting of nanoparticle suspensions. *Methods Mol. Biol.* (2012). doi:10.1007/978-1-61779-953-2_41

206. Webber, J. & Clayton, A. How pure are your vesicles? *J. Extracell. Vesicles* **2**, 19861 (2013).

207. Jung, M. K. & Mun, J. Y. Sample Preparation and Imaging of Exosomes by Transmission Electron Microscopy. *J. Vis. Exp.* (2018).

208. Choi, H. & Mun, J. Y. Structural Analysis of Exosomes Using Different Types of Electron Microscopy. *Appl. Microsc.* **47**, 171–175 (2017).

209. Chernyshev, V. S. *et al.* Size and shape characterization of hydrated and desiccated exosomes. *Anal. Bioanal. Chem.* **407**, 3285–3301 (2015).

210. Emelyanov, A. *et al.* Cryo-electron microscopy of extracellular vesicles from cerebrospinal fluid. *PLoS One* **15**, e0227949 (2020).

211. Cizmar, P. & Yuana, Y. Detection and Characterization of Extracellular Vesicles by Transmission and Cryo-Transmission Electron Microscopy. in *Methods in molecular biology (Clifton, N.J.)* 221–232 (2017).

212. Harris, V. M. Protein Detection by Simple Western™ Analysis. in *Western Blotting: Methods and Protocols* 465–468 (2015).

213. Nguyen, U., Squaglia, N., Boge, A. & Fung, P. A. The Simple Western™: a gel-free, blot-free, hands-free Western blotting reinvention. *Nat. Methods* **8**, v–vi (2011).

214. Montecalvo, A. *et al.* Mechanism of transfer of functional microRNAs between mouse dendritic cells via exosomes. *Blood* **119**, 756–766 (2012).

215. Skog, J. *et al.* Glioblastoma microvesicles transport RNA and proteins that promote tumour growth and provide diagnostic biomarkers. *Nat. Cell Biol.* **10**, 1470–1476 (2008).

216. Ibrahim, A. G.-E., Cheng, K. & Marbán, E. Exosomes as Critical

Agents of Cardiac Regeneration Triggered by Cell Therapy. *Stem Cell Reports* **2**, 606–619 (2014).

217. Geiger, A., Walker, A. & Nissen, E. Human fibrocyte-derived exosomes accelerate wound healing in genetically diabetic mice. *Biochem. Biophys. Res. Commun.* **467**, 303–309 (2015).

218. Costa Verdera, H., Gitz-Francois, J. J., Schiffelers, R. M. & Vader, P. Cellular uptake of extracellular vesicles is mediated by clathrin-independent endocytosis and macropinocytosis. *J. Control. Release* **266**, 100–108 (2017).

219. Tian, T., Wang, Y., Wang, H., Zhu, Z. & Xiao, Z. Visualizing of the cellular uptake and intracellular trafficking of exosomes by live-cell microscopy. *J. Cell. Biochem.* **111**, 488–496 (2010).

220. Smyth, T. *et al.* Biodistribution and delivery efficiency of unmodified tumor-derived exosomes. *J. Control. Release* **199**, 145–155 (2015).

221. Rashid, M. H. *et al.* Differential in vivo biodistribution of 131I-labeled exosomes from diverse cellular origins and its implication for theranostic application. *Nanomedicine Nanotechnology, Biol. Med.* **21**, 102072 (2019).

222. Yi, Y. W. *et al.* Advances in Analysis of Biodistribution of Exosomes by Molecular Imaging. *Int. J. Mol. Sci.* **21**, 665 (2020).

223. Christianson, H. C., Svensson, K. J., van Kuppevelt, T. H., Li, J.-P. & Belting, M. Cancer cell exosomes depend on cell-surface heparan sulfate proteoglycans for their internalization and functional activity. *Proc. Natl. Acad. Sci.* **110**, 17380–17385 (2013).

224. Escrevente, C., Keller, S., Altevogt, P. & Costa, J. Interaction and uptake of exosomes by ovarian cancer cells. *BMC Cancer* **11**, 108 (2011).

225. Mulcahy, L. A., Pink, R. C. & Carter, D. R. F. Routes and mechanisms of extracellular vesicle uptake. *J. Extracell. Vesicles* **3**, 24641 (2014).

226. Morelli, A. E. *et al.* Endocytosis, intracellular sorting, and processing of exosomes by dendritic cells. *Blood* **104**, 3257–3266 (2004).

227. Feng, D. *et al.* Cellular Internalization of Exosomes Occurs Through Phagocytosis. *Traffic* **11**, 675–687 (2010).

228. Fitzner, D. *et al.* Selective transfer of exosomes from oligodendrocytes to microglia by macropinocytosis. *J. Cell Sci.* **124**, 447–458 (2011).

229. Tian, T. *et al.* Exosome Uptake through Clathrin-mediated Endocytosis and Macropinocytosis and Mediating miR-21 Delivery. *J. Biol. Chem.* **289**, 22258–22267 (2014).

230. Parolini, I. *et al.* Microenvironmental pH Is a Key Factor for Exosome Traffic in Tumor Cells. *J. Biol. Chem.* **284**, 34211–34222 (2009).

231. Rana, S., Yue, S., Stadel, D. & Zöller, M. Toward tailored exosomes:

The exosomal tetraspanin web contributes to target cell selection. *Int. J. Biochem. Cell Biol.* **44**, 1574–1584 (2012).

232. Franzen, C. A. *et al.* Characterization of Uptake and Internalization of Exosomes by Bladder Cancer Cells. *Biomed Res. Int.* **2014**, 1–11 (2014).

233. Gangadaran, P. *et al.* A new bioluminescent reporter system to study the biodistribution of systematically injected tumor-derived bioluminescent extracellular vesicles in mice. *Oncotarget* **8**, 109894–109914 (2017).

234. Imai, T. *et al.* Macrophage-dependent clearance of systemically administered B16BL6-derived exosomes from the blood circulation in mice. *J. Extracell. Vesicles* **4**, 1–8 (2015).

235. GRANGE, C. *et al.* Biodistribution of mesenchymal stem cell-derived extracellular vesicles in a model of acute kidney injury monitored by optical imaging. *Int. J. Mol. Med.* **33**, 1055–1063 (2014).

236. Di Rocco, G., Baldari, S. & Toietta, G. Towards Therapeutic Delivery of Extracellular Vesicles: Strategies for In Vivo Tracking and Biodistribution Analysis. *Stem Cells Int.* **2016**, 1–12 (2016).

237. Liu, Y. *et al.* Targeted exosome-mediated delivery of opioid receptor Mu siRNA for the treatment of morphine relapse. *Sci. Rep.* **5**, 17543 (2015).

238. Lai, C. P. *et al.* Visualization and tracking of tumour extracellular vesicle delivery and RNA translation using multiplexed reporters. *Nat. Commun.* **6**, 1–12 (2015).

239. Peinado, H. *et al.* Melanoma exosomes educate bone marrow progenitor cells toward a pro-metastatic phenotype through MET. *Nat. Med.* **18**, 883–891 (2012).

240. Chen, C. C. *et al.* Elucidation of Exosome Migration Across the Blood–Brain Barrier Model In Vitro. *Cell. Mol. Bioeng.* **9**, 509–529 (2016).

241. Pardridge, W. M. The blood-brain barrier: Bottleneck in brain drug development. *NeuroRX* **2**, 3–14 (2005).

242. Yuan, D. *et al.* Macrophage exosomes as natural nanocarriers for protein delivery to inflamed brain. *Biomaterials* **142**, 1–12 (2017).

243. El-Andaloussi, S. *et al.* Exosome-mediated delivery of siRNA in vitro and in vivo. *Nat. Protoc.* **7**, 2112–2126 (2012).

244. Pardridge, W. M. Drug Transport across the Blood–Brain Barrier. *J. Cereb. Blood Flow Metab.* **32**, 1959–1972 (2012).

245. Daneman, R. & Prat, A. The Blood–Brain Barrier. *Cold Spring Harb. Perspect. Biol.* **7**, a020412 (2015).

246. Zhou, Y., Peng, Z., Seven, E. S. & Leblanc, R. M. Crossing the blood-brain barrier with nanoparticles. *J. Control. Release* **270**, 290–303

(2018).

247. Thomi *et al.* Intranasally Administered Exosomes from Umbilical Cord Stem Cells Have Preventive Neuroprotective Effects and Contribute to Functional Recovery after Perinatal Brain Injury. *Cells* **8**, 855 (2019).

248. Guo, S. *et al.* Intranasal Delivery of Mesenchymal Stem Cell Derived Exosomes Loaded with Phosphatase and Tensin Homolog siRNA Repairs Complete Spinal Cord Injury. *ACS Nano* **13**, 10015–10028 (2019).

249. Long, Q. *et al.* Intranasal MSC-derived A1-exosomes ease inflammation, and prevent abnormal neurogenesis and memory dysfunction after status epilepticus. *Proc. Natl. Acad. Sci.* **114**, E3536–E3545 (2017).

250. Kodali, M. *et al.* Intranasally Administered Human MSC-Derived Extracellular Vesicles Pervasively Incorporate into Neurons and Microglia in both Intact and Status Epilepticus Injured Forebrain. *Int. J. Mol. Sci.* **21**, 181 (2019).

251. Illum, L. Transport of drugs from the nasal cavity to the central nervous system. *Eur. J. Pharm. Sci.* **11**, 1–18 (2000).

252. Richards, P. M., Saunders, C. J. & Silver, W. L. Functional neuroanatomy of the upper airway in experimental animals. in *Toxicology of the Nose and Upper Airways* (2016).

253. Labiris, N. R. & Dolovich, M. B. Pulmonary drug delivery. Part I: Physiological factors affecting therapeutic effectiveness of aerosolized medications. *Br. J. Clin. Pharmacol.* **56**, 588–599 (2003).

254. Imai, T. *et al.* Macrophage-dependent clearance of systemically administered B16BL6-derived exosomes from the blood circulation in mice. *J. Extracell. Vesicles* (2015). doi:10.3402/jev.v4.26238

255. Hazan-Halevy, I. *et al.* Cell-specific uptake of mantle cell lymphoma-derived exosomes by malignant and non-malignant B-lymphocytes. *Cancer Lett.* **364**, 59–69 (2015).

256. Hood, J. L., San, R. S. & Wickline, S. A. Exosomes Released by Melanoma Cells Prepare Sentinel Lymph Nodes for Tumor Metastasis. *Cancer Res.* **71**, 3792–3801 (2011).

257. Tran, P. H. L. *et al.* Development of a nanoamorphous exosomal delivery system as an effective biological platform for improved encapsulation of hydrophobic drugs. *Int. J. Pharm.* **566**, 697–707 (2019).

258. Fuhrmann, G., Herrmann, I. K. & Stevens, M. M. Cell-derived vesicles for drug therapy and diagnostics: Opportunities and challenges. *Nano Today* **10**, 397–409 (2015).

259. Denzer, K. *et al.* Follicular Dendritic Cells Carry MHC Class II-Expressing Microvesicles at Their Surface. *J. Immunol.* **165**, 1259–1265 (2000).

260. Clayton, A. *et al.* Adhesion and signaling by B cell-derived exosomes: the role of integrins. *FASEB J.* **18**, 977–979 (2004).

261. Atay, S., Gercel-Taylor, C. & Taylor, D. D. Human Trophoblast-Derived Exosomal Fibronectin Induces Pro-Inflammatory Il-1β Production by Macrophages. *Am. J. Reprod. Immunol.* **66**, 259–269 (2011).

262. Delcayre, A. *et al.* Exosome Display technology: Applications to the development of new diagnostics and therapeutics. *Blood Cells, Mol. Dis.* **35**, 158–168 (2005).

263. Hartman, Z. C. *et al.* Increasing vaccine potency through exosome antigen targeting. *Vaccine* **29**, 9361–9367 (2011).

264. Rountree, R. B. *et al.* Exosome Targeting of Tumor Antigens Expressed by Cancer Vaccines Can Improve Antigen Immunogenicity and Therapeutic Efficacy. *Cancer Res.* **71**, 5235–5244 (2011).

265. Véron, P., Segura, E., Sugano, G., Amigorena, S. & Théry, C. Accumulation of MFG-E8/lactadherin on exosomes from immature dendritic cells. *Blood Cells, Mol. Dis.* **35**, 81–88 (2005).

266. Bliss, C. M. *et al.* Targeting Antigen to the Surface of EVs Improves the In Vivo Immunogenicity of Human and Non-human Adenoviral Vaccines in Mice. *Mol. Ther. - Methods Clin. Dev.* **16**, 108–125 (2020).

267. Srivastava, A., Quinn-Allen, M. A., Kim, S. W., Kane, W. H. & Lentz, B. R. Soluble Phosphatidylserine Binds to a Single Identified Site in the C2 Domain of Human Factor V a †. *Biochemistry* **40**, 8246–8255 (2001).

268. Pratt, K. P. *et al.* Structure of the C2 domain of human factor VIII at 1.5 Å resolution. *Nature* **402**, 439–442 (1999).

269. Shi, J., Heegaard, C. W., Rasmussen, J. T. & Gilbert, G. E. Lactadherin binds selectively to membranes containing phosphatidyl-l-serine and increased curvature. *Biochim. Biophys. Acta - Biomembr.* **1667**, 82–90 (2004).

270. Van Dongen, H. M., Masoumi, N., Witwer, K. W. & Pegtel, D. M. Extracellular Vesicles Exploit Viral Entry Routes for Cargo Delivery. *Microbiol. Mol. Biol. Rev.* **80**, 369–386 (2016).

271. Meyer, C. *et al.* Pseudotyping exosomes for enhanced protein delivery in mammalian cells. *Int. J. Nanomedicine* **Volume 12**, 3153–3170 (2017).

272. Moreno-Gonzalo, O., Fernandez-Delgado, I. & Sanchez-Madrid, F. Post-translational add-ons mark the path in exosomal protein sorting. *Cell. Mol. Life Sci.* **75**, 1–19 (2018).

273. Metcalf, D. & Isaacs, A. M. The role of ESCRT proteins in fusion events involving lysosomes, endosomes and autophagosomes. *Biochem. Soc. Trans.* **38**, 1469–1473 (2010).

274. Cheng, Y. & Schorey, J. S. Targeting soluble proteins to exosomes

using a ubiquitin tag. *Biotechnol. Bioeng.* **113**, 1315–1324 (2016).

275. Buschow, S. I., Liefhebber, J. M. P., Wubbolts, R. & Stoorvogel, W. Exosomes contain ubiquitinated proteins. *Blood Cells, Mol. Dis.* **35**, 398–403 (2005).

276. Smith, V. L., Jackson, L. & Schorey, J. S. Ubiquitination as a Mechanism To Transport Soluble Mycobacterial and Eukaryotic Proteins to Exosomes. *J. Immunol.* **195**, 2722–2730 (2015).

277. Zuccato, E. *et al.* Sorting of Fas ligand to secretory lysosomes is regulated by mono-ubiquitylation and phosphorylation. *J. Cell Sci.* **120**, 191–199 (2006).

278. Buschow, S. I., Liefhebber, J. M. P., Wubbolts, R. & Stoorvogel, W. Exosomes contain ubiquitinated proteins. *Blood Cells, Mol. Dis.* **35**, 398–403 (2005).

279. Burke, M. C., Oei, M. S., Edwards, N. J., Ostrand-Rosenberg, S. & Fenselau, C. Ubiquitinated Proteins in Exosomes Secreted by Myeloid-Derived Suppressor Cells. *J. Proteome Res.* **13**, 5965–5972 (2014).

280. Ha, D., Yang, N. & Nadithe, V. Exosomes as therapeutic drug carriers and delivery vehicles across biological membranes: current perspectives and future challenges. *Acta Pharm. Sin. B* **6**, 287–296 (2016).

281. Gomari, H., Forouzandeh Moghadam, M. & Soleimani, M. Targeted cancer therapy using engineered exosome as a natural drug delivery vehicle. *Onco. Targets. Ther.* **11**, 5753–5762 (2018).

282. Batrakova, E. V. & Kim, M. S. Using exosomes, naturally-equipped nanocarriers, for drug delivery. *J. Control. Release* **219**, 396–405 (2015).

283. Witwer, K. W. *et al.* Standardization of sample collection, isolation and analysis methods in extracellular vesicle research. *J. Extracell. Vesicles* **2**, 1–25 (2013).

284. Jeyaram, A. & Jay, S. M. Preservation and Storage Stability of Extracellular Vesicles for Therapeutic Applications. *AAPS J.* **20**, 1 (2018).

285. Lőrincz, Á. M. *et al.* Effect of storage on physical and functional properties of extracellular vesicles derived from neutrophilic granulocytes. *J. Extracell. Vesicles* **3**, 25465 (2014).

286. Kreke, M., Smith, R., HANSCOME, P., PECK, K. & Ibrahim, A. Processes for producing stable exosome formulations. *Google Patent* (2014).

287. Wang, W. Lyophilization and development of solid protein pharmaceuticals. *Int. J. Pharm.* **203**, 1–60 (2000).

288. Emami, F., Vatanara, A., Park, E. & Na, D. Drying Technologies for the Stability and Bioavailability of Biopharmaceuticals. *Pharmaceutics* **10**,

131 (2018).

289. Roy, I. & Gupta, M. N. Freeze-drying of proteins: some emerging concerns. *Biotechnol. Appl. Biochem.* **39**, 165 (2004).

290. Khairnar, S., Kini, R., Harwalker, M., Slaunkhe, K. & Chaudhari, S. A review on freeze drying process and pharmaceuticals. *Int. J. Res. Pharm. Sci.* **2**, 76–94 (2013).

291. Nail, S. L., Jiang, S., Chongprasert, S. & Knopp, S. A. Fundamentals of Freeze-Drying. in *Pharmaceutical biotechnology* 281–360 (2002).

292. Bahr, M. M., Amer, M. S., Abo-El-Sooud, K., Abdallah, A. N. & El-Tookhy, O. S. Preservation techniques of stem cells extracellular vesicles: a gate for manufacturing of clinical grade therapeutic extracellular vesicles and long-term clinical trials. *Int. J. Vet. Sci. Med.* **8**, 1–8 (2020).

293. Matejtschuk, P. Lyophilization of Proteins. in *Methods in molecular biology (Clifton, N.J.)* 59–72 (2007).

294. Liu, W. R., Langer, R. & Klibanov, A. M. Moisture-induced aggregation of lyophilized proteins in the solid state. *Biotechnol. Bioeng.* **37**, 177–184 (1991).

295. Costantino, H. R., Langer, R. & Klibanov, A. M. Aggregation of a Lyophilized Pharmaceutical Protein, Recombinant Human Albumin: Effect of Moisture and Stabilization by Excipients. *Nat. Biotechnol.* **13**, 493–496 (1995).

296. Charoenviriyakul, C., Takahashi, Y., Nishikawa, M. & Takakura, Y. Preservation of exosomes at room temperature using lyophilization. *Int. J. Pharm.* **553**, 1–7 (2018).

297. Bari, E. *et al.* Pilot Production of Mesenchymal Stem/Stromal Freeze-Dried Secretome for Cell-Free Regenerative Nanomedicine: A Validated GMP-Compliant Process. *Cells* **7**, 190 (2018).

298. Frank, J. *et al.* Extracellular vesicles protect glucuronidase model enzymes during freeze-drying. *Sci. Rep.* **8**, 12377 (2018).

299. El Baradie, K. B. Y. *et al.* Freeze-Dried Extracellular Vesicles From Adipose-Derived Stem Cells Prevent Hypoxia-Induced Muscle Cell Injury. *Front. Cell Dev. Biol.* **8**, (2020).

300. Mensink, M. A., Frijlink, H. W., van der Voort Maarschalk, K. & Hinrichs, W. L. J. How sugars protect proteins in the solid state and during drying (review): Mechanisms of stabilization in relation to stress conditions. *Eur. J. Pharm. Biopharm.* **114**, 288–295 (2017).

301. Jain, N. K. & Roy, I. Effect of trehalose on protein structure. *Protein Sci.* (2008). doi:10.1002/pro.3

302. Lane, R. E., Korbie, D., Trau, M. & Hill, M. M. Purification Protocols for Extracellular Vesicles. in *Methods in molecular biology (Clifton, N.J.)* 111–130 (2017).

303. Nordin, J. Z. *et al.* Ultrafiltration with size-exclusion liquid chromatography for high yield isolation of extracellular vesicles preserving intact biophysical and functional properties. *Nanomedicine Nanotechnology, Biol. Med.* **11**, 879–883 (2015).

304. Maroto, R. *et al.* Effects of storage temperature on airway exosome integrity for diagnostic and functional analyses. *J. Extracell. Vesicles* **6**, 1359478 (2017).

305. Carpenter, J. F., Manning, M. C. & Randolph, T. W. Long-Term Storage of Proteins. *Curr. Protoc. Protein Sci.* **27**, (2002).

306. McGann, L. E. Differing actions of penetrating and nonpenetrating cryoprotective agents. *Cryobiology* **15**, 382–390 (1978).

307. Hood, J. L., Scott, M. J. & Wickline, S. A. Maximizing exosome colloidal stability following electroporation. *Anal. Biochem.* **448**, 41–49 (2014).

308. Date, P. V., Samad, A. & Devarajan, P. V. Freeze Thaw: A Simple Approach for Prediction of Optimal Cryoprotectant for Freeze Drying. *AAPS PharmSciTech* **11**, 304–313 (2010).

309. Manning, M. C., Patel, K. & Borchardt, R. T. Stability of protein pharmaceuticals. *Pharm. Res.* **6**, 903–18 (1989).

310. Bansal, A., Lale, S. & Goyal, M. Development of lyophilization cycle and effect of excipients on the stability of catalase during lyophilization. *Int. J. Pharm. Investig.* **1**, 214 (2011).

311. Sun, A. Lysosomal storage disease overview. *Ann. Transl. Med.* **6**, 476.-476. (2018).

312. Lundstrom, K. Latest development in viral vectors for gene therapy. *Trends Biotechnol.* **21**, 117–122 (2003).

313. Misra, S. Human gene therapy: a brief overview of the genetic revolution. *J. Assoc. Physicians India* **61**, 127–33 (2013).

314. Gonçalves, G. A. R. & Paiva, R. de M. A. Gene therapy: advances, challenges and perspectives. *Einstein (São Paulo)* **15**, 369–375 (2017).

315. Van Haasteren, J., Hyde, S. C. & Gill, D. R. Lessons learned from lung and liver in-vivo gene therapy: implications for the future. *Expert Opin. Biol. Ther.* **18**, 959–972 (2018).

316. Wiklander, O. P. B. *et al.* Systematic Methodological Evaluation of a Multiplex Bead-Based Flow Cytometry Assay for Detection of Extracellular Vesicle Surface Signatures. *Front. Immunol.* **9**, (2018).

317. Johnsen, K. B. *et al.* Evaluation of electroporation-induced adverse effects on adipose-derived stem cell exosomes. *Cytotechnology* **68**, 2125–2138 (2016).

# Appendices

## I. Chapter 3

*Characterisation of naïve EVs from different cell lines*

The size and concentration of EVs from naïve non-transduced HEK293T, THP-1 and BMSCs were measured using the NTA to establish which cell line produced the highest yield of EVs within the size range of 40-150 nm. As can be seen in Fig. 16, the vesicle suspensions are moderately polydisperse with the majority of vesicles derived from BMSC cells being within the size range of EVs, whereas the percentage of vesicles derived from HEK293T cells that is within the size range of EVs is smaller in comparison and it is smallest for veiscles derived from THP-1 cells. It has been noted that this heterogeneity in size distribution between vesicles derived from different cell lines could be a result of several reasons, one being that different cells produce different levels of vesicles that are within the size range of EVs and also the biogenesis of EVs differs to some extent between different cell lines, leading to the production of different sized vesicles [39]. Another reason could be due to the centrifugation purification method not being specific, and the fact that it may allow the debris of other materials to be co-isolated in the process, including extracellular vesicles other than EVs. Moreover, a possible explanation for the larger structures observed is the aggregation of EVs of various phenotypes and morphologies [141].

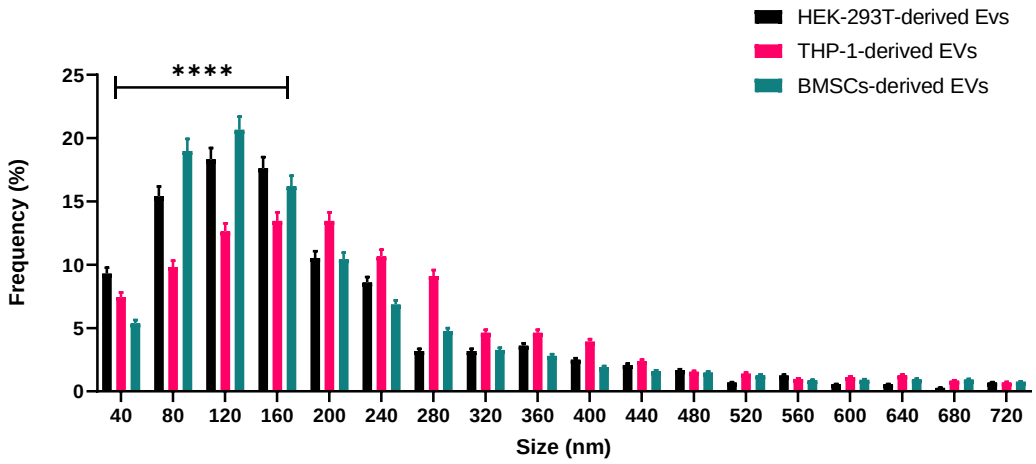


**Figure A.I. 1**: A histogram of size distribution of isolated vesicles derived from HEK293T, THP-1 and BMSCs cells as analysed by NTA. Five independent experiments were performed and results presented as mean ± SD. Statistical analysis: two-way ANOVA, Tukey's multiple test, ****p < 0.0001.

*q-PCR amplification plots*

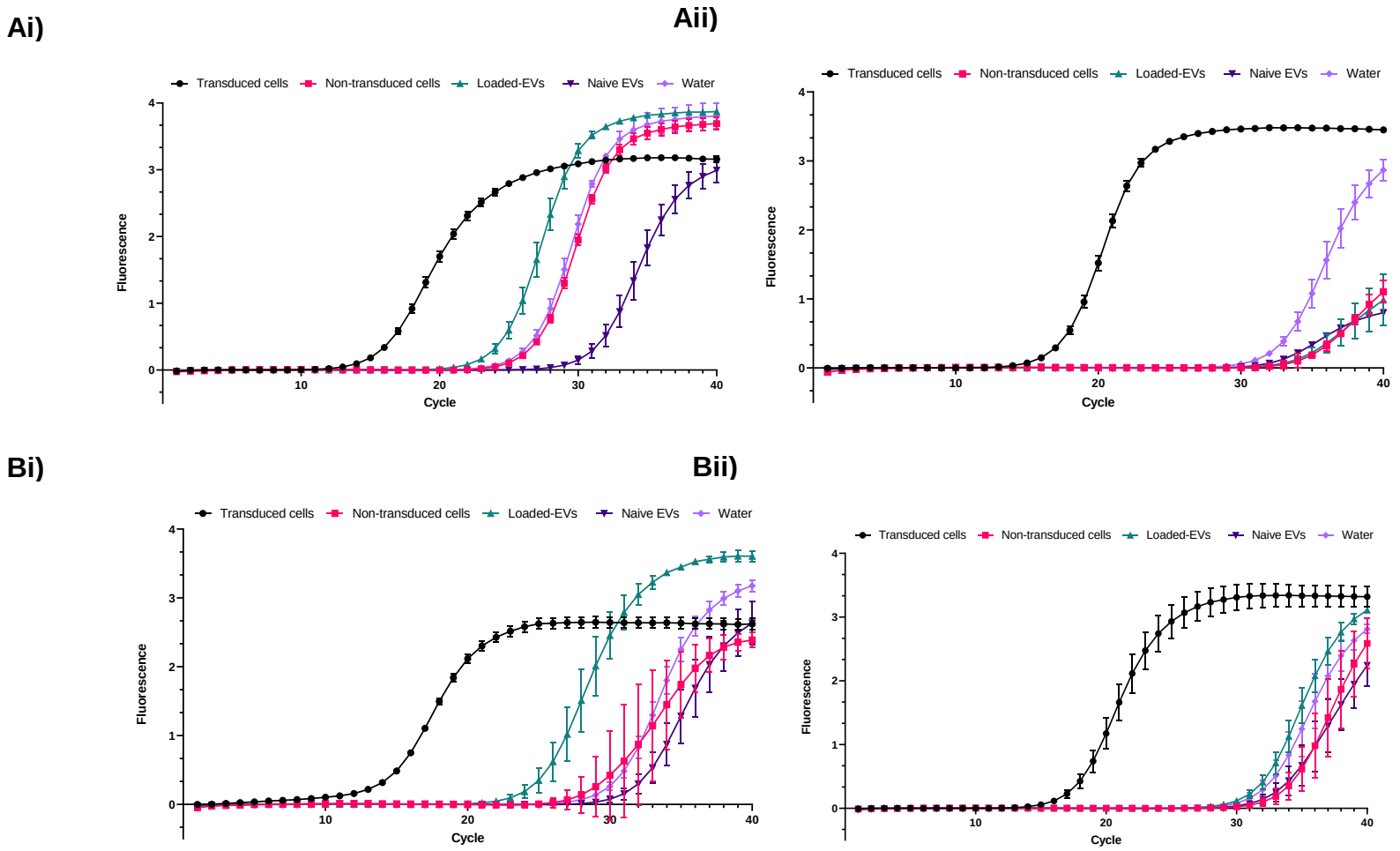


**Figure A.I. 2**: Amplification plots using ai) primer set 1 and large RNA as source, aii) primer set 1 and total RNA as a source, bi) primer set 2 and large RNA as a source, and bii) primer set 2 and total RNA as source, extracted from sorted-transduced and non-transduced HEK293T cells, loaded-EVs, naïve EVs, and water. Three independent experiments were performed and data presented as mean ± SD.

## II.Chapter 7

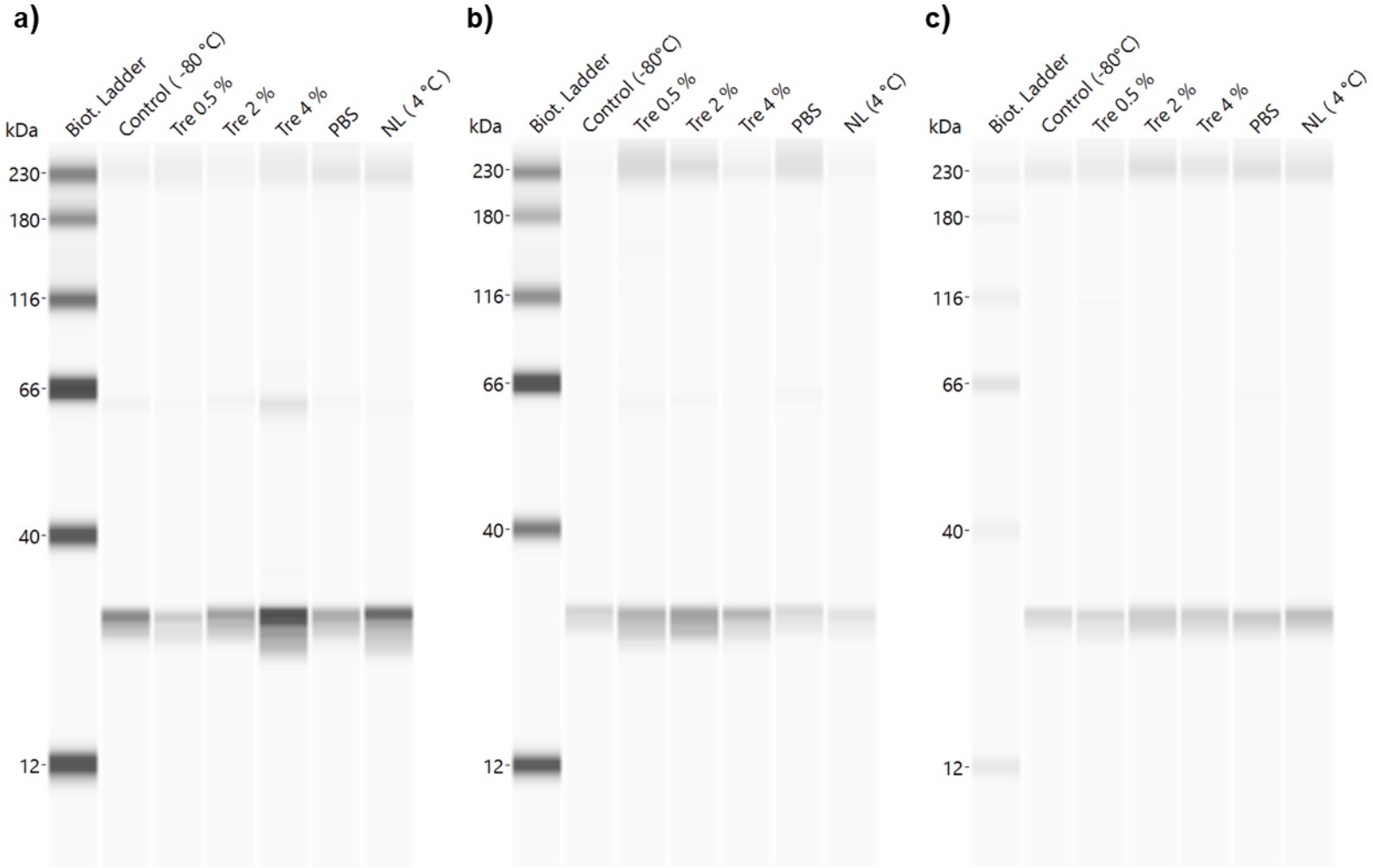


**Figure AII. 1:** Representative western blots obtained by WES for CD9 in different samples of naive HEK293T-derived EVs following storage at -80 °C, 4 °C or lyophilisation with 0.5-4 % of trehalose or without trehalose and storage at 4 °C after a) 1 week b) 2 weeks and c) 4 weeks.

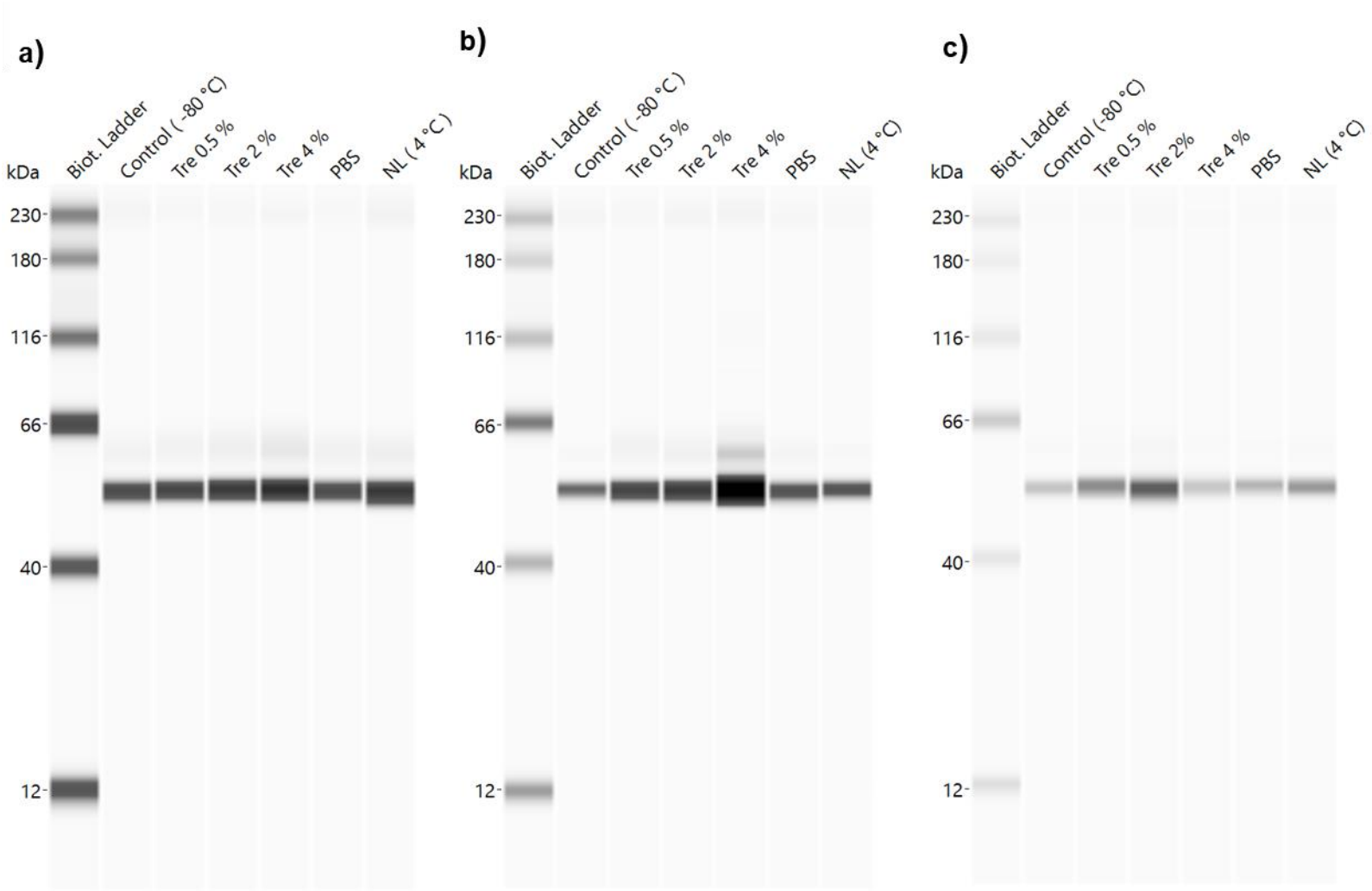


**Figure AII. 2:** Representative western blots as obtained by simple western for the EV surface marker TSG101 in different samples of naive HEK293T-derived EVs following storage at -80 °C, 4 °C or lyophilisation with 0.5-4 % of trehalose or without trehalose and storage at 4 °C after a) 1 week b) 2 weeks and c) 4 weeks.

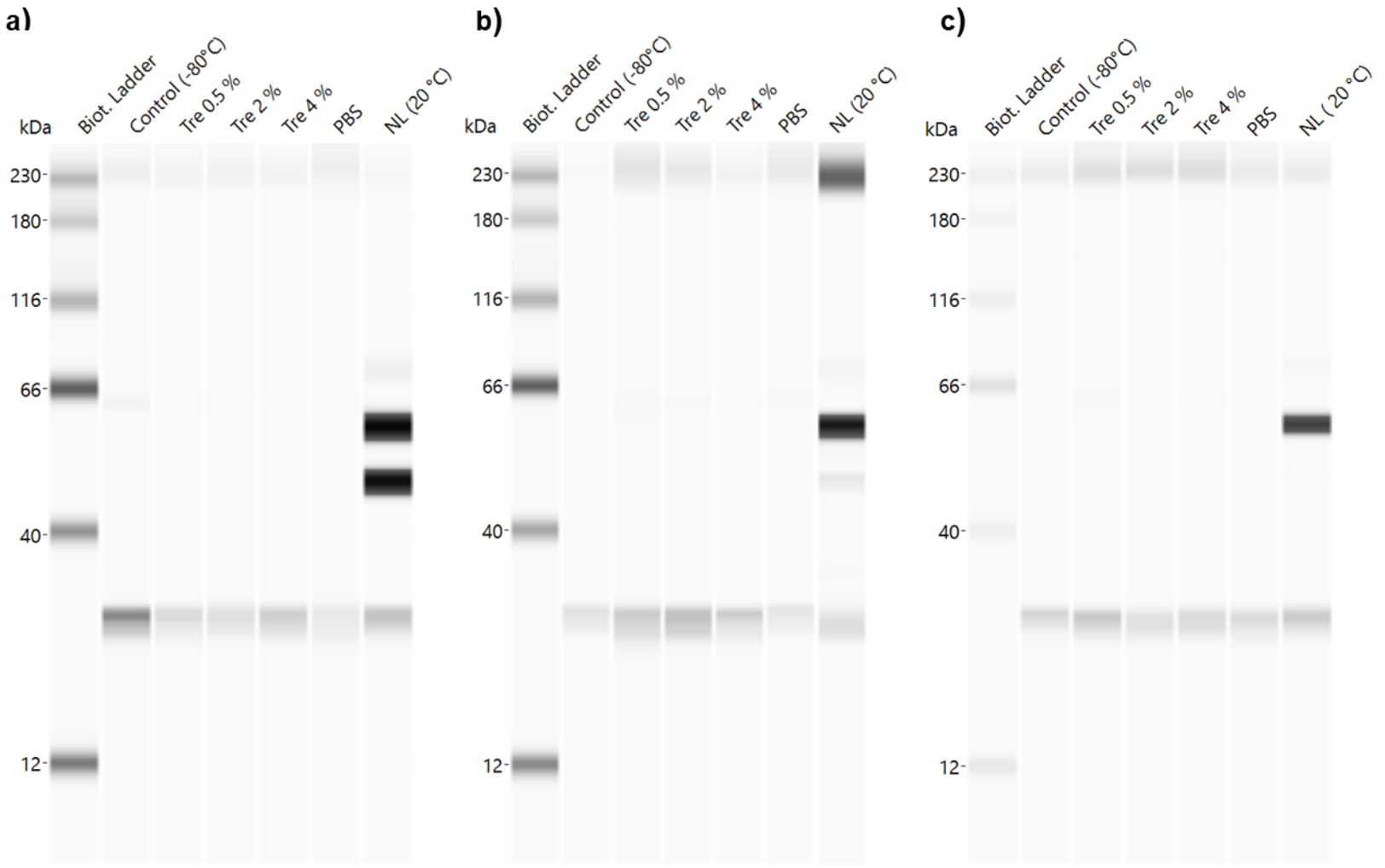


**Figure AII. 3:** Representative western blots as obtained by simple western for the EV surface marker CD9 in different samples of naive HEK293T-derived EVs following storage at -80 °C, 20 °C or lyophilisation with 0.5-4 % of trehalose or without trehalose and storage at 20 °C after a) 1 week b) 2 weeks and c) 4 weeks.

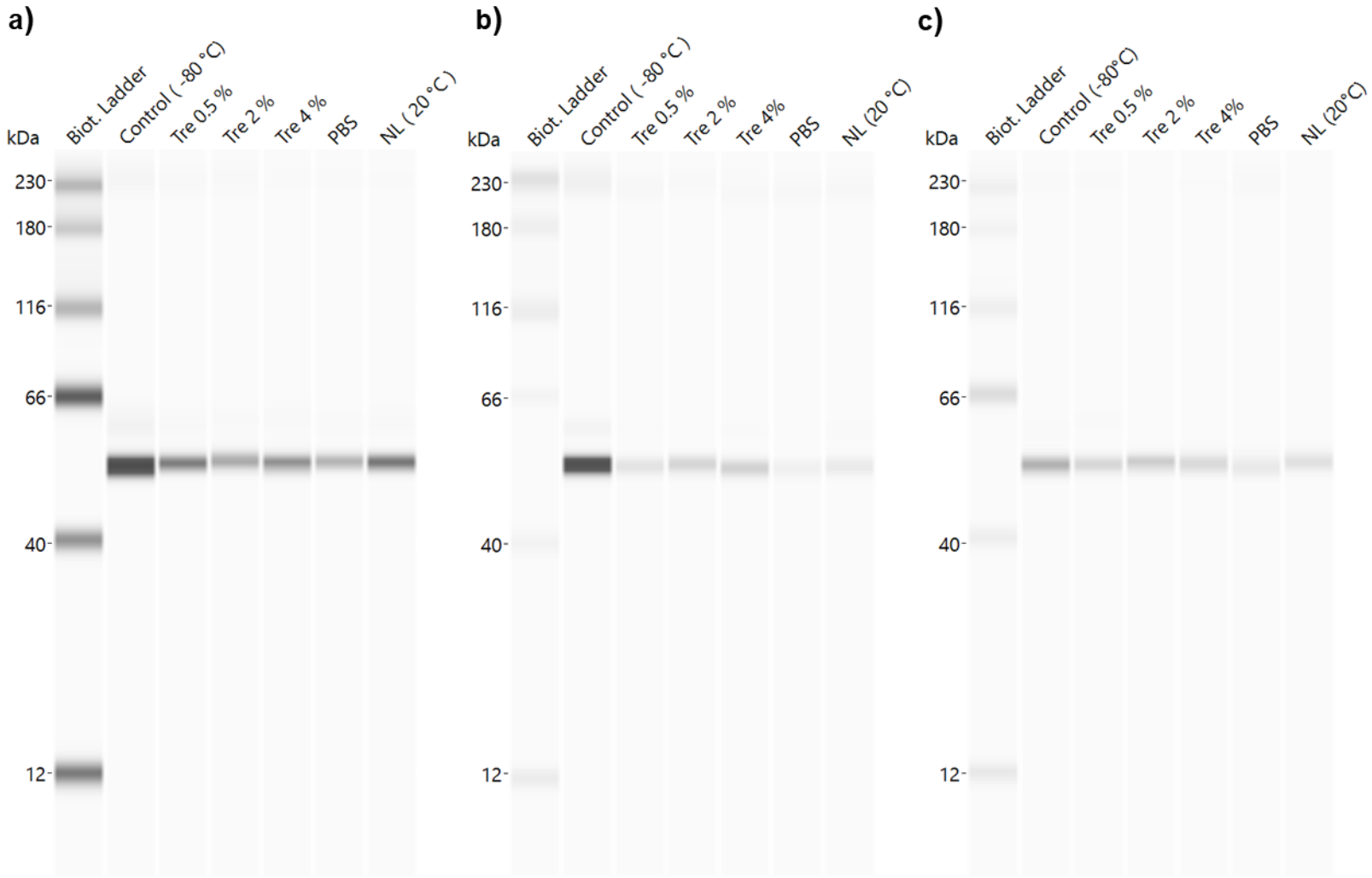


**Figure AII. 4:** Representative western blots as obtained by simple western for the EV surface marker TSG101 in different samples of naive HEK293T-derived EVs following storage at -80 °C, 20 °C or lyophilisation with 0.5-4 % of trehalose or without trehalose and storage at 20 °C after a) 1 week b) 2 weeks and c) 4 weeks.

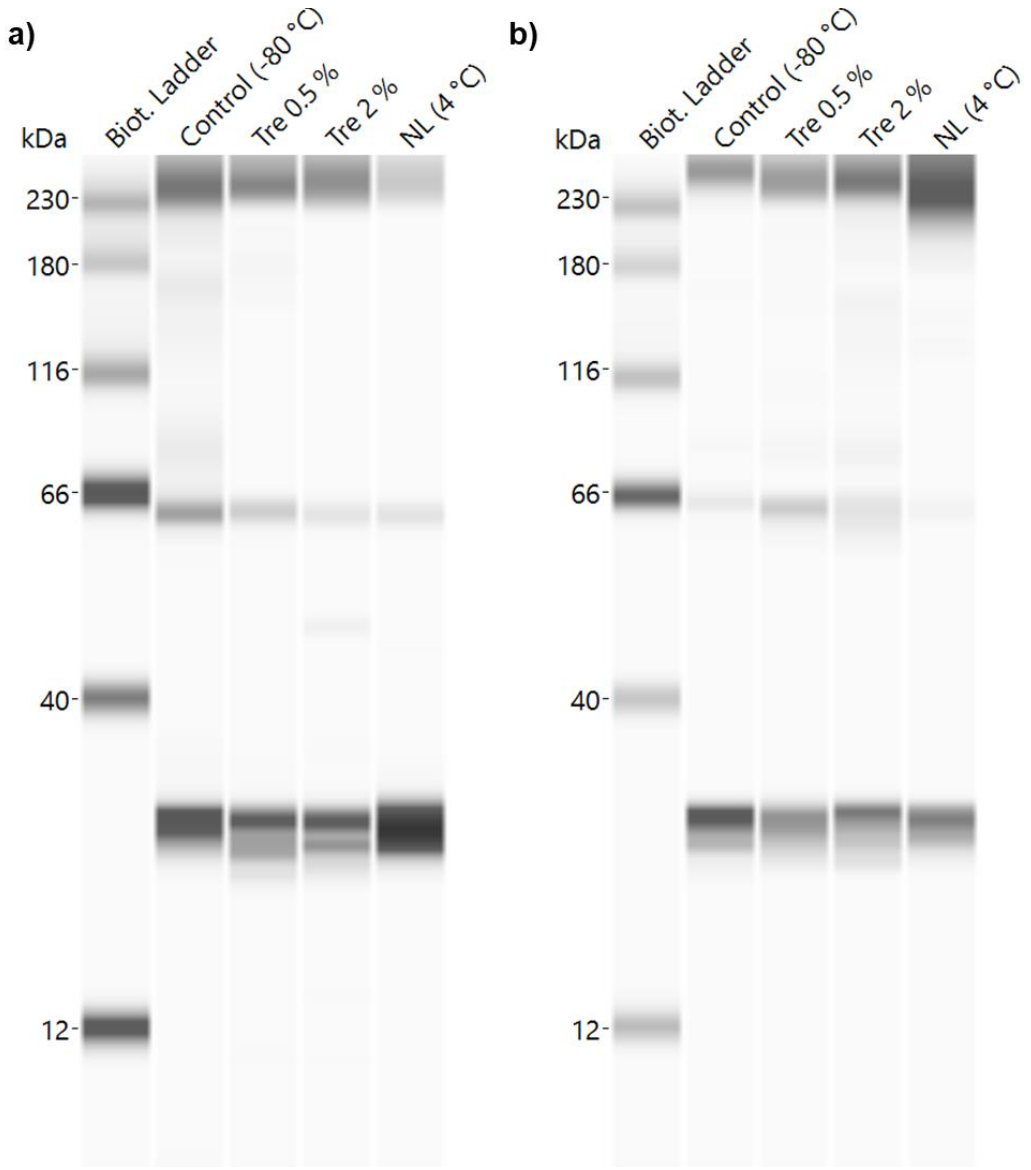


**Figure AII. 5:** Representative western blots as obtained by simple western for the EV surface marker CD9 in different samples of loaded-EVs derived from transduced-sorted HEK293T-cells following storage at -80 °C, 4 °C or lyophilisation with 0.5-2 % of trehalose and storage at 4 °C after a) 1 week and b) 2 weeks.

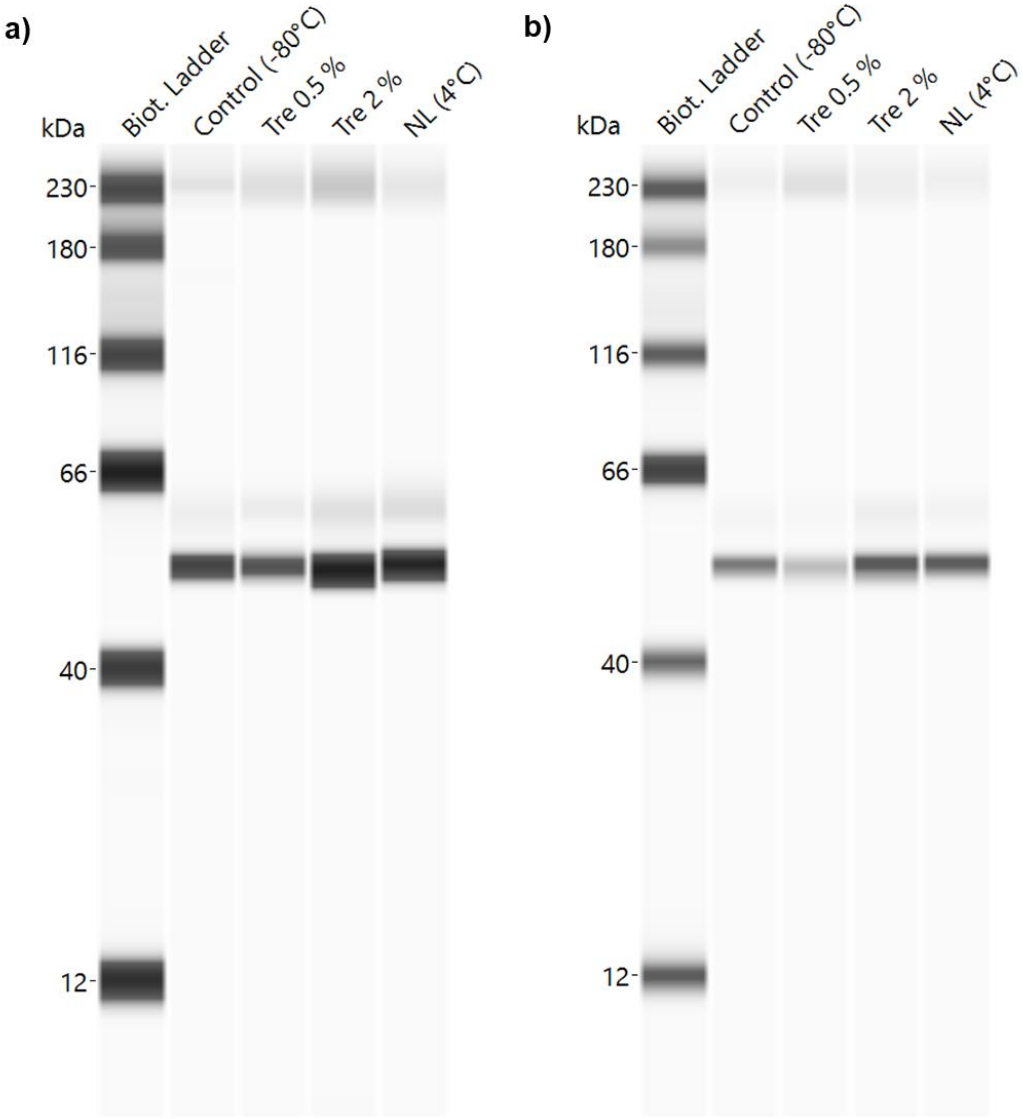


**Figure AII. 6:** Representative western blots as obtained by simple western for the EV surface marker TSG101 in different samples of loaded-EVs derived from transduced-sorted HEK293T-cells following storage at -80 °C, 4 °C or lyophilisation with 0.5-2 % of trehalose and storage at 4 °C after a) 1 week and b) 2 weeks.

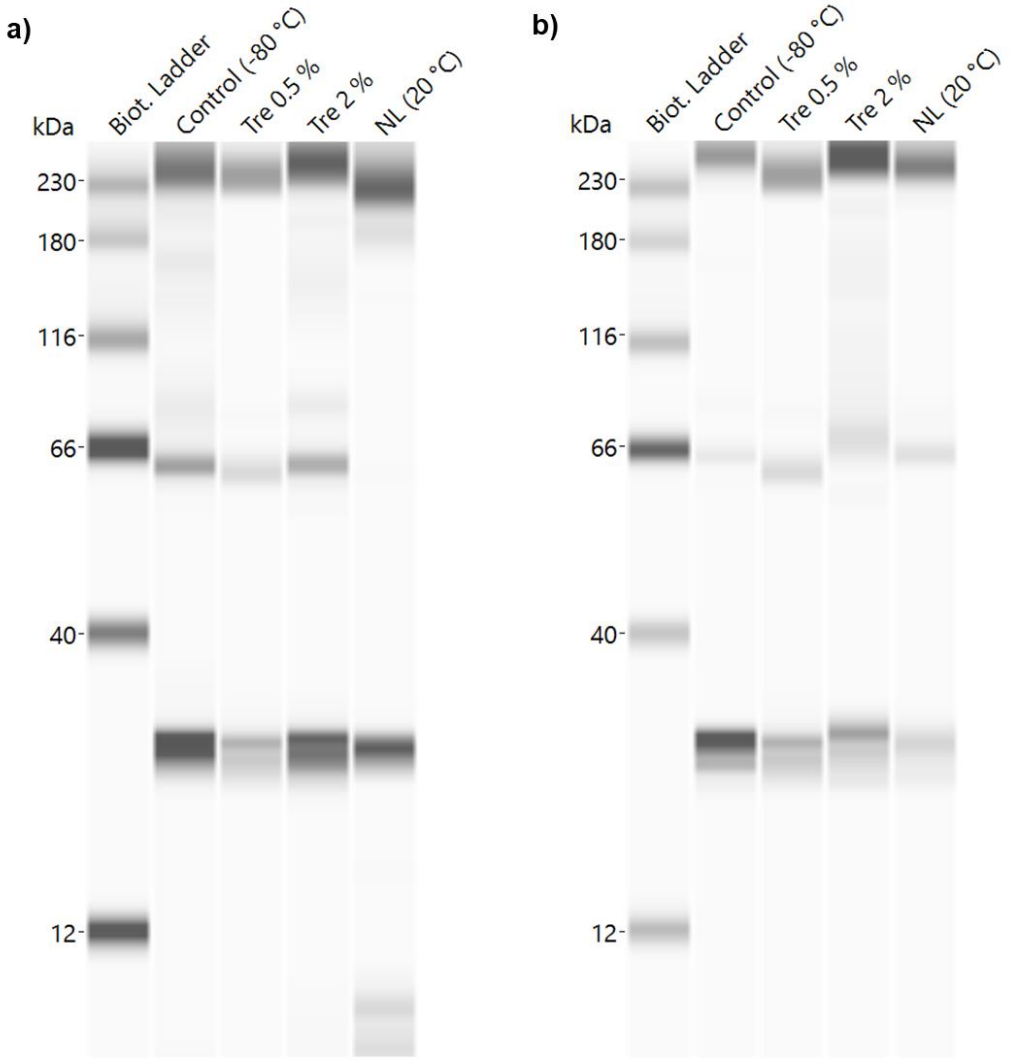


**Figure AII. 7:** Representative western blots as obtained by simple western for the EV surface marker CD9 in different samples of loaded-EVs derived from transduced-sorted HEK293T-cells following storage at -80 °C, 20 °C or lyophilisation with 0.5-2 % of trehalose and storage at 20 °C after a) 1 week and b) 2 weeks.

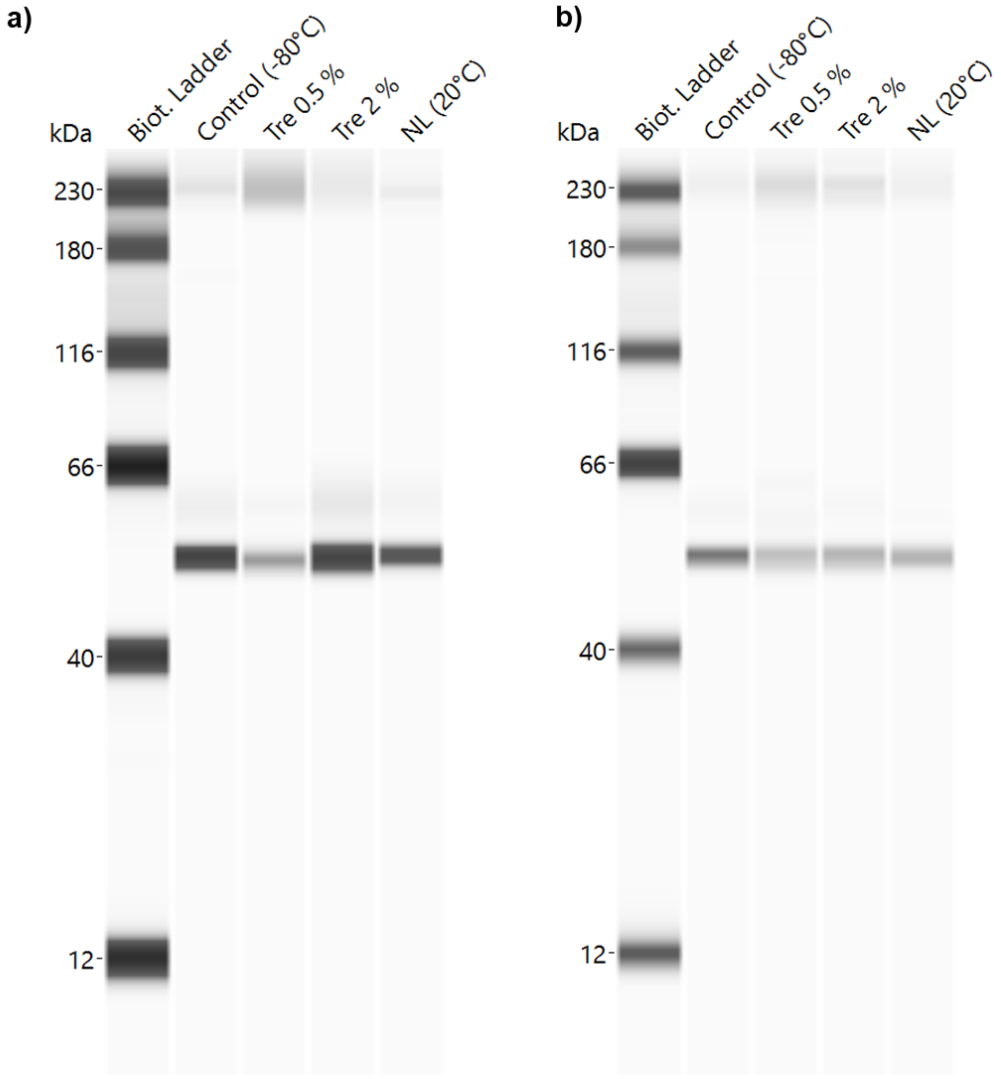


**Figure AII. 8:** Representative western blots as obtained by simple western for the EV surface marker TSG101 in different samples of loaded-EVs derived from transduced-sorted HEK293T-cells following storage at -80 °C, 20 °C or lyophilisation with 0.5-2 % of trehalose and storage at 20°C after a) 1 week and b) 2 weeks.